NEW GENERATION METAMATERIAL FOR ENERGY HARVESTING

A THESIS SUBMITTED TO THE BOARD OF GRADUATE PROGRAMS

OF

MIDDLE EAST TECHNICAL UNIVERSITY, NORTHERN CYPRUS CAMPUS

BY

MEHMET PAŞA ÜSTÜNSOY

IN PARTIAL FULFILLMENT OF THE REQUIREMENTS

FOR

THE DEGREE OF MASTER OF SCIENCE

IN

SUSTAINABLE ENVIRONMENT AND ENERGY SYSTEMS

AUGUST 2017

Approval of the Board of Graduate Programs

_____
Prof. Dr. Gürkan Karakaş
Chair person

I certify that this thesis satisfies all the requirements as a thesis for the degree of Master of
Science.

_____
Assist. Prof. Dr. Carter Mandrik
Program Coordinator

This is to certify that we have read this thesis and that in our opinion it is fully adequate, in scope and quality, as a thesis for the degree of Master of Science.

_____
Assoc. Prof. Dr. Cumali Sabah
Supervisor

Examining Committee Members

Assoc. Prof. Dr. Cumali Sabah	Electrical and Electronics Engineering Dept. METU NCC	_____
Assoc. Prof. Dr. Tayfun Nesimoğlu	Electrical and Electronics Engineering Dept. METU NCC	_____
Assoc. Prof. Dr. Hüseyin Ademgil	Computer Engineering Dept. European University of Lefke	_____

I hereby declare that all information in this document has been obtained and presented in accordance with academic rules and ethical conduct. I also declare that, as required by these rules and conduct, I have fully cited and referenced all material and results that are not original to this work.

Name, Last name: Mehmet Paşa Üstünsoy

Signature:

ABSTRACT

NEW GENERATION METAMATERIAL FOR ENERGY HARVESTING

Üstünsoy, Mehmet Paşa

M.Sc. Sustainable Environment and Energy Systems Program

Supervisor: Assoc. Prof. Dr. Cumali Sabah

August 2017, 150 pages

Scientists and researchers have been working for many years to find alternative energy sources for gathering the energy demand in which solar energy is a kind of renewable energy source. The proposed structures can be used in several applications such as antennas, EM filters, sensors, THz imaging systems, infrared spectroscopy, infrared cameras, solar cells, and so on. The aim of this thesis is to design and analyze new metamaterial absorbers and energy harvesters with different materials. In addition to this, metamaterial on antennas is designed and analyzed. Furthermore, the designed structures are numerically simulated and subjected to some enhancement techniques.

Keywords: Metamaterial, absorber, energy harvesting, antennas, solar cells

ÖZ

ENERJİNİN TOPLANMASI İÇİN YENİ NESİL METAMALZEME

Üstünsoy, Mehmet Paşa

Yüksek Lisans, Sürdürülebilir Çevre ve Enerji Sistemleri Programı

Tez Yöneticisi: Doç. Dr. Cumali Sabah

Ağustos 2017, 150 sayfa

Yenilenebilir enerji kaynaklarının bir türü olan güneş enerjisi enerji talebini karşılamak için birçok yıldır bilim insanları ve araştırmacılar alternatif enerji kaynakları bulmak için çalışıyorlar. Hazırlanan bu yapılar, örneğin antenler, elektromanyetik filtreler, sensörler, THz görüntüleme sistemleri, kızılötesi spektroskopisi, kızılötesi kameralar, güneş pilleri, ve benzer birçok uygulama için kullanılabilir. Bu tezin amacı, farklı malzemelerle yeni metamalzeme soğurucular ve enerji toplayıcılar tasarlamak ve analiz etmektir. Buna ek olarak, anten üzerinde metamalzeme tasarlanıp, analiz edilmiştir. Ek olarak, tasarlanmış yapılar sayısal olarak simüle edildi ve bazı geliştirme teknikleri uygulandı.

Anahtar kelimeler: Metamalzeme, soğurucu, enerji toplayıcı, antenler, güneş pilleri

DEDICATION

To my family

ACKNOWLEDGEMENTS

I would first like thank to my thesis supervisor, Assoc. Prof. Dr. Cumali Sabah whose enormous experience, comprehension, useful comments, contribution to my graduate experience. During learning, searching and completing of this study, his patience and leadership always helped me.

In addition, special thanks to all my Jury members.

I also mention other colleagues in the metamaterial research group; Patrick Rufangura and Batuhan Mulla for their positive ideas during this study.

Finally, I would like sincerely thank my family for their support and encouragement during my research.

TABLE OF CONTENTS

ETHICAL DECLARATION……..iii

ABSTRACT……...iv

ÖZ……v

DEDICATION……vi

ACKNOWLEDGEMENTS……...vii

TABLE OF CONTENTS……..viii

LIST OF FIGURES……..xiii

LIST OF TABLES……...xxx

NOMENCLATURE……...xxxii

CHAPTER 1

INTRODUCTION……1

1.1. Maxwell`s equations……..1

1.2. Metamaterials…….....3

1.3. Metamaterial absorber……4

1.4. Metamaterial absorber based energy harvester……..7

1.5. Numerical Validation of a previous study in literature……..9

CHAPTER 2

HIGH FREQUENCY METAMATERIAL ABSORBER BASED ON PATCH RESONATOR AND ITS APPLICATIONS FOR ENERGY HARVESTING……..12

2.1. Introduction……..12

2.2. Dual-Band Near Perfect Metamaterial Absorber…….....12

2.2.1. Design and Simulation……...12

2.2.2. Result and Discussion……13

2.3. Dual-Band Near Perfect Metamaterial Absorber`s Enhancement with Graphene Layers……..23

2.3.1. Design and Simulation……..24

2.3.2. Result and Discussion……24

2.4. Dual-Band Near Perfect Metamaterial Absorber Energy Harvesting……..26

2.4.1. Design and Simulation……..27

2.4.2. Result and Discussion……29

2.5. Conclusion……38

CHAPTER 3

ENEGRY HARVESTING OF METAMATERIAL ABSORBER FOR MICROWAVE, SUB-TERAHERTZ, AND INFRARED FREQUENCY REGIONS……...39

3.1. Introduction……..39

3.2. Dual band metamaterial absorber based energy harvester in microwave (GHz) regime for energy harvesting……..39

3.2.1. Design and Simulation……..39

3.2.2. Result and Discussion……40

3.3. Single band metamaterial absorber based energy harvester in sub-THz regime for energy harvesting…….....52

3.3.1. Design and Simulation……..52

3.3.2. Result and Discussion……53

3.4. Single band metamaterial absorber based energy harvester in infrared regime for energy harvesting……....60

3.4.1. Design and Simulation……..60

3.4.2. Result and Discussion……61

3.5. Conclusion……65

CHAPTER 4

TOPOLOGICAL STUDY OF ENERGY HARVESTING OF METAMATERIAL ABSORBER FOR MICROWAVE, SUB-TERAHERTZ, AND INFRARED FREQUENCY REGIONS……..67

4.1. Introduction…….....67

4.2. Single band metamaterial absorber based energy harvester topology in microwave (GHz) regime for energy harvesting…….....67

4.2.1. Design and Simulation……..67

4.2.2. Result and Discussion……69

4.3. Single band metamaterial absorber based energy harvester topology in sub-THz regime for energy harvesting……...74

4.3.1. Design and Simulation……..74

4.3.2. Result and Discussion……76

4.4. Single band metamaterial absorber based energy harvester topology in infrared regime for energy harvesting……...82

4.4.1. Design and Simulation……..82

4.4.2. Result and Discussion……83

4.5. Conclusion……89

CHAPTER 5

PARAMETRIC STUDY FOR ENERGY HARVESTING OF METAMATERIAL ABSORBER FOR HIGH FREQUENCY REGION AND ENHANCEMENT TECHNIQUES……...91

5.1. Introduction……..91

5.2. Design and Simulation……..91

5.3. Result and Discussion……...92

5.4. Enhancement Methods of Results…….....96

5.4.1. Hole at the metal plate……96

5.4.2. Adding different materials into the hole……97

5.4.3. Graphene……...99

5.5. Conclusion……..105

CHAPTER 6

ENERGY HARVESTING APPLICATION OF METAMATERIAL ABSORBER INTEGRATED TO THE MICROSTRIP PATCH ANTENNA FOR WIRELESS COMMUNICATION……106

6.1. Introduction……106

6.2. A microstrip patch antenna in 2.4 GHz operation and a metamaterial absorber based energy harvester with FR4 substrate with/without FR4 substrate legs on its patch……..106

6.2.1. Design and Simulation…….....106

6.2.2. Result and Discussion……..108

6.3. A microstrip patch antenna in 2.4 GHz operation and a metamaterial absorber based energy harvester with Rogers RT5880 substrate with/without Rogers RT5880 substrate legs on its patch……..122

6.3.1. Design and Simulation…….....122

6.3.2. Result and Discussion……..124

6.4. Conclusion…….....138

CHAPTER 7

CONCLUSION AND FUTURE WORK…….....140

BIBLIOGRAPHY…….....142

LIST OF FIGURES

Figure 1-1. ((a) The geometric design with dimensions, (b) gathered power efficiency – resistance diagram with load, (c) simulation setup, and (d) absorption results with and without load) obtained by Almoneef and Ramahi [57]……10

Figure 1-2. Absorption results for not only obtained by Almoneef and Ramahi [57] but also obtained by recreated and reanalysed structure……11

Figure 1-3. Efficiency not for only obtained by Almoneef and Ramahi [57] but also obtained by recreated and reanalysed structure……...11

Figure 2-1. The design and dimensions of the unit cell of the metamaterial absorber based on patch resonator……13

Figure 2-2. The reflectance and absorption results for $\sigma_{aluminum} = 3.56\times10^{7}$S/m, $\tan\delta_{GaAs} = 0.006$, and $\varepsilon_{GaAs} = 12.94$ materials` properties……14

Figure 2-3. The reflectance and absorption results when materials have Drude model properties…….....15

Figure 2-4. The reflectance and absorption results when materials have Drude model properties without (patch resonator) top metallic layer……16

Figure 2-5. Parametric study for the thickness of the top square patch resonator (c)…16

Figure 2-6. Parametric study for the length of the bottom square metal and square substrate (d).……17

Figure 2-7. Parametric study for the length of the bottom square metal and square substrate (d). …….....17

Figure 2-8. Parametric study for the length of the top square patch resonator (e).....18

Figure 2-9. Parametric study for the length of the top square patch resonator (e).....18

Figure 2-10. (a) Impedance and its real and imaginary part, and (b) real parts of permittivity and permeability.……19

Figure 2-11. Magnitude and phase of S_{11}……20

Figure 2-12. Absorption results for different polarization angles (φ) at normal incidence. …….....20

Figure 2-13. Absorption results for transverse electric (TE) mode for different incident angles (θ)……21

Figure 2-14. Absorption results for transverse magnetic (TM) mode for different incident angles (θ)……..21

Figure 2-15. (a) Electric field distributions of the metamaterial absorber structure at 197.25THz, (b) Electric field distributions of the metamaterial absorber structure at 514.5THz, (c) Surface current distributions of the metamaterial absorber structure at 197.25THz, and (d) Surface current distributions of the metamaterial absorber structure at 514.5THz.……22

Figure 2-16. The structure and dimensions of the unit cell of the metamaterial absorber based on patch resonator with integrated graphene layer(s) (a) under the metal patch resonator, (b) at the top of the metal patch resonator, (c) not only under the metal patch resonator but also at the top of the metal patch resonator.……..24

Figure 2-17. Parametric study for four graphene thicknesses (t) for (a) under the metal patch resonator, (b) at the top of the metal patch resonator, (c) not only under the metal patch resonator but also at the top of the metal patch resonator.……25

Figure 2-18. The view and dimensions of metamaterial energy harvester based on near perfect metamaterial absorber unit cell design with the square ring shaped resonator and two resistors.……28

Figure 2-19. The view and dimensions of metamaterial energy harvester based on near perfect metamaterial absorber unit cell design with the circular ring shaped resonator and two resistors.……28

Figure 2-20. Reflection and absorption results for (Aluminum (Palik) (metal plate), GaAs (Palik) (substrate) and Aluminum (Palik) (resonator)) structure (for the proposed (square ring shaped resonator) unit cell structure) (The resonance frequencies at 142.40 and 204.80 THz).……30

Figure 2-21. Reflection and absorption results for (Silver (Johnson) (metal plate), Silica (Ghosh) (substrate) and Silver (Johnson) (resonator)) structure (for the proposed (square ring shaped resonator) unit cell structure) (The resonance frequency at 240.00 THz)……...30

Figure 2-22. Reflection and absorption results for (Aluminum (Palik) (metal plate), GaAs (Palik) (substrate) and Aluminum (Palik) (resonator)) structure (for the proposed (circular ring shaped resonator) unit cell structure) (The resonance frequencies at 140.80 and 209.60 THz)…….31

Figure 2-23. Reflection and absorption results for (Silver (Johnson) (metal plate), Silica (Ghosh) (substrate) and Silver (Johnson) (resonator)) structure (for the proposed (circular ring shaped resonator) unit cell structure) (The resonance frequencies at 219.20 and 248.00 THz)…….31

Figure 2-24. Parametric study gathered power frequency diagram for selected different "g" parameters and resistors between 500-3000 ohm for (Aluminum (Palik) (metal plate), GaAs (Palik) (substrate) and Aluminum (Palik) (resonator)) structure (for the proposed (square ring shaped resonator) unit cell structure)……..32

Figure 2-25. Parametric study gathered power frequency diagram for selected different "g" parameters and resistors between 500-3000 ohm for (Silver (Johnson) (metal plate), Silica (Ghosh) (substrate) and Silver (Johnson) (resonator)) structure (for the proposed (square ring shaped resonator) unit cell structure)…….33

Figure 2-26. Parametric study gathered power frequency diagram for selected different "g" parameters and resistors between 500-3000 ohm for (Aluminum (Palik) (metal plate), GaAs (Palik) (substrate) and Aluminum (Palik) (resonator)) structure (for the proposed (circular ring shaped resonator) unit cell structure)……33

Figure 2-27. Parametric study gathered power frequency diagram for selected different "g" parameters and resistors between 500-3000 ohm for (Silver (Johnson) (metal plate), Silica (Ghosh) (substrate) and Silver (Johnson) (resonator)) structure (for the proposed (circular ring shaped resonator) unit cell structure)……34

Figure 2-28. Simulated lumped element power magnitude for both cases with and without metal plate for 500 ohm resistor for (Aluminum (Palik) (metal plate), GaAs

(Palik) (substrate) and Aluminum (Palik) (resonator)) structure (for the proposed (square ring shaped resonator) unit cell structure).....34

Figure 2-29. Simulated lumped element power magnitude for both cases with and without metal plate for 500 ohm resistor for (Silver (Johnson) (metal plate), Silica (Ghosh) (substrate) and Silver (Johnson) (resonator)) structure (for the proposed (square ring shaped resonator) unit cell structure).....35

Figure 2-30. Simulated lumped element power magnitude for both cases with and without metal plate for 500 ohm resistor for (Aluminum (Palik) (metal plate), GaAs (Palik) (substrate) and Aluminum (Palik) (resonator)) structure (for the proposed (circular ring shaped resonator) unit cell structure).....35

Figure 2-31. Simulated lumped element power magnitude for both cases with and without metal plate for 500 ohm resistor for (Silver (Johnson) (metal plate), Silica (Ghosh) (substrate) and Silver (Johnson) (resonator)) structure (for the proposed (circular ring shaped resonator) unit cell structure).....35

Figure 2-32. For (Aluminum (Palik) (metal plate), GaAs (Palik) (substrate) and Aluminum (Palik) (resonator)) structure (for the proposed (square ring shaped resonator) unit cell structure) (a) Electric field distribution at the resonance frequency of 142.40 THz (b) Magnetic field distribution at the resonance frequency of 142.40 THz (c) Surface current distribution at the resonance frequency of 142.40 THz (d) Electric field distribution at the resonance frequency of 204.80 THz (e) Magnetic field distribution at the resonance frequency of 204.80 THz (f) Surface current distribution at the resonance frequency of 204.80 THz.....36

Figure 2-33. For (Silver (Johnson) (metal plate), Silica (Ghosh) (substrate) and Silver (Johnson) (resonator)) structure (for the proposed (square ring shaped resonator) unit cell structure) (a) Electric field distribution at the resonance frequency of 240.00 THz (b) Magnetic field distribution at the resonance frequency of 240.00 THz (c) Surface current distribution at the resonance frequency of 240.00 THz.....37

Figure 2-34. For (Aluminum (Palik) (metal plate), GaAs (Palik) (substrate) and Aluminum (Palik) (resonator)) structure (for the proposed (circular ring shaped resonator) unit cell structure) (a) Electric field distribution at the resonance frequency

of 140.80 THz (b) Magnetic field distribution at the resonance frequency of 140.80 THz (c) Surface current distribution at the resonance frequency of 140.80 THz (d) Electric field distribution at the resonance frequency of 209.60 THz (e) Magnetic field distribution at the resonance frequency of 209.60 THz (f) Surface current distribution at the resonance frequency of 209.60 THz.……37

Figure 2-35. For (Silver (Johnson) (metal plate), Silica (Ghosh) (substrate) and Silver (Johnson) (resonator)) structure (for the proposed (circular ring shaped resonator) unit cell structure) (a) Electric field distribution at the resonance frequency of 219.20 THz (b) Magnetic field distribution at the resonance frequency of 219.20 THz (c) Surface current distribution at the resonance frequency of 219.20 THz (d) Electric field distribution at the resonance frequency of 248.00 THz (e) Magnetic field distribution at the resonance frequency of 248.00 THz (f) Surface current distribution at the resonance frequency of 248.00 THz.……...38

Figure 3-1. (a) Substrate, resonator and resistors, (b) metal plate, (c) dimensions of near perfect metamaterial absorber based energy harvester unit cell structure in microwave (GHz) range.……40

Figure 3-2. Reflectance and absorption results for (Copper (metal plate), FR4 (substrate) and Copper (resonator)) structure (The resonance frequencies at 5.42 and 12.72 GHz).……43

Figure 3-3. Gathered power frequency diagram for selected different resistors between 400-2900 ohm for (Copper (metal plate), FR4 (substrate) and Copper (resonator)) structure.……..44

Figure 3-4. Simulated lumped element power magnitude for both cases with and without metal plate for 400 ohm resistor for (Copper (metal plate), FR4 (substrate) and Copper (resonator)) structure.……44

Figure 3-5. For (Copper (metal plate), FR4 (substrate) and Copper (resonator)) structure (a) Electric field distribution at the resonance frequency of 5.42 GHz (b) Electric field distribution at the resonance frequency of 12.72 GHz (c) Surface current distribution at the resonance frequency of 5.42 GHz (d) Surface current distribution at the resonance frequency of 12.72 GHz……...……45

Figure 3-6. Reflectance and absorption results for (Copper (metal plate), Polyimide (substrate) and Copper (resonator)) structure (The resonance frequencies at 5.80 and 13.62 GHz).....46

Figure 3-7. Gathered power frequency diagram for selected different resistors between 600-2600 ohm for (Copper (metal plate), Polyimide (substrate) and Copper (resonator)) structure.....46

Figure 3-8. Simulated lumped element power magnitude for both cases with and without metal plate for 600 ohm resistor for (Copper (metal plate), Polyimide (substrate) and Copper (resonator)) structure.....47

Figure 3-9. For (Copper (metal plate), Polyimide (substrate) and Copper (resonator)) structure (a) Electric field distribution at the resonance frequency of 5.80 GHz (b) Electric field distribution at the resonance frequency of 13.62 GHz (c) Surface current distribution at the resonance frequency of 5.80 GHz (d) Surface current distribution at the resonance frequency of 13.62 GHz.....47

Figure 3-10. Reflectance and absorption results for (Copper (metal plate), Arlon AD 350 (substrate) and Copper (resonator)) structure (The resonance frequencies at 5.74 and 14.44 GHz).....48

Figure 3-11. Gathered power frequency diagram for selected different resistors between 600-2600 ohm for (Copper (metal plate), Arlon AD 350 (substrate) and Copper (resonator)) structure.....48

Figure 3-12. Simulated lumped element power magnitude for both cases with and without metal plate for 600 ohm resistor for (Copper (metal plate), Arlon AD 350 (substrate) and Copper (resonator)) structure.....49

Figure 3-13. For (Copper (metal plate), Arlon AD 350 (substrate) and Copper (resonator)) structure (a) Electric field distribution at the resonance frequency of 5.74 GHz (b) Electric field distribution at the resonance frequency of 14.44 GHz (c) Surface current distribution at the resonance frequency of 5.74 GHz (d) Surface current distribution at the resonance frequency of 14.44 GHz.....49

Figure 3-14. Reflectance and absorption results for (Copper (metal plate), Rogers RT 5880 (substrate) and Copper (resonator)) structure (The resonance frequencies at 7.00 and 16.98 GHz)……..50

Figure 3-15. Gathered power frequency diagram for selected different resistors between 500-3000 ohm for (Copper (metal plate), Rogers RT 5880 (substrate) and Copper (resonator)) structure……50

Figure 3-16. Simulated lumped element power magnitude for both cases with and without metal plate for 500 ohm resistor for (Copper (metal plate), Rogers RT 5880 (substrate) and Copper (resonator)) structure……51

Figure 3-17. For (Copper (metal plate), Rogers RT 5880 (substrate) and Copper (resonator)) structure (a) Electric field distribution at the resonance frequency of 7.00 GHz (b) Electric field distribution at the resonance frequency of 16.98 GHz (c) Surface current distribution at the resonance frequency of 7.00 GHz (d) Surface current distribution at the resonance frequency of 16.98 GHz……51

Figure 3-18. (a) Substrate, resonator and resistors, (b) metal plate, (c) dimensions of near perfect metamaterial absorber based energy harvester unit cell structure in sub-THz range……...52

Figure 3-19. Reflectance and absorption results for (Silver (metal plate), Quartz (substrate) and Silver (resonator)) structure (The resonance frequency at 0.694 THz)……...53

Figure 3-20. Gathered power frequency diagram for selected different resistors between 500-3000 ohm for (Silver (metal plate), Quartz (substrate) and Silver (resonator)) structure……..54

Figure 3-21. Simulated lumped element power magnitude for both cases with and without metal plate for 500 ohm resistor for (Silver (metal plate), Quartz (substrate) and Silver (resonator)) structur……55

Figure 3-22. For (Silver (metal plate), Quartz (substrate) and Silver (resonator)) structure (a) Electric field distribution at the resonance frequency of 0.694 THz (b) Surface current distribution at the resonance frequency of 0.694 THz……..56

Figure 3-23. Lumped element power value according to different metals with Quartz substrate……..56

Figure 3-24. Lumped element power value according to different metals with Polyimide substrate…….57

Figure 3-25. Lumped element power value according to different metals with Teflon substrate……..57

Figure 3-26. Lumped element power value according to different metals with Silicon substrate……..58

Figure 3-27. Lumped element power value according to different metals with Rogers TMM4 substrate…….....58

Figure 3-28. Lumped element power value according to different metals with Rogers RT5880 substrate…….....59

Figure 3-29. (a) Substrate, resonator and resistors, (b) metal plate, (c) dimensions of near perfect metamaterial absorber based energy harvester unit cell structure in infrared range.....60

Figure 3-30. Reflectance and absorption results for (Silver (Johnson) (metal plate), Silicon (substrate) and Silver (Johnson) (resonator)) structure (The resonance frequency at 96.15 THz)……..61

Figure 3-31. Gathered power frequency diagram for selected different resistors between 500-3000 ohm for (Silver (Johnson) (metal plate), Silicon (substrate) and Silver (Johnson) (resonator)) structure.……...62

Figure 3-32. Simulated lumped element power magnitude for both cases with and without metal plate for 500 ohm resistor for (Silver (Johnson) (metal plate), Silicon (substrate) and Silver (Johnson) (resonator)) structure……63

Figure 3-33. For (Silver (Johnson) (metal plate), Silicon (substrate) and Silver (Johnson) (resonator)) structure (a) Electric field distribution at the resonance frequency of 96.15 THz (b) Magnetic field distribution at the resonance frequency of

96.15 THz (c) Surface current distribution at the resonance frequency of 96.15 THz.……64

Figure 3-34. Lumped element power value according to different metals with Silica (Silicon Dioxide) substrate.……64

Figure 3-35. Lumped element power value according to different metals with Silicon substrate……..65

Figure 4-1. (a) Substrate, resonators and resistors, (b) metal plate, (c) dimensions of near perfect metamaterial absorber based energy harvester unit cell structure in microwave (GHz) range……..68

Figure 4-2. Reflectance and absorption result for (Copper (metal plate), Rogers RT 5880 (substrate) and Copper (resonator)) structure (The resonance frequency at 4.800 GHz)……...69

Figure 4-3. Gathered power frequency diagram for selected different resistors between 500-3000 ohm for (Copper (metal plate), Rogers RT 5880 (substrate) and Copper (resonator)) structure.……..70

Figure 4-4. When (n) resonators and (n-1) resistors are exist, (a1 - j1) views from the top, (a2 – j2) reflectance and absorption results, and (a3 – j3) Lumped element power values for different geometric designs at 500 ohm (Changed geometric parameters are separately given left side of each design).……71

Figure 4-5. Simulated lumped element power magnitude for both cases with and without metal plate for 500 ohm resistor for (Copper (metal plate), Rogers RT 5880 (substrate) and Copper (resonator)) structure (This structure can be seen in either Figure 4-1 or Figure 4-4j1 because the same structure is shown in both Figures.).……73

Figure 4-6. For (Copper (metal plate), Rogers RT 5880 (substrate) and Copper (resonator)) structure (This structure can be seen in either Figure 4-1 or Figure 4-4j1 because the same structure is shown in both Figures.) (a) Electric field distribution (b) Magnetic field distribution (c) Surface current distribution at the resonance frequency of 4.800 GHz at 500 ohm……74

Figure 4-7. (a) Substrate, metal plate, resonators and resistors, (b1 and b2) dimensions of near perfect metamaterial absorber based energy harvester unit cell structure in sub-THz range……75

Figure 4-8. Reflectance and absorption result for (Silver (metal plate), Quartz (substrate) and Silver (resonator)) structure (The resonance frequency at 0.5595 THz)……...76

Figure 4-9. Gathered power frequency diagram for selected different resistors between 300-2800 ohm for (Silver (metal plate), Quartz (substrate) and Silver (resonator)) structure.....77

Figure 4-10. When (n) resonators and (n-1) resistors are exist, (a1 - j1) views from the top, (a2 – j2) reflectance and absorption results, and (a3 – j3) Lumped element power values for different geometric designs at 300 ohm (Changed geometric parameters are separately given left side of each design)……78

Figure 4-11. Simulated lumped element power magnitude for both cases with and without metal plate for 300 ohm resistor for (Silver (metal plate), Quartz (substrate) and Silver (resonator)) structure (This structure can be seen in either Figure 4-7 or Figure 4-10j1 because the same structure is shown in both Figures.)……80

Figure 4-12. For (Silver (metal plate), Quartz (substrate) and Silver (resonator)) structure (This structure can be seen in either Figure 4-7 or Figure 4-10j1 because the same structure is shown in both Figures.) (a) Electric field distribution (b) Magnetic field distribution (c) Surface current distribution at the resonance frequency of 0.5595 THz at 300 ohm……..81

Figure 4-13. (a) Substrate, metal plate, resonators and resistors, (b1 and b2) dimensions of near perfect metamaterial absorber based energy harvester unit cell structure in infrared range……..83

Figure 4-14. Reflectance and absorption result for (Silver (Johnson) (metal plate), Silica (substrate) and Silver (Johnson) (resonator)) structure (The resonance frequency at 252.8 THz……84

Figure 4-15. Gathered power frequency diagram for selected different resistors between 400-2900 ohm for (Silver (Johnson) (metal plate), Silica (substrate) and Silver (Johnson) (resonator)) structure.....85

Figure 4-16. When (n) resonators and (n-1) resistors are exist, (a1 - j1) views from the top, (a2 – j2) reflectance and absorption results, and (a3 – j3) Lumped element power values for different geometric designs at 400 ohm (Changed geometric parameters are separately given left side of each design).....86

Figure 4-17. Simulated lumped element power magnitude for both cases with and without metal plate for 400 ohm resistor for (Silver (Johnson) (metal plate), Silica (substrate) and Silver (Johnson) (resonator)) structure (This structure can be seen in either Figure 4-13 or Figure 4-16j1 because the same structure is shown in both Figures.).....88

Figure 4-18. For (Silver (Johnson) (metal plate), Silica (substrate) and Silver (Johnson) (resonator)) structure (This structure can be seen in either Figure 4-13 or Figure 4-16j1 because the same structure is shown in both Figures.) (a) Electric field distribution (b) Magnetic field distribution (c) Surface current distribution at the resonance frequency of 252.8 THz at 400 ohm.....89

Figure 5-1. (a) Substrate, metal plate, resonator and resistors, (b and c) dimensions of near perfect metamaterial absorber based energy harvester unit cell structure in infrared and visible range.....92

Figure 5-2. Reflectance and absorption result for the structure in Figure 5-1 (The resonance frequencies at 363 THz, 468.7 THz and 529.6 THz).....92

Figure 5-3. Gathered power frequency diagram for four 900 ohm resistors for the structure in Figure 5-1.....93

Figure 5-4. Simulated lumped element power magnitude for both cases with and without metal plate for 900 ohm resistor for the structure in Figure 5-1.....93

Figure 5-5. For the structure in Figure 5-1 (a1) Electric field distribution (a2) Magnetic field distribution (a3) Surface current distribution at the resonance frequency of 363 THz at 900 ohm, (b1) Electric field distribution (b2) Magnetic field distribution (b3)

Surface current distribution at the resonance frequency of 468.7 THz at 900 ohm, (c1) Electric field distribution (c2) Magnetic field distribution (c3) Surface current distribution at the resonance frequency of 529.6 THz at 900 ohm.……94

Figure 5-6. Gathered absorption frequency diagram for selected different resistors between 900-3000 ohm for the structure in Figure 5-1……..95

Figure 5-7. Gathered power frequency diagram for selected different resistors between 900-3000 ohm for the structure in Figure 5-1…….95

Figure 5-8. View of created hole at the metal plate with dimensions for parametric study……96

Figure 5-9. Gathered power frequency diagram for selected different “h” parameters for the structure when R=900 ohm in Figure 5-8.……97

Figure 5-10. View of adding different material in created hole at the metal plate for the structure in Figure 5-8 when h=20 nm and R=900 ohm.……..98

Figure 5-11. Gathered power frequency diagram for four different materials which are separately adding in created hole at the metal plate and analysed when h=20 nm and R=900 ohm for the structure in Figure 5-8.…….98

Figure 5-12. View of adding Graphene layer(s) at the bottom of the metal plate and a-Si substrate material in created hole in the middle of metal plate for the structure in Figure 5-10 when h=20 nm and R=900 ohm.……..99

Figure 5-13. Gathered absorption frequency diagram for the parametric study with three graphene thicknesses for the structure in Figure 5-12.……..100

Figure 5-14. Gathered power frequency diagram for the parametric study with three graphene thicknesses for the structure in Figure 5-12.……..100

Figure 5-15. Simulated absorption magnitude for both cases with and without hole & hole substrate & Graphene for the structures in Figure 5-1 and Figure 5-12……102

Figure 5-16. Simulated total power values of lumped elements magnitude for both cases with and without hole & hole substrate & Graphene for the structures in Figure 5-1 and Figure 5-12…….....103

Figure 5-17. For the structure in Figure 5-12 (a1) Electric field distribution (a2) Magnetic field distribution (a3) Surface current distribution at the resonance frequency of 355.3 THz at 900 ohm, (b1) Electric field distribution (b2) Magnetic field distribution (b3) Surface current distribution at the resonance frequency of 462.4 THz at 900 ohm, (c1) Electric field distribution (c2) Magnetic field distribution (c3) Surface current distribution at the resonance frequency of 514.9 THz at 900 ohm (for the with hole & hole substrate (a-Si) & Graphene (Graphene thickness = 1.005 nm (3-layers)) situation)……..105

Figure 6-1. (a) Substrate, patch, edge-fed, quarter wavelength and waveport (b) dimensions, (c) ground metal plate and dimensions of waveport for a 2.4 GHz microstrip patch antenna in microwave (GHz) range……...107

Figure 6-2. Reflectance result for a 2.4 GHz microstrip patch antenna design in Figure 6-1 in microwave (GHz) range from 1 GHz to 5 GHz (The resonance frequencies at 2.380 GHz, 3.320 GHz and 4.788 GHz)……108

Figure 6-3. (a) Adding four FR4 substrate legs and metamaterial absorber based energy harvester on a 2.4 GHz microstrip patch antenna in microwave (GHz) range (b1) Dimensions, FR4 substrate, Copper resonator and four resistors for a metamaterial absorber based energy harvester (b2) FR4 (substrate) legs and Copper metal plate, (b3) dimensions of FR4 (substrate) legs . ……109

Figure 6-4. Reflectance and absorption results for the design in Figure 6-3a in microwave (GHz) range from 1 GHz to 5 GHz (The resonance frequencies at 2.348 GHz, 3.156 GHz and 4.804 GHz)…….....110

Figure 6-5. Gathered power frequency diagram for four 10 ohm resistors for the design in Figure 6-3a in microwave (GHz) range from 1 GHz to 5 GHz (The resonance frequencies at 2.424 GHz, 2.764 GHz and 4.908 GHz)……110

Figure 6-6. Adding ten layers metamaterial absorber based energy harvester with their legs on a 2.4 GHz microstrip patch antenna in microwave (GHz) range (Each layer have four 10 ohm resistors)……..111

Figure 6-7. Gathered absorption frequency diagram for selected different quantities of adding layers between 2 – 10 layers for the structure in Figure 6-6…….....112

Figure 6-8. Gathered power frequency diagram for selected different quantities of adding layers between 2 – 10 layers for the structure in Figure 6-6.…….113

Figure 6-9. For the structure (adding 10 – layers metamaterial absorber based energy harvester with their legs on the designed 2.4 GHz microstrip patch antenna in microwave (GHz) range) in Figure 6-6 (a) Electric field distribution (b) Magnetic field distribution (c) Surface current distribution at the resonance frequency of 2.344 GHz at 10 ohm.……..114

Figure 6-10. For the structure (adding 10 – layers metamaterial absorber based energy harvester with their legs on the designed 2.4 GHz microstrip patch antenna in microwave (GHz) range) in Figure 6-6 (a) typical radiation pattern (b1) and (b2) view of three – dimensional far – field pattern from two different sides at the resonance frequency of 2.344 GHz at 10 ohm……115

Figure 6-11. (a) Adding metamaterial absorber based energy harvester on a 2.4 GHz microstrip patch antenna in microwave (GHz) range (b1) Dimensions, FR4 substrate, Copper resonator and four resistors for a metamaterial absorber based energy harvester (b2) Copper metal plate for a metamaterial absorber based energy harvester.……..116

Figure 6-12. Reflectance and absorption results for the design in Figure 6-11a in microwave (GHz) range from 1 GHz to 5 GHz (The resonance frequencies at 2.376 GHz, 3.336 GHz and 4.860 GHz).…….117

Figure 6-13. Gathered power frequency diagram for four 10 ohm resistors for the design in Figure 6-11a in microwave (GHz) range from 1 GHz to 5 GHz (The resonance frequencies at 2.372 GHz, 3.740 GHz and 4.908 GHz).……..117

Figure 6-14. Adding thirteen layers metamaterial absorber based energy harvesters without their Copper metal plates (excluded for the first layer) on a 2.4 GHz microstrip patch antenna in microwave (GHz) range (Each layer have four 10 ohm resistors).……...118

Figure 6-15. Gathered absorption frequency diagram for selected different quantities of adding layers between 2 – 13 layers for the structure in Figure 6-14.……..119

Figure 6-16. Gathered power frequency diagram for selected different quantities of adding layers between 2 – 13 layers for the structure in Figure 6-14……..120

Figure 6-17. For the structure (adding 13 – layers metamaterial absorber based energy harvester without their Copper metal plate (excluded for the first layer) on the designed 2.4 GHz microstrip patch antenna in microwave (GHz) range) in Figure 6-14 (a) Electric field distribution (b) Magnetic field distribution (c) Surface current distribution at the resonance frequency of 2.348 GHz at 10 ohm……121

Figure 6-18. For the structure (adding 13 – layers metamaterial absorber based energy harvester without their Copper metal plate (excluded for the first layer) on the designed 2.4 GHz microstrip patch antenna in microwave (GHz) range) in Figure 6-14 (a) typical radiation pattern (b1) and (b2) view of three – dimensional far – field pattern from two different sides at the resonance frequency of 2.348 GHz at 10 ohm……..122

Figure 6-19. (a) Substrate, patch, edge-fed, quarter wavelength and waveport (b) dimensions, (c) ground metal plate and dimensions of waveport for a 2.4 GHz microstrip patch antenna in microwave (GHz) range……...123

Figure 6-20. Reflectance result for a 2.4 GHz microstrip patch antenna design in Figure 6-19 in microwave (GHz) range from 1 GHz to 5 GHz (The resonance frequencies at 2.324 GHz, 3.852 GHz and 4.796 GHz)……...124

Figure 6-21. (a) Adding four Rogers RT5880 substrate legs and metamaterial absorber based energy harvester on a 2.4 GHz microstrip patch antenna in microwave (GHz) range (b1) Dimensions, Rogers RT5880 substrate, Copper resonator and four resistors for a metamaterial absorber based energy harvester (b2) Rogers RT5880 (substrate) legs and Copper metal plate, (b3) dimensions of Rogers RT5880 (substrate) legs...125

Figure 6-22. Reflectance and absorption results for the design in Figure 6-21a in microwave (GHz) range from 1 GHz to 5 GHz (The resonance frequencies at 2.312 GHz, 3.860 GHz and 4.760 GHz)….....126

Figure 6-23. Gathered power frequency diagram for four 4700 ohm resistors for the design in Figure 6-21a in microwave (GHz) range from 1 GHz to 5 GHz (The resonance frequency at 2.304 GHz)……..126

Figure 6-24. Adding six layers metamaterial absorber based energy harvester with their legs on a 2.4 GHz microstrip patch antenna in microwave (GHz) range (Each layer have four 4700 ohm resistors)……..127

Figure 6-25. Gathered absorption frequency diagram for selected different quantities of adding layers between 2 – 6 layers for the structure in Figure 6-24.…….128

Figure 6-26. Gathered power frequency diagram for selected different quantities of adding layers between 2 – 6 layers for the structure in Figure 6-24.……..129

Figure 6-27. For the structure (adding 6 – layers metamaterial absorber based energy harvester with their legs on the designed 2.4 GHz microstrip patch antenna in microwave (GHz) range) in Figure 6-24 (a) Electric field distribution (b) Magnetic field distribution (c) Surface current distribution at the resonance frequency of 2.304 GHz at 4700 ohm.……..130

Figure 6-28. For the structure (adding 6 – layers metamaterial absorber based energy harvester with their legs on the designed 2.4 GHz microstrip patch antenna in microwave (GHz) range) in Figure 6-24 (a) typical radiation pattern (b1) and (b2) view of three – dimensional far – field pattern from two different sides at the resonance frequency of 2.304 GHz at 4700 ohm….....131

Figure 6-29. (a) Adding metamaterial absorber based energy harvester on a 2.4 GHz microstrip patch antenna in microwave (GHz) range (b1) Dimensions, Rogers RT5880 substrate, Copper resonator and four resistors for a metamaterial absorber based energy harvester (b2) Copper metal plate for a metamaterial absorber based energy harvester.....132

Figure 6-30. Reflectance and absorption results for the design in Figure 6-29a in microwave (GHz) range from 1 GHz to 5 GHz (The resonance frequencies at 2.336 GHz, 3.820 GHz and 4.584 GHz).…….133

Figure 6-31. Gathered power frequency diagram for four 4700 ohm resistors for the design in Figure 6-29a in microwave (GHz) range from 1 GHz to 5 GHz (The resonance frequency at 2.240 GHz).…….....133

Figure 6-32. Adding thirty layers metamaterial absorber based energy harvesters without their Copper metal plates (excluded for the first layer) on a 2.4 GHz microstrip patch antenna in microwave (GHz) range (Each layer have four 4700 ohm resistors)…….....134

Figure 6-33. Gathered absorption frequency diagram for selected different quantities of adding layers between 2 – 30 layers for the structure in Figure 6-32……..135

Figure 6-34. Gathered power frequency diagram for selected different quantities of adding layers between 2 – 30 layers for the structure in Figure 6-32……..136

Figure 6-35. For the structure (adding 30 – layers metamaterial absorber based energy harvester without their Copper metal plate (excluded for the first layer) on the designed 2.4 GHz microstrip patch antenna in microwave (GHz) range) in Figure 6-32 (a) Electric field distribution (b) Magnetic field distribution (c) Surface current distribution at the resonance frequency of 2.284 GHz at 4700 ohm……..137

Figure 6-36. For the structure (adding 30 – layers metamaterial absorber based energy harvester without their Copper metal plate (excluded for the first layer) on the designed 2.4 GHz microstrip patch antenna in microwave (GHz) range) in Figure 6-32 (a) typical radiation pattern (b1) and (b2) view of three – dimensional far – field pattern from two different sides at the resonance frequency of 2.284 GHz at 4700 ohm.…138

LIST OF TABLES

Table 1-1. Materials` properties and their availabilities according to their EM properties.....4

Table 1-2. Brief comparison for three simulation techniques……6

Table 1-3. Summarized literature review……...8

Table 3-1. Output power, power efficiency and resonance frequency values according to different substrate and metal materials.……...59

Table 3-2. Output power, power efficiency and resonance frequency values according to different substrate and metal materials.……...65

Table 4-1. Absorption and resonance frequency values (which are received from the results in Figure 4-4)……72

Table 4-2. Output power, power efficiency and resonance frequency values (which are received from the results in Figure 4-4)……...72

Table 4-3. Absorption and resonance frequency values (which are received from the results in Figure 4-10)……79

Table 4-4. Output power, power efficiency and resonance frequency values (which are received from the results in Figure 4-10).……79

Table 4-5. Absorption and resonance frequency values (which are received from the results in Figure 4-16)……..87

Table 4-6. Output power, power efficiency and resonance frequency values (which are received from the results in Figure 4-16)……87

Table 5-1. Output power, power efficiency and resonance frequency values according to four different substrate materials in hole and without any substrate materials in hole for at first, second and third resonances due to comparison.……..99

Table 5-2. Absorption and resonance frequency values (which are received from the results in Figure 5-13) according to adding three different Graphene thicknesses for

the structure in Figure 5-12 for at first, second and third resonances due to comparison.……...101

Table 5-3. Output power, power efficiency and resonance frequency values (which are received from the results in Figure 5-14) according to adding three different Graphene thicknesses for the structure in Figure 5-12 for at first, second and third resonances due to comparison.……101

Table 5-4. Absorption and resonance frequency values (which are received from the results in Figure 5-15) according to both cases with and without hole & hole substrate & Graphene for the structures in Figure 5-1 and Figure 5-12 at first, second and third resonances due to comparison.…….....103

Table 5-5. Output power, power efficiency and resonance frequency values (which are received from the results in Figure 5-16) according to both cases with and without hole & hole substrate & Graphene for the structures in Figure 5-1 and Figure 5-12 at first, second and third resonances due to comparison.…….....104

NOMENCLATURE

MTM	Metamaterial
MA	Metamaterial Absorber
EH	Energy Harvester
EM	Electromagnetic
EMR	Electromagnetic Radiation
MHz	Megahertz
GHz	Gigahertz
THz	Terahertz
mm	millimeter
μm	micrometer
nm	nanometer
λ	Wavelength of electromagnetic radiation
IR	Infrared
$\vec{D}$	Electric flux density ($C.m^{-2}$)
$\vec{B}$	Magnetic flux density (T)
E	Electric field ($V.m^{-1}$)
H	Magnetic field ($A.m^{-1}$)
ω	Angular frequency (Hz)
C	Speed of light ($m.s^{-1}$)
k	Extinction coefficient
ε	Electric permittivity
μ	Magnetic permeability
Z_0	Impedance of free space
ε_0	Permittivity of free space (8.85×10^{-12} F/m)
$Z(\omega)$	Frequency dependent impedance
e	Charge of electron ($1.60217657 \times 10^{-19}$ C)
TE	Transverse Electric
TM	Transverse Magnetic

FIT	Finite Integration Technique
FBW	Frequency Bandwidth
δ	Skin depth
$R(\omega)$	Frequency dependent reflection coefficient
$T(\omega)$	Frequency dependent transmission coefficient
$A(\omega)$	Frequency dependent absorption coefficient
V	Voltage
P_{in}	Input power (0.5 W)
P_{out}	Output power (< 0.5 W)
R	Resistance
ITO	Indium Tin Oxide
σ	Electric conductivity ($S.m^{-1}$)
$tan\delta$	Electrical loss tangent
σ_g	Conductivity of Graphene
$f_d(\varepsilon)$	Fermi-Dirac distribution
$\hbar$	Planck`s constant ($6.62606957 \times 10^{-34}$ $m^2 kg\ s^{-1}$)
Al	Aluminum
Ag	Silver
Au	Gold
Cu	Copper
GaAs	Gallium Arsenide
Si	Silicon
SiO_2	Silica (Silicon Dioxide)
a-Si	Amorphous Silicon
ZnO	Zinc Oxide
SRR	Split Ring Resonator

CHAPTER 1

INTRODUCTION

The rising world population, growing industry and advancing technology are reasons of the increasing energy demand. Petroleum, coal, crude oil, etc. as energy resources, which are called as fossil fuel, are commonly utilized in order to supply 80% of the energy demand of the world. They will be eventually depleted due to non – renewable. According to Li et al. [1], the remaining oil, natural gas and coal will last in around next 40, 60 and 200 years, respectively. The electricity prices are dramatically increasing in order to supply energy need with available fossil fuels. By burning them in power plants and cars, releasing green – house gases cause global warming. On the other hand, renewable energy resources (solar energy, wind, hydropower, tidal, geothermal, etc.) can be safely utilized due to environmental friendly. Although low usage of them, they are richly available in nature and they will not vanish. Solar energy, which appears one of the best substitute to the utilization of fossil fuels, is between renewable energy resources. Annual power consumption of the world can be met by the delivering power in one hour from the sun radiation [2], but adequately harvest method is not exist. In visible regime, solar cells can incompletely convert solar radiation into electricity [3, 4] due to optical and recombination losses. Microwave (between 0.3 GHz (λ=1000 mm) and 300 GHz (λ=1mm)), sub – THz (between 0.3 THz (λ=1000 μm) and 3 THz (λ=100 μm)), infrared (IR) (between 3 THz (λ=100000 nm) and 430 THz (λ=700 nm)) and visible (light) (between 430 THz (λ=700 nm) and 790 THz (λ=400 nm)) are regions in electromagnetic radiation (EMR) spectrum. Metamaterials can be utilized to solve this inefficiency [5].

1.1. Maxwell`s equations

Maxwell`s equations in an isotropic medium are studied to understand the interaction between light radiation and matter. Their differential forms are given in the following equations (1.1 – 1.4):

$$\nabla . \vec{D} = 0 \qquad \text{Gauss`s law for electricity} \qquad (1.1)$$

Meaning of equation 1.1: Electric field is created by electric loads.

$$\nabla . \vec{B} = 0 \qquad \text{Gauss`s law for magnetism} \qquad (1.2)$$

Meaning of equation 1.2: Magnetic load is not the source of magnetic field.

$$\nabla \times \vec{E} = -\frac{\partial \vec{B}}{\partial t} \qquad \text{Faraday`s law of induction} \qquad (1.3)$$

Meaning of equation 1.3: Changeable magnetic field generates electric field.

$$\nabla \times \vec{H} = \frac{\partial \vec{D}}{\partial t} \qquad \text{Ampère`s law (as extended by Maxwell)} \qquad (1.4)$$

Meaning of equation 1.4: Loads and changeable electric fields` generate magnetic field.

In given four equations above, the electric flux density, the magnetic flux density, electric field and magnetic field are symbolized by *D*, *B*, *E*, and *H*, respectively. In the following equations (1.5 and 1.6), *D* and *B* are presented in homogeneous isotropic medium.

$$\vec{D} = \varepsilon \vec{E} \qquad (1.5)$$

$$\vec{B} = \mu \vec{H} \qquad (1.6)$$

According to equations (1.5 and 1.6), rewritten Maxwell`s equations in isotropic medium can be seen by the following equations (1.7 – 1.10):

$$\nabla . \varepsilon \vec{E} = 0 \qquad (1.7)$$

$$\nabla . \mu \vec{H} = 0 \qquad (1.8)$$

$$\nabla \times \vec{E} = -\mu \frac{\partial \vec{H}}{\partial t} \qquad (1.9)$$

$$\nabla \times \vec{H} = \varepsilon \frac{\partial \vec{E}}{\partial t} \qquad (1.10)$$

In the following equations (1.11 and 1.12), *E* and *H* are presented. $\vec{z}$ is the direction of propagation.

$$\vec{E}(\omega, \vec{k}) = \vec{E}_0 e^{i(\vec{k}\vec{Z} - \omega t)} \qquad (1.11)$$

$$\vec{B} = \vec{B}_0 e^{i(\vec{k}\,\vec{Z} - \omega t)} \qquad (1.12)$$

According to equations (1.11 and 1.12), re-arranged Maxwell`s equations are shown in the following equations (1.13 and 1.14):

$$\vec{k} \times \vec{E} = -\frac{\omega}{c}\mu H \tag{1.13}$$

$$\vec{k} \times \vec{H} = \frac{\omega}{c}\varepsilon \vec{E} \tag{1.14}$$

where speed of light in free space, angular frequency of electromagnetic wave and wave vector are symbolized by c , ω, and $\vec{k}$, respectively.

Relation between light and matter interactions can be explain based on Maxwell equations. Behaviour of metamaterials is presented by Maxwell equations.

1.2. Metamaterials

The features of metamaterials (MTMs) with unusual electromagnetic (EM) properties, which are negative permittivity (ε (ω)) and negative permeability (μ (ω)) [6], can not be simultaneously found in nature [7] as a conventional material because of artificial. Refractive index (or index of refraction) ($\tilde{n}$) is utilized in order to see optical response of a material. Negative refractive index [7 – 12] occurs when both ε (ω) and μ (ω) are negative. The permittivity, the permeability and refractive index in complex function can be seen by the following equations (1.15 – 1.17):

$$\varepsilon(\omega) = \varepsilon'(\omega) + i\varepsilon''(\omega) \tag{1.15}$$

$$\mu(\omega) = \mu'(\omega) + i\mu''(\omega) \tag{1.16}$$

$$\tilde{n} = n + ik \tag{1.17}$$

where the real part and the imaginary part of the index are symbolized by n and k, respectively.

Table 1-1. Materials` properties and their availabilities according to their EM properties

	Materials` properties according to their EM properties		
Availability in nature	Permittivity (ε)	Permeability (μ)	
Plasmas, Metals at optical frequency region	ε<0	μ>0	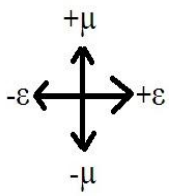
Isotropic dielectrics	ε>0	μ>0	
Magnetic materials	ε>0	μ<0	
Artificially	ε<0	μ<0	

Materials` properties and their existence in nature can be seen in Table 1-1 according to their EM properties.

The initial experimental metamaterial study was realized in 2000s [13, 14]. MTM topics in EM science and technology have been attracted the interest of the MTM researchers in recent years. Exotic application areas of MTMs can be categorized super lenses [13, 15 - 18], antennas [19], sensing [20], sensors [21 - 26], EM cloaking [17, 18, 22, 27 - 31], EM filters [32], absorbers [3, 18, 33 - 43], and so on. Furthermore, EM energy harvesting was paid attention as a new application area.

1.3. Metamaterial absorber

The geometry and size of metamaterial absorber (MA) are attentively set with proper materials according to their working frequency regimes, so impedance matching can be realized at the resonance frequency. Perfect absorption is the result of impedance matching [44]. The impedance of free space (Z_0) matches with the impedance of the MA ($Z(\omega)$). The impedance of free space and the MA are shown in the following equations (1.18 – 1.19):

$$Z_0 = \sqrt{\frac{\mu_0}{\varepsilon_0}} = 120\pi\Omega = 377\Omega \tag{1.18}$$

$$Z\ (\omega) = \sqrt{\frac{\mu\ (\omega)}{\varepsilon\ (\omega)}} \tag{1.19}$$

where electric permittivity of free space, magnetic permeability of free space, electric permittivity of MA and magnetic permeability of MA are symbolized by ε_0, μ_0, ε (ω) and μ (ω), respectively.

By commercial full-wave EM solver, which is based on Finite Integration Technique (FIT), results can be achieved. This technique, which is a simulation method by Weiland [45], uses the integral form of Maxwell`s equations. Time domain or frequency domain can be utilized. Structure is divided to the small parts, which are called mesh, by the simulator. Tetrahedral mesh or hexahedral mesh can be utilized.

Reliability of results is based on the number of mesh cells and sufficient number of mesh cells are obtained by using adaptive mesh refreshment. Adaptive mesh refreshment automatically enhances number of produced mesh cells during the simulation processes until the variation of the results remain stable. Therefore, the reliability of the results are obtained.

In this thesis, hexahedral mesh type were used in time domain solver because of analyzing energy harvesters. Accuracy and reliability of results are based on value of dividing maximum mesh step to minimum mesh step and mesh line ratio limit. Mesh line ratio limit is constant and equal to 10. Value, which is obtained after division, has to be lesser than mesh line ratio limit.

Finite Element Method (FEM), Finite Difference Time Domain Method (FDTD), and Finite Integration Technique (FIT) are solver methods, so their brief comparison is summarized in Table 1-2.

Table 1-2. Brief comparison for three simulation techniques

FEM	FDTD	FIT
Solve differential form of Maxwell equations	Solve differential form of Maxwell equations	Solve integral form of Maxwell equations
Divide space to smaller parts	Not iterative	Solve complex designs
Easy designing structure	Necessity: Very long time	Lesser memory and mesh
Necessity: High computer property		

The calculation of the frequency-dependent absorption is realized by the following equation (1.20):

$$A(\omega) = 1 - R(\omega) - T(\omega) \tag{1.20}$$

where absorption, reflection and transmission are symbolized by $A(\omega)$, $R(\omega)$ and $T(\omega)$, respectively. By the scattering parameters (S), which is obtained from the output of the simulation software, the equation (1.20) can be shown like in the equation (1.21).

$$A(\omega) = 1 - |S_{11}|^2 - |S_{21}|^2 \tag{1.21}$$

The maximization of the absorption is only realized by the minimization of the reflection and transmission [46, 47]. By using metallic layer (as metal plate) at the bottom of the structure, approximately zero transmission ($T(\omega) \approx 0$) is obtained. Therefore, transmission can be ignored. In this way, the absorption will directly rely on the reflection. The equation (1.21) reduces to equation (1.22).

$$A(\omega) = 1 - |S_{11}|^2 \tag{1.22}$$

The reflection is minimized by the usage of metallic layer (as resonator) at the top of the structure. Therefore, near perfect absorption can be achieved. In other words, all the incident EM wave is absorbed by MA [48 - 50]. As note, both bottom metal (as

metal plate) and top metal (as resonator) have to be same material in designs. The lateral direction of a designed structure has to be less than the wavelength of incident wave [51]. The first recommendation and experimental verification of a near perfect metamaterial absorber have been done by Landy *et al* [39].

1.4. Metamaterial absorber based energy harvester

EM energy harvesting was ascertained as a new application area as it is mentioned above. By EM waves, motivation of resonators is succeeded due to the production of EM energy by those waves is absorbed by the MTM structures. By lumped network elements, which are resistors or varicaps, this EM energy can be harvested. A gap on the resonator is created according to the electric field direction in order to use this EM energy as a voltage source. This EM energy is harvested by a placed lumped network element on the gap. With the both sides of the metamaterial absorber (MA) structures, strong combination of the electric field and inducement of free electric response are realized when activation of the surface charges with the electric field and creation a magnetic response and resonance absorption. By a resistor in this proposed mechanism, which is not the same with the conventional MAs, the incident energy within the gap of the resonator is harvested at the resonance frequency. By a resistor, which means a load, an effect on the amplitude of the harvested energy is realized. The selection of the resistance value is done according to the numerical results. EM MTM energy harvesting topic has an increasing importance because of limited energy resources [52] although it is a fresh topic. General creation of power harvesting devices are depended on for converting one type of energy to another which generally turns into DC [53, 54]. Existence of EM energy harvesting studies with MTMs in the literature is few [52, 55 - 58] even though flexible design opportunities are provided and can be adapted to various energy harvesting studies by EM MTMs. By Ramahi et al. [55], a 611 mV voltage is firstly generated at 5.8 GHz by using EM MTMs. By Hawkes et al. [56], 36.8% power efficiency is experimentally succeeded at 900 MHz by using a split ring resonator (SRR) and a resistor. By Almoneef and Ramahi [57], 3-D MTM stacked arrays are created in order to increase conversion efficiency. By Gunduz and Sabah [58], conversion of 0.25 W output power, which is 50% of the input power, is realized to obtain real power by the resistive load at 5.88 GHz. By Bakir et al. [52], 83.6% of the input power, which is 0.418 W (output power), is numerically

harvested at 2.40 GHz. In Table 1-3, literature review can be summarized by giving power efficiencies.

Table 1-3. Summarized literature review

Reference study	Title	Power efficiency results
Ramahi et al. (2012)	Metamaterial particles for electromagnetic energy harvesting	76% (numerically) (array)
Hawkes et al. (2013)	A microwave metamaterial with integrated power harvesting functionality	65% (numerically) (array) 36.8% (experimentally) (array)
Almoneef and Ramahi (2014)	A 3-dimensional stacked metamaterial arrays for electromagnetic energy harvesting	48% (numerically) (unit cell) 68% (numerically) (array)
Gunduz and Sabah (2015)	Polarization angle independent perfect multiband metamaterial absorber and energy harvesting application	50% (numerically) Input power:0.5 Watt Output power:0.25 Watt
Bakir, Karaaslan, Dincer, Delihacioglu, and Sabah (2015)	Perfect metamaterial absorber-based energy harvesting and sensor applications in the industrial, scientific, and medical band	83.6% efficiency (numerically&experimentally) Input power:1 Watt Output power:0.836 Watt

In this thesis, differences are exist according to the other MTM energy harvesting studies in literature. Due to simple geometry of proposed structures, productions of proposed structures can be easily achieved. Furthermore, both MA and adaptation of

MA to MA based energy harvester (EH) with different materials is the basis of this thesis. The physics of the energy harvesting mechanism can be briefly explained by the basic equations in the following equations (1.23 – 1.25).

$$V = E \times d \tag{1.23}$$

$$P = \frac{V^2}{2 \times R} \tag{1.24}$$

$$Power\ efficiency\ (\%) = \frac{P_{out}}{P_{in}} \times 100 \tag{1.25}$$

where the voltage, the electric field, the length of the gap, the power, the resistance value of lumped network element (resistor), the input power and the output power are symbolized by V, E, d, P, R, P_{in} and P_{out}, respectively. Briefly, the electric field means the voltage according to equation (1.23). The same voltage means the power according to equation (1.24). Therefore, the relation between E and P is based on V. Power efficiency of the resistor can be calculated by equation (1.25). P_{out} has to be lower than P_{in}.

1.5. Numerical Validation of a previous study in literature

The accuracy of FIT based numerical simulator is tested by recreating and reanalysing a previous study in literature. Study of Almoneef and Ramahi [57] was selected in order to numerically validate the accuracy of solver. In Figure 1-1b, power efficiencies with their loads (with load means a resistor is available across the gap) can be seen according to different resistances between 0 kΩ and 20 kΩ. By Almoneef and Ramahi, maximum power efficiency is obtained when resistance is 3.5 kΩ as shown in Figure 1-1b. Simulation setup, which obtained by Almoneef and Ramahi, can be seen in Figure 1-1c. In Figure 1-1c, a single SRR is placed in a waveguide with near perfect electric and magnetic boundaries at y-z and x-z planes, respectively. This SRR is obtained by adding copper metal ring at the top of Rogers RO 4003 substrate. The thickness, loss tangent, relative permittivity and relative permeability of the Rogers RO 4003 substrate material are 0.813 mm, 0.0027, 3.55 and 1, respectively. Also, electrical conductivity of the copper is 5.8001×10^7 S/m. Thickness of copper is 0.035 mm. In Figure 1-1a, the parametric dimensions of design L, W, and g are given as 5.3,

0.5, and 0.5 mm, respectively. the length and width of square substrate is same and equal to 8.8 mm. Dimensions of SRR are set to resonate at around 5.8 GHz by Almoneef and Ramahi [57]. In Figure 1-1d, absorption with load is enhanced of 4.5 times according to without load (without load means a resistor is unavailable across the gap). For not only obtained by Almoneef and Ramahi [57] but also obtained by recreated and reanalysed structure, absorption results and power efficiency can be seen in Figure 1-2 and in Figure 1-3, respectively. According to these two figures, numerical simulator gives accurate results in this thesis.

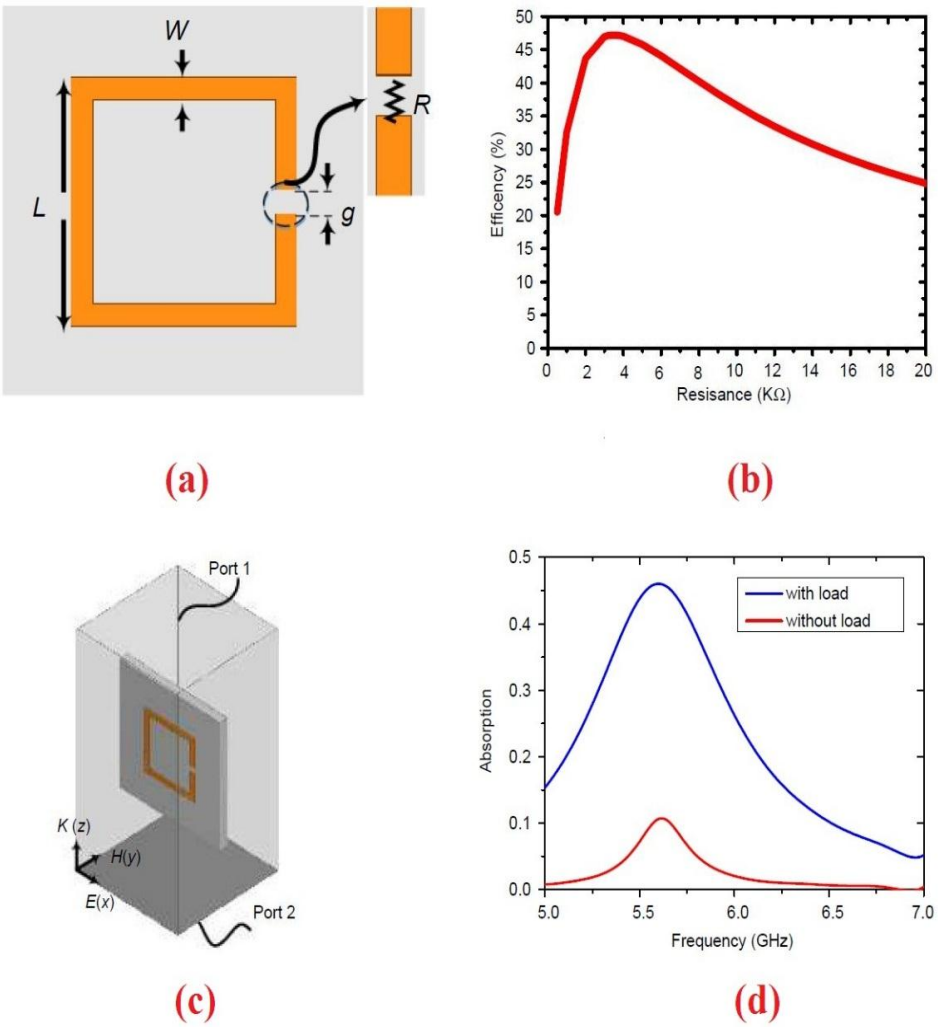

Figure 1-1. ((a) The geometric design with dimensions, (b) gathered power efficiency – resistance diagram with load, (c) simulation setup, and (d) absorption results with and without load) obtained by Almoneef and Ramahi [57].

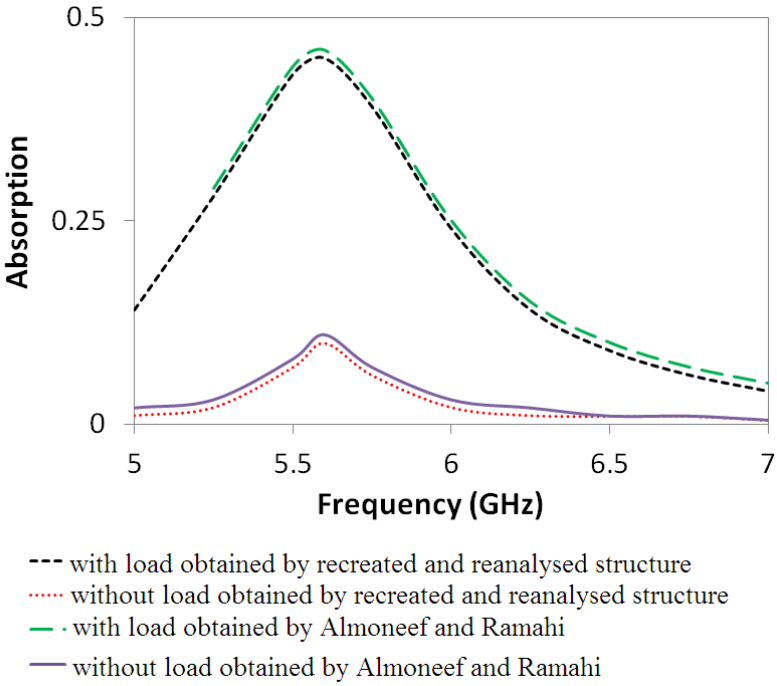

Figure 1-2. Absorption results for not only obtained by Almoneef and Ramahi [57] but also obtained by recreated and reanalysed structure.

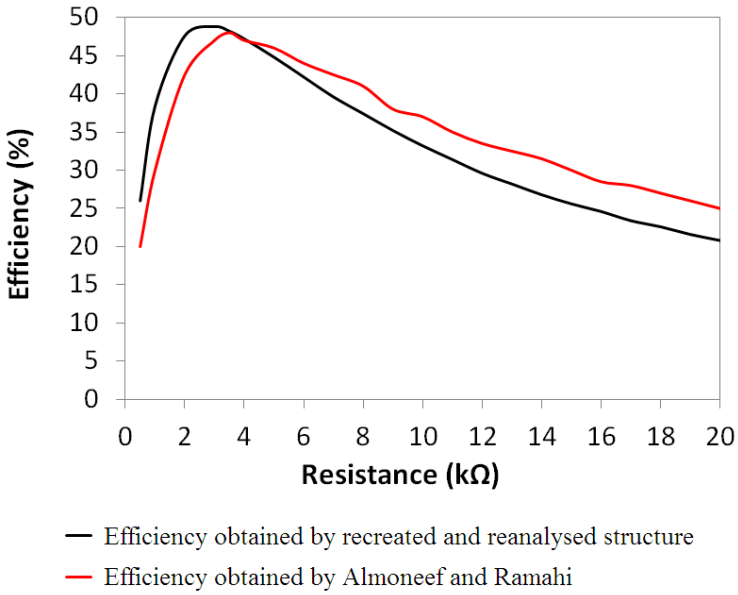

Figure 1-3. Efficiency not for only obtained by Almoneef and Ramahi [57] but also obtained by recreated and reanalysed structure.

CHAPTER 2

HIGH FREQUENCY METAMATERIAL ABSORBER BASED ON PATCH RESONATOR AND ITS APPLICATIONS FOR ENERGY HARVESTING

2.1. Introduction

The definition of metamaterials, and the related information's that can be used for analyzing and characterizing metamaterial absorbers are given in the first chapter. In addition to these, the related theories for near perfect absorptions, methods for calculating power efficiency are presented. Moreover, a design is also validated in the first chapter. In this chapter, one design is analysed in Section 2.2, the same design is enhanced with graphene in Section 2.3. After the conversion of the same design to two metamaterial absorber based energy harvesters with some modifications, two new designs are created and they analysed again in Section 2.4.

By commercial full-wave EM solver, which is based on Finite Integration Technique (FIT), all results were achieved. Numerical options are selected according to working frequency region in electromagnetic spectrum. Geometrically simple structures were designed and analyzed in order to easily fabricate them.

2.2. Dual-Band Near Perfect Metamaterial Absorber

2.2.1. Design and Simulation

The shape of a high frequency metamaterial absorber based on patch resonator in the infrared and visible regime is shown with dimensions in Figure 2-1. The transmission is prevented by the usage of aluminum as a metallic layer at the bottom of the structure. As a dielectric substrate layer, gallium arsenide (GaAs) is used on to the top of the bottom metallic aluminum layer. GaAs has been selected because of its optical absorption characteristics. It has a good absorption response to the visible light. In addition to these it is also insensitive to heat and it can be easily obtained. According to gold (Au) and silver (Ag), aluminum material cheaper. Also, it has lower skin depth. The reflection is minimized by the usage of same aluminum as a patch resonator at the top of the structure (on to the top of the GaAs layer). At first, electrical conductivity of aluminum ($\sigma_{aluminum}$) = 3.56×10^{7}S/m, the electrical loss tangent of GaAs ($\tan\delta_{GaAs}$) = 0.006 and the dielectric constant of GaAs (ε_{GaAs}) = 12.94. For more realistic results,

the materials of the same design are defined and analysed according to Drude model. Movement properties of electrons in materials is called Drude model. The optical properties of aluminum and GaAs for infrared and visible frequency regimes for Drude model can be found in Ref. [59]. Plasma frequency of aluminum and GaAs are 2.38×10^{16} rad/s and 3.67×10^{14} rad/s, respectively. Collision frequency of aluminum and GaAs are 9.43×10^{14} 1/s and 4.26×10^{13} 1/s, respectively.

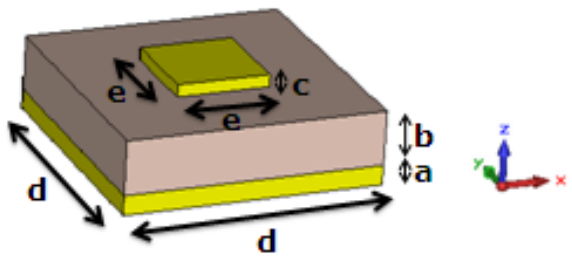

Figure 2-1. The design and dimensions of the unit cell of the metamaterial absorber based on patch resonator.

When perfectly matched boundary is chosen along the z-axis, the boundary conditions along the x- and y-axis are chosen as periodic. Therefore, the symmetry is realized along x- and y-axis, and also, the wave comes perpendicularly onto the z-axis (the direction of the propagation (a waveguide port)) [60 – 62]. Wide frequency range is chosen for simulations in order to realize the efficient usage of solar energy.

The calculation of the frequency-dependent absorption is realized by $A(\omega) = 1 - R(\omega) - T(\omega)$ where $A(\omega)$, $R(\omega)$ and $T(\omega)$ are absorption, reflection and transmission, correspondingly. The maximization of the absorption is only realized by the minimization of the reflection and transmission [46, 47]. By using metallic layer at the bottom of the structure, zero transmission ($T(\omega) = 0$) is obtained. In this way, the absorption will directly rely on the reflection. By the scattering parameters (S), which is obtained from the simulation, reflection ($R(\omega) = |S_{11}(\omega)|^2$) can be calculated.

2.2.2. Result and Discussion

Achievements of all numerical results is based on FIT by commercial full-wave EM solver. When used materials` properties are $\sigma_{aluminum} = 3.56\times10^7$S/m, $\tan\delta_{GaAs} = 0.006$, and $\varepsilon_{GaAs} = 12.94$, maximum absorptions are obtained around 99.99% and 99% at

558.75 THz and 216.75 THz, respectively. The reflectance (S_{11}) and absorption results are shown in Figure 2-2. The thickness of the bottom square metal (aluminum) is a = 40 nm, the thickness of the square substrate (GaAs) is b = 110 nm, the thickness of the top square patch resonator metal (aluminum) is c = 25 nm, the lengths of the bottom square metal and square substrate are same value which is d = 500 nm, and the length of the top square patch resonator metal is e = 179.5 nm. The skin depths are calculated for each resonance frequencies by using the following equation (2.1) in Ref. [59, 63]:

$$\delta = \frac{C}{\omega \tilde{k}(\omega)} \tag{2.1}$$

where δ is the optical skin depth, C is the velocity of light, ω is the frequency of electromagnetic (EM) wave and $\tilde{k}$ is the extinction coefficient. The skin depths are 15.73 nm and 13.04 nm for the first (216.75 THz) and second (558.75 THz) resonance frequencies, respectively. Both skin depths are less than the thickness of the bottom square metal (a = 40 nm). Thus, greater than 99% of the non-transmitted incident wave with minimum reflected wave is absorbed by this metamaterial absorber.

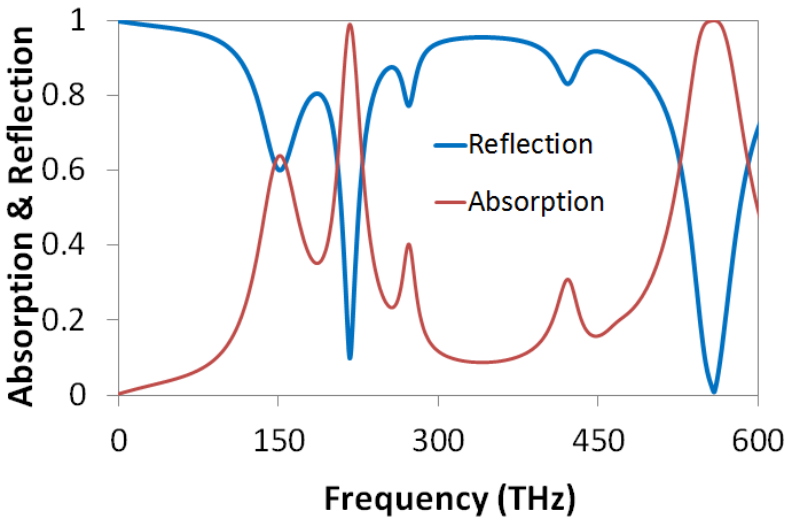

Figure 2-2. The reflectance and absorption results for $\sigma_{aluminum} = 3.56\times10^{7}$S/m, $\tan\delta_{GaAs} = 0.006$, and $\varepsilon_{GaAs} = 12.94$ materials` properties .

When used materials are defined according to Drude model with the same geometric parameters as before, maximum absorptions are obtained around 99.96% and 99.63%

at 514.5THz and 197.25THz, respectively. In Figure 2-3, reflectance and absorption results can be seen. A third resonance is also become around 87.63% at 141THz. Although it has not a perfect percentage, it is acceptable because of above 85%. The skin depths are found as 15.82 nm, 15.71 nm and 13.25 nm for 141THz, 197.25THz and 514.5THz, correspondingly. The thickness of the bottom square metal (a = 40 nm) is greater than these three skin depths. Therefore, the incident wave is absorbed by the structure with no transmission, as it is mentioned before.

The top metallic plate, which is also called as a patch resonator, is removed and simulation is repeated in order to understand physical mechanism of the resonances. Reflectance and absorption results are given in Figure 2-4 for this situation. Two resonances, which are also called as a dual band, are exist according to Figure 2-4. Although they are not near perfect absorption resonances, their resonances` locations are almost the same with the resonances` locations in Figure 2-3. With the usage of the top metallic plate (the patch resonator) in the structure, the enhancements are realized at 197.25THz and 514.5THz resonances in Figure 2-3. With the third resonance at 141THz, a wide band is obtained for both 141THz and 197.25THz resonances [64]. Because of the interaction between the top metal and substrate/bottom metal, these two resonances are expected. Also, as obtained [65, 66] the plasmonic resonances can be created by surface plasmonic polaritons in high frequency regime. Moving electrons are collected at the metals` surface, so this is called as surface plasmons (SPs).

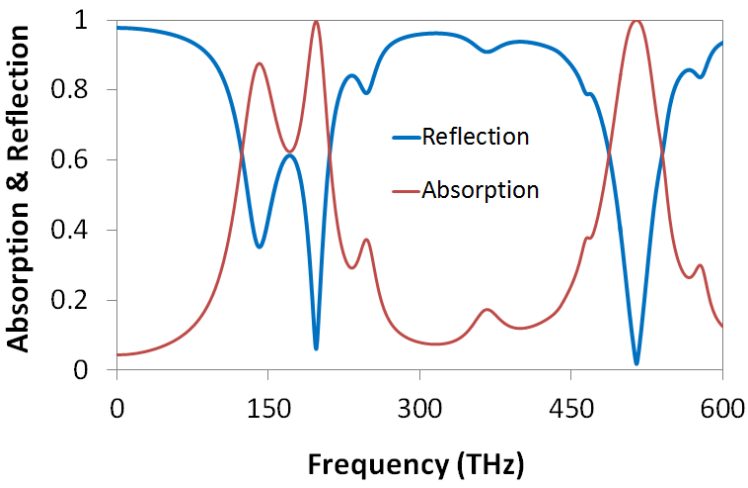

Figure 2-3. Reflectance and absorption results when materials have Drude model properties.

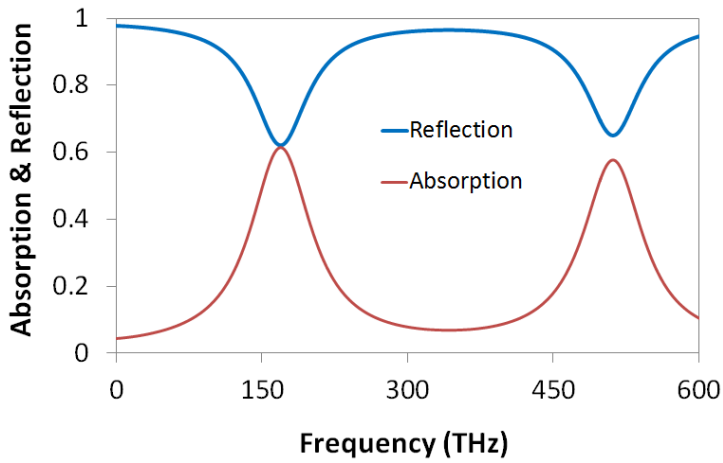

Figure 2-4. Reflectance and absorption results when materials have Drude model properties without (patch resonator) top metallic layer.

The effects of the geometrical parameters ("c", "d", and "e") of the metamaterial structure on the absorption can be seen in from Figure 2-5 to Figure 2-9. Although resonances` frequencies sometimes shift to the lower or higher frequencies, the percentages of the absorptions remain almost same.

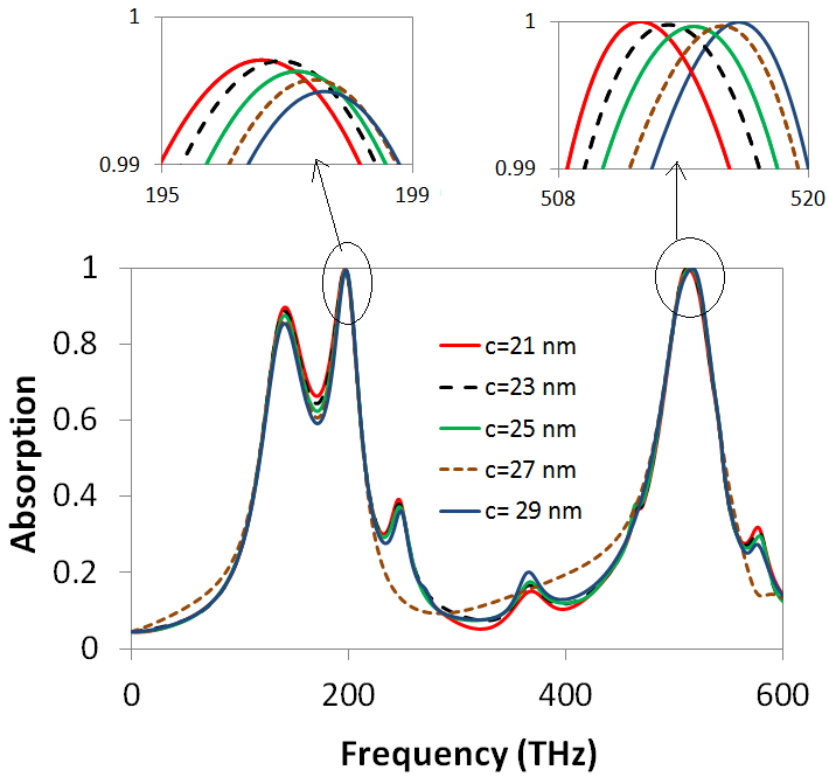

Figure 2-5. Parametric study for the thickness of the top square patch resonator (c).

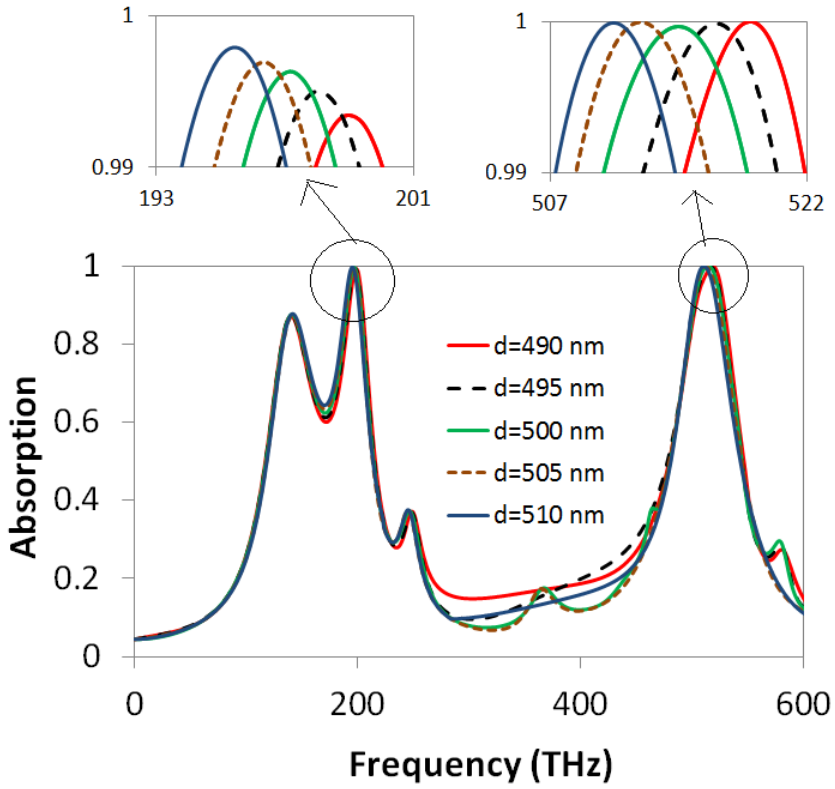

Figure 2-6. Parametric study for the length of the bottom square metal and square substrate (d).

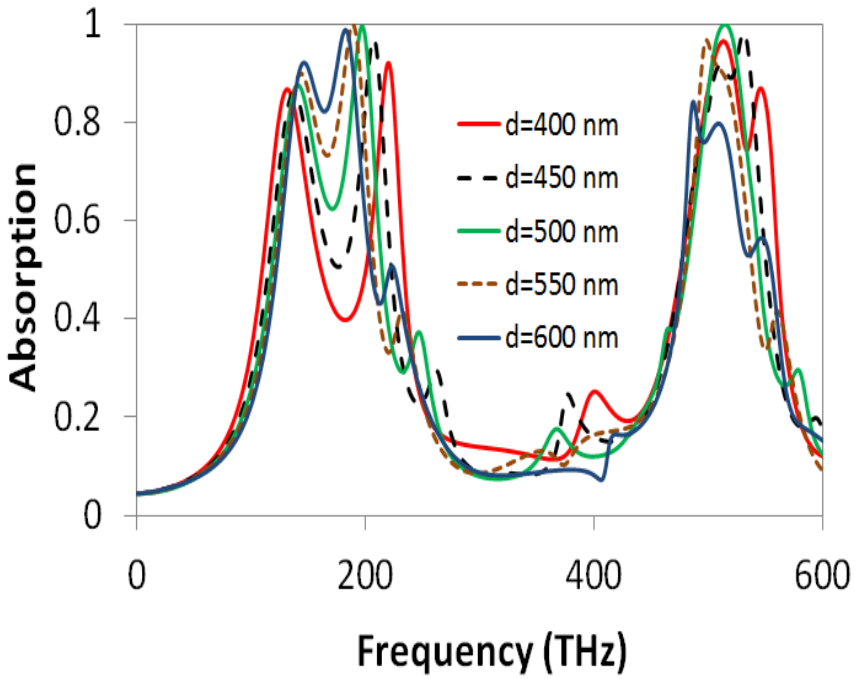

Figure 2-7. Parametric study for the length of the bottom square metal and square substrate (d).

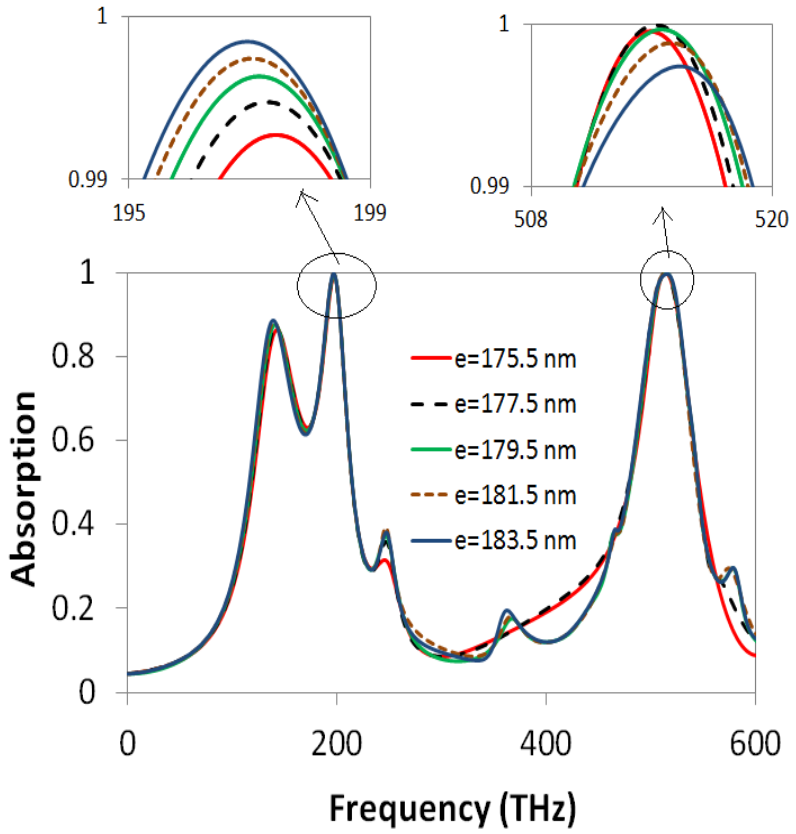

Figure 2-8. Parametric study for the length of the top square patch resonator (e).

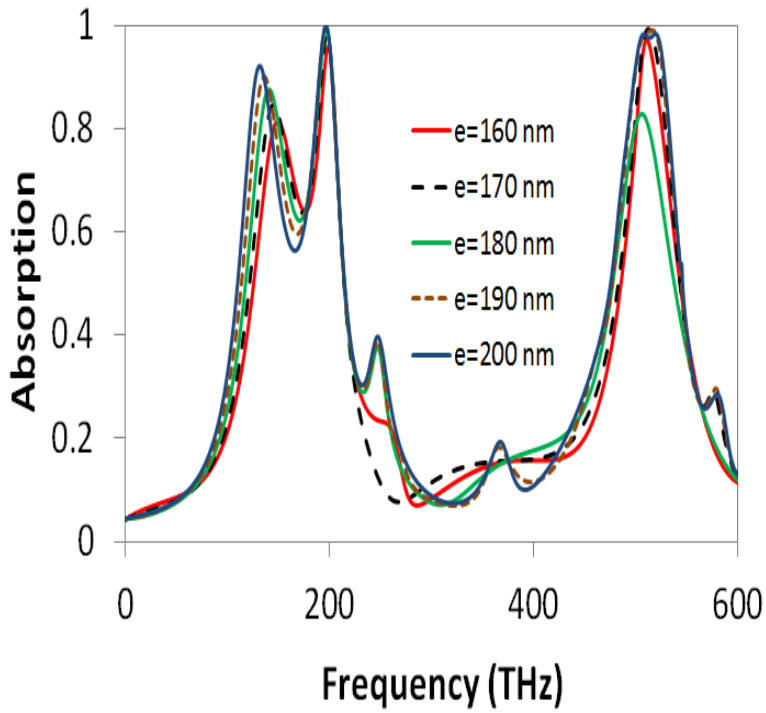

Figure 2-9. Parametric study for the length of the top square patch resonator (e).

Impedance matching is realized when real part (Re (z)) and imaginary part (Im (z)) of normalized impedance are approximately 1 and 0, respectively. In Figure 2-10a, Re (z) and Im (z) can be seen for three resonance frequency. Re (z) and Im (z) of 197.25 THz and 514.5 THz are confirmed near perfect absorption. Re (z) and Im (z) of 141 THz are lower and higher than 1 and 0, respectively. This situation is confirmed that 87.63% absorption is not a near perfect. In addition to this, real part of permeability and permittivity are given in Figure 2-10b. Linear magnitude and phase of S_{11} are given in Figure 2-11. Three resonance frequencies of them are approximately same.

In Figure 2-12, absorption results of the metamaterial absorber for different polarization angles at normal incidence are shown. The polarization angle can be defined as the angle variation on x-y plane (see Figure 2-1) for the incident wave. 90° polarization angle refers to the electric field component of the polarization wave rotating on x-y plane [67]. With 30° steps on x (u) – y (v) plane in Figure 2-12, the polarization angles are increased from 0° to 90°. For all polarization angles, same near perfect absorptions are obtained for the metamaterial absorber based on patch resonator. Therefore, the structure is polarization angle independent can be said.

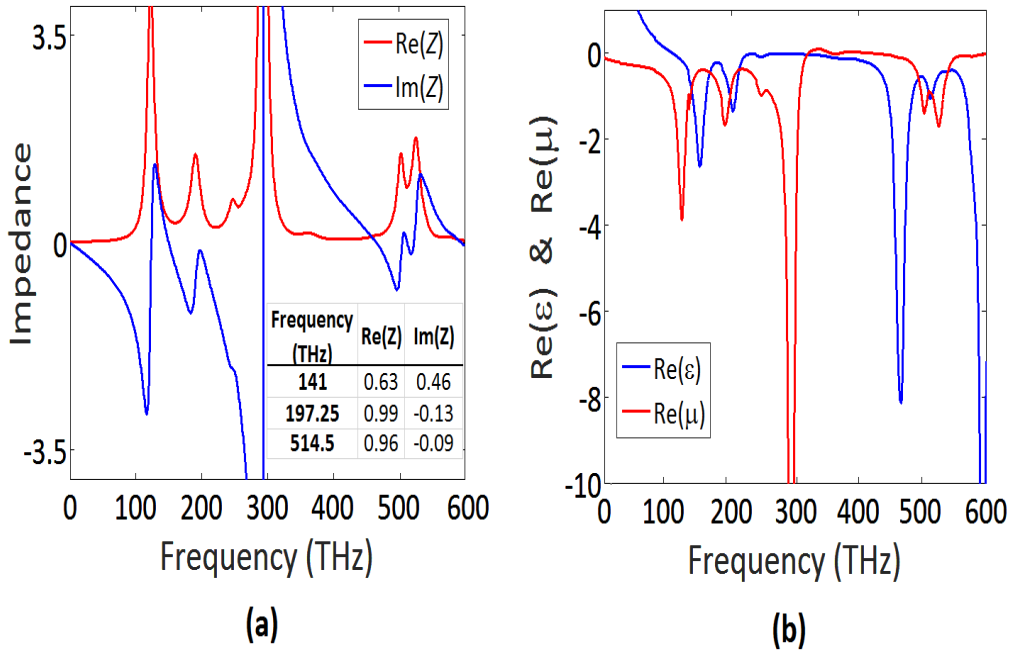

Figure 2-10. (a) Impedance and its real and imaginary part, and (b) real parts of permittivity and permeability.

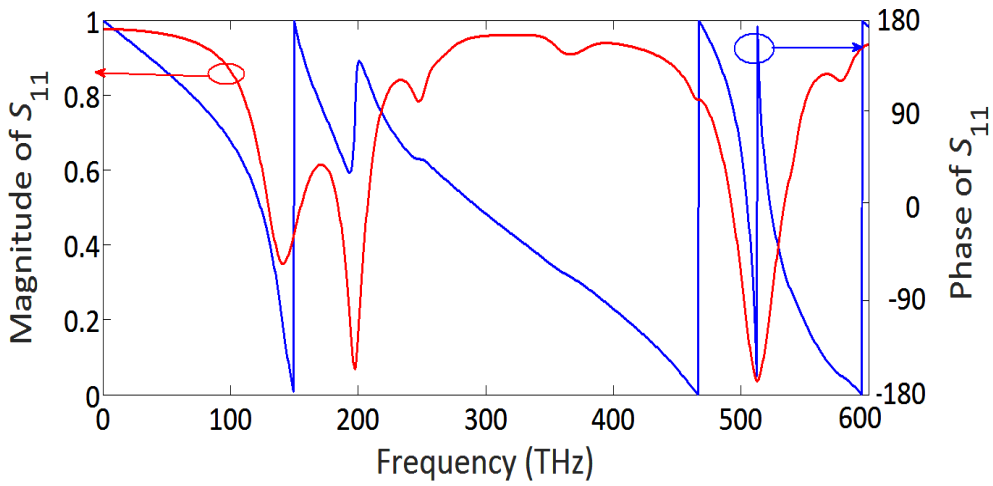

Figure 2-11. Magnitude and phase of S_{11}.

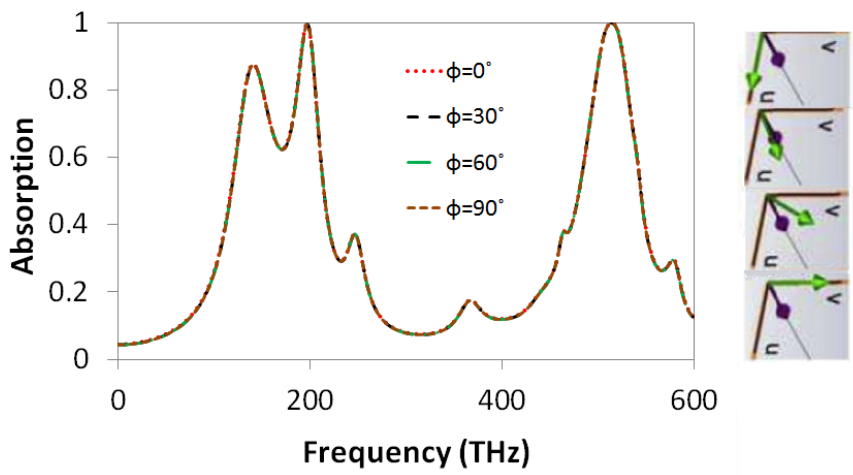

Figure 2-12. Absorption results for different polarization angles (φ) at normal incidence.

All simulations until now in this structure are realized for normal incidence. The transverse electric (TE) (the electric field is perpendicular to the direction of the propagation while the magnetic field is normal to the direction of the propagation) and transverse magnetic (TM) (the magnetic field is perpendicular to the direction of the propagation while the electric field is normal to the direction of the propagation) absorption results for different incident angles (θ) are given in Figure 2-13 and Figure 2-14, respectively. Absorption results remain the same with some slight changes according to absorption result in Figure 2-3, so the structure is incident angle independent can be said [18].

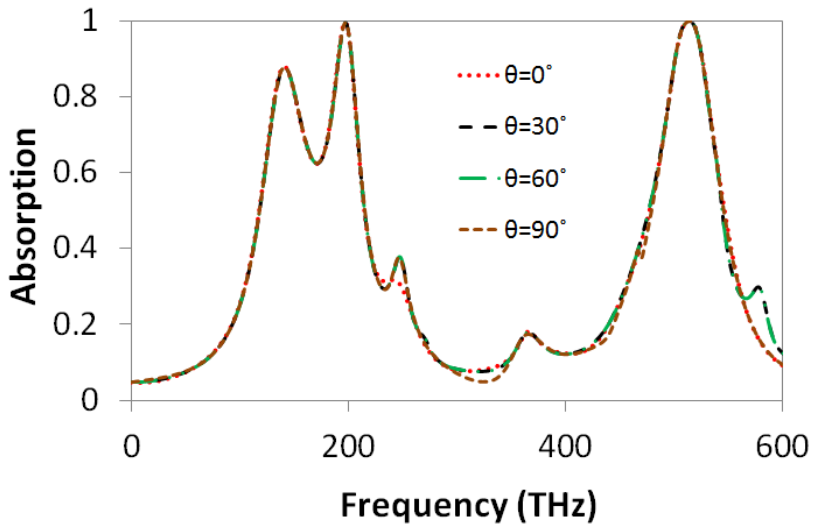

Figure 2-13. Absorption results for transverse electric (TE) mode for different incident angles (θ).

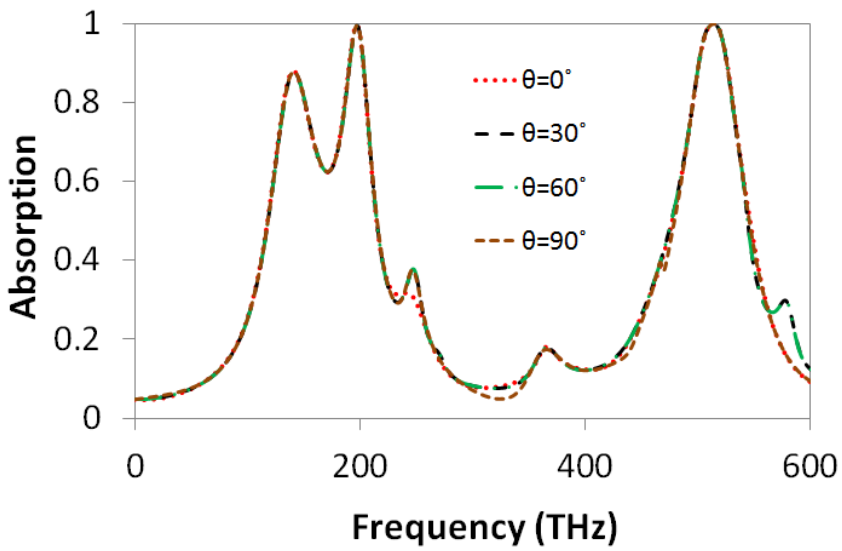

Figure 2-14. Absorption results for transverse magnetic (TM) mode for different incident angles (θ).

In Figure 2-15 (from a to d), electric field and surface current distributions can be seen for 197.25THz and 514.5THz (main resonance frequencies). The operation mechanism of the structure is understood by these distributions. Although the electric field in Figure 2-15a is stronger than in Figure 2-15b, the strong electric fields are taking place on the two sides of the top square metal plate for both electric field distribution figures. Locations of the electric field are responsible for the absorption. Electric field also behave like an electric dipole in these two figures. In Figure 2-15c and Figure 2-15d, the strong parallel surface currents are localizing on the two sides of the structure. In Figure 2-15d, the strong anti-parallel surface currents also take

place in the middle of the structure by circulating surface currents at the four sides of the structure. The parallel surface currents are the reason of the electric resonance. The circulating and anti-parallel surface currents are the reason of the magnetic resonance. At the resonance frequencies, near perfect absorptions are become by matching of the electric and magnetic responses to incident electromagnetic wave.

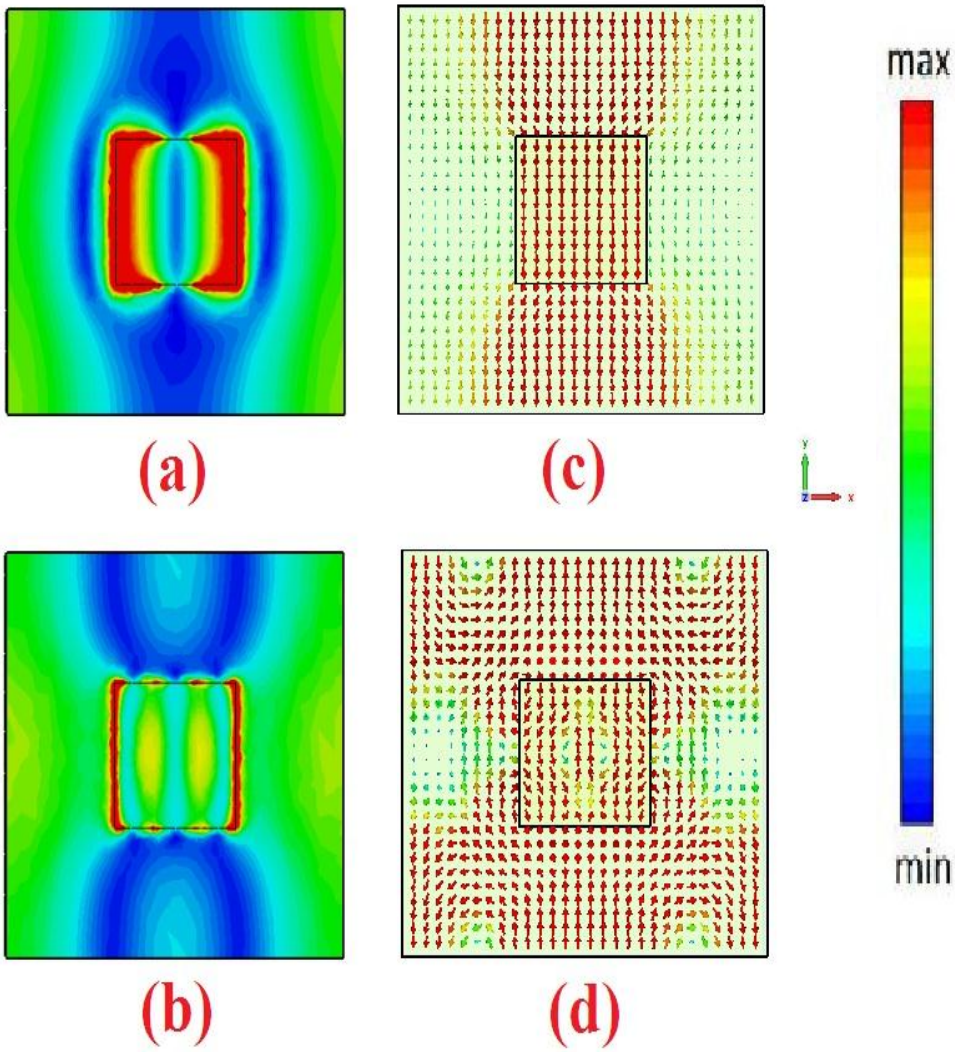

Figure 2-15. (a) Electric field distributions of the metamaterial absorber structure at 197.25THz, (b) Electric field distributions of the metamaterial absorber structure at 514.5THz, (c) Surface current distributions of the metamaterial absorber structure at 197.25THz, and (d) Surface current distributions of the metamaterial absorber structure at 514.5THz.

2.3. Dual-Band Near Perfect Metamaterial Absorber`s Enhancement with Graphene Layers

By integrating graphene (a kind of carbon atoms) layer(s) to the structure, the performance of the metamaterial absorber is enhanced. The first single (mono) – layer graphene has been fabricated in 2004. At high (terahertz) frequency, electrical, optical, and mechanical properties can be seen by graphene material [68]. Graphene motivates surface plasmonic polaritons, so a new reply is become in order to enhance previously obtained results. High conductivity can be obtained by using graphene. High conductivity is one of the main advantage of the graphene based structure [69, 70]. Correspondingly, one can control the EM wave by controlling the conductivity (and relatedly dielectric constant) of the graphene in which it provides additional flexibility in the design and fabrication of various device configurations. For example, the absorption level has been enhanced by the coupling of the MTM and graphene layers [71 - 75]. The conductivity of graphene (σ_g) is calculated by using Kubo formula [70, 76 – 78] as:

$$\sigma_g(\omega, \mu_c, \tau, T) = \sigma_{intra} + \sigma_{inter} \tag{2.2}$$

$$\sigma_g(\omega, \mu_c, \tau, T) = \frac{je^2(\omega - j\tau^{-1})}{\pi\hbar^2} \times \left[\frac{1}{(\omega - j\tau^{-1})^2}\int_0^\infty \frac{\partial f_d(\varepsilon)}{\partial \varepsilon} - \frac{\partial f_d(-\varepsilon)}{\partial \varepsilon}\partial\varepsilon - \int_0^\infty \frac{f_d(-\varepsilon) - f_d(\varepsilon)}{(\omega - j\tau^{-1})^2 - 4(\varepsilon/\hbar)^2}\partial\varepsilon\right] \tag{2.3}$$

where j is the imaginary unit, $f_d(\varepsilon)$ is the Fermi-Dirac distribution, ε is the energy of the incident wave, $\hbar$ is the reduced Planck`s constant, and τ is the scattering time. σ_{intra} and σ_{inter} come from the intra-band and inter-band transitions, correspondingly. The dielectric constant of graphene (ε_g) is calculated by using the following equation (2.4):

$$\varepsilon_g = 1 + j\frac{\sigma_g}{\omega\varepsilon_0\Delta} \tag{2.4}$$

where ε_0 is the permittivity of free space and Δ is the thickness of the graphene layer(s).

In the numerical simulations, the conductivity and the dielectric constant of graphene are controlled. With the effect of the adding graphene layer(s), the absorption result is enhanced. The reason of this situation is the graphene provides additional degree of freedom to match the impedance of the metamaterial absorber structure to the impedance of free space. Therefore, a fascinating possibility is apparent for controlling the electromagnetic wave by tuning the optical and electronic properties of the overall structure.

2.3.1. Design and Simulation

Three kinds of the integration of 3-dimensional graphene into the metamaterial absorber structure is shown Figure 2-16. In Figure 2-16a, graphene layer is under the metal patch resonator while in Figure 2-16b, graphene layer is at the top of the metal patch resonator. In Figure 2-16c, two graphene layers are located not only under the metal patch resonator but also at the top of the metal patch resonator with the same thicknesses at the same time. The standard thickness of a single (mono)-layer graphene is 0.335 nm [79]. Thicknesses of graphene layer(s) should be in the order of 0.335 nm. In Figure 2-16, designs of three structures are set in order to realize numerical simulations according to multiples of 0.335 nm.

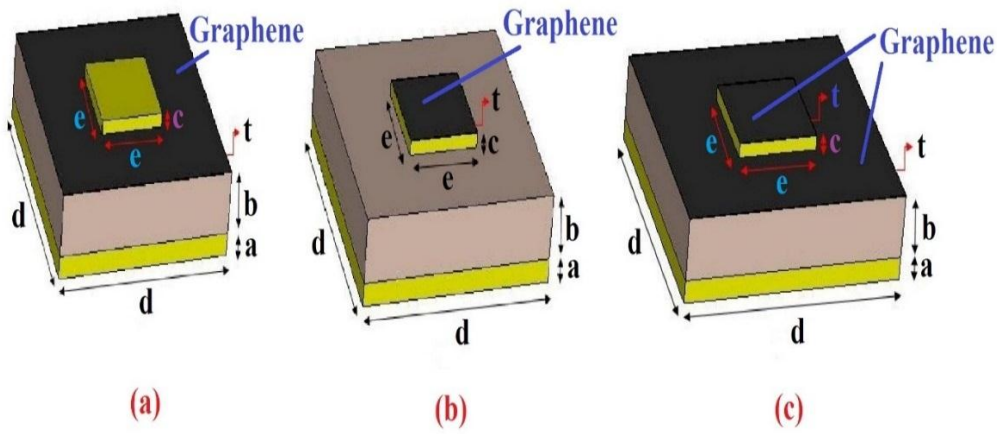

Figure 2-16. The structure and dimensions of the unit cell of the metamaterial absorber based on patch resonator with integrated graphene layer(s) (a) under the metal patch resonator, (b) at the top of the metal patch resonator, (c) not only under the metal patch resonator but also at the top of the metal patch resonator.

2.3.2. Result and Discussion

Achievements of all numerical results is based on FIT by commercial full-wave EM solver. Numerical simulations are realized for three different kind graphene integrations. The thickness of the single graphene layer is t = 0.335 nm. Absorption results are given in Figure 2-17a-c for from single to four graphene layer(s). When t = 0.335 nm (single – layer), absorption results are better than the remaining layers (2 -

4) for all three configurations which are shown in Figure 2-16. Utilization of a single layer graphene at the top and bottom of patch resonator at the same time is more practical in the structure.

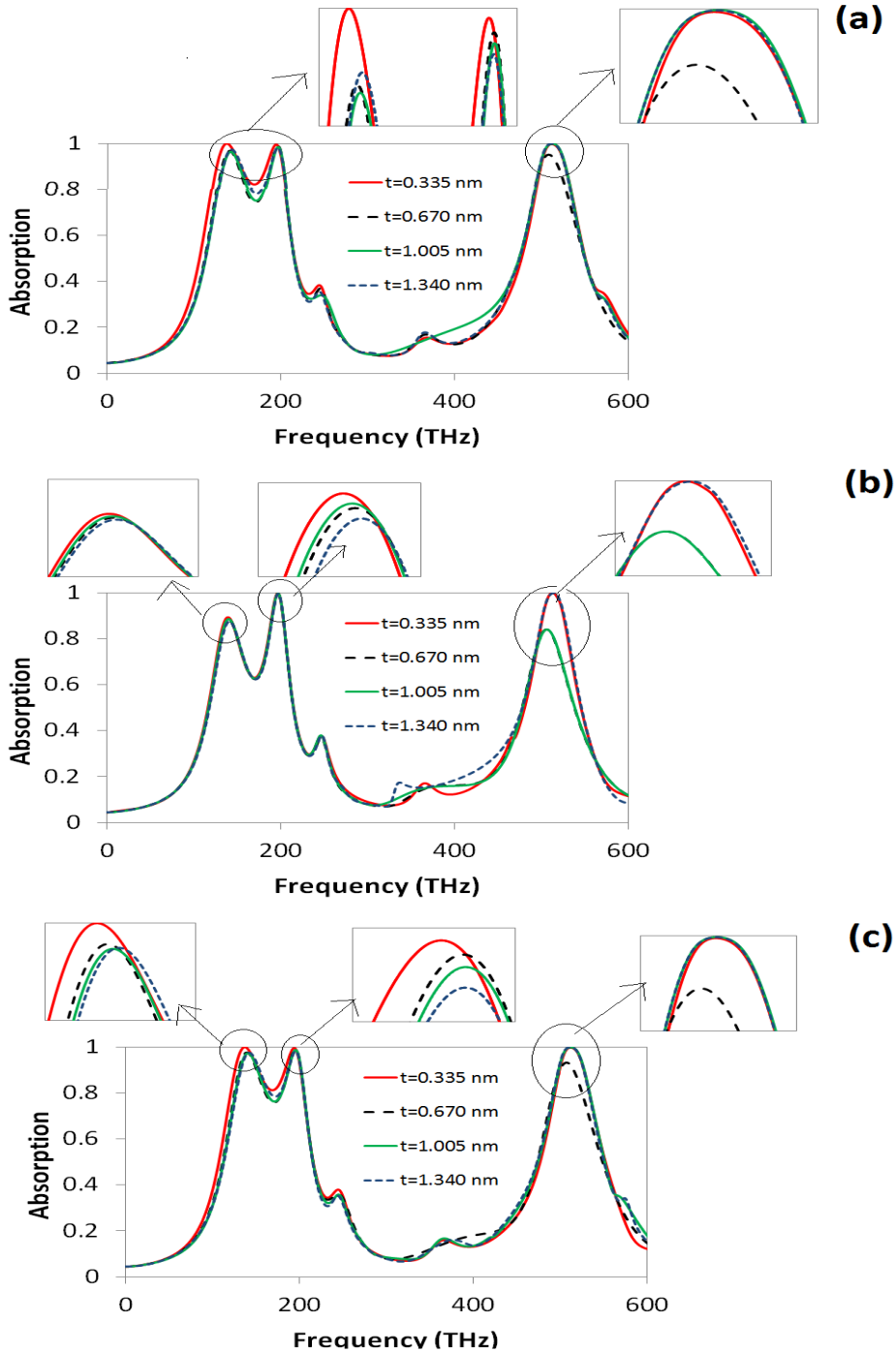

Figure 2-17. Parametric study for four graphene thicknesses (t) for (a) under the metal patch resonator, (b) at the top of the metal patch resonator, (c) not only under the metal patch resonator but also at the top of the metal patch resonator.

In Figure 2-17a, 99.98%, 99.59%, and 99.72% absorption results are obtained at 137.25THz, 193.50THz, and 511.50THz resonance frequencies, respectively. In Figure 2-17b, 89.39%, 99.89%, and 99.97% absorption results are obtained at 139.50THz, 196.50THz, and 513THz resonance frequencies, respectively. In Figure 2-17c, 99.99%, 99.60%, and 99.74% absorption results are obtained at 137.25THz, 194.25THz, and 511.50THz resonance frequencies, respectively. In Figure 2-17c, absorption results are the highest ones among three graphene situations as percentages when graphene thickness is t = 0.335 nm (single – layer). High conductivity graphene layers are given the reason of this enhancement.

Fractional bandwidth (FBW) calculations are done for Figure 2-3 and Figure 2-17 (when t = 0.335 nm). FBW can be found with $\Delta f / f_0$ where Δf is the half – power bandwidth and f_0 is the center frequency. Information is supplied about an absorber`s quality by FBW [80 – 82]. In Figure 2-3, Δf = 29.25THz, f_0 = 141THz and FBW ≈ 20.74% for the first resonance, Δf = 25.50THz, f_0 = 197.25THz and FBW ≈ 12.93% for the second resonance, and Δf = 42.75THz, f_0 = 514.50THz and FBW ≈ 8.31% for the third resonance. In Figure 2-17a, Δf = 91.50THz, f_0 = 168.75THz and FBW ≈ 54.22% for the first and second resonances, Δf = 48.75THz, f_0 = 511.50THz and FBW ≈ 9.53% for the third resonance. In Figure 2-17b, Δf = 30.75THz, f_0 = 139.50THz and FBW ≈ 22.04% for the first resonance, Δf = 27THz, f_0 = 196.50THz and FBW ≈ 13.74% for the second resonance, and Δf = 41.25THz, f_0 = 513THz and FBW ≈ 8.04% for the third resonance. In Figure 2-17c, Δf = 90.75THz, f_0 = 168.75THz and FBW ≈ 53.78% for the first and second resonances, Δf = 48.75THz, f_0 = 511.50THz and FBW ≈ 9.53% for the third resonance. Higher FBW, which means better quality absorber, is seen in some cases above.

2.4. Dual-Band Near Perfect Metamaterial Absorber Energy Harvesting

At the bottom of the structure, the usage of metal layer are confined electromagnetic energy within the structure as in the metamaterial absorber studies [3, 37]. The near perfect absorption is obtained at the resonance frequency when the impedance of free – space matches with the frequency dependent effective impedance of the metamaterial absorber [44, 83].

2.4.1. Design and Simulation

The structure, which is shown in Figure 2-1, can be used a metamaterial absorber based energy harvester with the realization of some small modifications. Two new structures, which are obtained by adding square or circular ring shaped resonator and two resistors (lumped network elements), can be seen in Figure 2-18 and Figure 2-19 with dimensions. Gaps are become between patch resonator and square or circular ring shaped resonator. Across created gaps, resistors are located as lumped network elements. With these processes, two new structures are prepared for energy harvesting. The reason of adding ring to the structure is electric fields were collected around the two sides of square patch resonator for the structure in Figure 2-1. Collected electric fields can be seen in Figure 2-15a and Figure 2-15b. As it is mentioned before in section 1.4 in chapter 1, electric field means voltage and voltage means power. Therefore, two different shaped rings are separately adding in order to create gaps, add resistors, and receive collected power by resistors. The reason of selecting two different shaped rings is to enable the comparison of the effects of the geometrical resonators on optical and electrical responses. After many parametric studies are done with finite integration technique (FIT) – based numerical simulator, these resistors` numerical values are chosen.

At first, same Aluminum (Palik) and GaAs (Palik) materials are used for separately analysing two new structures. Later, Silver (Johnson) as a metal and Silica (Silicon Dioxide) (Ghosh) as a substrate are used in two new structure in order to enhance results. Optical properties of Aluminum and GaAs can be found in Ref [59] as they are used before. For the infrared frequency regimes, the optical properties of Silica and Silver can be separately found in Ref [84] and Ref [85], respectively. Materials, which are used in two structure, are defined according to Drude model. Dimensions of these designs a, b, c, d, e, f and g are numerically given as 40, 110, 25, 500, 180, 440, and 30 nm, respectively. They can be seen in Figure 2-18c, d and Figure 2-19c, d.

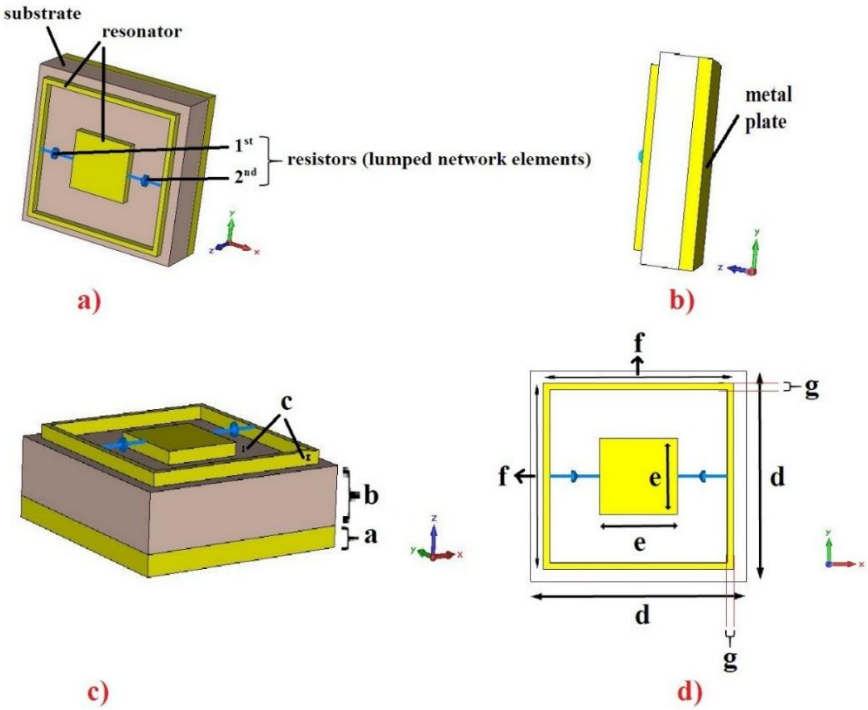

Figure 2-18. The view and dimensions of metamaterial energy harvester based on near perfect metamaterial absorber unit cell design with the square ring shaped resonator and two resistors.

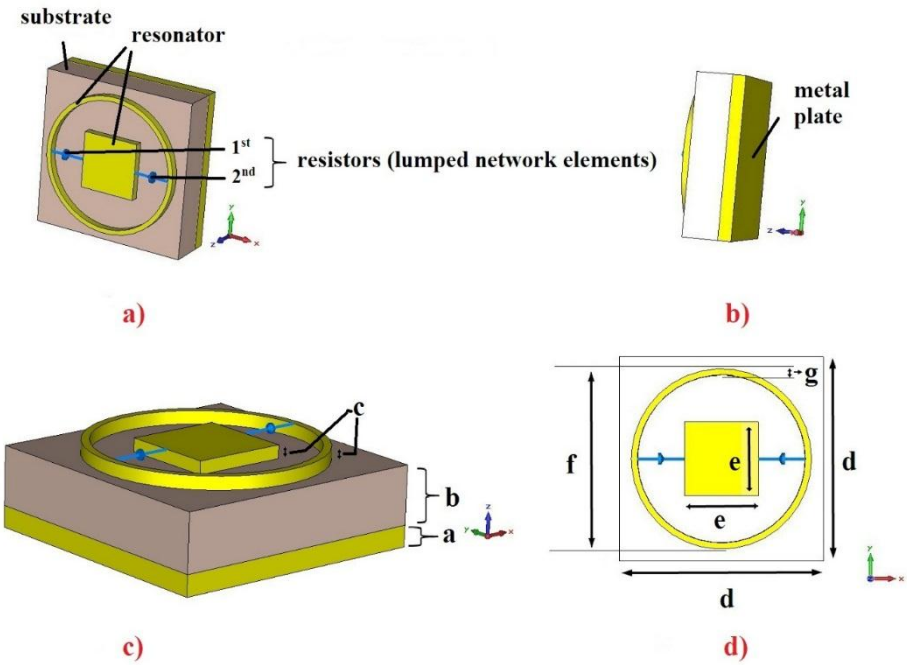

Figure 2-19. The view and dimensions of metamaterial energy harvester based on near perfect metamaterial absorber unit cell design with the circular ring shaped resonator and two resistors.

The wave comes perpendicularly onto the z-axis because of the position of the direction of the propagation (a waveguide port). Boundary conditions are set periodic, periodic, and open along x-, y-, and z- directions, respectively. Along the x- and y-directions, the electric and magnetic field components of the incident plane wave are polarized, respectively [60 – 62].

2.4.2. Result and Discussion

Achievements of all numerical results is based on FIT by commercial full-wave EM solver. In Figure 2-20, numerical reflection and absorption results are given for (Aluminum (Palik) (metal plate), GaAs (Palik) (substrate) and Aluminum (Palik) (resonator)) structure (for the proposed (square ring shaped resonator) unit cell structure as shown in Figure 2-18). 86.29% maximum absorption is obtained at 142.40 THz and 78.63% maximum absorption is obtained at 204.80 THz as shown in Figure 2-20. This absorption is become when two 500 ohm resistors are positioned across the gaps as two lumped network elements as shown in Figure 2-18a. In Figure 2-21, numerical reflection and absorption results are given for (Silver (Johnson) (metal plate), Silica (Ghosh) (substrate) and Silver (Johnson) (resonator)) structure (for the proposed (square ring shaped resonator) unit cell structure as shown in Figure 2-18). 98.66% maximum absorption is obtained at 240.00 THz as shown in Figure 2-21. This absorption is become when two 500 ohm resistors are positioned across the gaps as two lumped network elements as shown in Figure 2-18a. In Figure 2-22, numerical reflection and absorption results are given for (Aluminum (Palik) (metal plate), GaAs (Palik) (substrate) and Aluminum (Palik) (resonator)) structure (for the proposed (circular ring shaped resonator) unit cell structure as shown in Figure 2-19). 90.26% maximum absorption is obtained at 140.80 THz and 91.22% maximum absorption is obtained at 209.60 THz as shown in Figure 2-22. This absorption is become when two 500 ohm resistors are positioned across the gaps as two lumped network elements as shown in Figure 2-19a. In Figure 2-23, numerical reflection and absorption results are given for (Silver (Johnson) (metal plate), Silica (Ghosh) (substrate) and Silver (Johnson) (resonator)) structure (for the proposed (circular ring shaped resonator) unit cell structure as shown in Figure 2-19). 99.86% maximum absorption is obtained at

219.20 THz and 99.78% maximum absorption is obtained at 248.00 THz as shown in Figure 2-23. This absorption is become when two 500 ohm resistors are positioned across the gaps as two lumped network elements as shown in Figure 2-19a.

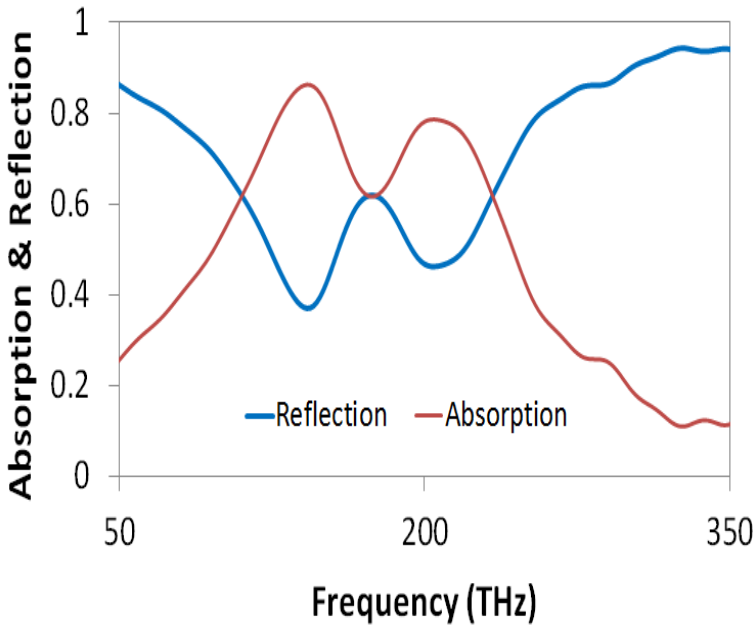

Figure 2-20. Reflection and absorption results for (Aluminum (Palik) (metal plate), GaAs (Palik) (substrate) and Aluminum (Palik) (resonator)) structure (for the proposed (square ring shaped resonator) unit cell structure) (The resonance frequencies at 142.40 and 204.80 THz).

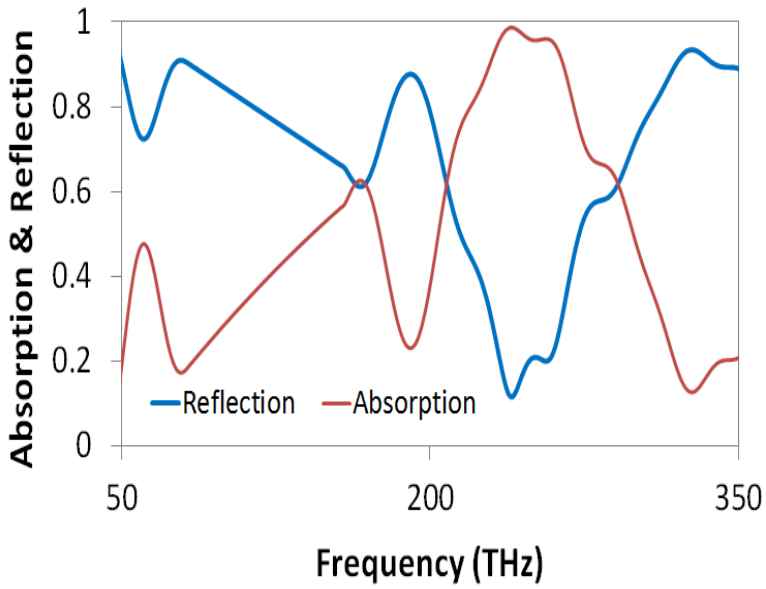

Figure 2-21. Reflection and absorption results for (Silver (Johnson) (metal plate), Silica (Ghosh) (substrate) and Silver (Johnson) (resonator)) structure (for the proposed (square ring shaped resonator) unit cell structure) (The resonance frequency at 240.00 THz).

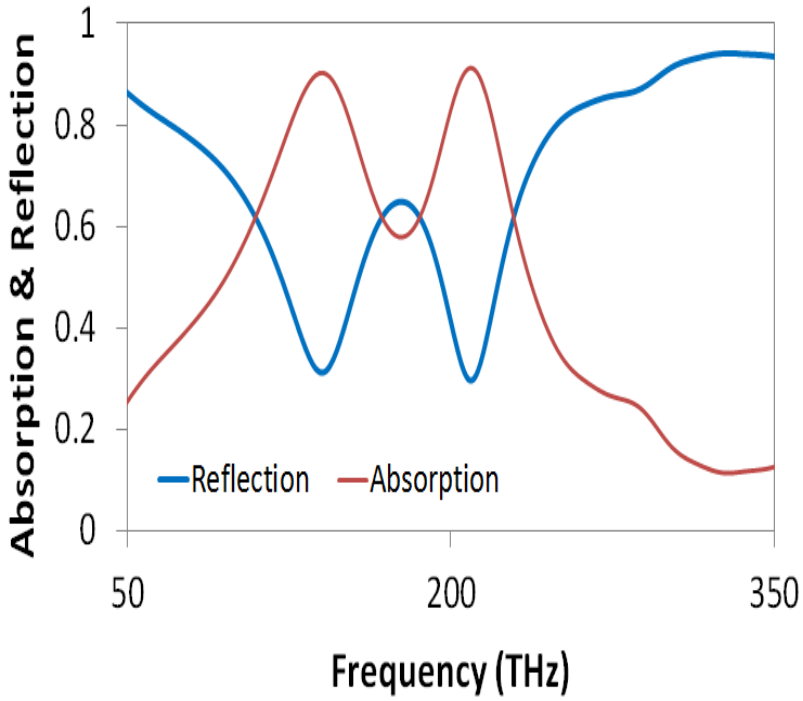

Figure 2-22. Reflection and absorption results for (Aluminum (Palik) (metal plate), GaAs (Palik) (substrate) and Aluminum (Palik) (resonator)) structure (for the proposed (circular ring shaped resonator) unit cell structure) (The resonance frequencies at 140.80 and 209.60 THz).

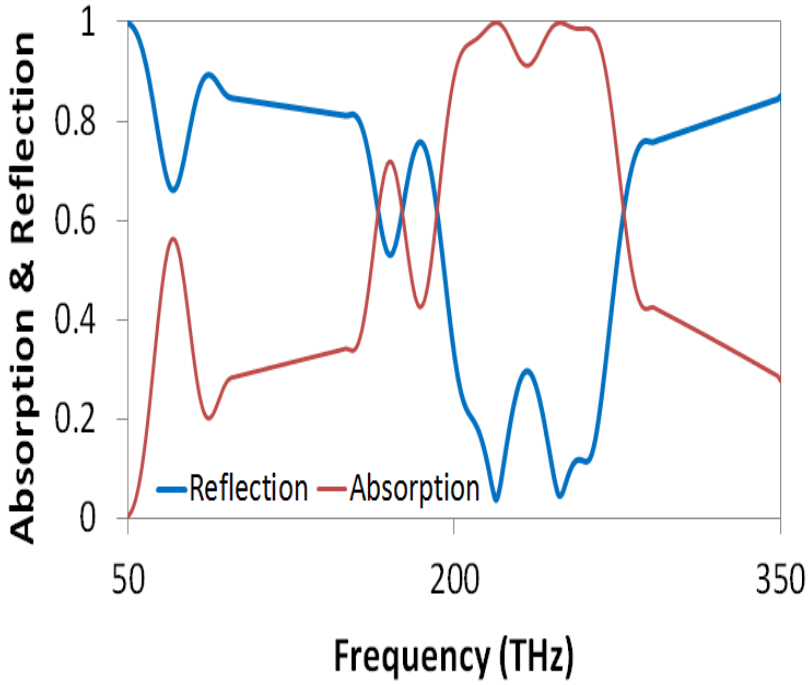

Figure 2-23. Reflection and absorption results for (Silver (Johnson) (metal plate), Silica (Ghosh) (substrate) and Silver (Johnson) (resonator)) structure (for the proposed (circular ring shaped resonator) unit cell structure) (The resonance frequencies at 219.20 and 248.00 THz).

By the resistance values and “g” parameters, the energies are affected as shown in Figure 2-24 - 27. At 500 ohm, the maximum efficiencies are achieved as seen from Figure 2-24 - 27. For all power harvesting simulations, input powers were taken 0.500 W. The lumped network elements (resistors) are placed parallel to x-axis (electric field direction) is shown in Figure 2-18 and 2-19. The output power value of the first resistor is the same with the output power value of the second resistor for all simulation. 20.4% (output power is 0.102 W) and 5.4% (output power is 0.027 W) maximum power efficiencies are obtained at 139.20 and 200.00 THz at 500 ohm as shown in Figure 2-24. 93.0% (output power is 0.465 W) maximum power efficiency is obtained at 240.00 at 500 ohm as shown in Figure 2-25. 21.4% (output power is 0.107 W) and 8.0% (output power is 0.040 W) maximum power efficiencies are obtained at 139.20 and 217.60 THz at 500 ohm as shown in Figure 2-26. 97.0% (output power is 0.485 W) and 98.2% (output power is 0.491 W) maximum power efficiencies are obtained at 212.80 and 252.80 THz at 500 ohm as shown in Figure 2-27.

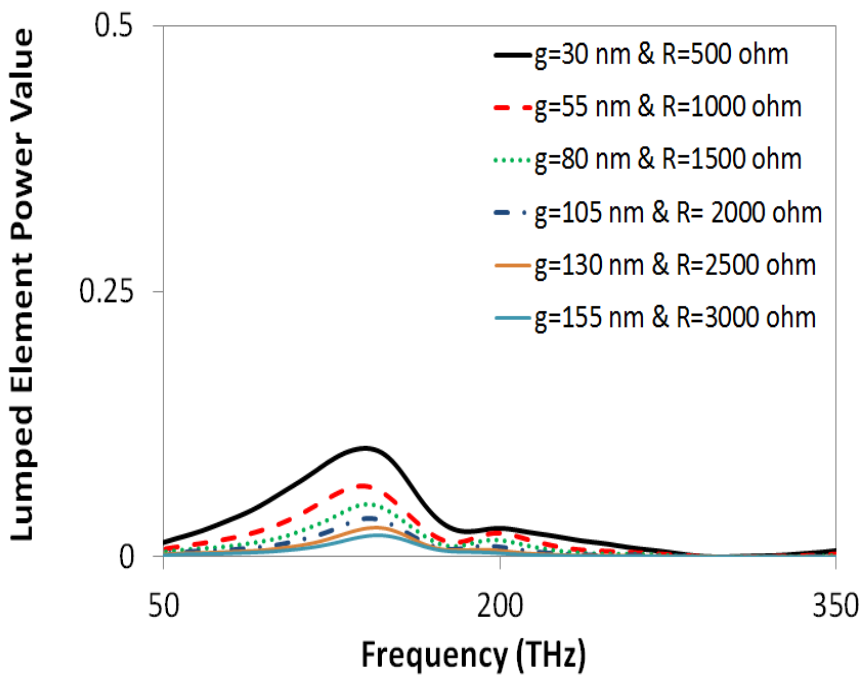

Figure 2-24. Parametric study gathered power frequency diagram for selected different “g” parameters and resistors between 500-3000 ohm for (Aluminum (Palik) (metal plate), GaAs (Palik) (substrate) and Aluminum (Palik) (resonator)) structure (for the proposed (square ring shaped resonator) unit cell structure).

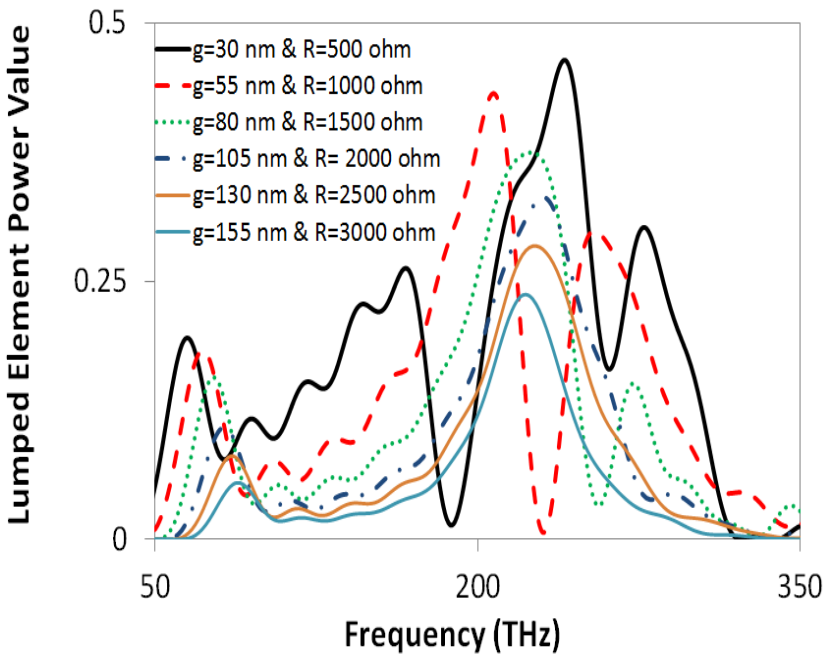

Figure 2-25. Parametric study gathered power frequency diagram for selected different "g" parameters and resistors between 500-3000 ohm for (Silver (Johnson) (metal plate), Silica (Ghosh) (substrate) and Silver (Johnson) (resonator)) structure (for the proposed (square ring shaped resonator) unit cell structure).

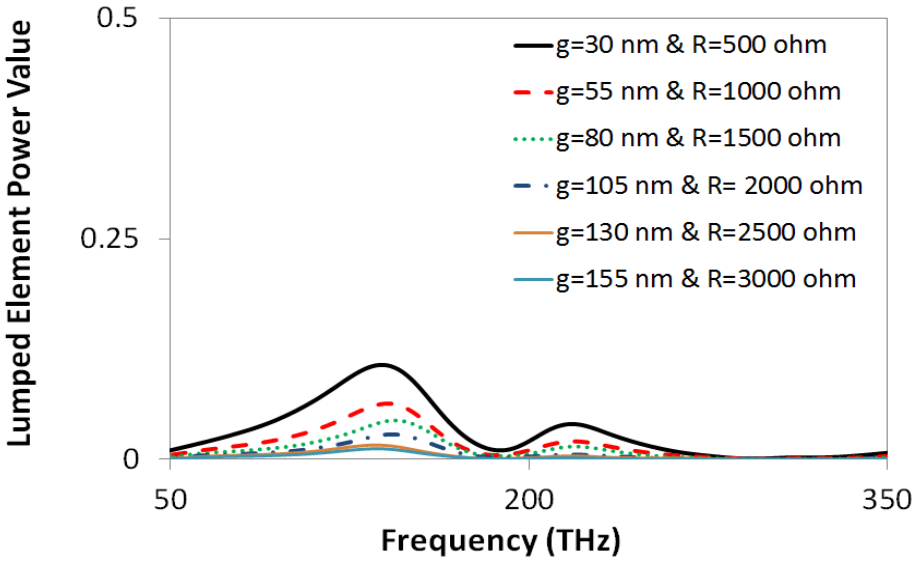

Figure 2-26. Parametric study gathered power frequency diagram for selected different "g" parameters and resistors between 500-3000 ohm for (Aluminum (Palik) (metal plate), GaAs (Palik) (substrate) and Aluminum (Palik) (resonator)) structure (for the proposed (circular ring shaped resonator) unit cell structure).

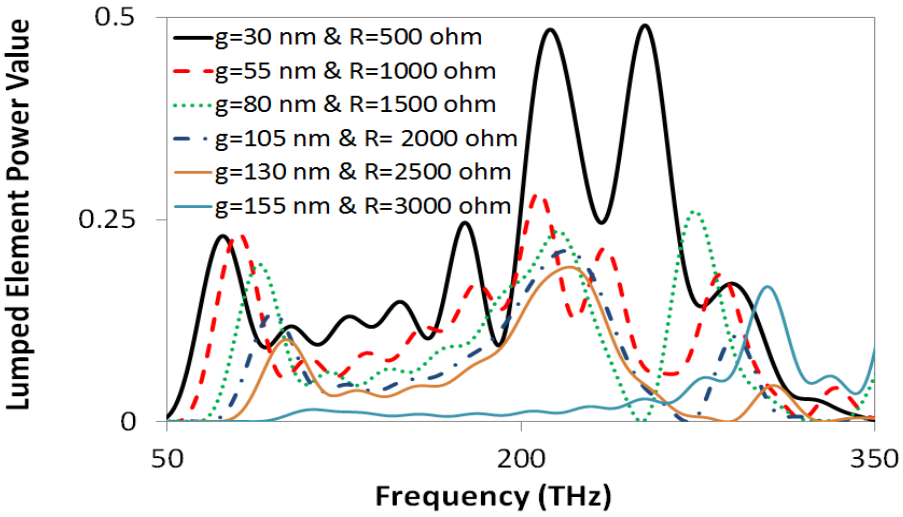

Figure 2-27. Parametric study gathered power frequency diagram for selected different "g" parameters and resistors between 500-3000 ohm for (Silver (Johnson) (metal plate), Silica (Ghosh) (substrate) and Silver (Johnson) (resonator)) structure (for the proposed (circular ring shaped resonator) unit cell structure).

In order to understand the effect of the metal plate existence, two numerical study results (with metal plate and without metal plate situations) for four situations on two kind structures are appreciated as shown in Figure 2-28 - 31. When metal plate exists at the bottom of the design, total lumped network elements` power value is high at 500 ohm in Figure 2-28 - 31. However, this value is decreased when the metal plate is removed from the design as shown in Figure 2-28 - 31. The harvested power is affected due to the effect of the metal plate on total capacitance value.

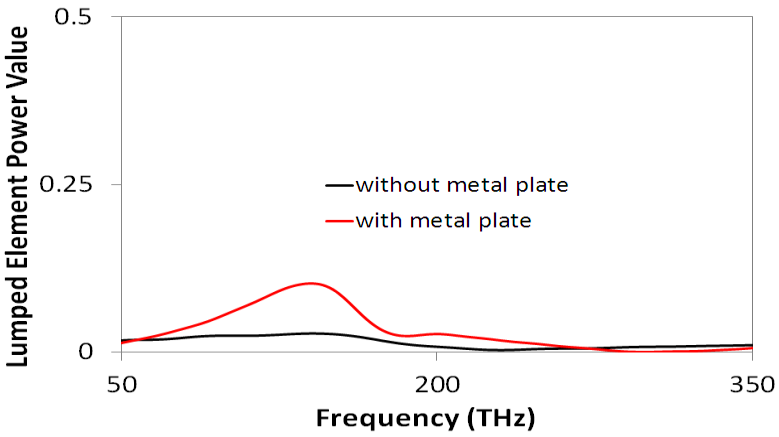

Figure 2-28. Simulated lumped element power magnitude for both cases with and without metal plate for 500 ohm resistor for (Aluminum (Palik) (metal plate), GaAs (Palik) (substrate) and Aluminum (Palik) (resonator)) structure (for the proposed (square ring shaped resonator) unit cell structure).

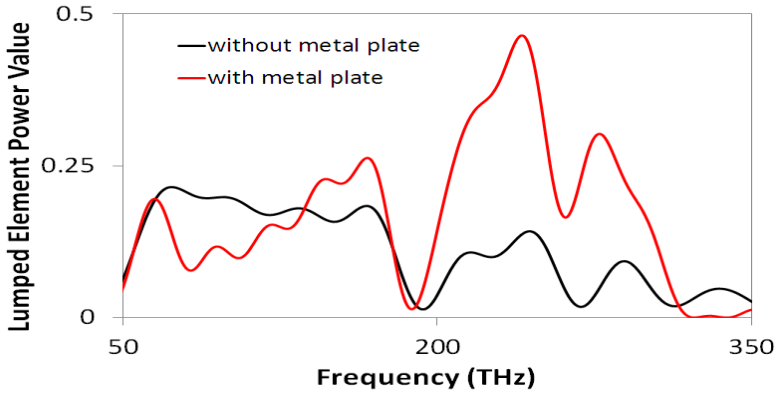

Figure 2-29. Simulated lumped element power magnitude for both cases with and without metal plate for 500 ohm resistor for (Silver (Johnson) (metal plate), Silica (Ghosh) (substrate) and Silver (Johnson) (resonator)) structure (for the proposed (square ring shaped resonator) unit cell structure).

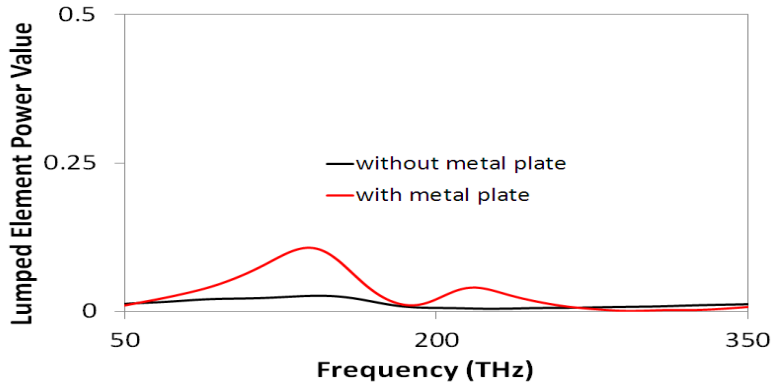

Figure 2-30. Simulated lumped element power magnitude for both cases with and without metal plate for 500 ohm resistor for (Aluminum (Palik) (metal plate), GaAs (Palik) (substrate) and Aluminum (Palik) (resonator)) structure (for the proposed (circular ring shaped resonator) unit cell structure).

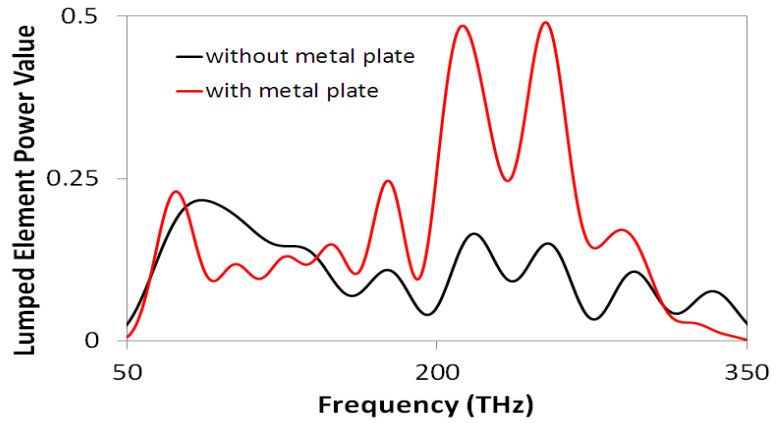

Figure 2-31. Simulated lumped element power magnitude for both cases with and without metal plate for 500 ohm resistor for (Silver (Johnson) (metal plate), Silica (Ghosh) (substrate) and Silver (Johnson) (resonator)) structure (for the proposed (circular ring shaped resonator) unit cell structure).

In Figure 2-32 – 35, the electric field, magnetic field and surface current distributions can be seen at the resonance frequency/frequencies in order to understand better the physical mechanism of the designs in power harvesting applications. The concentrations of these distributions are on two gaps of the structure where there are resistors because electric field directions are taken to be parallel to x-axis as it is mentioned before. Therefore, the structure act as an electric dipole at the resonance frequency. The basis of this study is the structure can be used as voltage source in order to achieve the confinement of the EM waves at the resonance frequency.

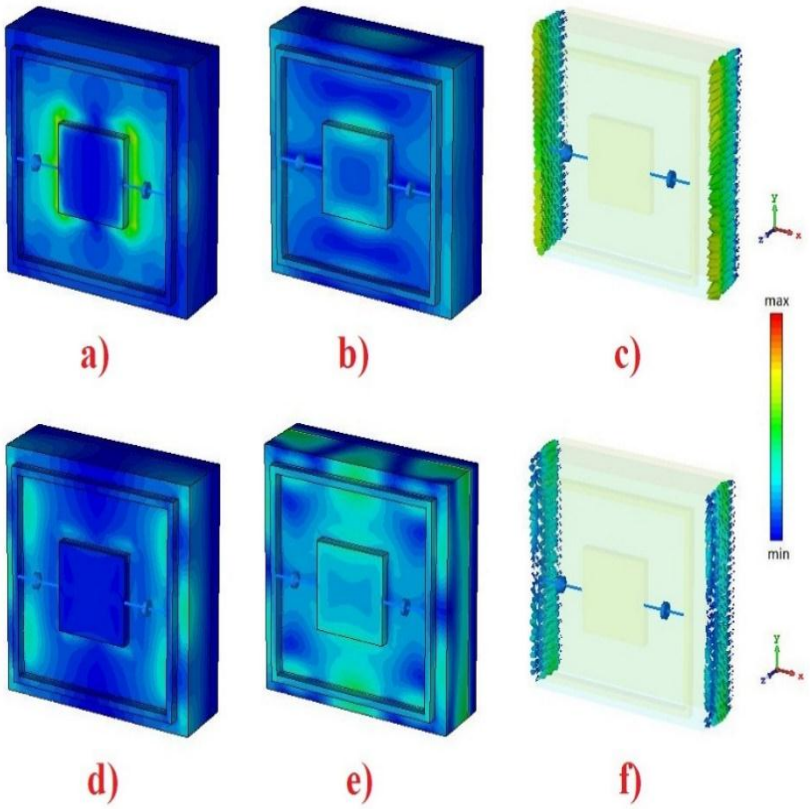

Figure 2-32. For (Aluminum (Palik) (metal plate), GaAs (Palik) (substrate) and Aluminum (Palik) (resonator)) structure (for the proposed (square ring shaped resonator) unit cell structure) (a) Electric field distribution at the resonance frequency of 142.40 THz (b) Magnetic field distribution at the resonance frequency of 142.40 THz (c) Surface current distribution at the resonance frequency of 142.40 THz (d) Electric field distribution at the resonance frequency of 204.80 THz (e) Magnetic field distribution at the resonance frequency of 204.80 THz (f) Surface current distribution at the resonance frequency of 204.80 THz.

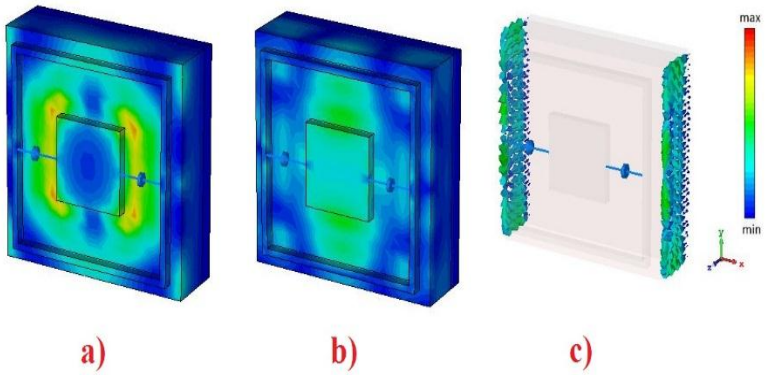

Figure 2-33. For (Silver (Johnson) (metal plate), Silica (Ghosh) (substrate) and Silver (Johnson) (resonator)) structure (for the proposed (square ring shaped resonator) unit cell structure) (a) Electric field distribution at the resonance frequency of 240.00 THz (b) Magnetic field distribution at the resonance frequency of 240.00 THz (c) Surface current distribution at the resonance frequency of 240.00 THz.

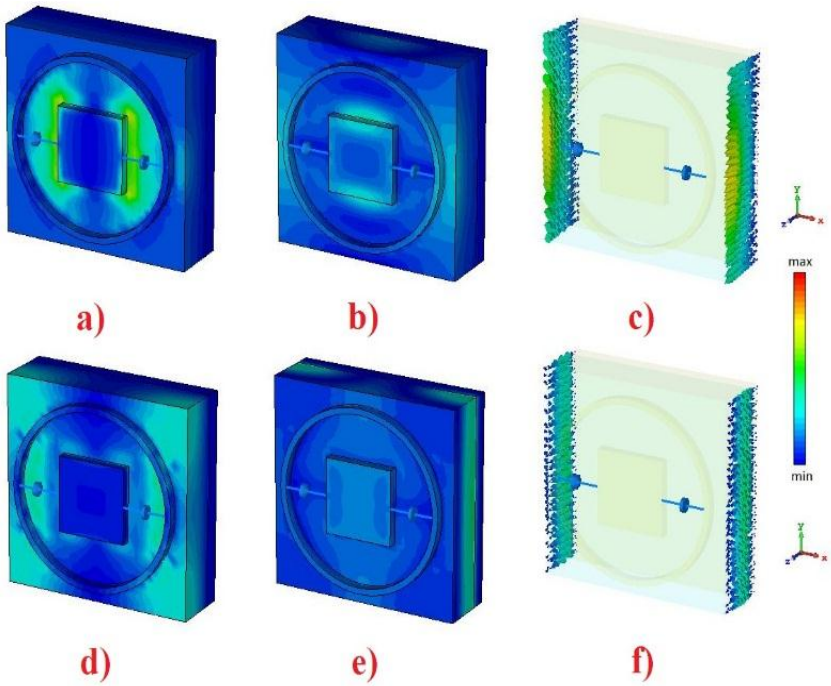

Figure 2-34. For (Aluminum (Palik) (metal plate), GaAs (Palik) (substrate) and Aluminum (Palik) (resonator)) structure (for the proposed (circular ring shaped resonator) unit cell structure) (a) Electric field distribution at the resonance frequency of 140.80 THz (b) Magnetic field distribution at the resonance frequency of 140.80 THz (c) Surface current distribution at the resonance frequency of 140.80 THz (d) Electric field distribution at the resonance frequency of 209.60 THz (e) Magnetic field distribution at the resonance frequency of 209.60 THz (f) Surface current distribution at the resonance frequency of 209.60 THz.

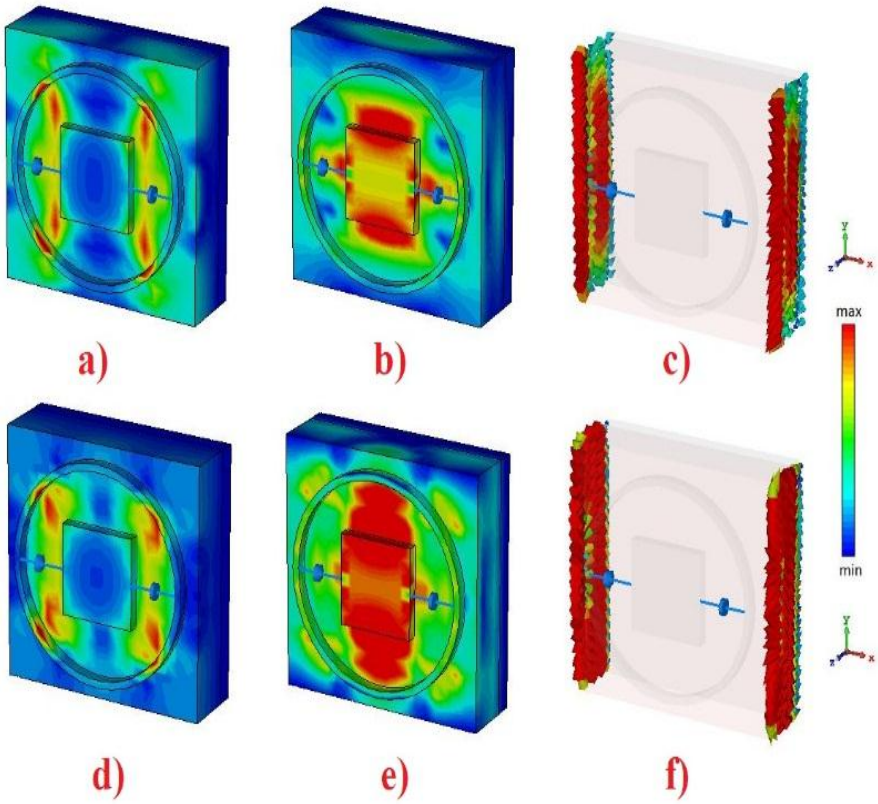

Figure 2-35. For (Silver (Johnson) (metal plate), Silica (Ghosh) (substrate) and Silver (Johnson) (resonator)) structure (for the proposed (circular ring shaped resonator) unit cell structure) (a) Electric field distribution at the resonance frequency of 219.20 THz (b) Magnetic field distribution at the resonance frequency of 219.20 THz (c) Surface current distribution at the resonance frequency of 219.20 THz (d) Electric field distribution at the resonance frequency of 248.00 THz (e) Magnetic field distribution at the resonance frequency of 248.00 THz (f) Surface current distribution at the resonance frequency of 248.00 THz.

2.5. Conclusion

In this chapter, a metamaterial absorber based on patch metal resonator, its enhancement with graphene layers, its conversion to two different energy harvester designs are realized and analysed. Reflectance, absorption, parametric studies, field distributions can be seen above. Also, the design are polarization and incident angles independent as they are mentioned in section 2.2. The possibility is available to use these absorbers in utilization of solar energy. Proposed structures can be used for many application such as infrared spectroscopy, infrared cameras, solar cells.

CHAPTER 3

ENEGRY HARVESTING OF METAMATERIAL ABSORBER FOR MICROWAVE, SUB-TERAHERTZ, AND INFRARED FREQUENCY REGIONS

3.1. Introduction

Although different dimensions and working frequency regimes, designs have a same view in this chapter. Metamaterial absorber based energy harvesters are analysed in microwave (GHz), sub-THz and infrared frequency regions in Section 3.2, Section 3.3 and Section 3.4, respectively.

3.2. Dual band metamaterial absorber based energy harvester in microwave (GHz) regime for energy harvesting

3.2.1. Design and Simulation

In Figure 3-1c, the parametric dimensions of the microwave (GHz) metamaterial absorber based energy harvester structure can be seen. There are four gaps on the resonator. Resistors are located as lumped network elements across the gaps on the resonator. Before selected numerical values of these resistors are specifically chosen, many parametric studies have been done with finite integration technique (FIT)-based numerical simulator. Copper metal element is used at the bottom layer (as metal plate) and top (as resonator) of this structure as a metallic layers as shown in Figure 3-1a and Figure 3-1b. Aim of the metal plate (as shown Figure 3-1b) on back side of the structure is the realization of approximately zero transmission (T(ω)) as it is mentioned before in previous chapters. Aim of the resonator (as shown Figure 3-1a) on front side of the structure is the minimization of the reflection as it is mentioned before in previous chapters. Thicknesses are same and equal to 0.035 mm for both bottom and top metallic layers. Also, electrical conductivity of the copper is 5.8001×10^{7} S/m. FR4, Polyimide, Arlon AD 350, Rogers RT 5880 are separately used as four different substrates with copper metal for metamaterial absorber based energy harvester as shown in Figure 3-1.

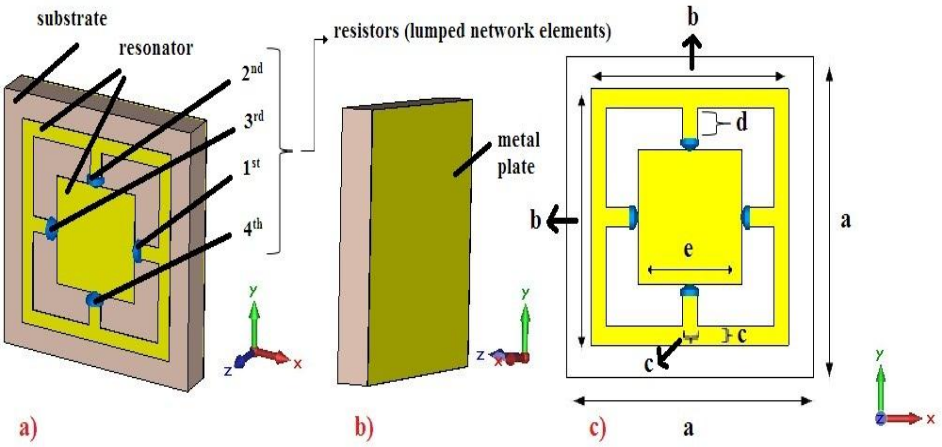

Figure 3-1. (a) Substrate, resonator and resistors, (b) metal plate, (c) dimensions of near perfect metamaterial absorber based energy harvester unit cell structure in microwave (GHz) range.

The thickness, loss tangent, relative permittivity and relative permeability of the FR4 substrate material are 1.6 mm, 0.025, 4.3 and 1, respectively. The thickness, loss tangent, relative permittivity and relative permeability of the Polyimide substrate material are 1.6 mm, 0.0027, 3.5 and 1, respectively. The thickness, loss tangent, relative permittivity and relative permeability of the Arlon AD 350 substrate material are 1.52 mm, 0.003, 3.5 and 1, respectively. The thickness, loss tangent, relative permittivity and relative permeability of the Rogers RT 5880 substrate material are 1.6 mm, 0.0009, 2.2 and 1, respectively.

Dimension values of except the (Copper, Arlon AD 350 and Copper) structure a, b, c, d and e are given as 10, 8, 0.6, 1, 4.2 mm, correspondingly [Figure 3-1c]. Dimension values of the (Copper, Arlon AD 350 and Copper) structure a, b, c, d and e are given as 10, 8, 0.6, 1.5 and 3.5 mm, correspondingly [Figure 3-1c].

Along the x- and y- directions, the magnetic and electric field components of the incident plane wave are polarized, respectively [60 – 62].

3.2.2. Result and Discussion

Numerical reflectance and absorption results can be seen in Figure 3-2 (for (Copper (metal plate), FR4 (substrate) and Copper (resonator)) structure), Figure 3-6 (for (Copper (metal plate), Polyimide (substrate) and Copper (resonator)) structure), Figure

3-10 (for (Copper (metal plate), Arlon AD 350 (substrate) and Copper (resonator)) structure) and Figure 3-14 (for (Copper (metal plate), Rogers RT 5880 (substrate) and Copper (resonator)) structure).

In Figure 3-2, maximum absorptions are obtained around 99.95% at 5.42 GHz and 99.99% at 12.72 GHz. These values are obtained when four 400 ohm resistor are placed across the gaps as four lumped network elements.

In Figure 3-6, maximum absorptions are obtained around 99.54% at 5.80 GHz and 99.92% at 13.62 GHz. These values are obtained when four 600 ohm resistor are placed across the gaps as four lumped network elements.

In Figure 3-10, maximum absorptions are obtained around 99.98% at 5.74 GHz and 99.17% at 14.44 GHz. These values are obtained when four 600 ohm resistor are placed across the gaps as four lumped network elements.

In Figure 3-14, maximum absorptions are obtained around 99.89% at 7.00 GHz and 99.81% at 16.98 GHz. These values are obtained when four 500 ohm resistor are placed across the gaps as four lumped network elements.

Results in Figure 3-3, Figure 3-7, Figure 3-11 and Figure 3-15 show that the energies are affected by the resistances. The maximum efficiencies are obtained at 400 ohm, 600 ohm, 600 ohm and 500 ohm as seen from Figure 3-3, Figure 3-7, Figure 3-11 and Figure 3-15, respectively. For all power harvesting simulations, input powers were chosen 0.500 W. The second and fourth lumped network elements (resistors) are located parallel to y-axis (electric field direction) and the first and third lumped network elements (resistors) are located parallel to x-axis (magnetic field direction) is shown in Figure 3-1. Therefore, the effect of the first and third resistors to output power is maximum 8.94% when this percentage compares with the effect of the second and fourth resistors. The output power value of the first resistor is the same with the output power value of the third resistor. The output power value of the second resistor is the same with the output power value of the fourth resistor. This situation can be opposite if electric and magnetic field directions are chosen to be parallel to x- and y-axis, respectively.

In Figure 3-3, maximum efficiencies are obtained around 71.80% (output power is 0.359 W) at 5.54 GHz and 86.20% (output power is 0.431 W) at 12.64 GHz at 400 ohm.

In Figure 3-7, maximum efficiencies are obtained around 87.60% (output power is 0.438 W) at 5.98 GHz and 98.40% (output power is 0.492 W) at 13.92 GHz at 600 ohm.

In Figure 3-11, maximum efficiencies are obtained around 85.60% (output power is 0.428 W) at 5.78 GHz and 98.80% (output power is 0.494 W) at 13.36 GHz at 600 ohm.

In Figure 3-15, maximum efficiencies are obtained around 91.60% (output power is 0.458 W) at 7.23 GHz and 99.80% (output power is 0.499 W) at 16.50 GHz at 500 ohm.

For each four different structure (four different structures mean they are separately created with four different substrate material), two numerical studies are achieved with metal plate and without metal plate situations as shown in Figure 3-4, Figure 3-8, Figure 3-12 and Figure 3-16 in order to see the effects of metal plate existence.

In Figure 3-4, total lumped elements` powers` values are 0.359 W at 5.54 GHz and 0.431 W at 12.64 GHz at 400 ohm when there is copper metal plate at the bottom of the structure. However, total lumped elements` powers` value is decreased to 0.200 W at 8.46 GHz at 400 ohm when the metal plate is removed from the structure.

In Figure 3-8, total lumped elements` powers` values are 0.438 W at 5.98 GHz and 0.492 W at 13.92 GHz at 600 ohm when there is copper metal plate at the bottom of the structure. However, total lumped elements` powers` value is decreased to 0.212 W at 9.18 GHz at 600 ohm when the metal plate is removed from the structure.

In Figure 3-12, total lumped elements` powers` values are 0.428 W at 5.78 GHz and 0.494 W at 13.36 GHz at 600 ohm when there is copper metal plate at the bottom of the structure. However, total lumped elements` powers` value is decreased to 0.221 W at 8.42 GHz at 600 ohm when the metal plate is removed from the structure.

In Figure 3-16, total lumped elements` powers` values are 0.458 W at 7.23 GHz and 0.499 W at 16.50 GHz at 500 ohm when there is copper metal plate at the bottom of the structure. However, total lumped elements` powers` value is decreased to 0.231 W at 10.60 GHz at 500 ohm when the metal plate is removed from the structure.

The harvested power is directly affected by metal plate due to the effects of the metal plate on total capacitance value.

The electric field and surface current distributions are given in Figure 3-5, Figure 3-9, Figure 3-13 and Figure 3-17 at the different resonance frequencies in order to understand better the physical mechanism of the designed four different structure (four different structures mean they are separately created with four different substrate material) in power harvesting applications. The concentrations of these distributions are on two gaps of the designed structure where there are resistors because electric field directions are chosen to be parallel to y-axis as it is mentioned before. Therefore, the structure act as an electric dipole at the resonance frequencies in four situations. The basis of this is the design can be used as a voltage source due to the confinement of the EM waves at the resonance frequencies.

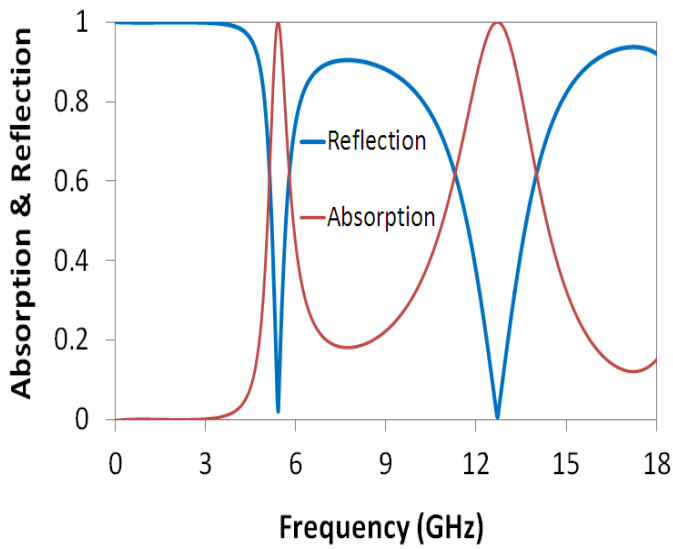

Figure 3-2. Reflectance and absorption results for (Copper (metal plate), FR4 (substrate) and Copper (resonator)) structure (The resonance frequencies at 5.42 and 12.72 GHz).

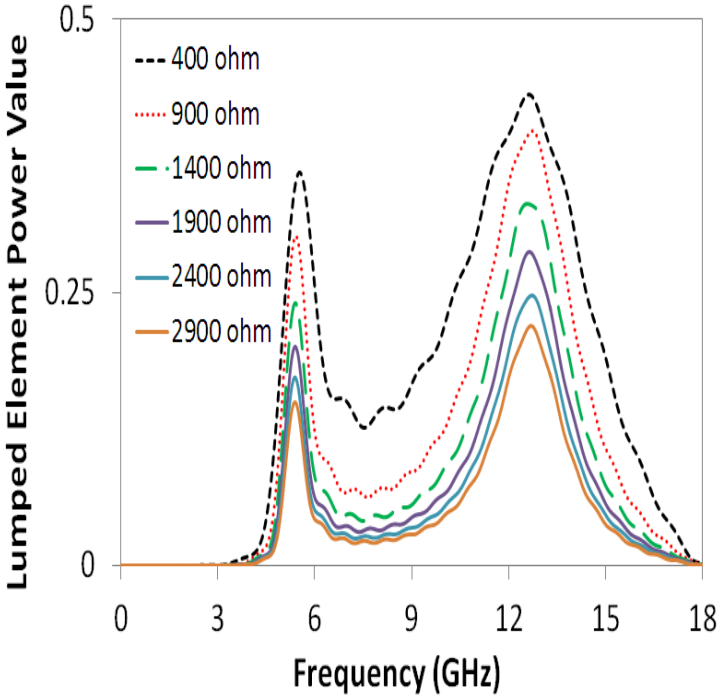

Figure 3-3. Gathered power frequency diagram for selected different resistors between 400-2900 ohm for (Copper (metal plate), FR4 (substrate) and Copper (resonator)) structure.

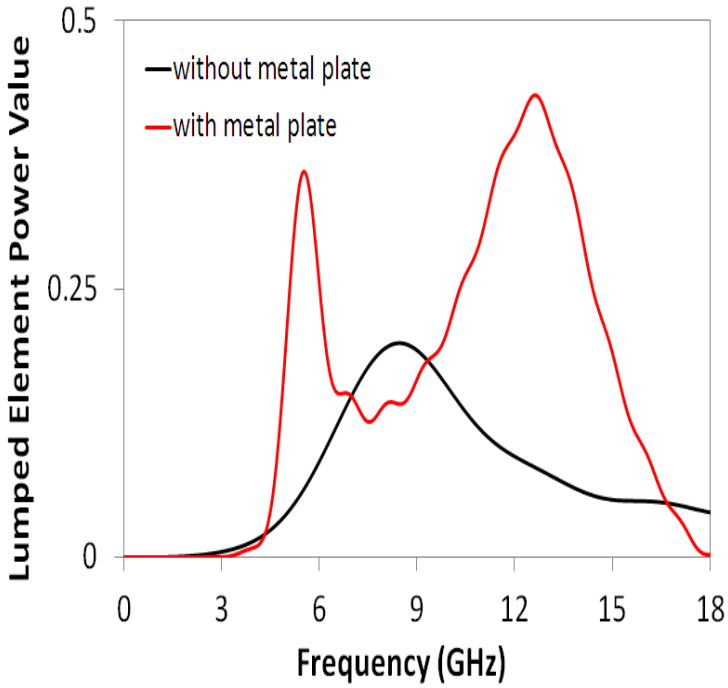

Figure 3-4. Simulated lumped element power magnitude for both cases with and without metal plate for 400 ohm resistor for (Copper (metal plate), FR4 (substrate) and Copper (resonator)) structure.

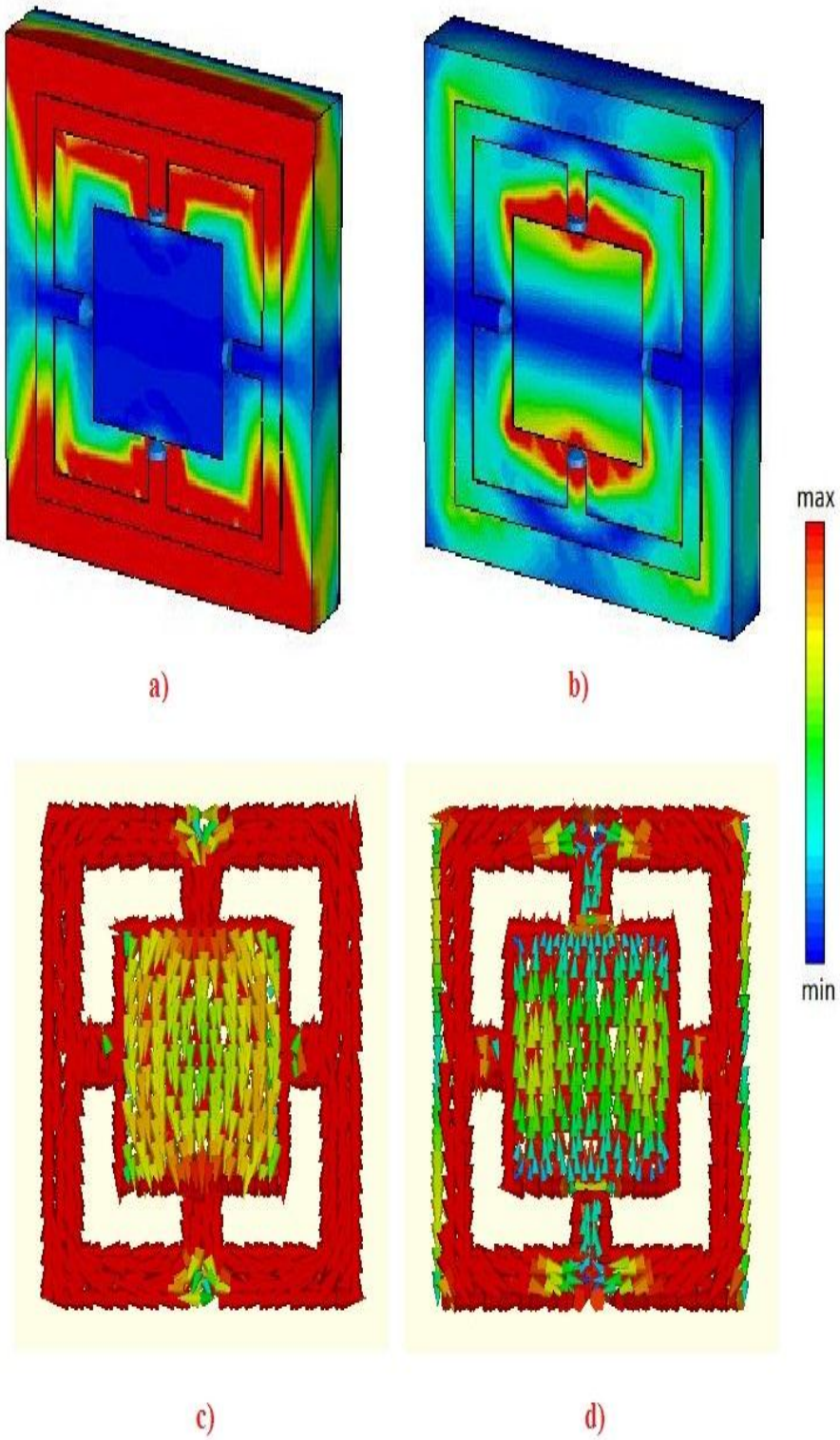

Figure 3-5. For (Copper (metal plate), FR4 (substrate) and Copper (resonator)) structure (a) Electric field distribution at the resonance frequency of 5.42 GHz (b) Electric field distribution at the resonance frequency of 12.72 GHz (c) Surface current distribution at the resonance frequency of 5.42 GHz (d) Surface current distribution at the resonance frequency of 12.72 GHz.

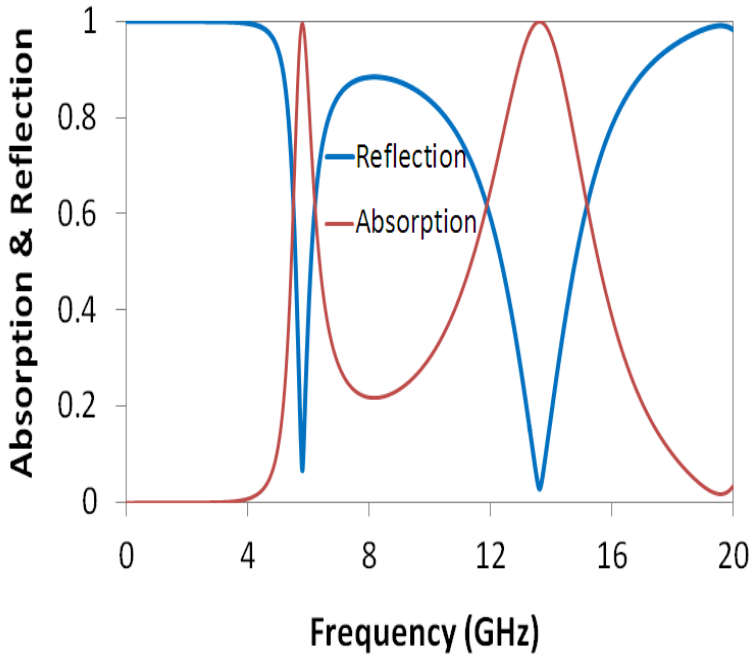

Figure 3-6. Reflectance and absorption results for (Copper (metal plate), Polyimide (substrate) and Copper (resonator)) structure (The resonance frequencies at 5.80 and 13.62 GHz).

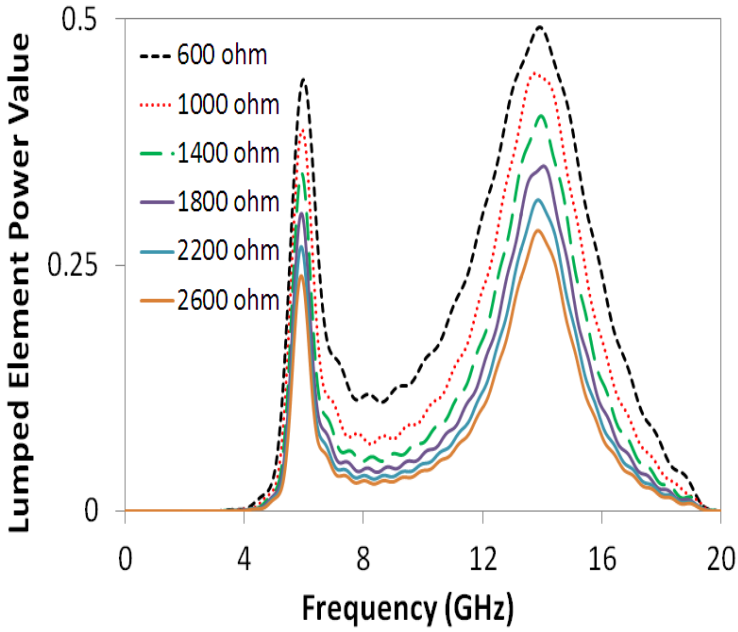

Figure 3-7. Gathered power frequency diagram for selected different resistors between 600-2600 ohm for (Copper (metal plate), Polyimide (substrate) and Copper (resonator)) structure.

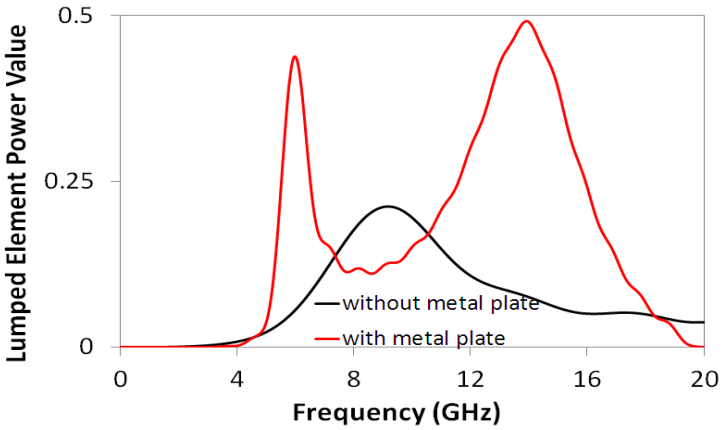

Figure 3-8. Simulated lumped element power magnitude for both cases with and without metal plate for 600 ohm resistor for (Copper (metal plate), Polyimide (substrate) and Copper (resonator)) structure.

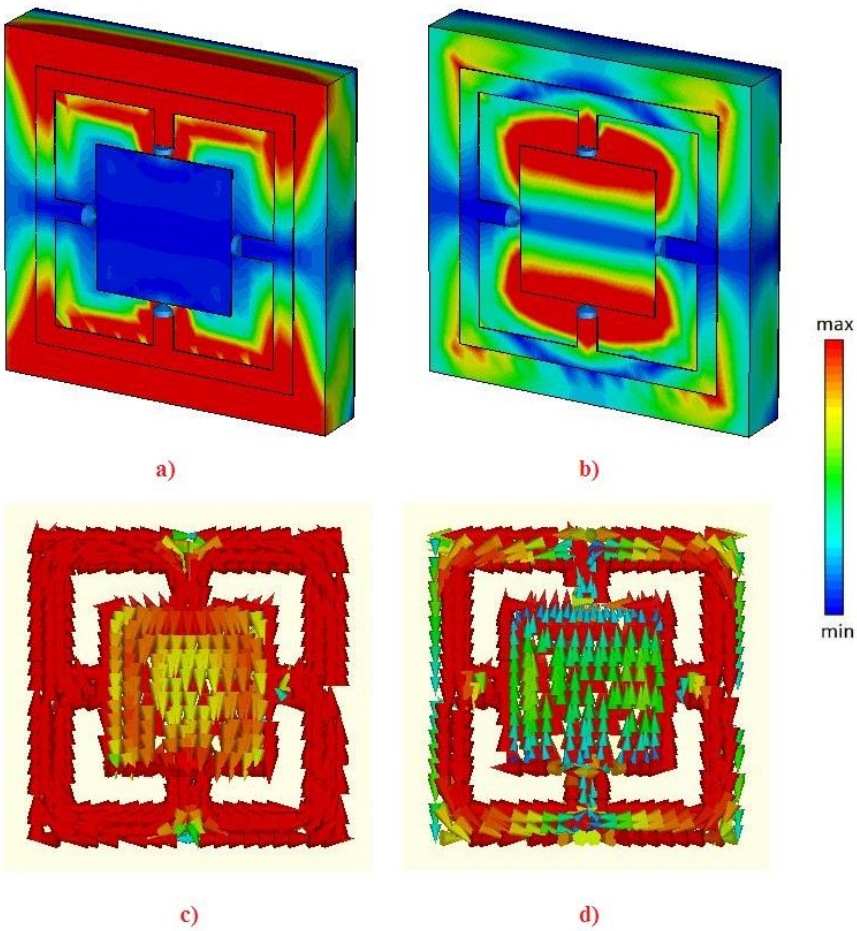

Figure 3-9. For (Copper (metal plate), Polyimide (substrate) and Copper (resonator)) structure (a) Electric field distribution at the resonance frequency of 5.80 GHz (b) Electric field distribution at the resonance frequency of 13.62 GHz (c) Surface current distribution at the resonance frequency of 5.80 GHz (d) Surface current distribution at the resonance frequency of 13.62 GHz.

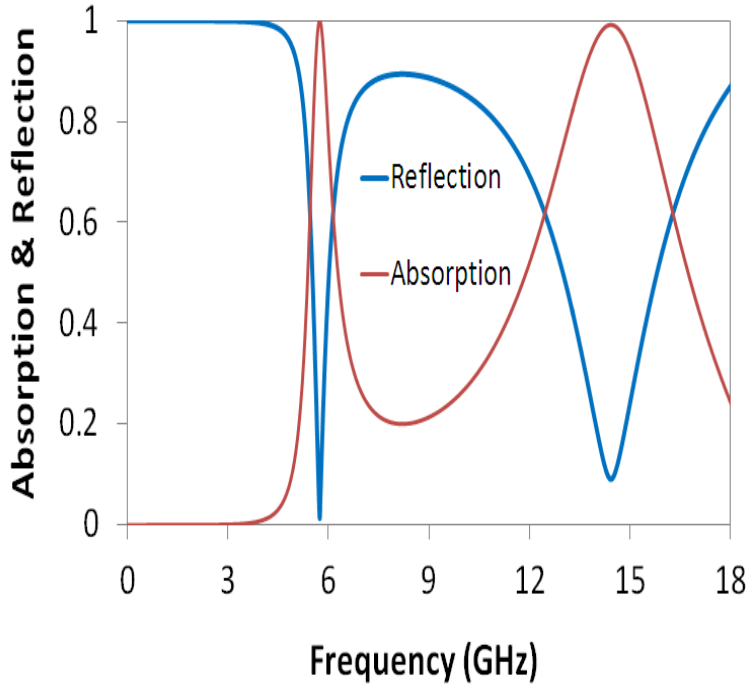

Figure 3-10. Reflectance and absorption results for (Copper (metal plate), Arlon AD 350 (substrate) and Copper (resonator)) structure (The resonance frequencies at 5.74 and 14.44 GHz).

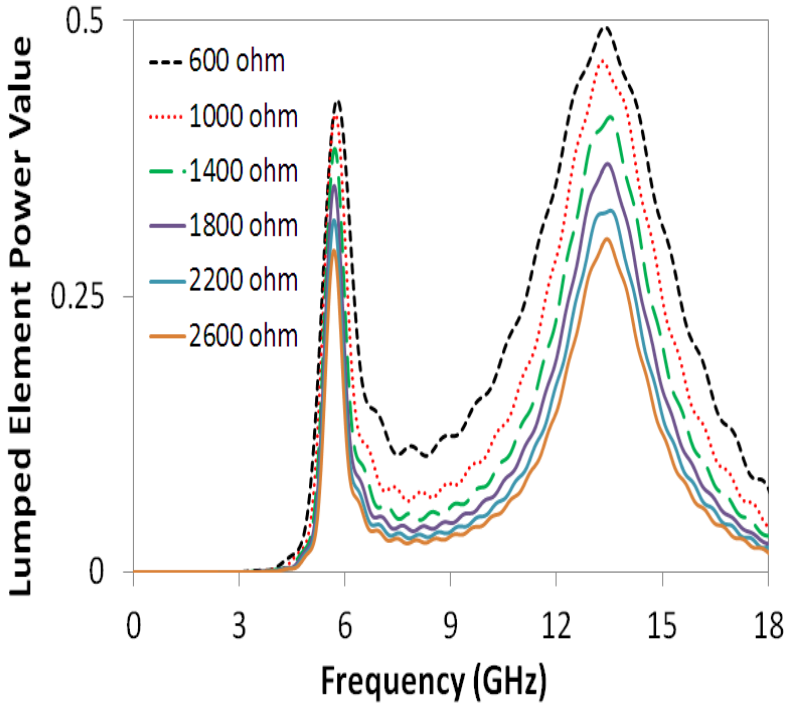

Figure 3-11. Gathered power frequency diagram for selected different resistors between 600-2600 ohm for (Copper (metal plate), Arlon AD 350 (substrate) and Copper (resonator)) structure.

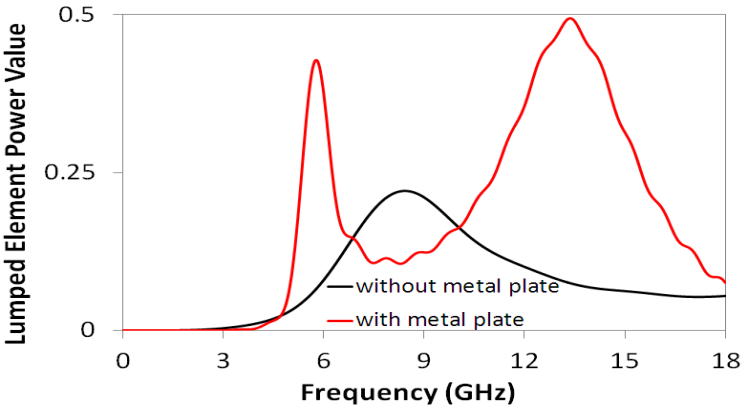

Figure 3-12. Simulated lumped element power magnitude for both cases with and without metal plate for 600 ohm resistor for (Copper (metal plate), Arlon AD 350 (substrate) and Copper (resonator)) structure.

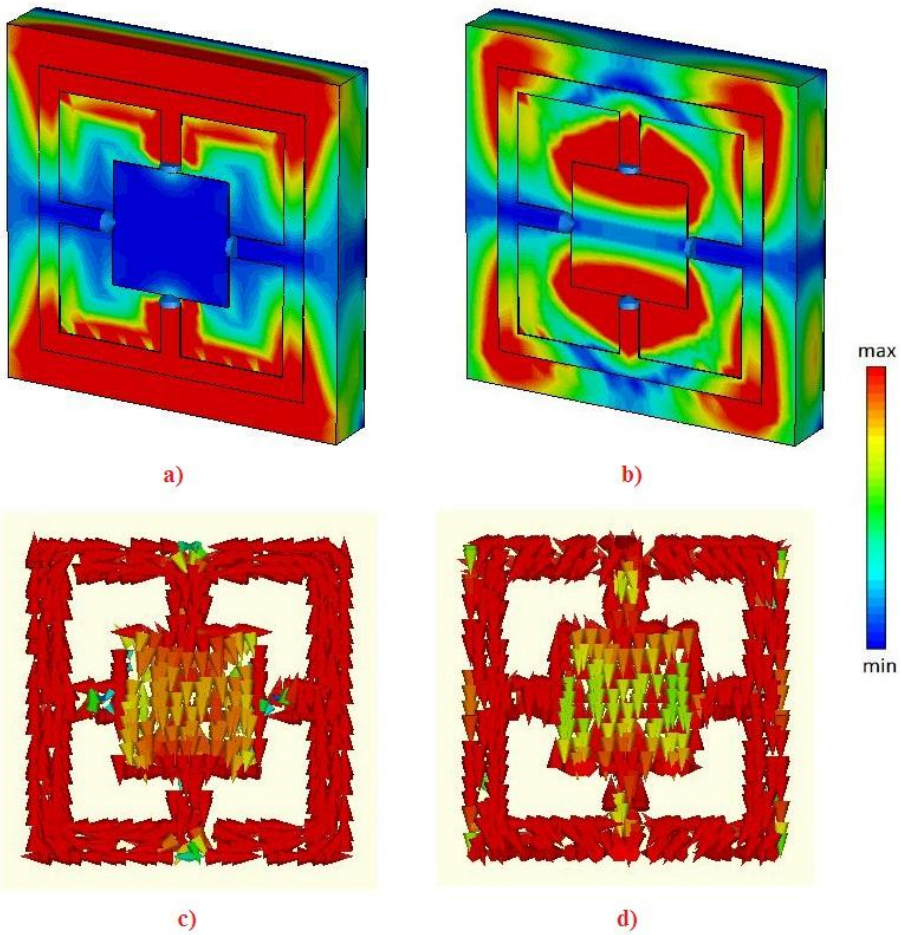

Figure 3-13. For (Copper (metal plate), Arlon AD 350 (substrate) and Copper (resonator)) structure (a) Electric field distribution at the resonance frequency of 5.74 GHz (b) Electric field distribution at the resonance frequency of 14.44 GHz (c) Surface current distribution at the resonance frequency of 5.74 GHz (d) Surface current distribution at the resonance frequency of 14.44 GHz.

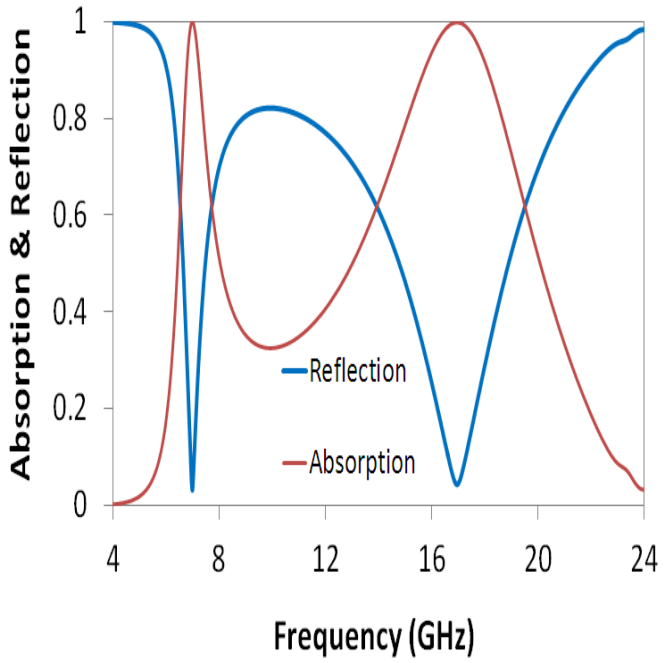

Figure 3-14. Reflectance and absorption results for (Copper (metal plate), Rogers RT 5880 (substrate) and Copper (resonator)) structure (The resonance frequencies at 7.00 and 16.98 GHz).

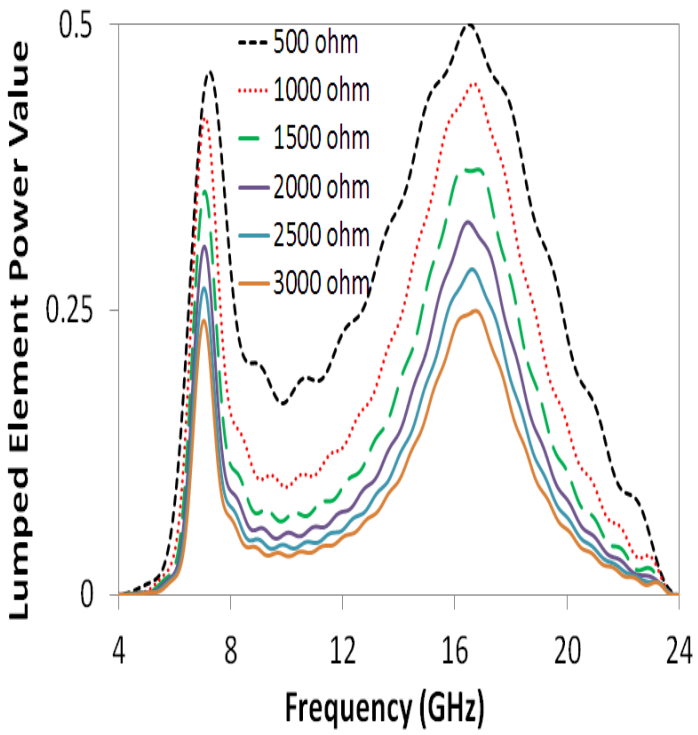

Figure 3-15. Gathered power frequency diagram for selected different resistors between 500-3000 ohm for (Copper (metal plate), Rogers RT 5880 (substrate) and Copper (resonator)) structure.

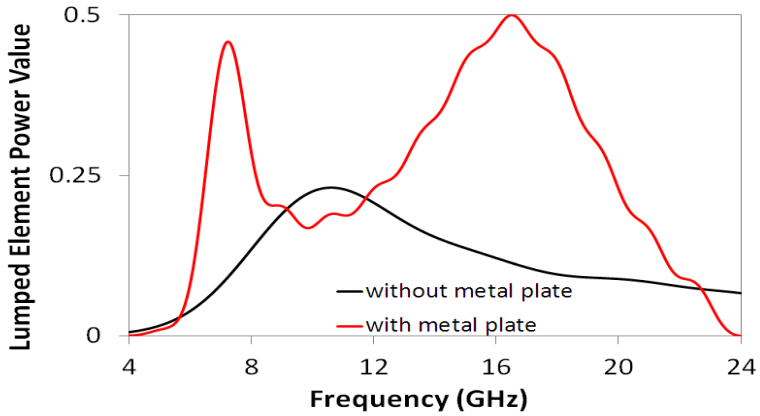

Figure 3-16. Simulated lumped element power magnitude for both cases with and without metal plate for 500 ohm resistor for (Copper (metal plate), Rogers RT 5880 (substrate) and Copper (resonator)) structure.

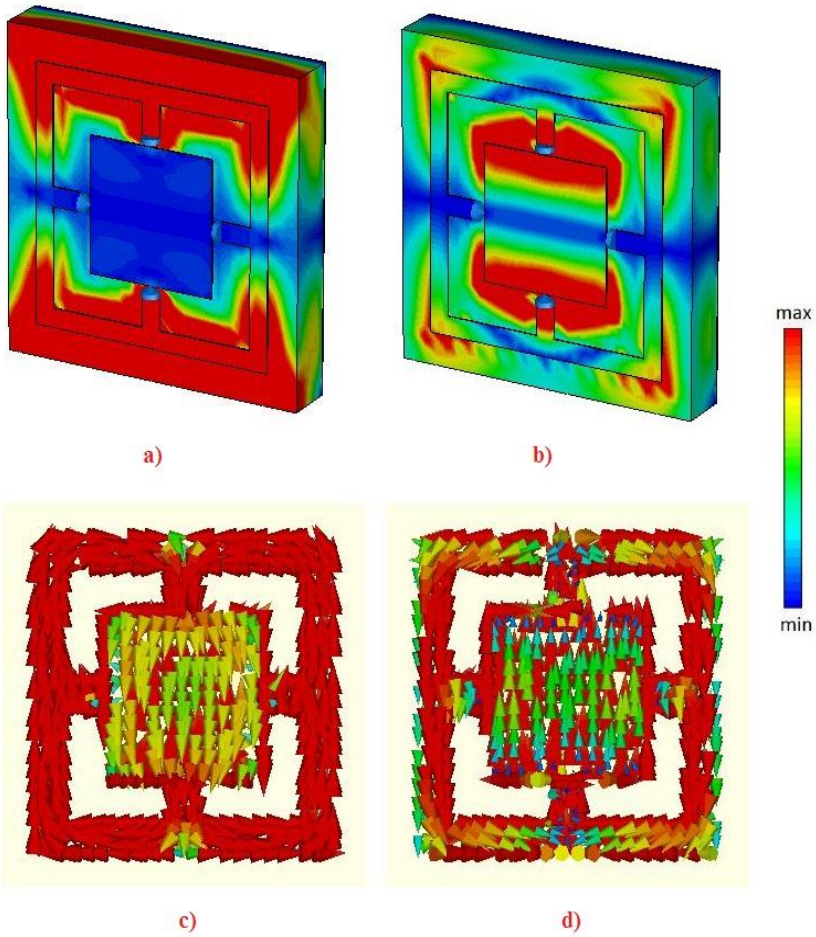

Figure 3-17. For (Copper (metal plate), Rogers RT 5880 (substrate) and Copper (resonator)) structure (a) Electric field distribution at the resonance frequency of 7.00 GHz (b) Electric field distribution at the resonance frequency of 16.98 GHz (c) Surface current distribution at the resonance frequency of 7.00 GHz (d) Surface current distribution at the resonance frequency of 16.98 GHz.

3.3. Single band metamaterial absorber based energy harvester in sub-THz regime for energy harvesting

3.3.1. Design and Simulation

In Figure 3-18c, the parametric dimensions of the sub-THz metamaterial absorber based energy harvester structure can be seen. There are four gaps on the resonator. Resistors are located as lumped network elements across the gaps on the resonator. Before selected numerical values of these resistors are specifically chosen, many parametric studies have been done with finite integration technique (FIT)-based numerical simulator. Silver, Gold and Aluminum metal elements are separately used at the bottom layer (as metal plate) and top (as resonator) of this structure as three different metallic layers as shown in Figure 3-18a and Figure 3-18b.

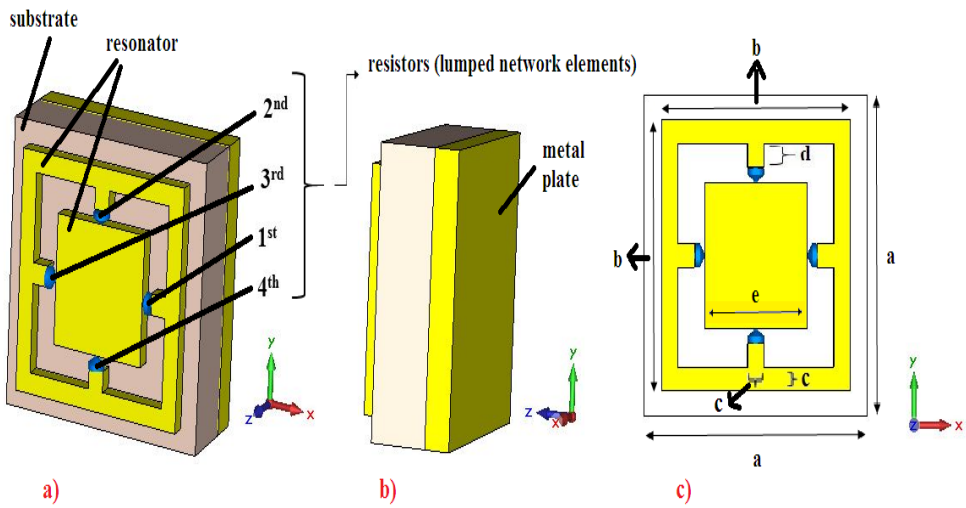

Figure 3-18. (a) Substrate, resonator and resistors, (b) metal plate, (c) dimensions of near perfect metamaterial absorber based energy harvester unit cell structure in sub-THz range.

The thicknesses of the bottom and top metallic layers are 18 and 10 µm, respectively. Also, electrical conductivities of the Silver, Gold and Aluminum are 6.3012×10^{7}, 4.561×10^{7}, 3.56×10^{7} S/m, respectively. Quartz, Polyimide, Teflon, Silicon, Rogers TMM4 and Rogers RT5880 are separately used as six different substrates with Silver, Gold and Aluminum for MA-based energy harvester as shown in Figure 3-18. The thickness of all these substrates is same and equal to 40 µm. The loss tangent, relative

permittivity and relative permeability of the Quartz material are 0.0004, 3.75 and 1, respectively. The loss tangent, relative permittivity and relative permeability of the Polyimide material are 0.0027, 3.5 and 1, respectively. The loss tangent, relative permittivity and relative permeability of the Teflon material are 0.0002, 2.1 and 1, respectively. The loss tangent, relative permittivity and relative permeability of the Silicon material are 0.00025, 11.9 and 1, respectively. The loss tangent, relative permittivity and relative permeability of the Rogers TMM4 material are 0.002, 4.5 and 1, respectively. The loss tangent, relative permittivity and relative permeability of the Rogers RT5880 material are 0.0009, 2.2 and 1, respectively. Dimension values of the design a, b, c, d and e are given as 150, 126, 11, 11 and 68 µm, correspondingly [Figure 3-18c].

3.3.2. Result and Discussion

Numerical reflection and absorption results can be seen in Figure 3-19 (for (Silver (metal plate), Quartz (substrate) and Silver (resonator)) structure). In Figure 3-19, maximum absorption is obtained around 99.94% at 0.694 THz. This value is obtained when four 500 ohm resistor are placed across the gaps as four lumped network elements.

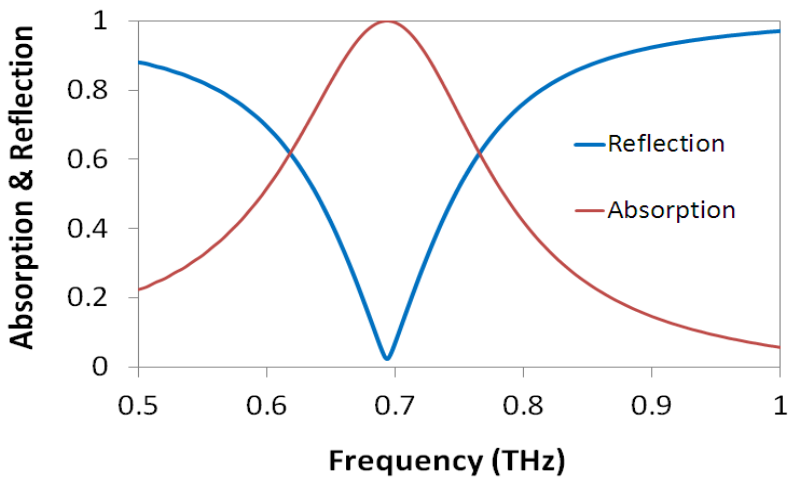

Figure 3-19. Reflectance and absorption results for (Silver (metal plate), Quartz (substrate) and Silver (resonator)) structure (The resonance frequency at 0.694 THz).

Results in Figure 3-20 show that the energies are affected by the resistances. The maximum efficiency is obtained at 500 ohm as seen from Figure 3-20. For all power harvesting simulations, input powers were chosen 0.500 W. The second and fourth lumped network elements (resistors) are located parallel to y-axis (electric field direction) and the first and third lumped network elements (resistors) are located parallel to x-axis (magnetic field direction) is shown in Figure 3-18. Therefore, the effect of the first and third resistors to output power is maximum 1.04% when this percentage compares with the effect of the second and fourth resistors. The output power value of the first resistor is the same with the output power value of the third resistor. The output power value of the second resistor is the same with the output power value of the fourth resistor. This situation can be opposite if electric and magnetic field directions are chosen to be parallel to x- and y-axis, respectively.

In Figure 3-20, maximum efficiency is obtained around 96.60% (output power is 0.483 W) at 0.692 THz at 500 ohm.

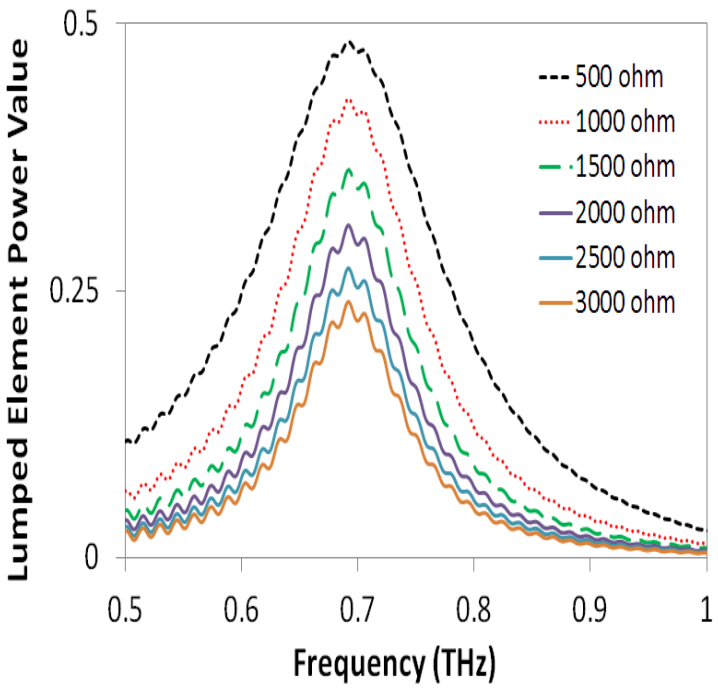

Figure 3-20. Gathered power frequency diagram for selected different resistors between 500-3000 ohm for (Silver (metal plate), Quartz (substrate) and Silver (resonator)) structure.

In order to understand the effect of the metal plate existence, two numerical studies for (Silver (metal plate), Quartz (substrate) and Silver (resonator)) structure are realized with metal plate and without metal plate situations as shown in Figure 3-21. When there is Silver metal plate at the bottom of the design, total lumped network elements` power value is 0.483 W at 0.692 THz at 500 ohm in Figure 3-21. However, this value is decreased to 0.154 W at 0.572 THz at 500 ohm when the metal plate is removed from the structure. Because of the effect of the metal plate on total capacitance value, the harvested power is affected.

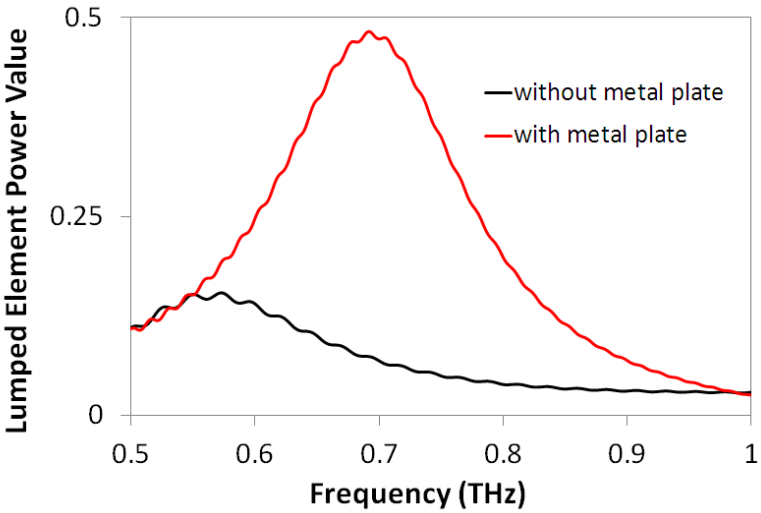

Figure 3-21. Simulated lumped element power magnitude for both cases with and without metal plate for 500 ohm resistor for (Silver (metal plate), Quartz (substrate) and Silver (resonator)) structure.

In Figure 3-22, the electric field and surface current distributions can be seen at the resonance frequency in order to understand better the physical mechanism of the design in power harvesting applications. The concentrations of these distributions are on two gaps of the design where there are resistors because electric field directions are selected to be parallel to y-axis as it is mentioned before. Therefore, the design act as an electric dipole at the resonance frequency. The basis of this is the design can be used as a voltage source because of the confinement of the EM waves at the resonance frequency.

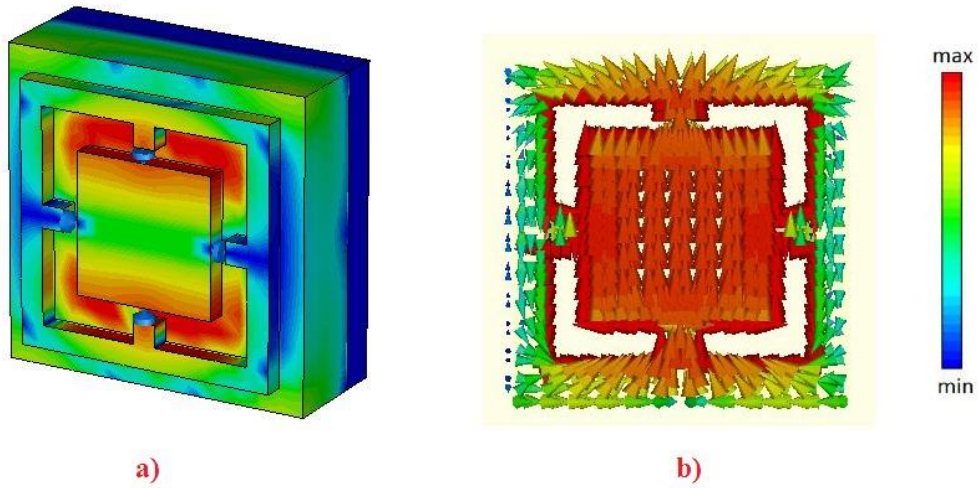

Figure 3-22. For (Silver (metal plate), Quartz (substrate) and Silver (resonator)) structure (a) Electric field distribution at the resonance frequency of 0.694 THz (b) Surface current distribution at the resonance frequency of 0.694 THz.

The relations between different (metal and substrate) materials and lumped element power are given in Figure 3 – 23-28. According to different (metal and substrate) materials, output power, power efficiency and resonance frequency values can be seen in Table 3-1.

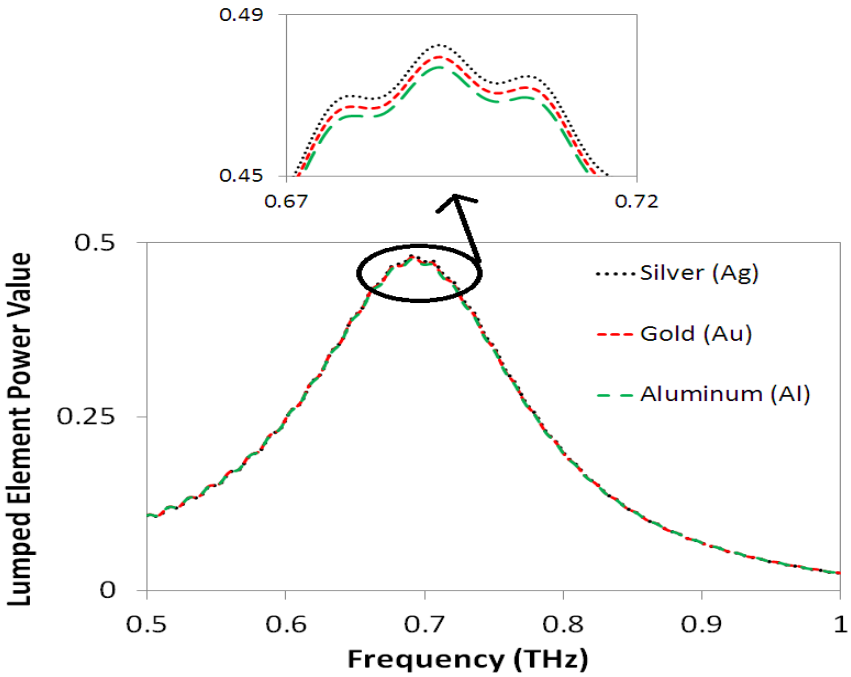

Figure 3-23. Lumped element power value according to different metals with Quartz substrate.

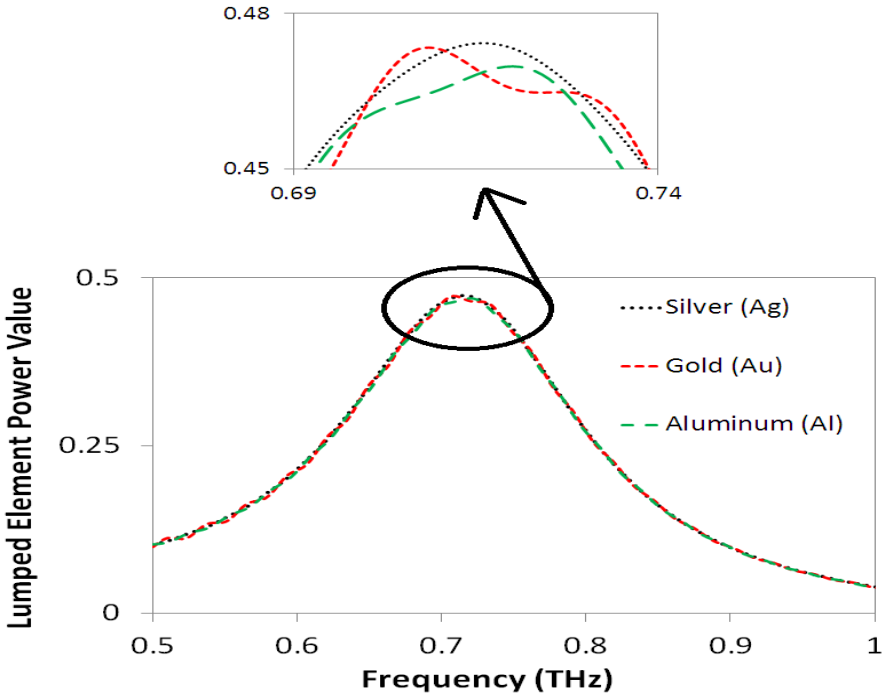

Figure 3-24. Lumped element power value according to different metals with Polyimide substrate.

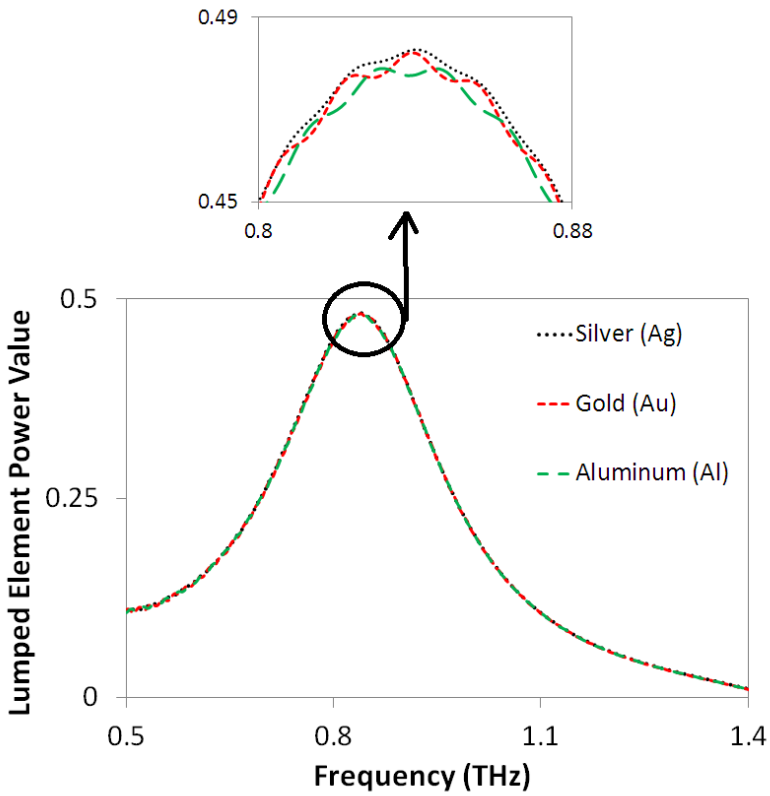

Figure 3-25. Lumped element power value according to different metals with Teflon substrate.

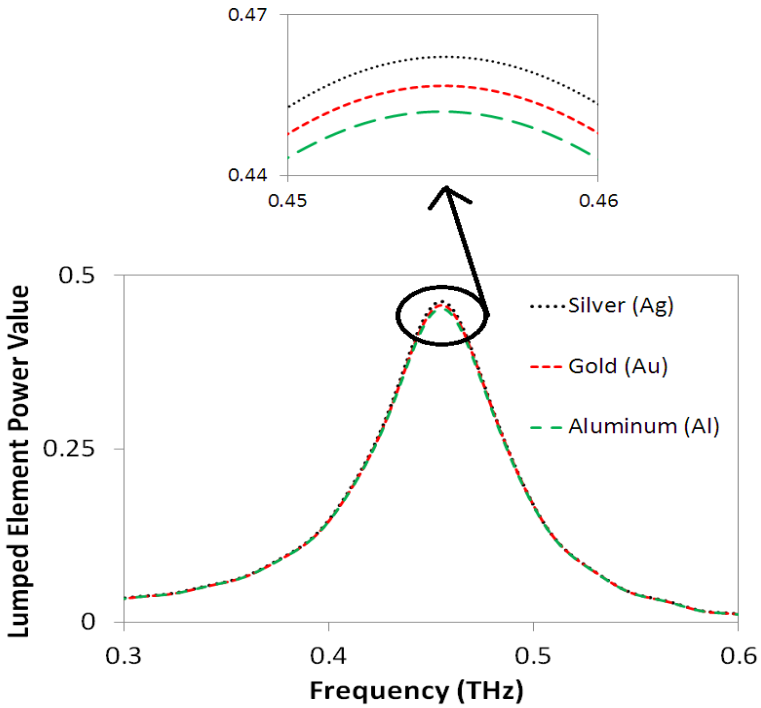

Figure 3-26. Lumped element power value according to different metals with Silicon substrate.

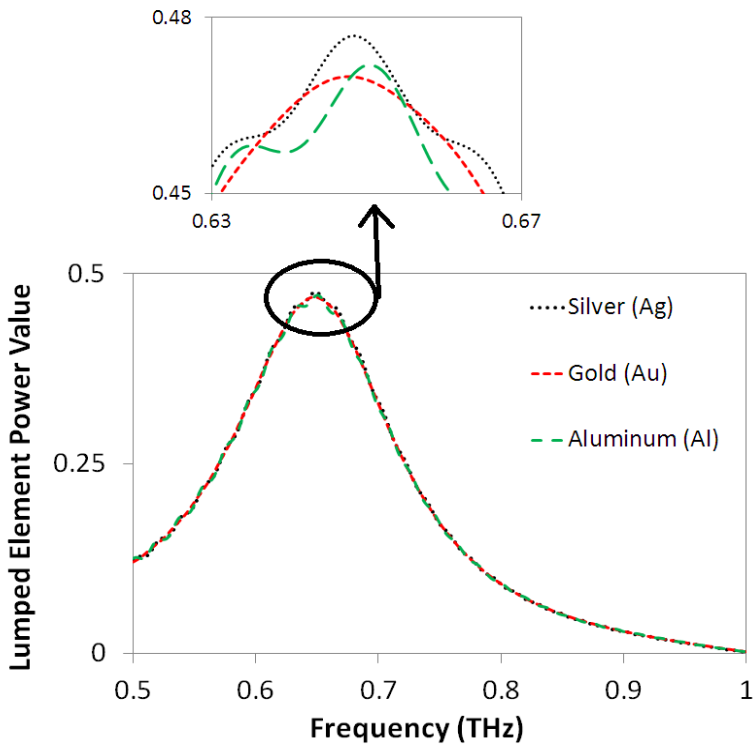

Figure 3-27. Lumped element power value according to different metals with Rogers TMM4 substrate.

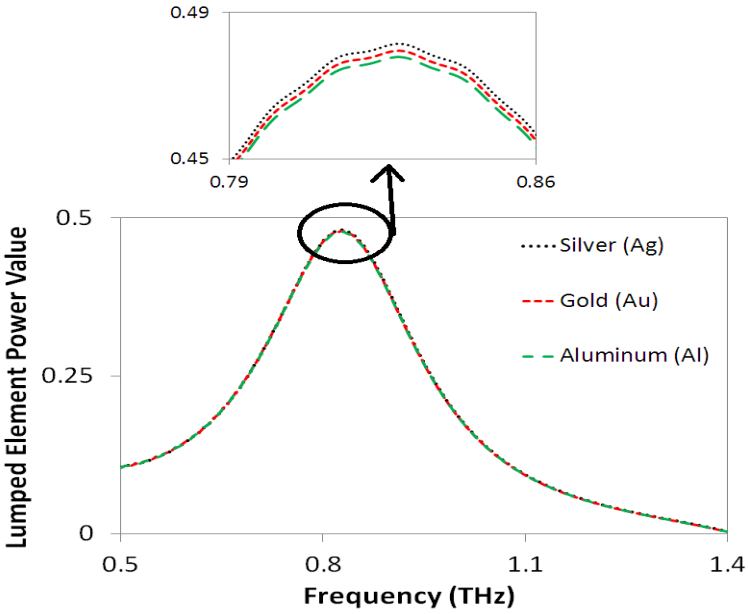

Figure 3-28. Lumped element power value according to different metals with Rogers RT5880 substrate.

Table 3-1. Output power, power efficiency and resonance frequency values according to different substrate and metal materials.

		Silver	Gold	Aluminum
Quartz	Output power (Watt)	0.483	0.480	0.477
	Power efficiency (%)	96.6	96.0	95.4
	Resonance frequency (THz)	0.692	0.692	0.692
Polyimide	Output power (Watt)	0.474	0.473	0.470
	Power efficiency (%)	94.8	94.6	94.0
	Resonance frequency (THz)	0.716	0.708	0.720
Teflon	Output power (Watt)	0.483	0.482	0.479
	Power efficiency (%)	96.6	96.4	95.8
	Resonance frequency (THz)	0.840	0.840	0.832
Silicon	Output power (Watt)	0.462	0.457	0.452
	Power efficiency (%)	92.4	91.4	90.4
	Resonance frequency (THz)	0.455	0.455	0.455
Rogers TMM4	Output power (Watt)	0.477	0.470	0.472
	Power efficiency (%)	95.4	94.0	94.4
	Resonance frequency (THz)	0.648	0.648	0.650
Rogers RT5880	Output power (Watt)	0.482	0.480	0.478
	Power efficiency (%)	96.4	96.0	95.6
	Resonance frequency (THz)	0.828	0.828	0.828

3.4. Single band metamaterial absorber based energy harvester in infrared regime for energy harvesting

3.4.1. Design and Simulation

In Figure 3-29c, the parametric dimensions of the infrared metamaterial absorber based energy harvester structure can be seen. There are four gaps on the resonator. Resistors are located as lumped network elements across the gaps on the resonator. Before selected numerical values of these resistors are specifically chosen, many parametric studies have been done with finite integration technique (FIT)-based numerical simulator. Silver (Palik), Silver (Johnson), Gold (Palik), Gold (Johnson) and Aluminum (Palik) metal elements are separately used at the bottom layer (as metal plate) and top (as resonator) of this structure as five different metallic layers as shown in Figure 3-29a and Figure 3-29b.

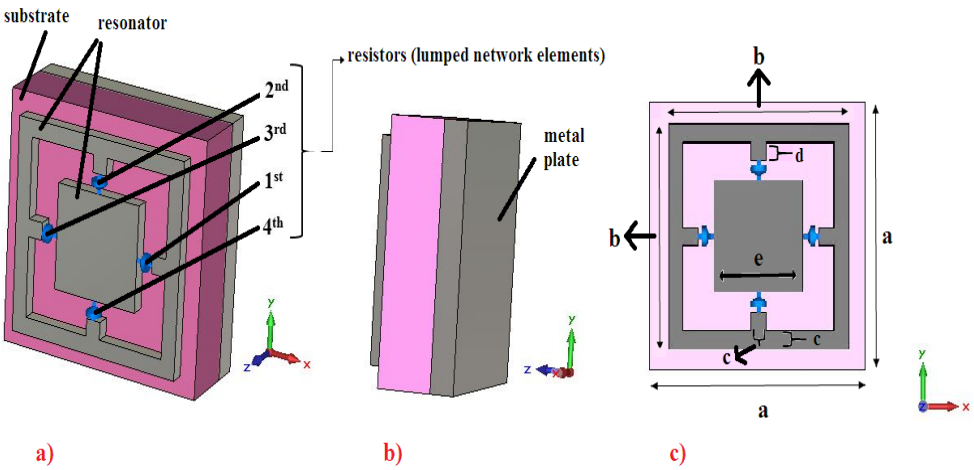

Figure 3-29. (a) Substrate, resonator and resistors, (b) metal plate, (c) dimensions of near perfect metamaterial absorber based energy harvester unit cell structure in infrared range.

The thicknesses of the bottom and top metallic layers are 70 and 40 nm, respectively. Silica (Silicon Dioxide) and Silicon are used as two different substrates with Silver (Palik), Silver (Johnson), Gold (Palik), Gold (Johnson) and Aluminum (Palik) for MA-based energy harvester as shown in Figure 3-29. The thickness of these two substrates is same and equal to 160 nm. The optical properties of Silver (Palik), Gold (Palik) and Aluminum (Palik) metals and Silicon substrate for infrared frequency ranges can be

found in Ref. [59]. The optical properties of Silica dielectric substrate for infrared frequency ranges can be found in Ref. [84]. The optical properties of Silver (Johnson) and Gold (Johnson) metals for infrared frequency ranges can be found in Ref. [85]. Dimension values of the design a, b, c, d and e are given as 650, 550, 45, 45 and 270 nm, correspondingly [Figure 3-29c].

3.4.2. Result and Discussion

Numerical reflectance and absorption results can be seen in Figure 3-30 (for (Silver (Johnson) (metal plate), Silicon (substrate) and Silver (Johnson) (resonator)) structure). In Figure 3-30, maximum absorption is obtained around 99.89% at 96.15 THz. This value is obtained when four 500 ohm resistor are placed across the gaps as four lumped network elements.

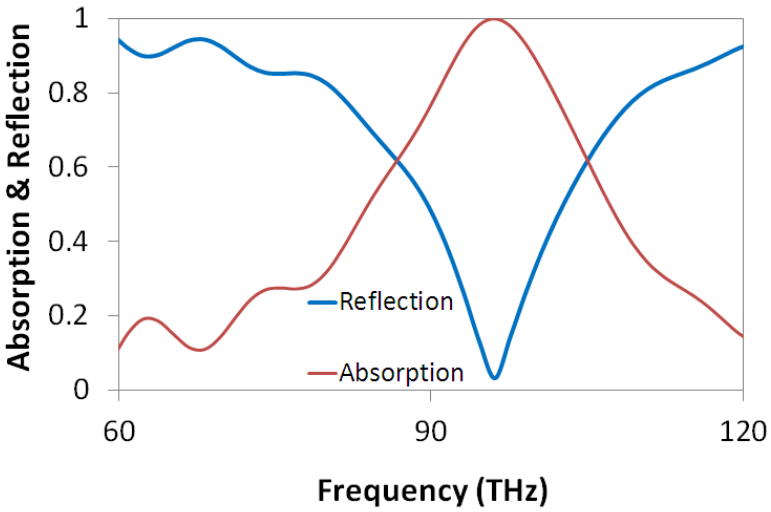

Figure 3-30. Reflectance and absorption results for (Silver (Johnson) (metal plate), Silicon (substrate) and Silver (Johnson) (resonator)) structure (The resonance frequency at 96.15 THz).

Results in Figure 3-31 show that the energies are affected by the resistances. The maximum efficiency is obtained at 500 ohm as seen from Figure 3-31. For all power harvesting simulations, input powers were chosen 0.500 W. The second and fourth lumped network elements (resistors) are located parallel to y-axis (electric field direction) and the first and third lumped network elements (resistors) are located parallel to x-axis (magnetic field direction) is shown in Figure 3-29. Therefore, the effect of the first and third resistors to output power is less than 1% when this

percentage compares with the effect of the second and fourth resistors. The output power value of the first resistor is the same with the output power value of the third resistor. The output power value of the second resistor is the same with the output power value of the fourth resistor. This situation can be opposite if electric and magnetic field directions are chosen to be parallel to x- and y-axis, respectively.

In Figure 3-31, maximum efficiency is obtained around 95.60% (output power is 0.478 W) at 97.62 THz at 500 ohm.

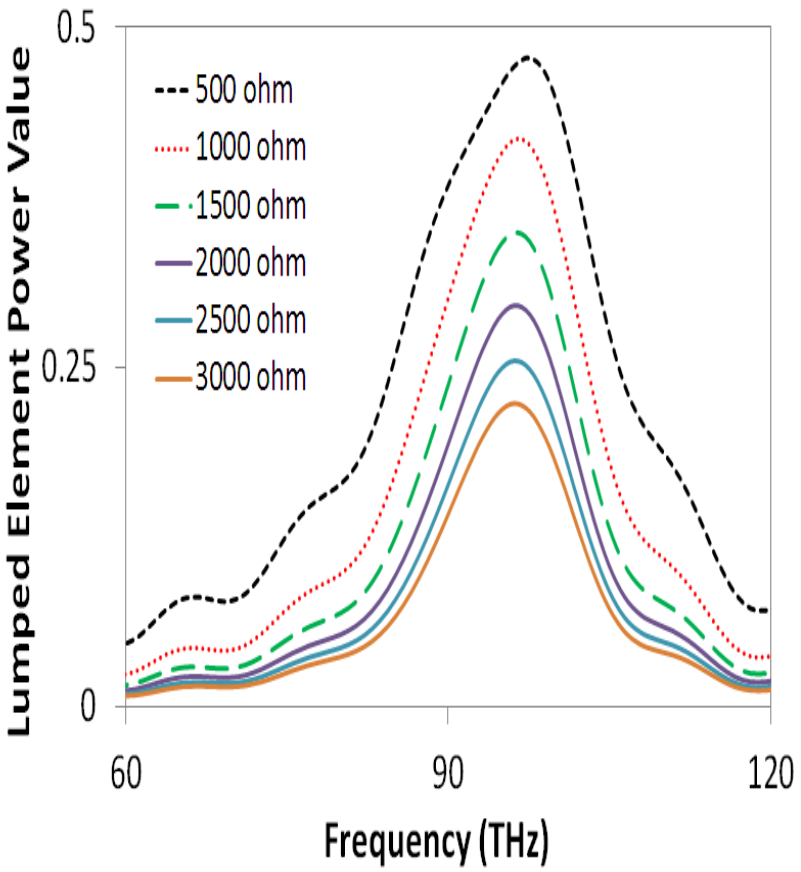

Figure 3-31. Gathered power frequency diagram for selected different resistors between 500-3000 ohm for (Silver (Johnson) (metal plate), Silicon (substrate) and Silver (Johnson) (resonator)) structure.

In order to understand the effect of the metal plate existence, two numerical studies for (Silver (Johnson) (metal plate), Silicon (substrate) and Silver (Johnson) (resonator)) structure are realized with metal plate and without metal plate situations as shown in

Figure 3-32. When there is Silver (Johnson) metal plate at the bottom of the design, total lumped network elements` power value is 0.478 W at 97.62 THz at 500 ohm in Figure 3-32. However, this value is decreased to 0.156 W at 63.81 THz at 500 ohm when the metal plate is removed from the structure. Because of the effect of the metal plate on total capacitance value, the harvested power is affected.

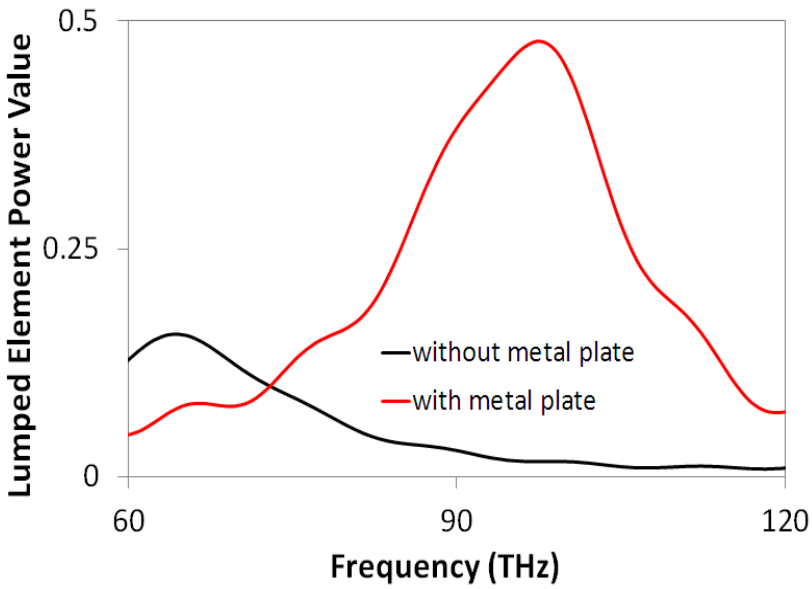

Figure 3-32. Simulated lumped element power magnitude for both cases with and without metal plate for 500 ohm resistor for (Silver (Johnson) (metal plate), Silicon (substrate) and Silver (Johnson) (resonator)) structure.

In Figure 3-33, the electric field, magnetic field and surface current distributions can be seen at the resonance frequency in order to understand better the physical mechanism of the design in power harvesting applications. The concentrations of these distributions are on two gaps of the design where there are resistors because electric field directions are selected to be parallel to y-axis as it is mentioned before. Therefore, the design act as an electric dipole at the resonance frequency. The basis of this is the design can be used as a voltage source because of the confinement of the EM waves at the resonance frequency.

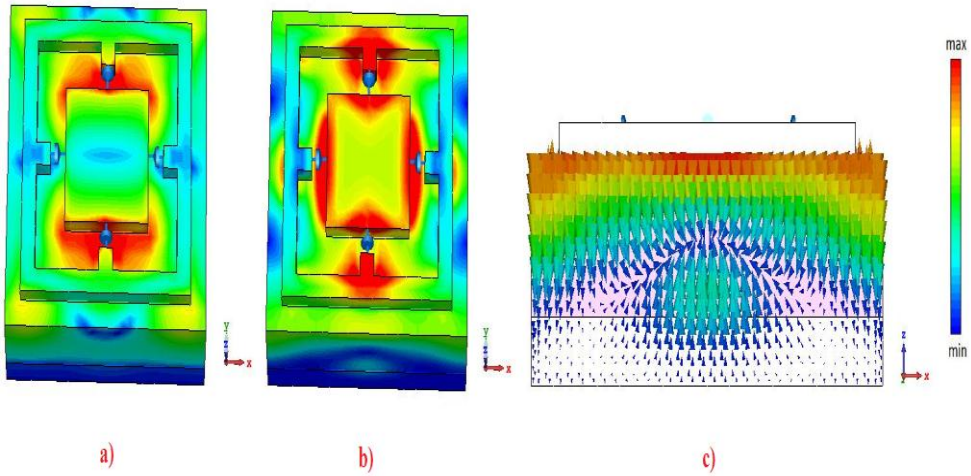

Figure 3-33. For (Silver (Johnson) (metal plate), Silicon (substrate) and Silver (Johnson) (resonator)) structure (a) Electric field distribution at the resonance frequency of 96.15 THz (b) Magnetic field distribution at the resonance frequency of 96.15 THz (c) Surface current distribution at the resonance frequency of 96.15 THz.

The relations between different (metal and substrate) materials and lumped element power are given in Figure 3 – 34-35. According to different (metal and substrate) materials, output power, power efficiency and resonance frequency values can be seen in Table 3-2.

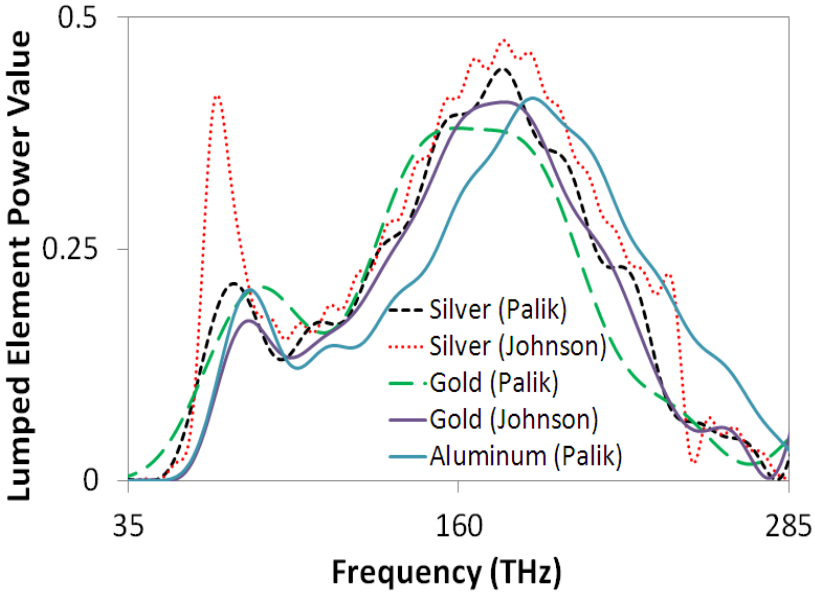

Figure 3-34. Lumped element power value according to different metals with Silica (Silicon Dioxide) substrate.

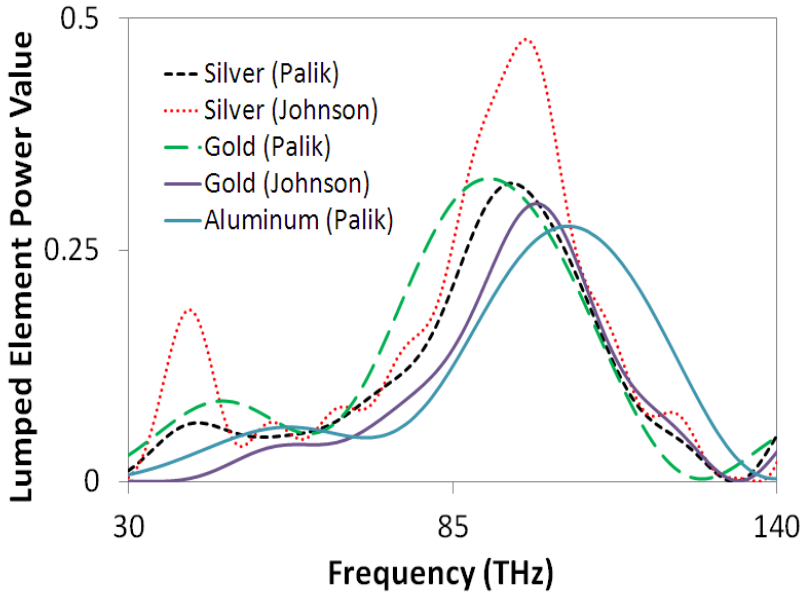

Figure 3-35. Lumped element power value according to different metals with Silicon substrate.

Table 3-2. Output power, power efficiency and resonance frequency values according to different substrate and metal materials.

		Silica	Silicon
Silver (Palik)	Output power (Watt)	0.445	0.322
	Power efficiency (%)	89.0	64.4
	Resonance frequency (THz)	177.00	94.68
Silver (Johnson)	Output power (Watt)	0.476	0.478
	Power efficiency (%)	95.2	95.6
	Resonance frequency (THz)	177.00	97.62
Gold (Palik)	Output power (Watt)	0.380	0.327
	Power efficiency (%)	76.0	65.4
	Resonance frequency (THz)	159.36	91.74
Gold (Johnson)	Output power (Watt)	0.409	0.300
	Power efficiency (%)	81.8	60.0
	Resonance frequency (THz)	177.00	99.09
Aluminum (Palik)	Output power (Watt)	0.413	0.276
	Power efficiency (%)	82.6	55.2
	Resonance frequency (THz)	188.76	104.97

3.5. Conclusion

In this chapter, high absorptions and lumped network element powers are obtained in microwave (GHz), sub-THz and infrared frequency regimes for metamaterial absorber

based energy harvesters. Also, reflection, parametric studies and field distributions can be seen above. Numerical results show that the usage of near perfect metamaterial absorbers can be efficient and easy for electromagnetic energy harvesters. Proposed structures can be used for many application such as antennas, EM filters, sensors, THz imaging systems, infrared spectroscopy, infrared cameras, solar cells.

CHAPTER 4

TOPOLOGICAL STUDY OF ENERGY HARVESTING OF METAMATERIAL ABSORBER FOR MICROWAVE, SUB-TERAHERTZ, AND INFRARED FREQUENCY REGIONS

4.1. Introduction

Although different dimensions and working frequency regimes, designs have a similar view in this chapter. The aim of this chapter is to understand effects of quantities of resonators and resistors by changing two parametric dimension sizes. For example, Gajibo *et al.* [86] numerically presented the effect of four small circular rings with a bigger circular ring patch on a metamaterial absorber in x-band operations. Metamaterial absorber based energy harvesters are analysed in microwave (GHz), sub-THz and infrared frequency regions in Section 4.2, Section 4.3 and Section 4.4, respectively.

4.2. Single band metamaterial absorber based energy harvester topology in microwave (GHz) regime for energy harvesting

4.2.1. Design and Simulation

In Figure 4-1c, the parametric dimensions of the microwave (GHz) metamaterial absorber based energy harvester structure can be seen. Fifteen resonators and fourteen resistors (1st – 14th) are exist. Resistors are located as lumped network elements across the gaps between middle rectangle shape resonator and other square shape resonators. Before selected numerical values of these resistors are specifically chosen, many parametric studies have been done with finite integration technique (FIT)-based numerical simulator. Copper metal element is used at the bottom layer (as a metal plate) and top (as resonators) of this structure as metallic layers as shown in Figure 4-1a and Figure 4-1b. Aim of the metal plate (as shown Figure 4-1b) on back side of the structure is the realization of approximately zero transmission ($T(\omega)$) as it is mentioned before in previous chapters. Aim of the resonator (as shown Figure 4-1a) on front side of the structure is the minimization of the reflection as it is mentioned before in previous chapters. Thicknesses are same and equal to 0.035 mm for both bottom and top metallic layers. Also, electrical conductivity of the copper is 5.8001×10^{7} S/m.

Rogers RT 5880 is used as a substrate with copper metal for metamaterial absorber based energy harvester as shown in Figure 4-1. The thickness, loss tangent, relative permittivity and relative permeability of the Rogers RT 5880 substrate material are 1.6 mm, 0.0009, 2.2 and 1, respectively. Dimension values of the (Copper, Rogers RT 5880 and Copper) structure a, b, c, d and w are given as 77, 30, 72, 9, 1.5 mm, correspondingly [Figure 4-1c]. Along the x- and y- directions, the magnetic and electric field components of the incident plane wave are polarized, respectively [60 – 62].

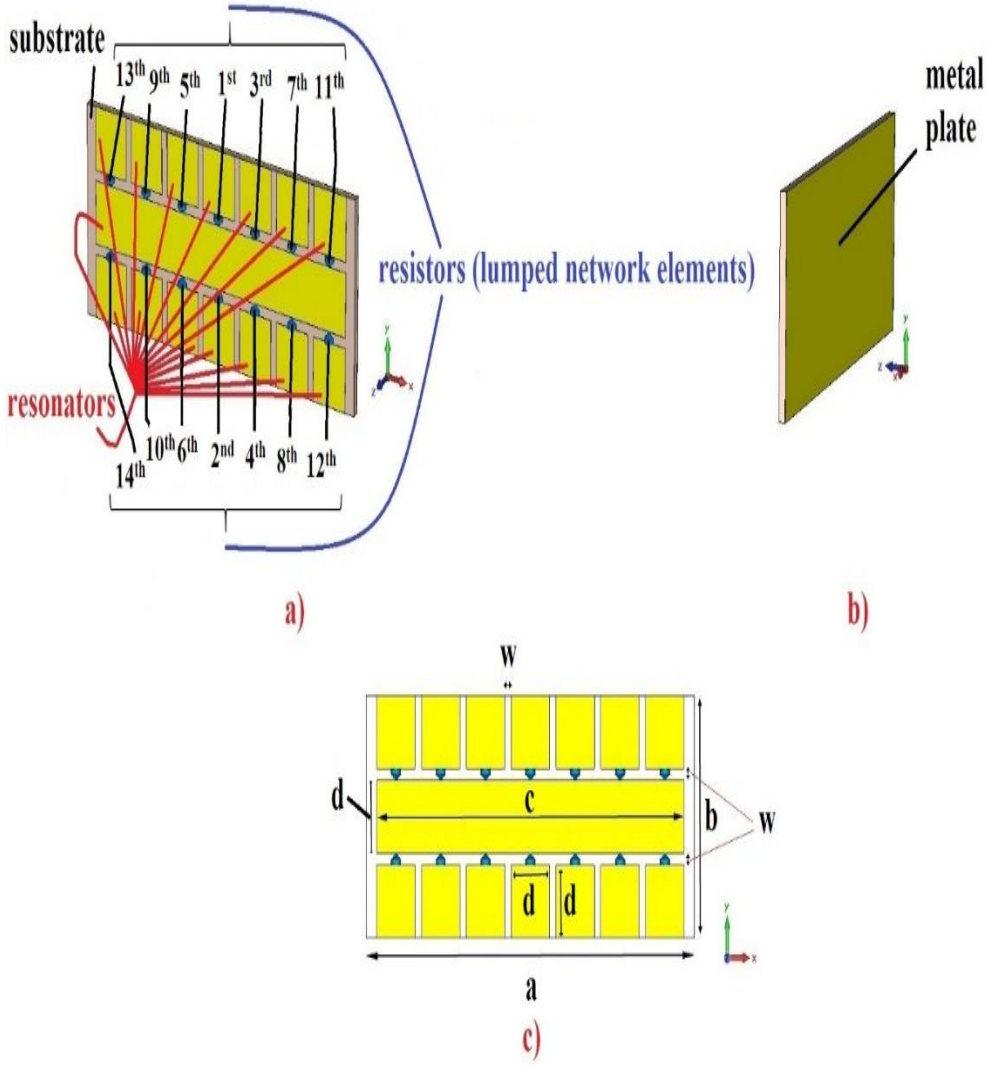

Figure 4-1. (a) Substrate, resonators and resistors, (b) metal plate, (c) dimensions of near perfect metamaterial absorber based energy harvester unit cell structure in microwave (GHz) range.

4.2.2. Result and Discussion

Numerical reflectance and absorption result can be seen in Figure 4-2 (for (Copper (metal plate), Rogers RT 5880 (substrate) and Copper (resonator)) structure). In Figure 4-2, maximum absorption is obtained around 99.53% at 4.800 GHz. This value is obtained when fourteen 500 ohm resistors are placed across the gaps between middle rectangle shape resonator and other resonators as fourteen lumped network elements.

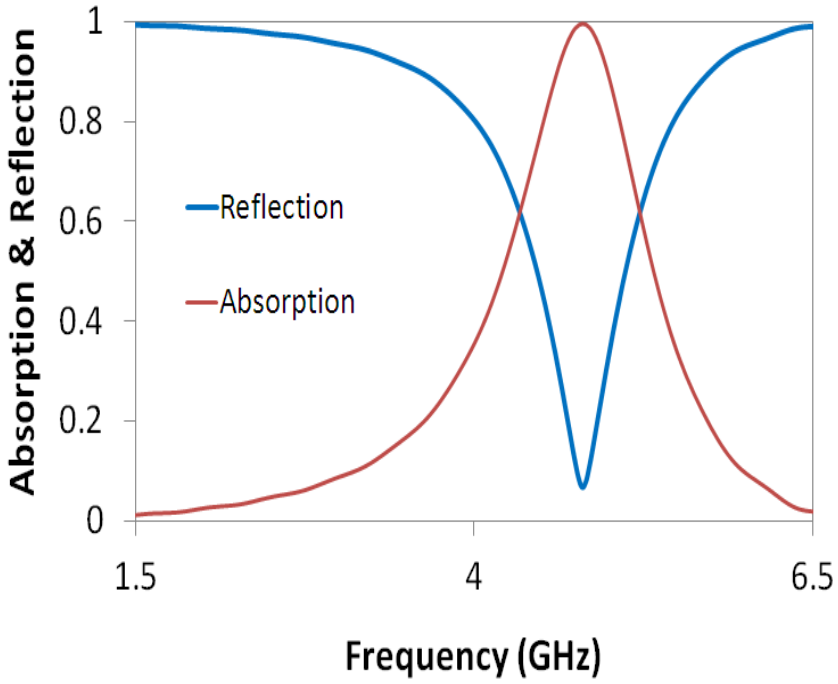

Figure 4-2. Reflectance and absorption result for (Copper (metal plate), Rogers RT 5880 (substrate) and Copper (resonator)) structure (The resonance frequency at 4.800 GHz).

Results in Figure 4-3 show that the energies are affected by the resistances. The maximum efficiency is obtained at 500 ohm as seen from Figure 4-3. For all power harvesting simulations, input powers were chosen 0.500 W. Fourteen lumped network elements (resistors) are located parallel to y-axis (electric field direction) is shown in Figure 4-1. In Figure 4-3, maximum efficiency is obtained around 98.80% (output power is 0.494 W) at 4.800 GHz at 500 ohm.

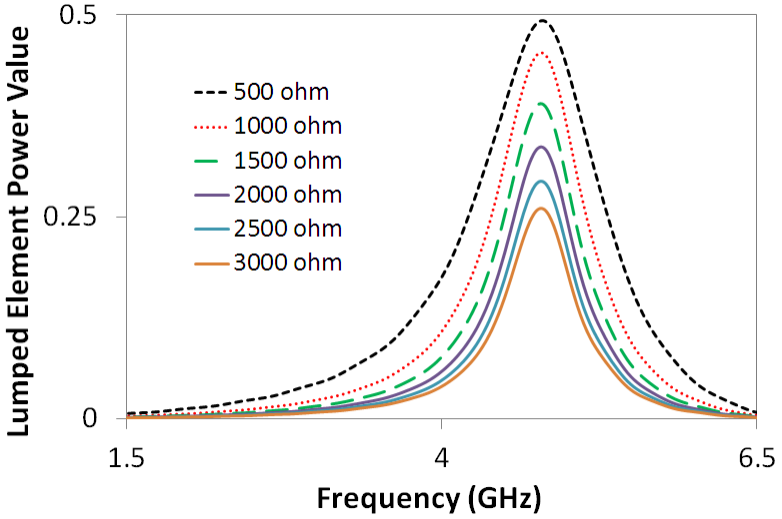

Figure 4-3. Gathered power frequency diagram for selected different resistors between 500-3000 ohm for (Copper (metal plate), Rogers RT 5880 (substrate) and Copper (resonator)) structure.

In Figure 4-4, views from the top, reflection, absorption, and Lumped element power values are shown for ten different geometric designs at 500 ohm when (n) resonators and (n-1) resistors are exist. “n” means any exact number, which is shown quantities of resonators. Quantities of resistors (n-1) are less one than quantities of resonators. Also, changed geometric parameters are separately given left side of each design in Figure 4-4. Structures are designed and analysed with increasing quantities of resonators and resistors, so dimensions are changed according to these quantities. Effects of increasing quantities of resonators and resistors with different “a” and “c” dimension values of designs can be seen in Figure 4-4. Although resonance frequency (4.800 GHz) is shifting lower (left side) or higher (right side) value between 1.5 and 6.5 GHz frequency range, both the highest absorption (the lowest reflectance) and the highest lumped element power value are obtained in Figure 4-4j2 and Figure 4-4j3 as percentages for the structure in Figure 4-4j1. The reasons of these good results are the impedance of free – space matches with the frequency dependent effective impedance of the metamaterial absorber [44, 83] and effectiveness between resonators. Absorption and resonance frequency values, which are received from the results in Figure 4-4, are given in Table 4-1. Output power, power efficiency and resonance frequency values, which are received from the results in Figure 4-4, are given in Table 4-2.

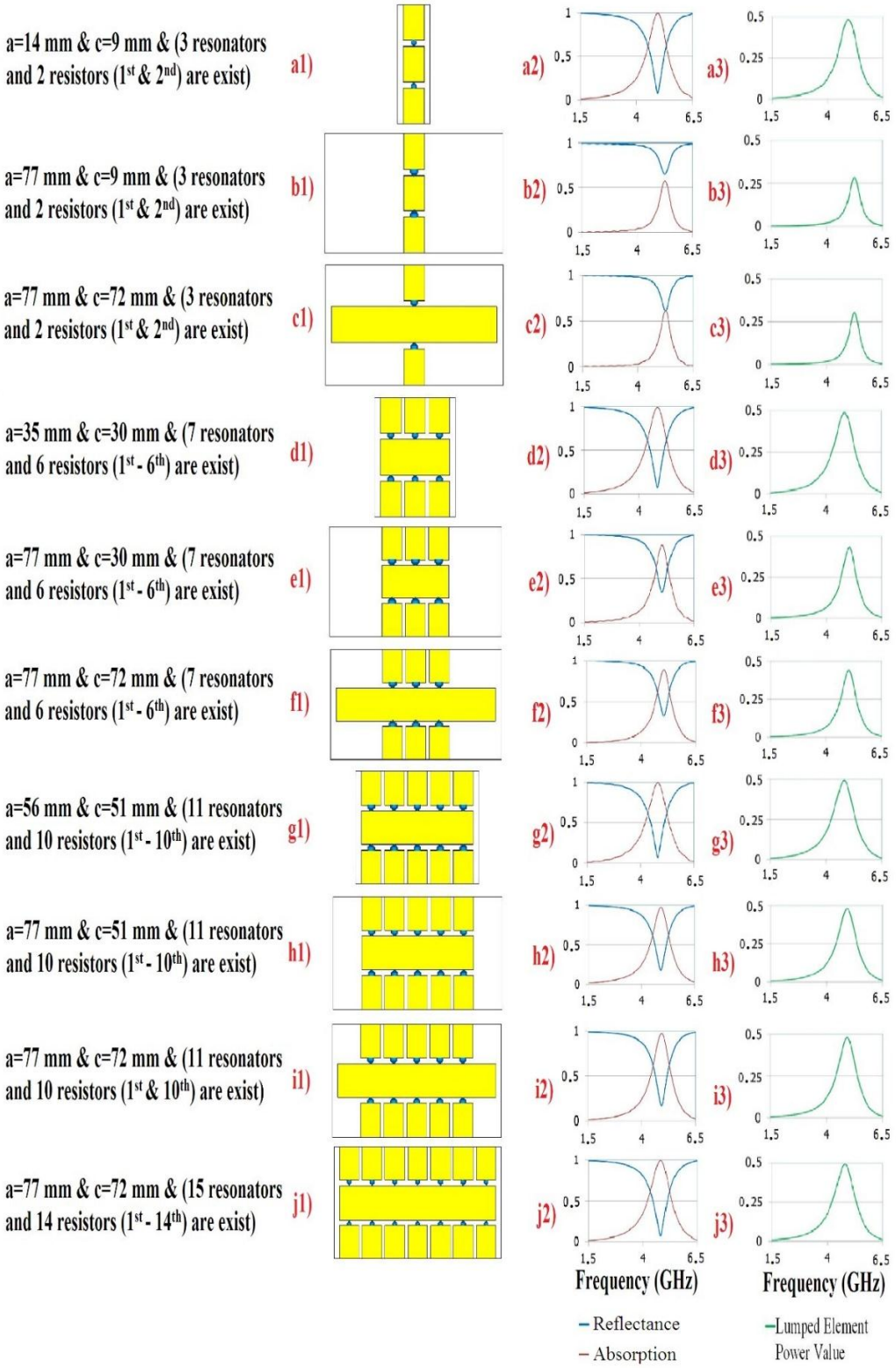

Figure 4-4. When (n) resonators and (n-1) resistors are exist, (a1 - j1) views from the top, (a2 – j2) reflectance and absorption results, and (a3 – j3) Lumped element power values for different geometric designs at 500 ohm (Changed geometric parameters are separately given left side of each design).

Table 4-1. Absorption and resonance frequency values (which are received from the results in Figure 4-4).

a (mm)	c (mm)	Quantities of resonators (n)	Quantities of resistors (n-1)	Structure from Figure	Results from Figure		
14	9	3	2	4-4a1	4-4a2	**Absorption (%)**	99.37
						Resonance frequency (GHz)	4.950
77	9	3	2	4-4b1	4-4b2	**Absorption (%)**	57.83
						Resonance frequency (GHz)	5.250
77	72	3	2	4-4c1	4-4c2	**Absorption (%)**	61.63
						Resonance frequency (GHz)	5.250
35	30	7	6	4-4d1	4-4d2	**Absorption (%)**	99.43
						Resonance frequency (GHz)	4.850
77	30	7	6	4-4e1	4-4e2	**Absorption (%)**	87.85
						Resonance frequency (GHz)	5.050
77	72	7	6	4-4f1	4-4f2	**Absorption (%)**	89.05
						Resonance frequency (GHz)	5.025
56	51	11	10	4-4g1	4-4g2	**Absorption (%)**	99.46
						Resonance frequency (GHz)	4.800
77	51	11	10	4-4h1	4-4h2	**Absorption (%)**	96.89
						Resonance frequency (GHz)	4.925
77	72	11	10	4-4i1	4-4i2	**Absorption (%)**	97.18
						Resonance frequency (GHz)	4.925
77	72	15	14	4-4j1	4-4j2	**Absorption (%)**	99.53
						Resonance frequency (GHz)	4.800

Table 4-2. Output power, power efficiency and resonance frequency values (which are received from the results in Figure 4-4).

a (mm)	c (mm)	Quantities of resonators (n)	Quantities of resistors (n-1)	Structure from Figure	Results from Figure		
14	9	3	2	4-4a1	4-4a3	**Output power (Watt)**	0.483
						Power efficiency (%)	96.60
						Resonance frequency (GHz)	4.950
77	9	3	2	4-4b1	4-4b3	**Output power (Watt)**	0.283
						Power efficiency (%)	56.60
						Resonance frequency (GHz)	5.250
77	72	3	2	4-4c1	4-4c3	**Output power (Watt)**	0.302
						Power efficiency (%)	60.40
						Resonance frequency (GHz)	5.250
35	30	7	6	4-4d1	4-4d3	**Output power (Watt)**	0.488
						Power efficiency (%)	97.60
						Resonance frequency (GHz)	4.825
77	30	7	6	4-4e1	4-4e3	**Output power (Watt)**	0.433
						Power efficiency (%)	86.60
						Resonance frequency (GHz)	5.050
77	72	7	6	4-4f1	4-4f3	**Output power (Watt)**	0.437
						Power efficiency (%)	87.40
						Resonance frequency (GHz)	5.050
56	51	11	10	4-4g1	4-4g3	**Output power (Watt)**	0.492
						Power efficiency (%)	98.40
						Resonance frequency (GHz)	4.800
77	51	11	10	4-4h1	4-4h3	**Output power (Watt)**	0.477
						Power efficiency (%)	95.40
						Resonance frequency (GHz)	4.925
77	72	11	10	4-4i1	4-4i3	**Output power (Watt)**	0.479
						Power efficiency (%)	95.80
						Resonance frequency (GHz)	4.925
77	72	15	14	4-4j1	4-4j3	**Output power (Watt)**	0.494
						Power efficiency (%)	98.80
						Resonance frequency (GHz)	4.800

For (Copper (metal plate), Rogers RT 5880 (substrate) and Copper (resonator)) structure, which can be seen in either Figure 4-1 or Figure 4-4j1 because the same structure is shown in both Figures, two numerical studies are achieved with metal plate and without metal plate situations as shown in Figure 4-5 in order to see the effects of metal plate existence. In Figure 4-5, total lumped elements` powers` values are 0.494 W at 4.800 GHz at 500 ohm when there is copper metal plate at the bottom of the structure. However, total lumped elements` powers` value is decreased when the metal plate is removed from the structure. The harvested power is directly affected by metal plate due to the effects of the metal plate on total capacitance value.

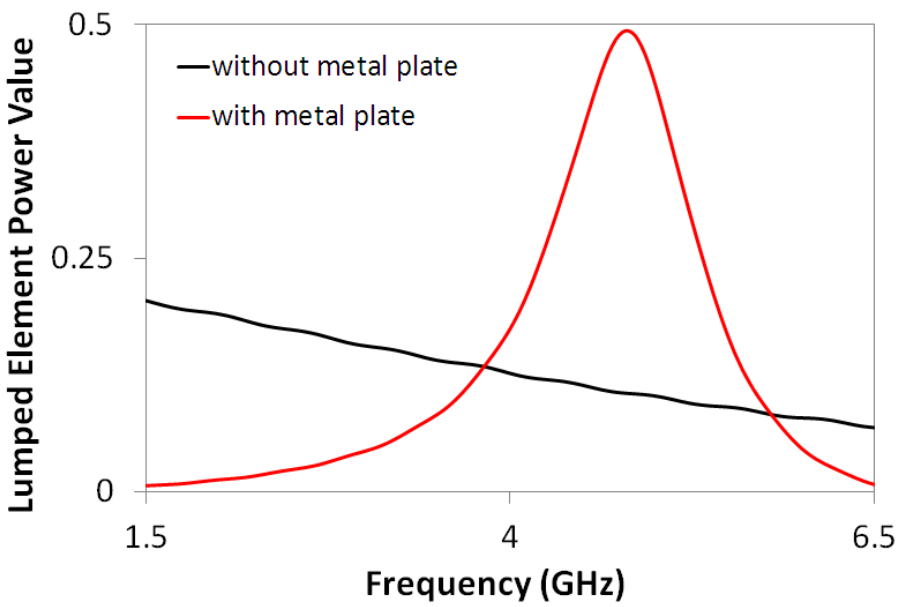

Figure 4-5. Simulated lumped element power magnitude for both cases with and without metal plate for 500 ohm resistor for (Copper (metal plate), Rogers RT 5880 (substrate) and Copper (resonator)) structure (This structure can be seen in either Figure 4-1 or Figure 4-4j1 because the same structure is shown in both Figures.).

The electric field, magnetic field, and surface current distributions are given in Figure 4-6 at the resonance frequency in order to understand better the physical mechanism of (Copper (metal plate), Rogers RT 5880 (substrate) and Copper (resonator)) structure (This structure can be seen in either Figure 4-1 or Figure 4-4j1 because the same

structure is shown in both Figures) in power harvesting applications. The concentrations of these distributions are on gaps and some parts of resonators of the designed structure where there are resistors because electric field directions are chosen to be parallel to y-axis as it is mentioned before. The basis of this is the design can be used as a voltage source due to the confinement of the EM waves at the resonance frequency.

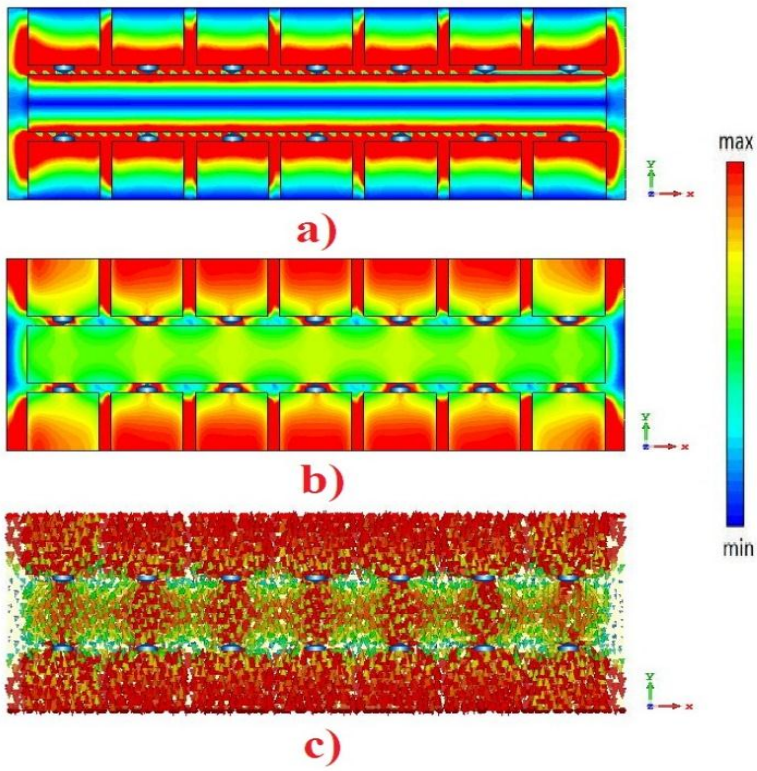

Figure 4-6. For (Copper (metal plate), Rogers RT 5880 (substrate) and Copper (resonator)) structure (This structure can be seen in either Figure 4-1 or Figure 4-4j1 because the same structure is shown in both Figures.) (a) Electric field distribution (b) Magnetic field distribution (c) Surface current distribution at the resonance frequency of 4.800 GHz at 500 ohm.

4.3. Single band metamaterial absorber based energy harvester topology in sub-THz regime for energy harvesting

4.3.1. Design and Simulation

In Figure 4-7b1 and Figure 4-7b2, the parametric dimensions of the sub-THz metamaterial absorber based energy harvester structure can be seen. Fifteen resonators and fourteen resistors (1st – 14th) are exist. Resistors are located as lumped network

elements across the gaps between middle rectangle shape resonator and other square shape resonators. Before selected numerical values of these resistors are specifically chosen, many parametric studies have been done with finite integration technique (FIT)-based numerical simulator. Silver metal element is used at the bottom layer (as a metal plate) and top (as resonators) of this structure as metallic layers as shown in Figure 4-7a. Aim of the metal plate (as shown Figure 4-7a) on back side of the structure is the realization of approximately zero transmission (T(ω)) as it is mentioned before. Aim of the resonator (as shown Figure 4-7a) on front side of the structure is the minimization of the reflection as it is mentioned before. Electrical conductivity of the silver is 6.3012×10^{7} S/m. Quartz is used as a substrate with silver metal for metamaterial absorber based energy harvester as shown in Figure 4-7. The loss tangent, relative permittivity and relative permeability of the Quartz substrate material are 0.0004, 3.75 and 1, respectively. Dimension values of the (Silver, Quartz and Silver) structure a, b, c, d, e, f, g, m, n and p are given as 120, 50, 114, 12, 5, 6, 10, 30, 35 and 22 μm, correspondingly [Figure 4-7b1 and Figure 4-7b2]. Along the x- and y-directions, the magnetic and electric field components of the incident plane wave are polarized, respectively [60 – 62].

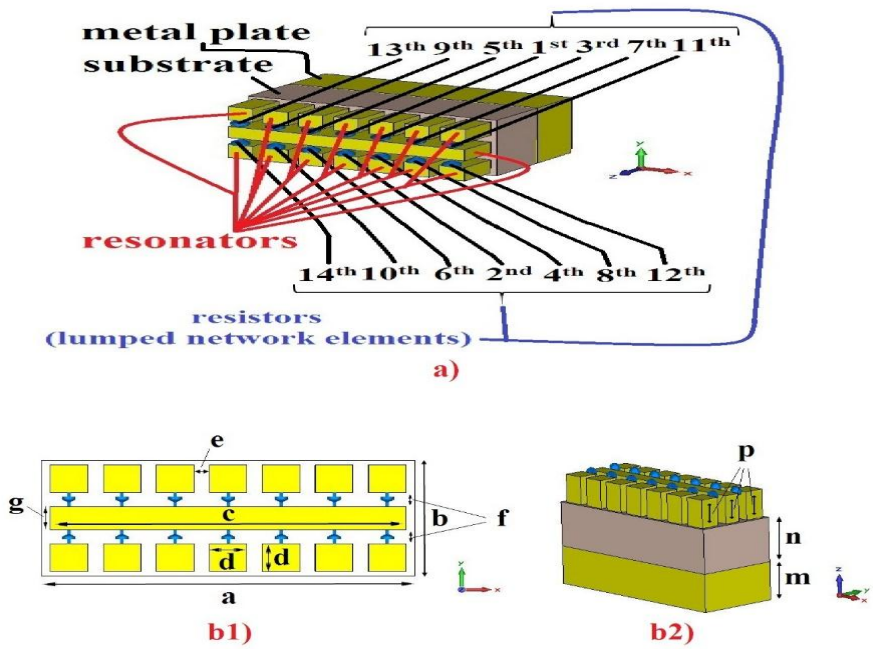

Figure 4-7. (a) Substrate, metal plate, resonators and resistors, (b1 and b2) dimensions of near perfect metamaterial absorber based energy harvester unit cell structure in sub-THz range.

4.3.2. Result and Discussion

Numerical reflectance and absorption result can be seen in Figure 4-8 (for (Silver (metal plate), Quartz (substrate) and Silver (resonator)) structure). In Figure 4-8, maximum absorption is obtained around 99.79% at 0.5595 THz. This value is obtained when fourteen 300 ohm resistors are placed across the gaps between middle rectangle shape resonator and other resonators as fourteen lumped network elements.

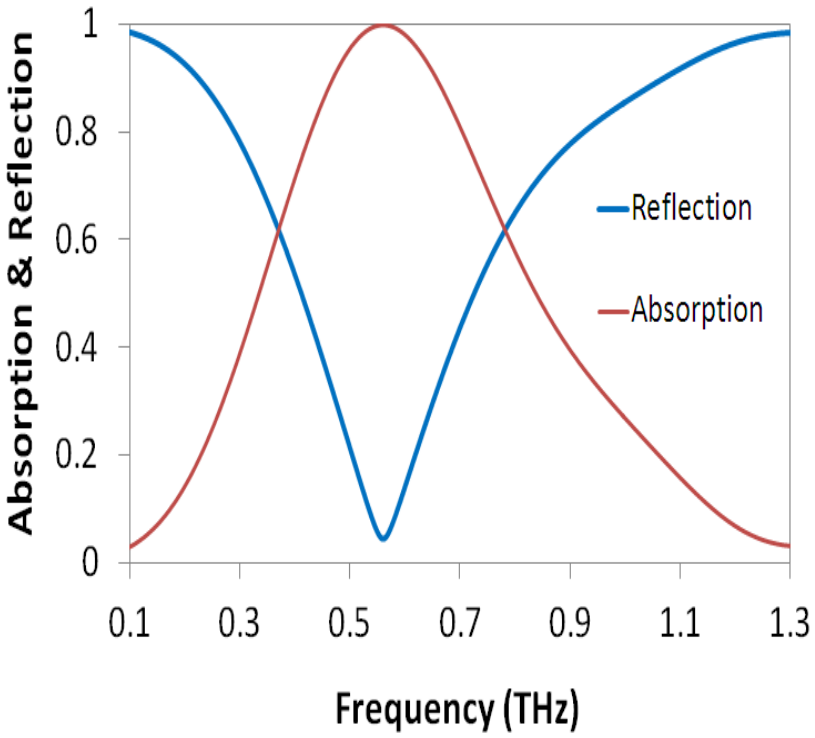

Figure 4-8. Reflectance and absorption result for (Silver (metal plate), Quartz (substrate) and Silver (resonator)) structure (The resonance frequency at 0.5595 THz).

Results in Figure 4-9 show that the energies are affected by the resistances. The maximum efficiency is obtained at 300 ohm as seen from Figure 4-9. For all power harvesting simulations, input powers were chosen 0.500 W. Fourteen lumped network elements (resistors) are located parallel to y-axis (electric field direction) is shown in Figure 4-7. In Figure 4-9, maximum efficiency is obtained around 96.60% (output power is 0.483 W) at 0.5580 THz at 300 ohm.

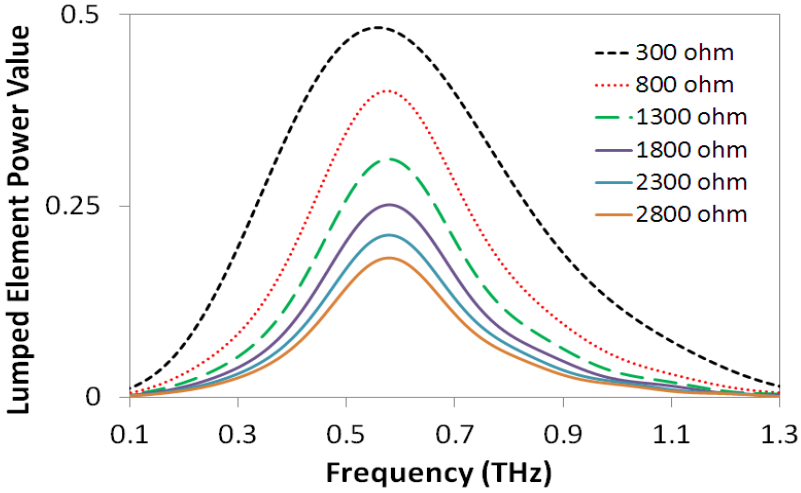

Figure 4-9. Gathered power frequency diagram for selected different resistors between 300-2800 ohm for (Silver (metal plate), Quartz (substrate) and Silver (resonator)) structure.

In Figure 4-10, views from the top, reflectance, absorption, and Lumped element power values are shown for ten different geometric designs at 300 ohm when (n) resonators and (n-1) resistors are exist. “n” means any exact number, which is shown quantities of resonators. Quantities of resistors (n-1) are less one than quantities of resonators. Also, changed geometric parameters are separately given left side of each design in Figure 4-10. Structures are designed and analysed with increasing quantities of resonators and resistors, so dimensions are changed according to these quantities. Effects of increasing quantities of resonators and resistors with different “a” and “c” dimension values of designs can be seen in Figure 4-10. Although resonance frequency (0.5595 THz for absorption and 0.5580 THz for lumped element power value) is shifting lower (left side) or higher (right side) value between 0.1 and 1.3 THz frequency range, both the highest absorption (the lowest reflectance) and the highest lumped element power value are obtained in Figure 4-10j2 and Figure 4-10j3 as percentages for the structure in Figure 4-10j1. The reasons of these good results are the impedance of free – space matches with the frequency dependent effective impedance of the metamaterial absorber [44, 83] and effectiveness between resonators. Absorption and resonance frequency values, which are received from the results in Figure 4-10, are given in Table 4-3. Output power, power efficiency and resonance frequency values, which are received from the results in Figure 4-10, are given in Table 4-4.

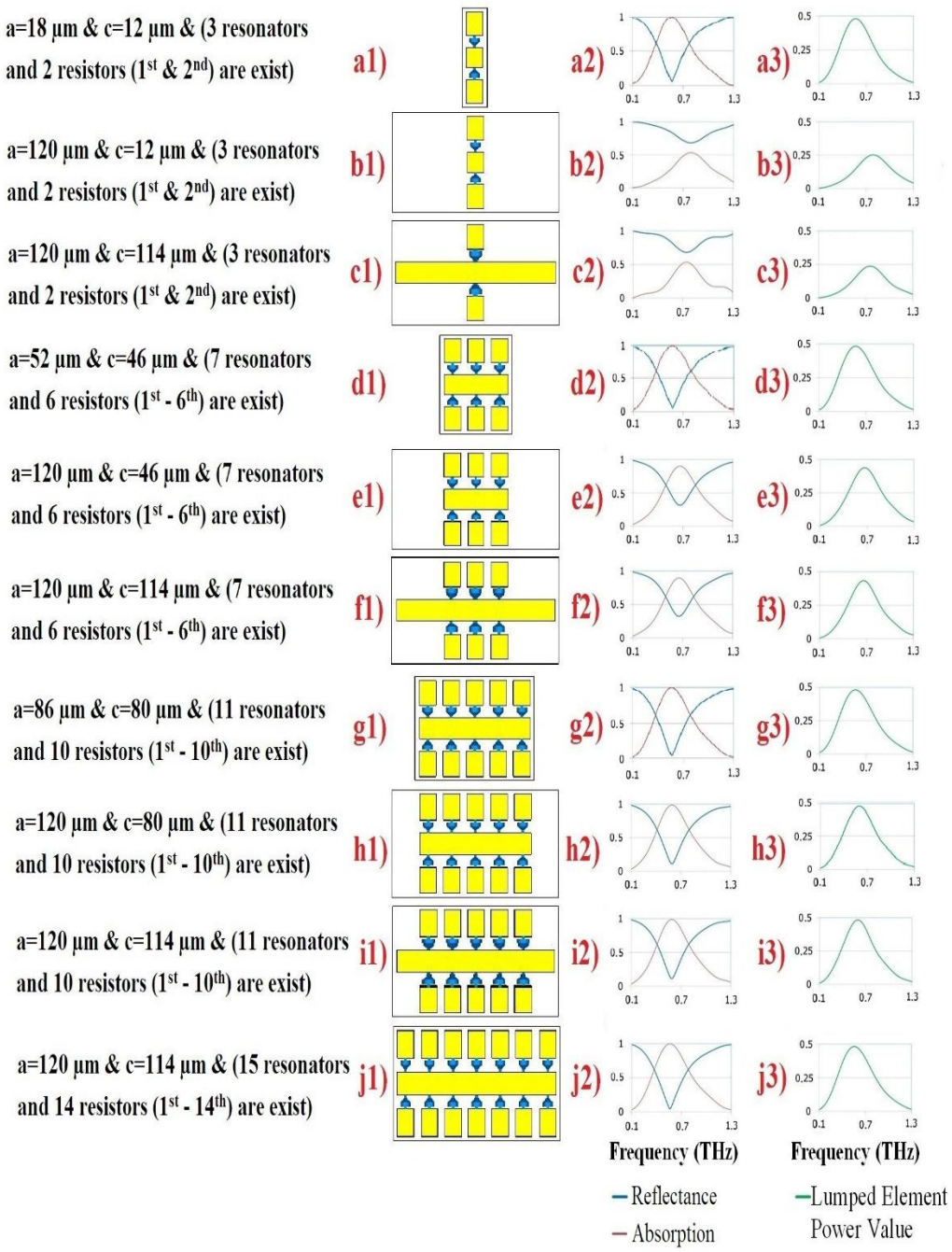

Figure 4-10. When (n) resonators and (n-1) resistors are exist, (a1 - j1) views from the top, (a2 – j2) reflectance and absorption results, and (a3 – j3) Lumped element power values for different geometric designs at 300 ohm (Changed geometric parameters are separately given left side of each design).

Table 4-3. Absorption and resonance frequency values (which are received from the results in Figure 4-10).

a (µm)	c (µm)	Quantities of resonators (n)	Quantities of resistors (n-1)	Structure From Figure	Results from Figure		
18	12	3	2	4-10a1	4-10a2	**Absorption (%)**	99.75
						Resonance frequency (THz)	0.5655
120	12	3	2	4-10b1	4-10b2	**Absorption (%)**	53.58
						Resonance frequency (THz)	0.7875
120	114	3	2	4-10c1	4-10c2	**Absorption (%)**	53.51
						Resonance frequency (THz)	0.7440
52	46	7	6	4-10d1	4-10d2	**Absorption (%)**	99.78
						Resonance frequency (THz)	0.5670
120	46	7	6	4-10e1	4-10e2	**Absorption (%)**	90.09
						Resonance frequency (THz)	0.6660
120	114	7	6	4-10f1	4-10f2	**Absorption (%)**	89.45
						Resonance frequency (THz)	0.6540
86	80	11	10	4-10g1	4-10g2	**Absorption (%)**	99.73
						Resonance frequency (THz)	0.5625
120	80	11	10	4-10h1	4-10h2	**Absorption (%)**	98.75
						Resonance frequency (THz)	0.5910
120	114	11	10	4-10i1	4-10i2	**Absorption (%)**	98.70
						Resonance frequency (THz)	0.5895
120	114	15	14	4-10j1	4-10j2	**Absorption (%)**	99.79
						Resonance frequency (THz)	0.5595

Table 4-4. Output power, power efficiency and resonance frequency values (which are received from the results in Figure 4-10).

a (µm)	c (µm)	Quantities of resonators (n)	Quantities of resistors (n-1)	Structure from Figure	Results from Figure		
18	12	3	2	4-10a1	4-10a3	**Output power (Watt)**	0.481
						Power efficiency (%)	96.20
						Resonance frequency (THz)	0.5655
120	12	3	2	4-10b1	4-10b3	**Output power (Watt)**	0.252
						Power efficiency (%)	50.40
						Resonance frequency (THz)	0.7890
120	114	3	2	4-10c1	4-10c3	**Output power (Watt)**	0.238
						Power efficiency (%)	47.60
						Resonance frequency (THz)	0.7575
52	46	7	6	4-10d1	4-10d3	**Output power (Watt)**	0.483
						Power efficiency (%)	96.60
						Resonance frequency (THz)	0.5670
120	46	7	6	4-10e1	4-10e3	**Output power (Watt)**	0.438
						Power efficiency (%)	87.60
						Resonance frequency (THz)	0.6705
120	114	7	6	4-10f1	4-10f3	**Output power (Watt)**	0.433
						Power efficiency (%)	86.60
						Resonance frequency (THz)	0.6615
86	80	11	10	4-10g1	4-10g3	**Output power (Watt)**	0.483
						Power efficiency (%)	96.60
						Resonance frequency (THz)	0.5610
120	80	11	10	4-10h1	4-10h3	**Output power (Watt)**	0.479
						Power efficiency (%)	95.80
						Resonance frequency (THz)	0.5985
120	114	11	10	4-10i1	4-10i3	**Output power (Watt)**	0.483
						Power efficiency (%)	96.60
						Resonance frequency (THz)	0.5970
120	114	15	14	4-10j1	4-10j3	**Output power (Watt)**	0.483
						Power efficiency (%)	96.60
						Resonance frequency (THz)	0.5580

For (Silver (metal plate), Quartz (substrate) and Silver (resonator)) structure, which can be seen in either Figure 4-7 or Figure 4-10j1 because the same structure is shown in both Figures, two numerical studies are achieved with metal plate and without metal plate situations as shown in Figure 4-11 in order to see the effects of metal plate existence. In Figure 4-11, total lumped elements` powers` values are 0.483 W at 0.5580 THz at 300 ohm when there is silver metal plate at the bottom of the structure. However, total lumped elements` powers` value is decreased when the metal plate is removed from the structure. The harvested power is directly affected by metal plate due to the effects of the metal plate on total capacitance value.

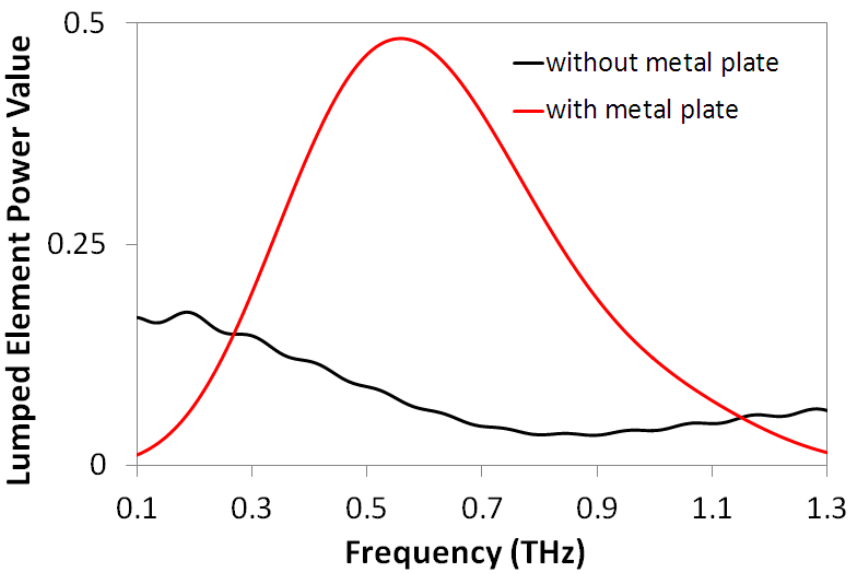

Figure 4-11. Simulated lumped element power magnitude for both cases with and without metal plate for 300 ohm resistor for (Silver (metal plate), Quartz (substrate) and Silver (resonator)) structure (This structure can be seen in either Figure 4-7 or Figure 4-10j1 because the same structure is shown in both Figures.).

The electric field, magnetic field, and surface current distributions are given in Figure 4-12 at the resonance frequency in order to understand better the physical mechanism of (Silver (metal plate), Quartz (substrate) and Silver (resonator)) structure (This structure can be seen in either Figure 4-7 or Figure 4-10j1 because the same structure is shown in both Figures) in power harvesting applications. The concentrations of these

distributions are on gaps and some parts of resonators of the designed structure where there are resistors because electric field directions are chosen to be parallel to y-axis as it is mentioned before. The basis of this is the design can be used as a voltage source due to the confinement of the EM waves at the resonance frequency.

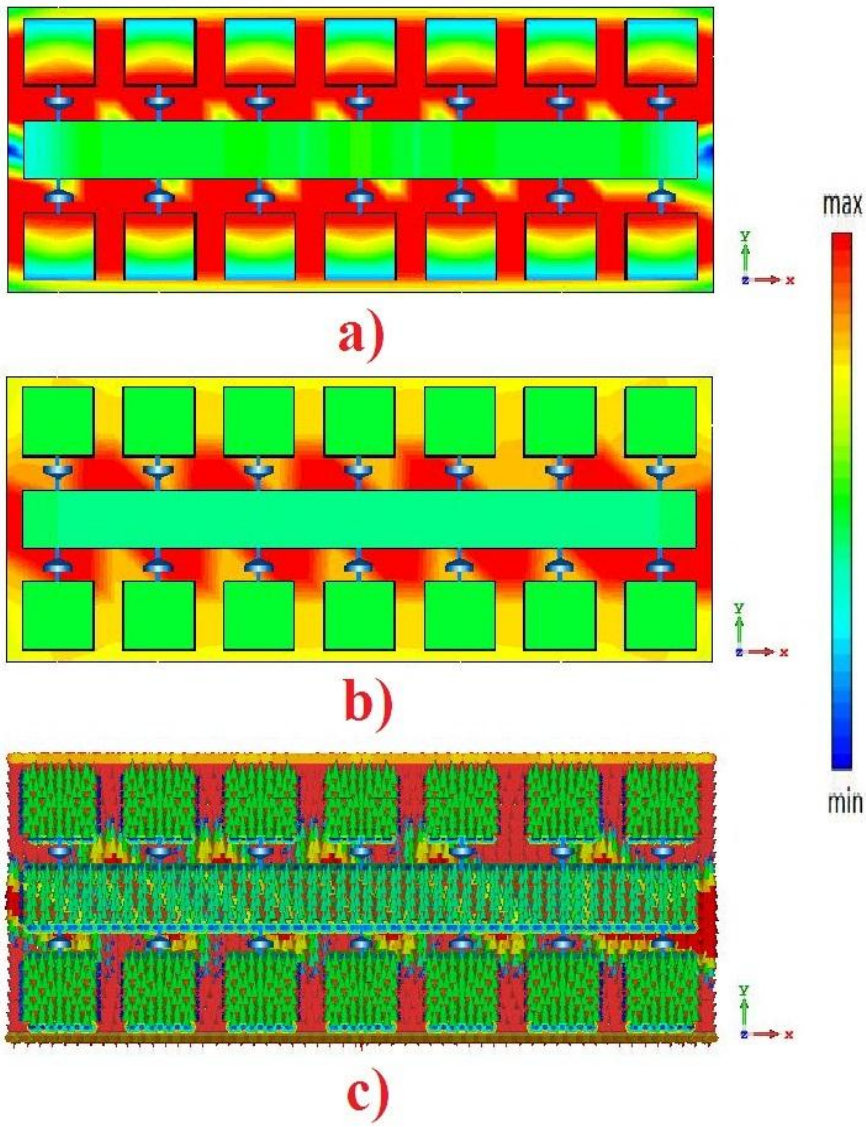

Figure 4-12. For (Silver (metal plate), Quartz (substrate) and Silver (resonator)) structure (This structure can be seen in either Figure 4-7 or Figure 4-10j1 because the same structure is shown in both Figures.) (a) Electric field distribution (b) Magnetic field distribution (c) Surface current distribution at the resonance frequency of 0.5595 THz at 300 ohm.

4.4. Single band metamaterial absorber based energy harvester topology in infrared regime for energy harvesting

4.4.1. Design and Simulation

In Figure 4-13b1 and Figure 4-13b2, the parametric dimensions of the infrared metamaterial absorber based energy harvester structure can be seen. Fifteen resonators and fourteen resistors (1st – 14th) are exist. Resistors are located as lumped network elements across the gaps between middle rectangle shape resonator and other square shape resonators. Before selected numerical values of these resistors are specifically chosen, many parametric studies have been done with finite integration technique (FIT)-based numerical simulator. Silver (Johnson) metal element is used at the bottom layer (as a metal plate) and top (as resonators) of this structure as metallic layers as shown in Figure 4-13a. Aim of the metal plate (as shown Figure 4-13a) on back side of the structure is the realization of approximately zero transmission ($T(\omega)$) as it is mentioned before. Aim of the resonator (as shown Figure 4-13a) on front side of the structure is the minimization of the reflection as it is mentioned before. Silica (Silicon Dioxide) is used as a substrate with Silver (Johnson) metal for metamaterial absorber based energy harvester as shown in Figure 4-13. The optical properties of Silica substrate and Silver (Johnson) metal can be found in Ref. [84] and in Ref. [85], respectively. Dimension values of the (Silver (Johnson), Silica and Silver(Johnson)) structure a, b, c, d, e, f, g, m, n and p are given as 575, 250, 550, 70, 10, 35, 20, 80, 80 and 20 nm, correspondingly [Figure 4-13b1 and Figure 4-13b2]. Along the x- and y-directions, the magnetic and electric field components of the incident plane wave are polarized, respectively [60 – 62].

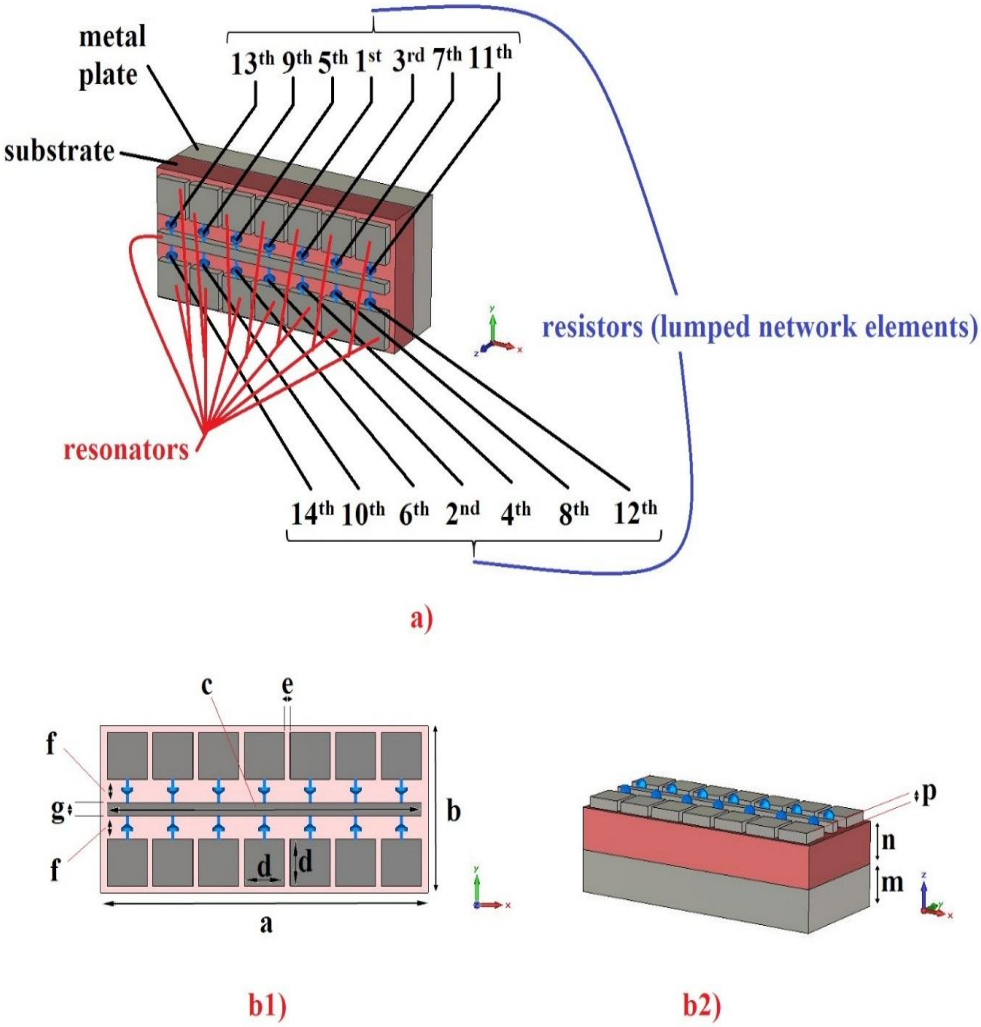

Figure 4-13. (a) Substrate, metal plate, resonators and resistors, (b1 and b2) dimensions of near perfect metamaterial absorber based energy harvester unit cell structure in infrared range.

4.4.2. Result and Discussion

Numerical reflectance and absorption result can be seen in Figure 4-14 (for (Silver (Johnson) (metal plate), Silica (substrate) and Silver (Johnson) (resonator)) structure). In Figure 4-14, maximum absorption is obtained around 99.99% at 252.8 THz. This value is obtained when fourteen 400 ohm resistors are placed across the gaps between middle rectangle shape resonator and other resonators as fourteen lumped network elements.

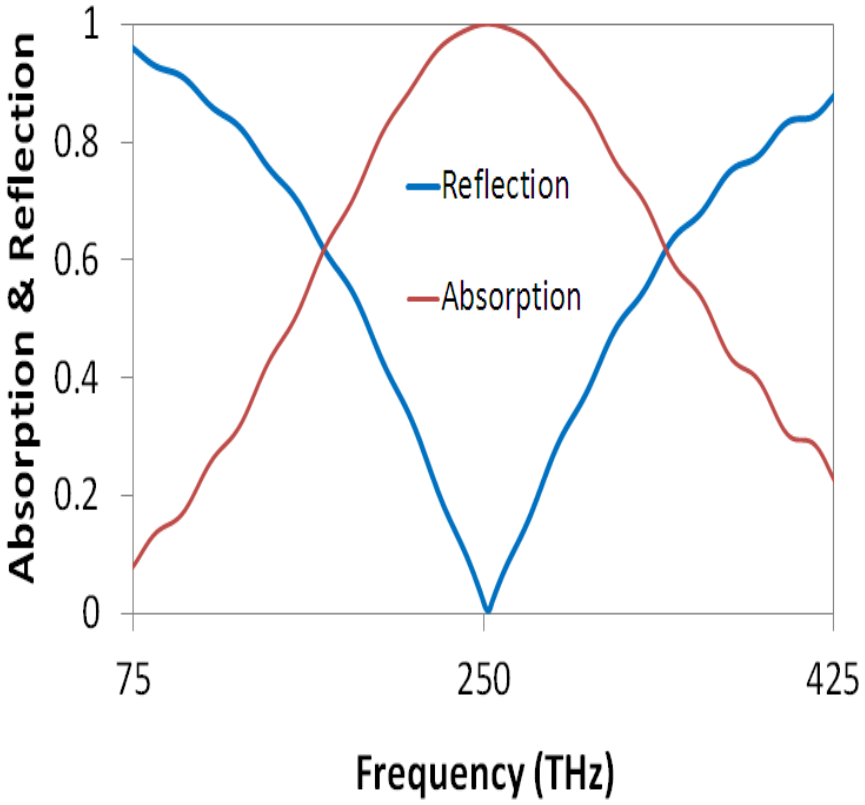

Figure 4-14. Reflectance and absorption result for (Silver (Johnson) (metal plate), Silica (substrate) and Silver (Johnson) (resonator)) structure (The resonance frequency at 252.8 THz).

Results in Figure 4-15 show that the energies are affected by the resistances. The maximum efficiency is obtained at 400 ohm as seen from Figure 4-15. For all power harvesting simulations, input powers were chosen 0.500 W. Fourteen lumped network elements (resistors) are located parallel to y-axis (electric field direction) is shown in Figure 4-13. In Figure 4-15, maximum efficiency is obtained around 98.80% (output power is 0.494 W) at 248.0 THz at 400 ohm.

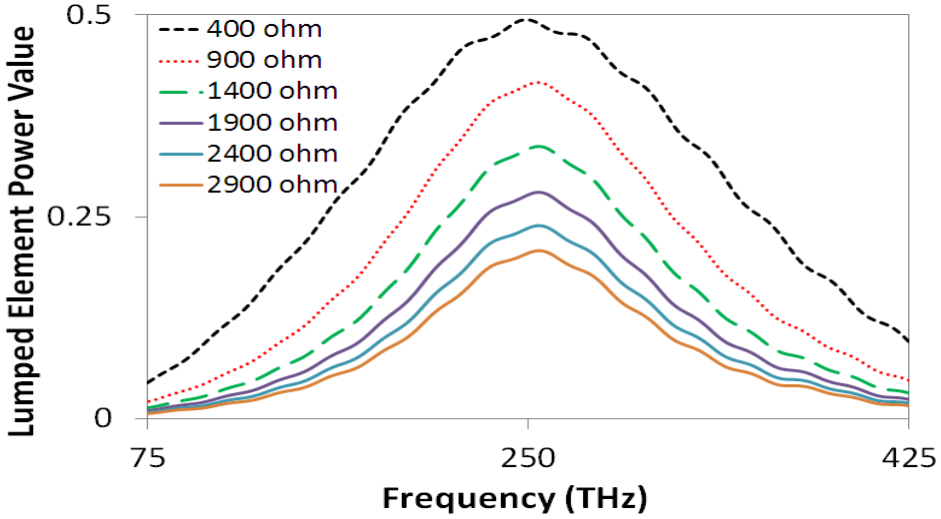

Figure 4-15. Gathered power frequency diagram for selected different resistors between 400-2900 ohm for (Silver (Johnson) (metal plate), Silica (substrate) and Silver (Johnson) (resonator)) structure.

In Figure 4-16, views from the top, reflectance, absorption, and Lumped element power values are shown for ten different geometric designs at 400 ohm when (n) resonators and (n-1) resistors are exist. “n” means any exact number, which is shown quantities of resonators. Quantities of resistors (n-1) are less one than quantities of resonators. Also, changed geometric parameters are separately given left side of each design in Figure 4-16. Structures are designed and analysed with increasing quantities of resonators and resistors, so dimensions are changed according to these quantities. Effects of increasing quantities of resonators and resistors with different “a” and “c” dimension values of designs can be seen in Figure 4-16. Although resonance frequency (252.8 THz for absorption and 248.0 THz for lumped element power value) is shifting lower (left side) or higher (right side) value between 75 and 425 THz frequency range, both the highest absorption (the lowest reflectance) and the highest lumped element power value are obtained in Figure 4-16j2 and Figure 4-16j3 as percentages for the structure in Figure 4-16j1. The reasons of these good results are the impedance of free – space matches with the frequency dependent effective impedance of the metamaterial absorber [44, 83] and effectiveness between resonators. Absorption and resonance frequency values, which are received from the results in Figure 4-16, are given in Table 4-5. Output power, power efficiency and resonance frequency values, which are received from the results in Figure 4-16, are given in Table 4-6.

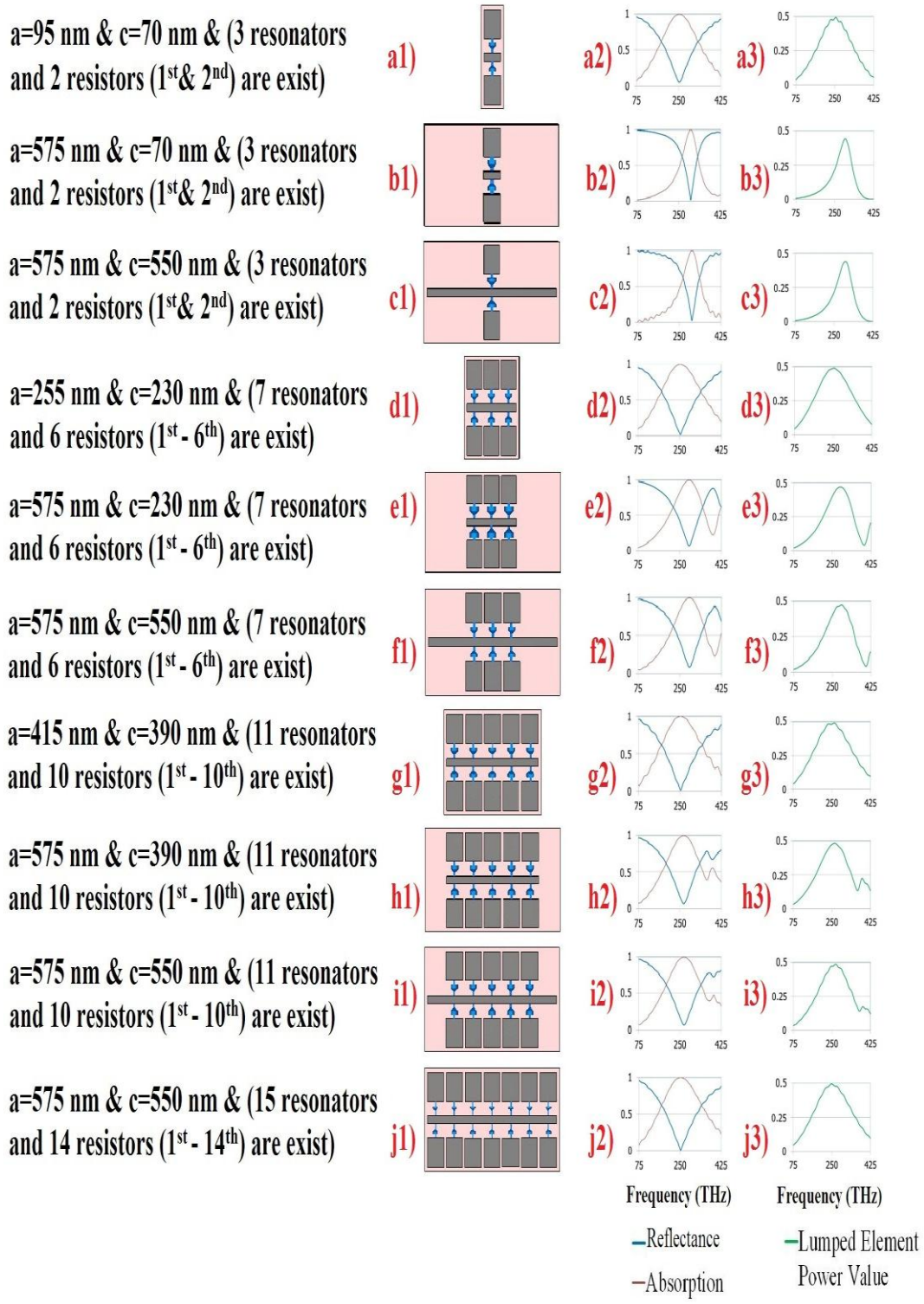

Figure 4-16. When (n) resonators and (n-1) resistors are exist, (a1 - j1) views from the top, (a2 – j2) reflectance and absorption results, and (a3 – j3) Lumped element power values for different geometric designs at 400 ohm (Changed geometric parameters are separately given left side of each design).

Table 4-5. Absorption and resonance frequency values (which are received from the results in Figure 4-16).

a (nm)	c (nm)	Quantities of resonators (n)	Quantities of resistors (n-1)	Structure from Figure	Results from Figure		
95	70	3	2	4-16a1	4-16a2	**Absorption (%)**	99.71
						Resonance frequency (THz)	252.8
575	70	3	2	4-16b1	4-16b2	**Absorption (%)**	99.97
						Resonance frequency (THz)	299.2
575	550	3	2	4-16c1	4-16c2	**Absorption (%)**	99.92
						Resonance frequency (THz)	302.4
255	230	7	6	4-16d1	4-16d2	**Absorption (%)**	99.98
						Resonance frequency (THz)	252.8
575	230	7	6	4-16e1	4-16e2	**Absorption (%)**	99.55
						Resonance frequency (THz)	289.6
575	550	7	6	4-16f1	4-16f2	**Absorption (%)**	99.31
						Resonance frequency (THz)	291.2
415	390	11	10	4-16g1	4-16g2	**Absorption (%)**	99.98
						Resonance frequency (THz)	252.8
575	390	11	10	4-16h1	4-16h2	**Absorption (%)**	99.60
						Resonance frequency (THz)	265.6
575	550	11	10	4-16i1	4-16i2	**Absorption (%)**	99.58
						Resonance frequency (THz)	267.2
575	550	15	14	4-16j1	4-16j2	**Absorption (%)**	99.99
						Resonance frequency (THz)	252.8

Table 4-6. Output power, power efficiency and resonance frequency values (which are received from the results in Figure 4-16).

a (nm)	c (nm)	Quantities of resonators (n)	Quantities of resistors (n-1)	Structure from Figure	Results from Figure		
95	70	3	2	4-16a1	4-16a3	**Output power (Watt)**	0.493
						Power efficiency (%)	98.60
						Resonance frequency (THz)	254.4
575	70	3	2	4-16b1	4-16b3	**Output power (Watt)**	0.443
						Power efficiency (%)	88.60
						Resonance frequency (THz)	297.6
575	550	3	2	4-16c1	4-16c3	**Output power (Watt)**	0.439
						Power efficiency (%)	87.80
						Resonance frequency (THz)	302.4
255	230	7	6	4-16d1	4-16d3	**Output power (Watt)**	0.490
						Power efficiency (%)	98.00
						Resonance frequency (THz)	252.8
575	230	7	6	4-16e1	4-16e3	**Output power (Watt)**	0.469
						Power efficiency (%)	93.80
						Resonance frequency (THz)	286.4
575	550	7	6	4-16f1	4-16f3	**Output power (Watt)**	0.473
						Power efficiency (%)	94.60
						Resonance frequency (THz)	292.8
415	390	11	10	4-16g1	4-16g3	**Output power (Watt)**	0.491
						Power efficiency (%)	98.20
						Resonance frequency (THz)	260.8
575	390	11	10	4-16h1	4-16h3	**Output power (Watt)**	0.482
						Power efficiency (%)	96.40
						Resonance frequency (THz)	262.4
575	550	11	10	4-16i1	4-16i3	**Output power (Watt)**	0.487
						Power efficiency (%)	97.40
						Resonance frequency (THz)	267.2
575	550	15	14	4-16j1	4-16j3	**Output power (Watt)**	0.494
						Power efficiency (%)	98.80
						Resonance frequency (THz)	248.0

For (Silver (Johnson) (metal plate), Silica (substrate) and Silver (Johnson) (resonator)) structure, which can be seen in either Figure 4-13 or Figure 4-16j1 because the same structure is shown in both Figures, two numerical studies are achieved with metal plate and without metal plate situations as shown in Figure 4-17 in order to see the effects of metal plate existence. In Figure 4-17, total lumped elements` powers` values are 0.494 W at 248.0 THz at 400 ohm when there is Silver (Johnson) metal plate at the bottom of the structure. However, total lumped elements` powers` value is decreased when the metal plate is removed from the structure. The harvested power is directly affected by metal plate due to the effects of the metal plate on total capacitance value.

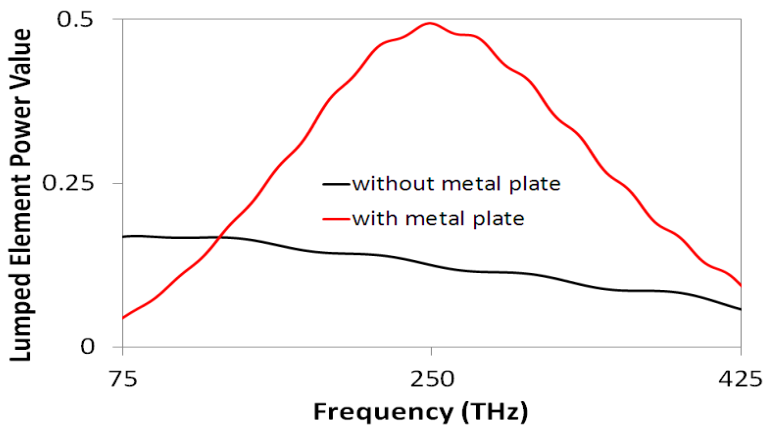

Figure 4-17. Simulated lumped element power magnitude for both cases with and without metal plate for 400 ohm resistor for (Silver (Johnson) (metal plate), Silica (substrate) and Silver (Johnson) (resonator)) structure (This structure can be seen in either Figure 4-13 or Figure 4-16j1 because the same structure is shown in both Figures.).

The electric field, magnetic field, and surface current distributions are given in Figure 4-18 at the resonance frequency in order to understand better the physical mechanism of (Silver (Johnson) (metal plate), Silica (substrate) and Silver (Johnson) (resonator)) structure (This structure can be seen in either Figure 4-13 or Figure 4-16j1 because the same structure is shown in both Figures) in power harvesting applications. The concentrations of these distributions are on gaps and some parts of resonators of the designed structure where there are resistors because electric field directions are chosen to be parallel to y-axis as it is mentioned before. The basis of this is the design can be used as a voltage source due to the confinement of the EM waves at the resonance frequency.

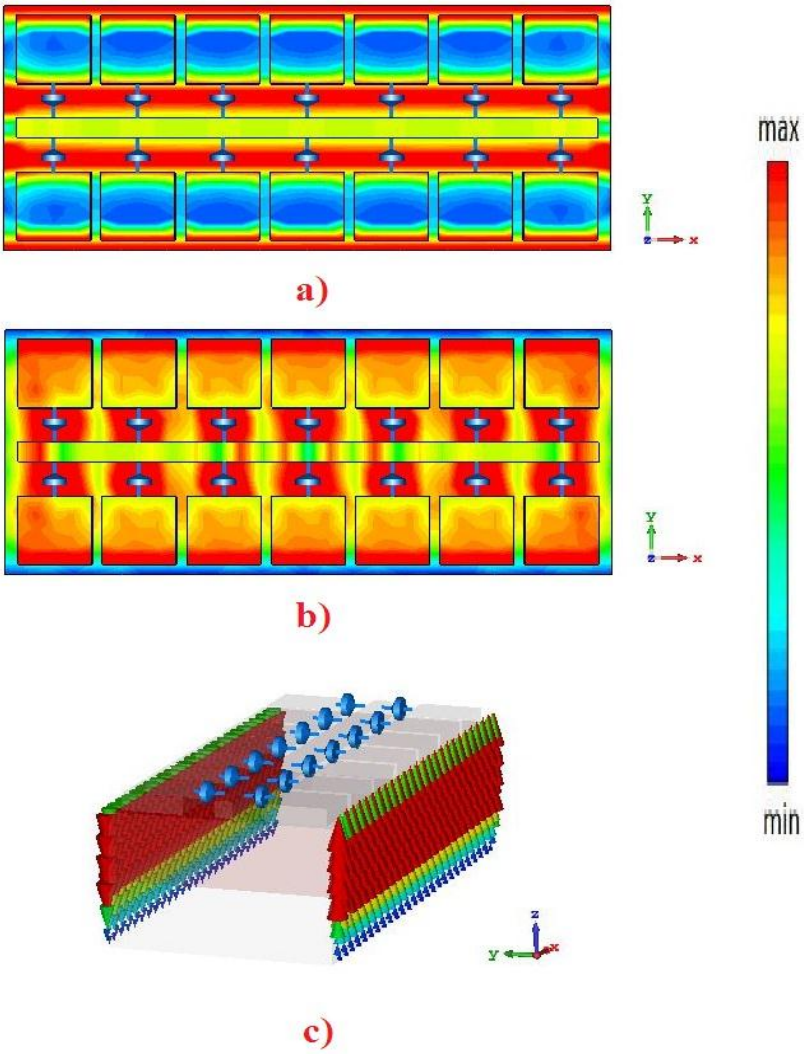

Figure 4-18. For (Silver (Johnson) (metal plate), Silica (substrate) and Silver (Johnson) (resonator)) structure (This structure can be seen in either Figure 4-13 or Figure 4-16j1 because the same structure is shown in both Figures.) (a) Electric field distribution (b) Magnetic field distribution (c) Surface current distribution at the resonance frequency of 252.8 THz at 400 ohm.

4.5. Conclusion

In this chapter, single band metamaterial absorber based energy harvester designs are analysed in microwave (GHz), sub-THz and infrared frequency regimes for single band topology by changing two geometric parameters and increasing quantities of resonators and resistors. Therefore, effects of quantities of resonators and resistors with different sizes of two parameters is understood. When adding all resonators and

resistors, high absorptions and lumped network element power values are obtained in microwave (GHz), sub-THz and infrared frequency regimes for metamaterial absorber based energy harvesters. Also, reflectance, effect of metal plate and field distributions can be seen above. Numerical results show that the usage of near perfect metamaterial absorbers can be efficient and easy for electromagnetic energy harvesters. Proposed structures can be used for many application such as antennas, EM filters, sensors, THz imaging systems, infrared spectroscopy, infrared cameras, solar cells.

CHAPTER 5

PARAMETRIC STUDY FOR ENERGY HARVESTING OF METAMATERIAL ABSORBER FOR HIGH FREQUENCY REGION AND ENHANCEMENT TECHNIQUES

5.1. Introduction

In this chapter, a triple band metamaterial absorber based energy harvester structure is designed. Information about the structure is given in Section 5.2. In Section 5.3, the design is analyzed. Results, which are obtained in Section 5.3, are enhanced in Section 5.4 by applying some techniques. Creation of a hole in the middle of metal plate, integration materials like Graphene [70, 76 – 78] or Indium Tin Oxide (ITO) [83 – 90] are called as enhancement methods. Parametric studies are carried in most of the results below. In addition, all simulation results are realized in both infrared and visible frequency regime at the same time.

5.2. Design and Simulation

In Figure 5-1b and Figure 5-1c, the parametric dimensions of the infrared and visible metamaterial absorber based energy harvester structure can be seen. Four resistors are used. Resistors are located as lumped network elements across the gaps on the resonator. Before selected numerical values of these resistors are specifically chosen, many parametric studies have been done with finite integration technique (FIT)-based numerical simulator. Silver (Johnson) metal element is used at the bottom layer (as a metal plate) and top (as a resonator) of this structure as metallic layers as shown in Figure 5-1a. The optical properties Silver (Johnson) metal can be found in Ref. [85]. Aim of the metal plate (as shown Figure 5-1a) on back side of the structure is the realization of approximately zero transmission ($T(\omega)$) as it is mentioned before in previous chapters. Aim of the resonator (as shown Figure 5-1a) on front side of the structure is the minimization of the reflection as it is mentioned before in previous chapters. Amorphous Silicon (a-Si) is used as a substrate with Silver (Johnson) metal for metamaterial absorber based energy harvester as shown in Figure 5-1. Dimension values of the structure a, b, c, d, e, m, n and p are given as 600, 440, 40, 90, 180, 100, 10 and 100 nm, correspondingly [Figure 5-1b and Figure 5-1c]. Along the x- and y-

directions, the magnetic and electric field components of the incident plane wave are polarized, respectively [60 – 62].

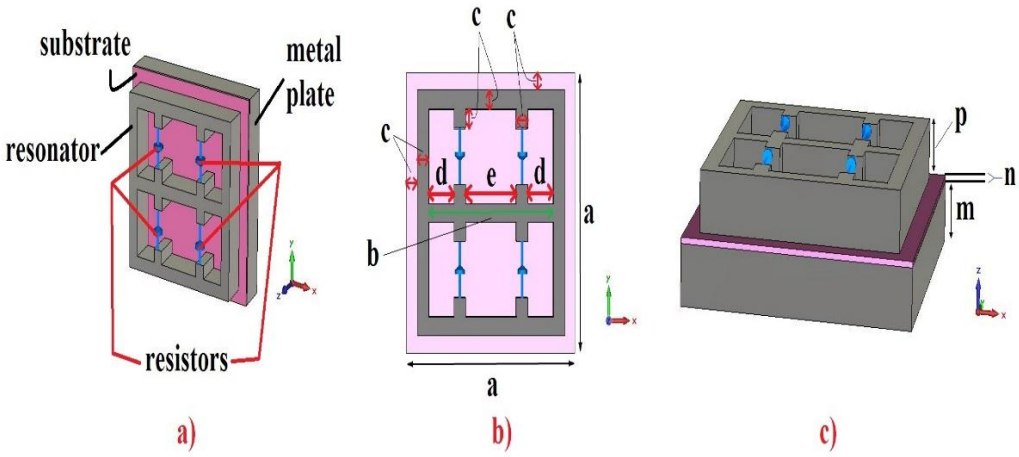

Figure 5-1. (a) Substrate, metal plate, resonator and resistors, (b and c) dimensions of near perfect metamaterial absorber based energy harvester unit cell structure in infrared and visible range.

5.3. Result and Discussion

Numerical reflectance and absorption result can be seen in Figure 5-2. In Figure 5-2, maximum absorptions are obtained around 99.98%, 83.72% and 92.77% at 363 THz, 468.7 THz and 529.6 THz, respectively. This values are obtained when four 900 ohm resistors are placed across the gaps.

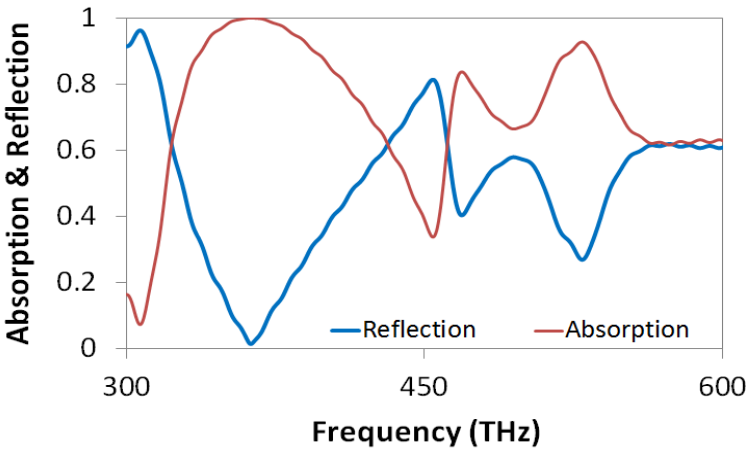

Figure 5-2. Reflectance and absorption result for the structure in Figure 5-1 (The resonance frequencies at 363 THz, 468.7 THz and 529.6 THz).

Four lumped network elements (resistors) are located parallel to y-axis (electric field direction) is shown in Figure 5-1. When input powers were chosen 0.500 W, maximum

efficiencies are obtained around 93.6% (output power is 0.468 W), 61.4% (output power is 0.307 W) and 14% (output power is 0.070 W) at 361.6 THz, 472.9 THz and 552 THz at 900 ohm in Figure 5-3.

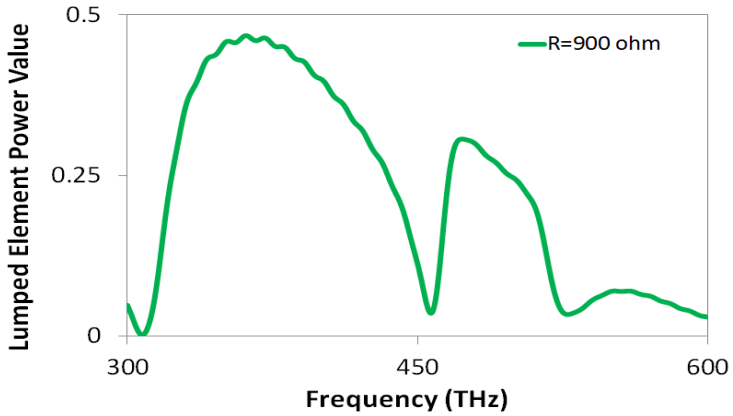

Figure 5-3. Gathered power frequency diagram for four 900 ohm resistors for the structure in Figure 5-1.

For the structure in Figure 5-1, two numerical studies are achieved with metal plate and without metal plate situations as shown in Figure 5-4 in order to see the effect of metal plate existence. In Figure 5-4, total lumped elements` powers` values are 0.468 W at 361.6 THz, 0.307 W at 472.9 THz and 0.070 W at 552 THz at 900 ohm when there is Silver (Johnson) metal plate at the bottom of the structure. However, total lumped elements` powers` value is decreased when the metal plate is removed from the structure. The harvested power is directly affected by metal plate due to the effects of the metal plate on total capacitance value.

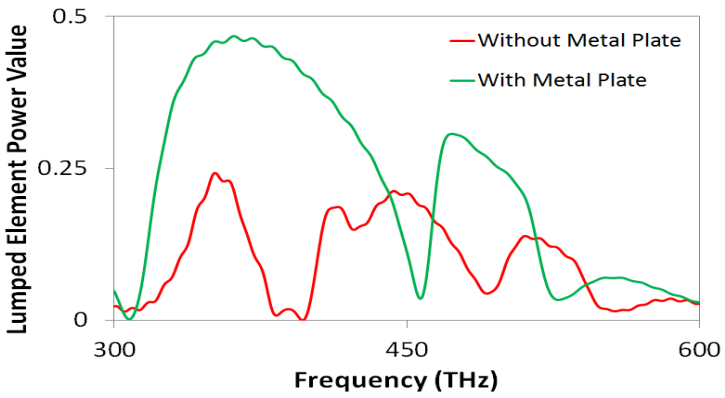

Figure 5-4. Simulated lumped element power magnitude for both cases with and without metal plate for 900 ohm resistor for the structure in Figure 5-1.

The electric fields, magnetic fields, and surface current distributions are given in Figure 5-5 at three resonance frequencies in order to understand better the physical mechanism of the structure in Figure 5-1 in power harvesting applications. When resonance frequency is 363 THz, electric field, magnetic field and surface current distribution are shown in Figure 5-5a1, in Figure 5-5a2 and Figure 5-5a3, respectively. When resonance frequency is 468.7 THz, electric field, magnetic field and surface current distribution are shown in Figure 5-5b1, in Figure 5-5b2 and Figure 5-5b3, respectively. When resonance frequency is 529.6 THz, electric field, magnetic field and surface current distribution are shown in Figure 5-5c1, in Figure 5-5c2 and Figure 5-5c3, respectively. The concentrations of these distributions are on gaps across the resonator of the designed structure where there are resistors because electric field directions are chosen to be parallel to y-axis as it is mentioned before. The basis of this is the design can be used as a voltage source due to the confinement of the EM waves at the resonance frequency.

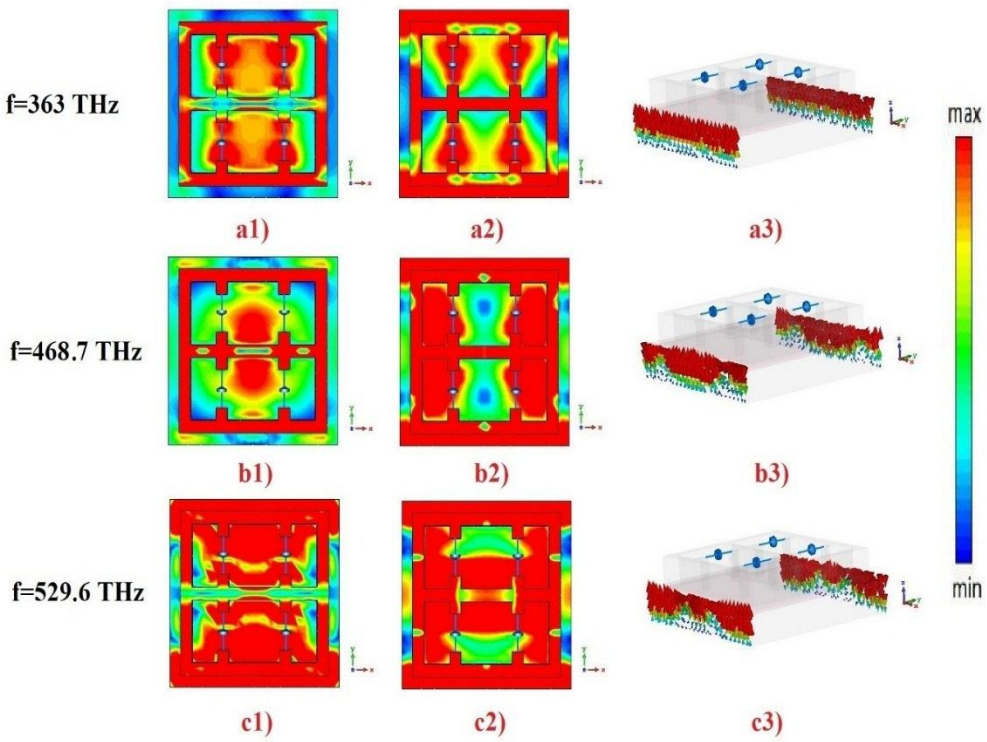

Figure 5-5. For the structure in Figure 5-1 (a1) Electric field distribution (a2) Magnetic field distribution (a3) Surface current distribution at the resonance frequency of 363 THz at 900 ohm, (b1) Electric field distribution (b2) Magnetic field distribution (b3) Surface current distribution at the resonance frequency of 468.7 THz at 900 ohm, (c1) Electric field distribution (c2) Magnetic field distribution (c3) Surface current distribution at the resonance frequency of 529.6 THz at 900 ohm.

As parametric studies, results in Figure 5-6 and in Figure 5-7 show that the energies are affected by the resistances. As percentages, maximum efficiencies are obtained at 900 ohm as seen from Figure 5-6 and Figure 5-7 for both absorption and total output power value of four lumped elements. Input powers were chosen 0.500 W. In previous, maximum efficiencies are given for both absorption and total output power value of four lumped elements at 900 ohm above when explanations have done for Figure 5-2 and Figure 5-3 about the structure in Figure 5-1.

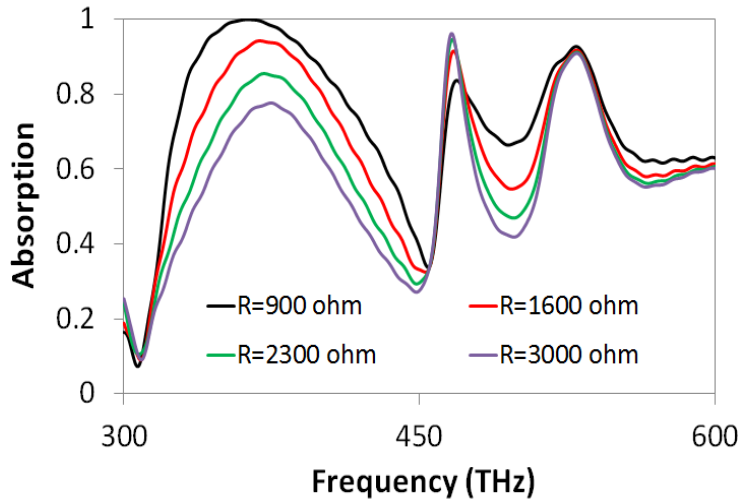

Figure 5-6. Gathered absorption frequency diagram for selected different resistors between 900-3000 ohm for the structure in Figure 5-1.

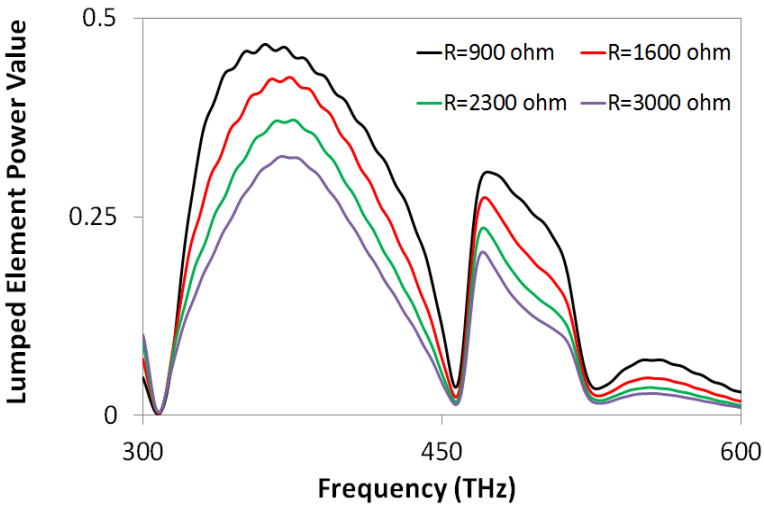

Figure 5-7. Gathered power frequency diagram for selected different resistors between 900-3000 ohm for the structure in Figure 5-1.

5.4. Enhancement Methods of Results

5.4.1. Hole at the metal plate

By opening a square shape hole in the middle of the metal plate, view of the back side of the metamaterial absorber based energy harvester structure in Figure 5-1 is reformed. Therefore, the modification in the structure can be seen in Figure 5-8 with dimension parameter “h”. A parametric study, which is shown in Figure 5-9, has realized for the “h” parameter. As percentages, maximum efficiencies are obtained around 94% (output power is 0.470 W), 62.6% (output power is 0.313 W) and 14.8% (output power is 0.074 W) at 365.1 THz, 474.3 THz and 553.4 THz at 900 ohm in Figure 5-9 when h=20 nm. These three percentage values (for when h=20 nm) are higher than other three percentage values (for when h=0 nm (without hole)) in Figure 5-9. The differences are shown with arrows at the top of the Figure 5-9 in order to make a comparison between h=0 nm (which means without any holes in metal plate) and h=20 nm (which means with a square shape hole in metal plate). According to given three resonance frequencies in Figure 5-3, new three resonance frequencies are shifting higher (right side) values between 300 and 600 THz frequency range in Figure 5-9. Total power values of maximum efficiencies are increased 0.4%, 1.2% and 0.8% as percentages for three resonances when value of the “h” parameter is increased from 0 nm to 20 nm in Figure 5-9. Although small rising in total power value, an enhancement is realized for three resonances by the creation a square shape hole at the metal plate. In this way, the small but positive effect of hole has been seen and understood on this metamaterial absorber based energy harvester unit cell structure in infrared and visible range.

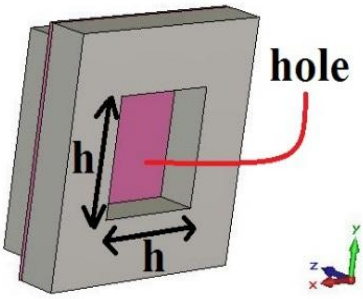

Figure 5-8. View of created hole at the metal plate with dimensions for parametric study.

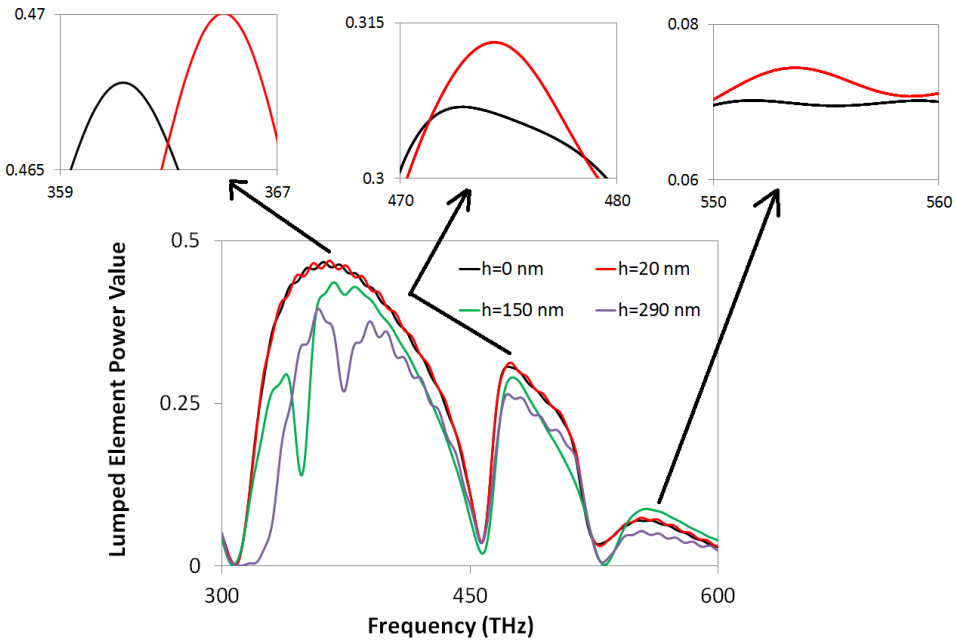

Figure 5-9. Gathered power frequency diagram for selected different "h" parameters for the structure when R=900 ohm in Figure 5-8.

5.4.2. Adding different materials into the hole

In Figure 5-10, adding a substrate material is shown in the created square shape hole at the metal plate. Simulations results are obtained in Figure 5-11 when h=20 nm and R=900 ohm because enhancement is realized with these two parameters above. Silicon Amorphous (a-Si), Indium Tin Oxide (ITO), Silicon Dioxide (SiO_2) and Zinc Oxide (ZnO) (Postava) are four different substrate materials. They are separately adding and used in hole for the same structure, which means there is a structure with a hole and this structure is separately analysed four times four different substrate materials, so behaviour and effect onto results of each material can be seen in Figure 5-11. For comparison of obtained previous enhanced result in Figure 5-9 with four different substrate materials, output power, power efficiency and resonance frequency values are given in Table 5-1 for three resonances. In this way, new small enhancements are realized in some power efficiencies at some resonance(s) as percentage(s) according to Table 5-1. Power efficiencies are same for the structure designed with Silicon Dioxide substrate material in hole, with Zinc Oxide substrate material in hole and without any substrate materials in hole at three resonances. Power efficiency is increasing at the first resonance for the structure designed with Amorphous Silicon substrate material in hole, but other two power efficiencies are decreasing at the second

and third resonances as percentages with shifting three resonance frequencies to lower (left side) values according to the results of the structure designed without any substrate materials in hole. Power efficiency is decreasing at the first resonance for the structure designed with Indium Tin Oxide substrate material in hole, but other two power efficiencies are increasing at the second and third resonances as percentages without any shifting at values of three resonance frequencies according to the results of the structure designed without any substrate materials in hole.

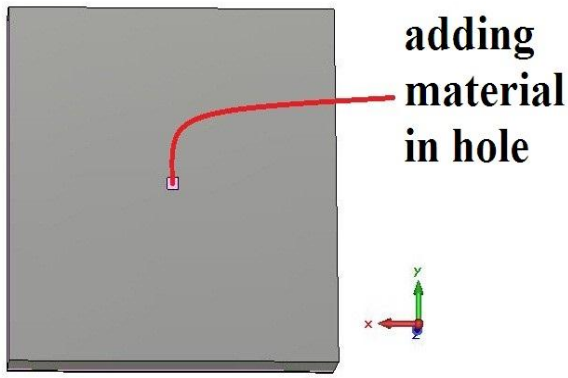

Figure 5-10. View of adding material in created hole at the metal plate for the structure in Figure 5-8 when h=20 nm and R=900 ohm.

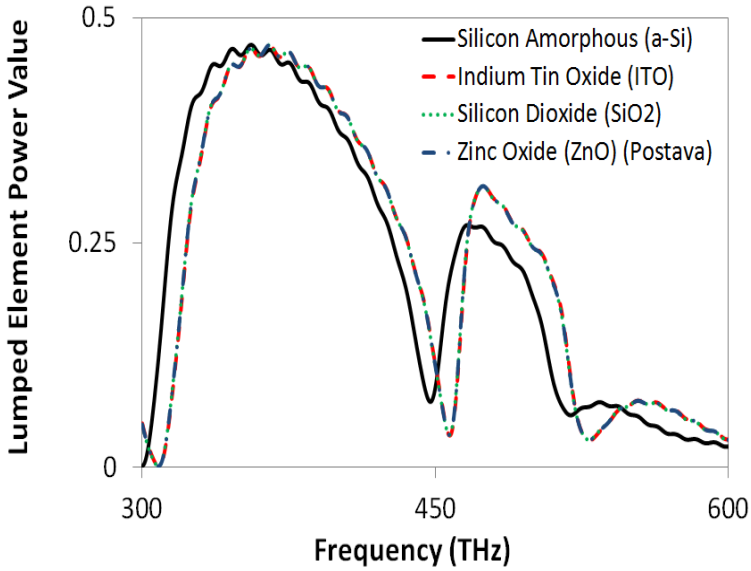

Figure 5-11. Gathered power frequency diagram for four different materials which are separately adding in created hole at the metal plate and analysed when h=20 nm and R=900 ohm for the structure in Figure 5-8.

Table 5-1. Output power, power efficiency and resonance frequency values according to four different substrate materials in hole and without any substrate materials in hole for at first, second and third resonances due to comparison.

		First resonance	Second resonance	Third resonance
Without any substrate materials in hole	Output Power (Watt)	0.470	0.313	0.074
	Power efficiency (%)	94.0	62.6	14.8
	Resonance frequency (THz)	365.1	474.3	553.4
Amorphous Silicon (a-Si)	Output Power (Watt)	0.471	0.270	0.073
	Power efficiency (%)	94.2	54.0	14.6
	Resonance frequency (THz)	356.0	466.6	533.8
Indium Tin Oxide (ITO)	Output Power (Watt)	0.470	0.314	0.075
	Power efficiency (%)	94.0	62.8	15.0
	Resonance frequency (THz)	365.1	474.3	553.4
Silicon Dioxide (SiO_2)	Output Power (Watt)	0.470	0.313	0.074
	Power efficiency (%)	94.0	62.6	14.8
	Resonance frequency (THz)	365.1	474.3	553.4
Zinc Oxide (ZnO) (Postava)	Output Power (Watt)	0.470	0.313	0.074
	Power efficiency (%)	94.0	62.6	14.8
	Resonance frequency (THz)	365.1	474.3	553.4

5.4.3. Graphene

The positive effect of using Graphene layer(s) has been seen on a metamaterial absorber structure in the Section 2.3 in the Chapter 2 of this thesis. The properties of Graphene and theory are briefly mentioned there. Instead of using Graphene layer(s) at top of the resonator or at the bottom of the resonator or at the both top and bottom of the resonator at the structure, Graphene is only used at the bottom of the metal plate and a-Si substrate material in created hole in the middle of metal plate here at the same time. In Figure 5-12, adding Graphene is shown.

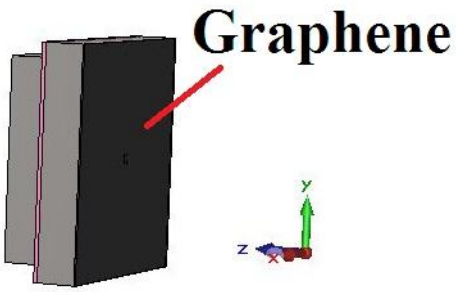

Figure 5-12. View of adding Graphene layer(s) at the bottom of the metal plate and a-Si substrate material in created hole in the middle of metal plate for the structure in Figure 5-10 when h=20 nm and R=900 ohm.

Two parametric studies are realized by changing Graphene thicknesses for the structure in Figure 5-12. Absorption and total power values of lumped element results can be seen in Figure 5-13 and Figure 5-14, respectively. About these results, which are shown in Figure 5-13 and Figure 5-14, details are given in Table 5-2 and Table 5-3 for comparison.

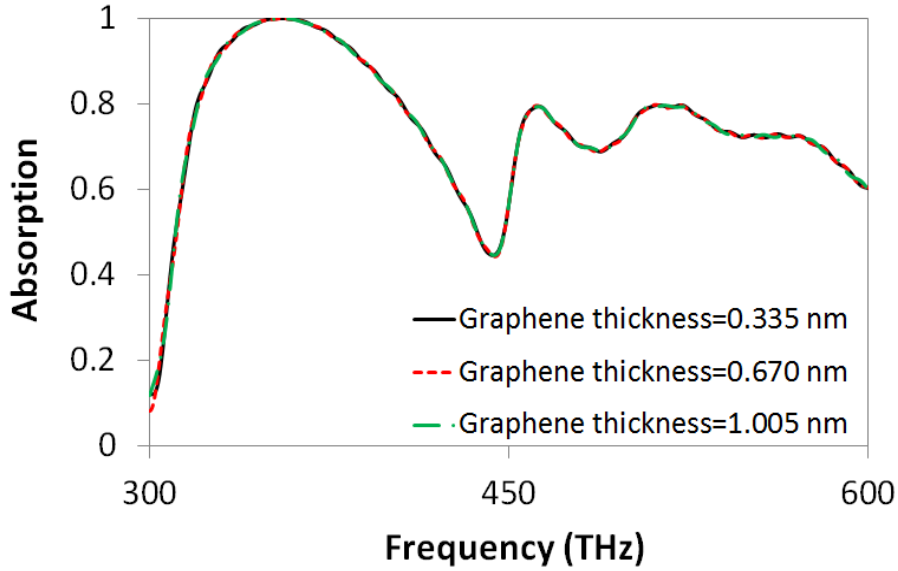

Figure 5-13. Gathered absorption frequency diagram for the parametric study with three graphene thicknesses for the structure in Figure 5-12.

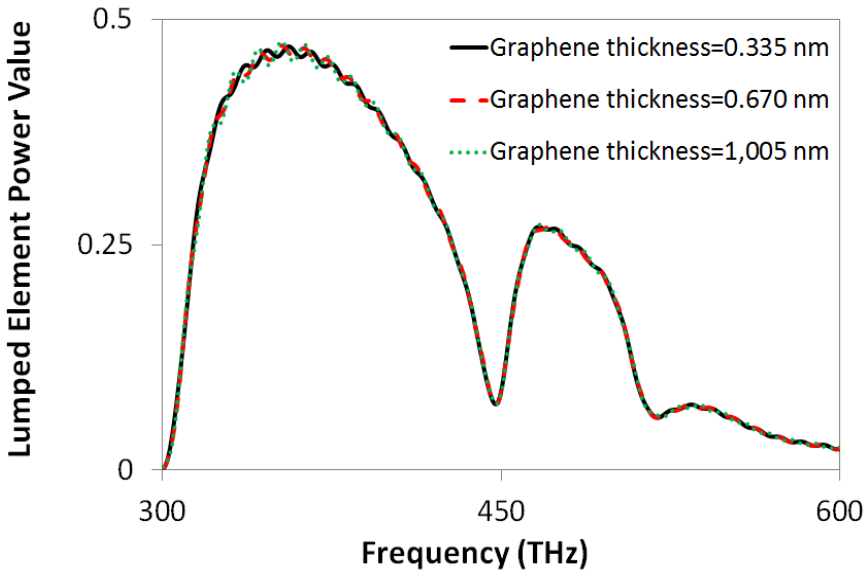

Figure 5-14. Gathered power frequency diagram for the parametric study with three graphene thicknesses for the structure in Figure 5-12.

Table 5-2. Absorption and resonance frequency values (which are received from the results in Figure 5-13) according to adding three different Graphene thicknesses for the structure in Figure 5-12 for at first, second and third resonances due to comparison.

Graphene thickness (nm)		**First resonance**	**Second resonance**	**Third resonance**
0.335 (1-layer)	Absorption (%)	99.97	79.41	79.73
	Resonance frequency (THz)	355.3	462.4	512.8
0.670 (2-layers)	Absorption (%)	99.96	79.64	79.84
	Resonance frequency (THz)	355.3	461.7	511.4
1.005 (3-layers)	Absorption (%)	99.99	79.42	79.65
	Resonance frequency (THz)	355.3	462.4	514.9

Table 5-3. Output power, power efficiency and resonance frequency values (which are received from the results in Figure 5-14) according to adding three different Graphene thicknesses for the structure in Figure 5-12 for at first, second and third resonances due to comparison.

Graphene thickness (nm)		**First resonance**	**Second resonance**	**Third resonance**
0.335 (1-layer)	Output Power (Watt)	0.471	0.270	0.073
	Power efficiency (%)	94.2	54.0	14.6
	Resonance frequency (THz)	356.0	466.6	534.5
0.670 (2-layers)	Output Power (Watt)	0.471	0.271	0.073
	Power efficiency (%)	94.2	54.2	14.6
	Resonance frequency (THz)	353.2	471.5	533.1
1.005 (3-layers)	Output Power (Watt)	0.477	0.273	0.073
	Power efficiency (%)	95.4	54.6	14.6
	Resonance frequency (THz)	352.5	466.6	537.3

Figure 5-15 and Figure 5-16 are become by receiving and using some obtained results, which are separately given in Figure 5-2, Figure 5-3, Figure 5-13 and Figure 5-14 above in this chapter, for comparison. For both cases with and without hole & hole substrate & Graphene for the structures in Figure 5-1 and Figure 5-12, two absorption and two total power values of lumped element results can be seen in Figure 5-15 and Figure 5-16, respectively. About these results, which are shown in Figure 5-15 and Figure 5-16, details are given in Table 5-4 and Table 5-5 for comparison. When passing from the without hole & hole substrate & Graphene situation to the with hole & hole substrate (a-Si) & Graphene (Graphene thickness = 1.005 nm (3-layers))

situation according to results in Table 5-4, as percentages absorption value of the first resonance is increasing 0.01%, but absorption values of the second and third resonances are decreasing 4.3% and 13.12%, respectively. When passing from the without hole & hole substrate & Graphene situation to the with hole & hole substrate (a-Si) & Graphene (Graphene thickness = 1.005 nm (3-layers)) situation according to results in Table 5-5, as percentages total power value of the second resonance is decreasing 6.8%, but total power value of the first and third resonances are increasing 1.8% and 0.6%, respectively. Moreover, three resonance frequencies are shifting lower (left side) values between 300 and 600 THz frequency range in both Figure 5-15 and Figure 5-16 for not only absorptions but also total power values when passing from the without hole & hole substrate & Graphene situation to the with hole & hole substrate (a-Si) & Graphene (Graphene thickness = 1.005 nm (3-layers)) situation according to results in both Table 5-4 and Table 5-5. In this way, new small enhancements are realized in an absorption value and two power efficiencies at some resonance(s) as percentage(s).

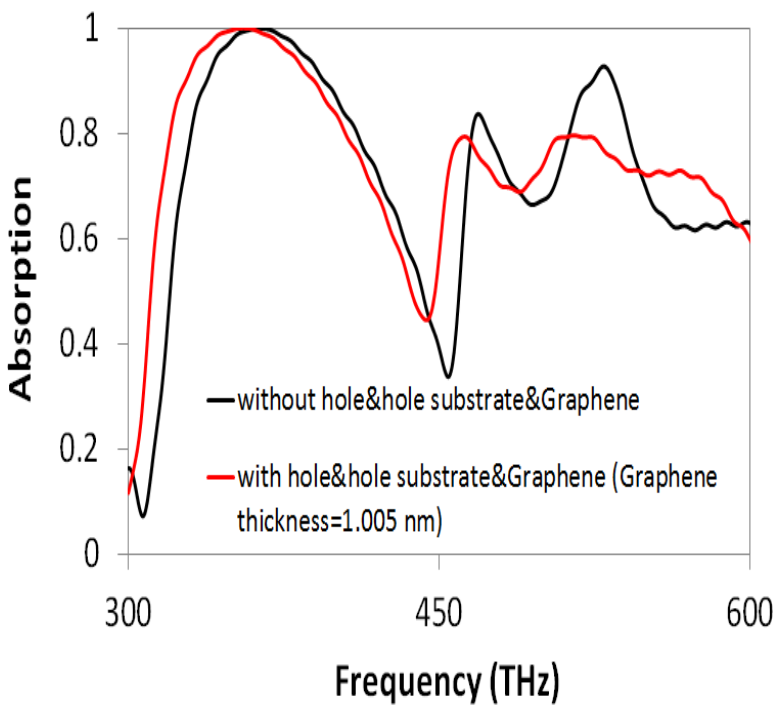

Figure 5-15. Simulated absorption magnitude for both cases with and without hole & hole substrate & Graphene for the structures in Figure 5-1 and Figure 5-12.

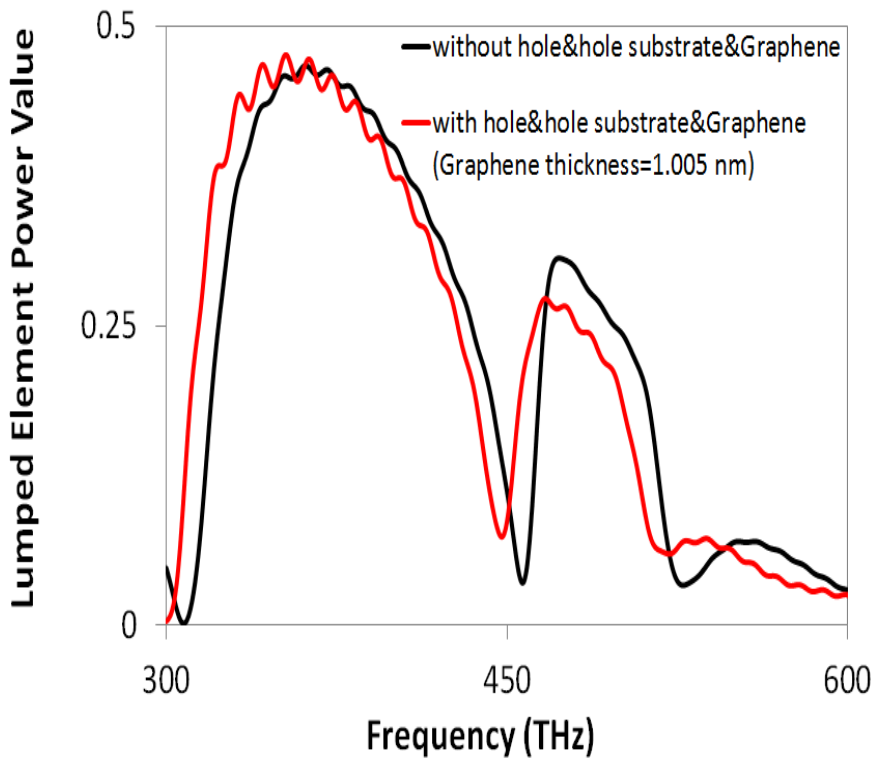

Figure 5-16. Simulated total power values of lumped elements magnitude for both cases with and without hole & hole substrate & Graphene for the structures in Figure 5-1 and Figure 5-12.

Table 5-4. Absorption and resonance frequency values (which are received from the results in Figure 5-15) according to both cases with and without hole & hole substrate & Graphene for the structures in Figure 5-1 and Figure 5-12 at first, second and third resonances due to comparison.

		First resonance	**Second resonance**	**Third resonance**
Without hole & hole substrate & Graphene	Absorption (%)	99.98	83.72	92.77
	Resonance frequency (THz)	363.0	468.7	529.6
With hole & hole substrate (a-Si) & Graphene (Graphene thickness = 1.005 nm (3-layers))	Absorption (%)	99.99	79.42	79.65
	Resonance frequency (THz)	355.3	462.4	514.9

Table 5-5. Output power, power efficiency and resonance frequency values (which are received from the results in Figure 5-16) according to both cases with and without hole & hole substrate & Graphene for the structures in Figure 5-1 and Figure 5-12 at first, second and third resonances due to comparison.

		First resonance	**Second resonance**	**Third resonance**
Without hole & hole substrate & Graphene	Output Power (Watt)	0.468	0.307	0.070
	Power efficiency (%)	93.6	61.4	14.0
	Resonance frequency (THz)	361.6	472.9	552.0
With hole & hole substrate (a-Si) & Graphene (Graphene thickness = 1.005 nm (3-layers))	Output Power (Watt)	0.477	0.273	0.073
	Power efficiency (%)	95.4	54.6	14.6
	Resonance frequency (THz)	352.5	466.6	537.3

The electric fields, magnetic fields, and surface current distributions are given in Figure 5-17 at three resonance frequencies in order to understand better the physical mechanism of the structure in Figure 5-12 in power harvesting applications. When resonance frequency is 355.3 THz, electric field, magnetic field and surface current distribution are shown in Figure 5-17a1, in Figure 5-17a2 and Figure 5-17a3, respectively. When resonance frequency is 462.4 THz, electric field, magnetic field and surface current distribution are shown in Figure 5-17b1, in Figure 5-17b2 and Figure 5-17b3, respectively. When resonance frequency is 514.9 THz, electric field, magnetic field and surface current distribution are shown in Figure 5-17c1, in Figure 5-17c2 and Figure 5-17c3, respectively. The concentrations of these distributions are on gaps across the resonator of the designed structure where there are resistors because electric field directions are chosen to be parallel to y-axis as it is mentioned before. The basis of this is the design can be used as a voltage source due to the confinement of the EM waves at the resonance frequency. Some differences, which are as either views or densities, are become when passing from the without hole & hole substrate & Graphene situation in Figure 5-5 to the with hole & hole substrate (a-Si) & Graphene (Graphene thickness = 1.005 nm (3-layers)) in Figure 5-17. These differences are

reasons of changes in both percentages of absorption and total power values and resonance frequencies.

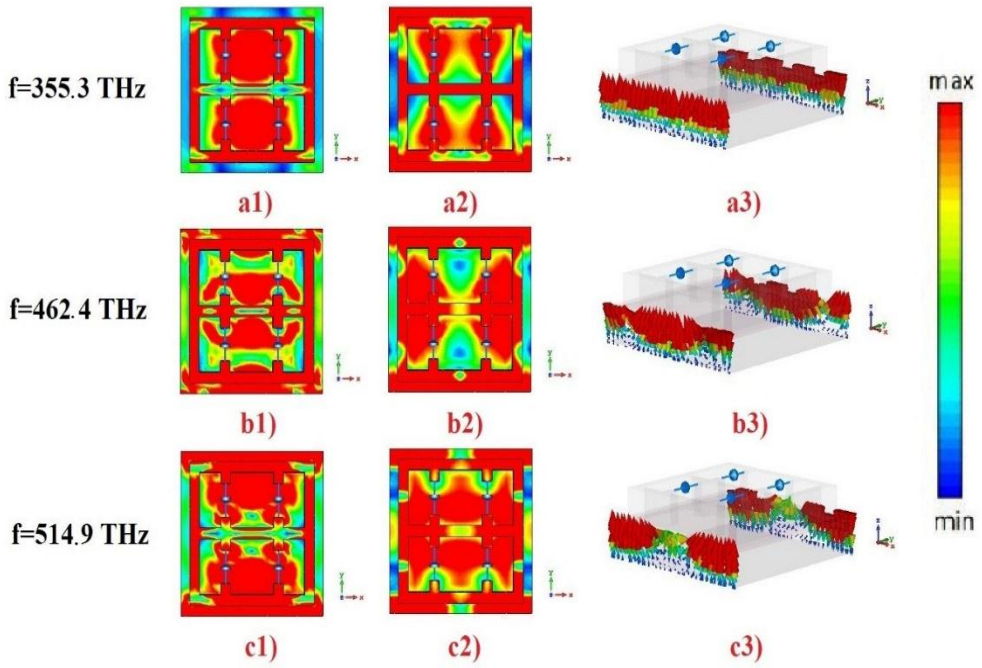

Figure 5-17. For the structure in Figure 5-12 (a1) Electric field distribution (a2) Magnetic field distribution (a3) Surface current distribution at the resonance frequency of 355.3 THz at 900 ohm, (b1) Electric field distribution (b2) Magnetic field distribution (b3) Surface current distribution at the resonance frequency of 462.4 THz at 900 ohm, (c1) Electric field distribution (c2) Magnetic field distribution (c3) Surface current distribution at the resonance frequency of 514.9 THz at 900 ohm (for the with hole & hole substrate (a-Si) & Graphene (Graphene thickness = 1.005 nm (3-layers)) situation).

5.5. Conclusion

Although all bands are not near perfect, triple band is obtained in infrared and visible frequency regime in this chapter. The aim of this chapter is realization of many different parametric studies with applying enhancement techniques in addition to reflectance, absorption, power efficiency, effect of metal plate, fields and surface current distribution results. As a result of this idea, behaviours and effects are seen on results for the structure when utilizing different materials and/or applying enhancement methods. Many comparison opportunities are also created between all results in this chapter above. Proposed structures can be used for many application such as infrared spectroscopy, infrared cameras, solar cells.

CHAPTER 6

ENERGY HARVESTING APPLICATION OF METAMATERIAL ABSORBER INTEGRATED TO THE MICROSTRIP PATCH ANTENNA FOR WIRELESS COMMUNICATION

6.1. Introduction

Microstrip patch antenna, which is utilized in communication technology, is one type of antennas [91, 92]. Main concepts about antennas in literature can be found in [91 – 97]. Here, two microstrip patch antennas are designed for 2.4 GHz operation. Each of them has a rectangular patch metal resonator. Some dimensions of them are different. Also, two different substrate materials are used in designs. According to width and length of each patch, two metamaterial absorber based energy harvesters are designed and horizontally and vertically adding at the top of patch. For each situation, quantities of adding metamaterials as layers are increased until obtain highest performance. Substrate legs between patch and metamaterial are only used during horizontal additions. A metal plate at the bottom of the first adding metamaterial is only used during vertical additions. Electromagnetic incident waves come from +x direction by a waveport (the direction of the propagation). Instead of placing waveport at +z direction (which is applying in previous chapters), waveport is located at +x direction (which is applying for this chapter). Usage of microstrip patch antenna designs in this chapter is the unique reason of this situation, so results can be negatively affected (near to 100% efficiencies can not be obtained because losses will become). Designs, simulations, results and discussions for FR4 substrate and Rogers RT5880 substrate are given in Section 6.2 and in Section 6.3, respectively. The Section 6.4 is the conclusion of this chapter.

6.2. A microstrip patch antenna in 2.4 GHz operation and a metamaterial absorber based energy harvester with FR4 substrate with/without FR4 substrate legs on its patch

6.2.1. Design and Simulation

In Figure 6-1b, the parametric dimensions of a 2.4 GHz (in the microwave (GHz) frequency regime) microstrip patch antenna structure can be seen. A ground metal

plate at the bottom of the structure, a substrate in the middle of the structure, patch, edge-fed and quarter wavelength at the top of the structure are exist. Study has been done with finite integration technique (FIT)-based numerical simulator. Copper metal element is used at the bottom layer (as a ground metal plate) and top (as patch, edge-fed and quarter wavelength) of this structure as metallic layers as shown in Figure 6-1a and Figure 6-1c. Thicknesses are same and equal to 0.035 mm for both bottom and top metallic layers. Also, electrical conductivity of the copper is 5.8001×10^{7} S/m. FR4 is used as a substrate with copper metal for microstrip patch antenna as shown in Figure 6-1. The thickness, loss tangent, relative permittivity and relative permeability of the FR4 substrate material are 1.6 mm, 0.025, 4.3 and 1, respectively. Dimension values of the (Copper, FR4 and Copper) microstrip patch antenna structure x, y, W, L, w_{qw}, I_{qw}, w_{50} and I_{50} are given as 110, 98.5, 22, 28, 0.72, 24.05, 4.84 and 15 mm, correspondingly [Figure 6-1b]. Dimension values of the rectangular waveport a (width) and b (height) are given as 50 and 15 mm, respectively [Figure 6-1c]. S-parameter settings are normalized to fixed impedance (50 ohms). For the x-, y-, and z-directions, open (add space) boundary conditions are selected.

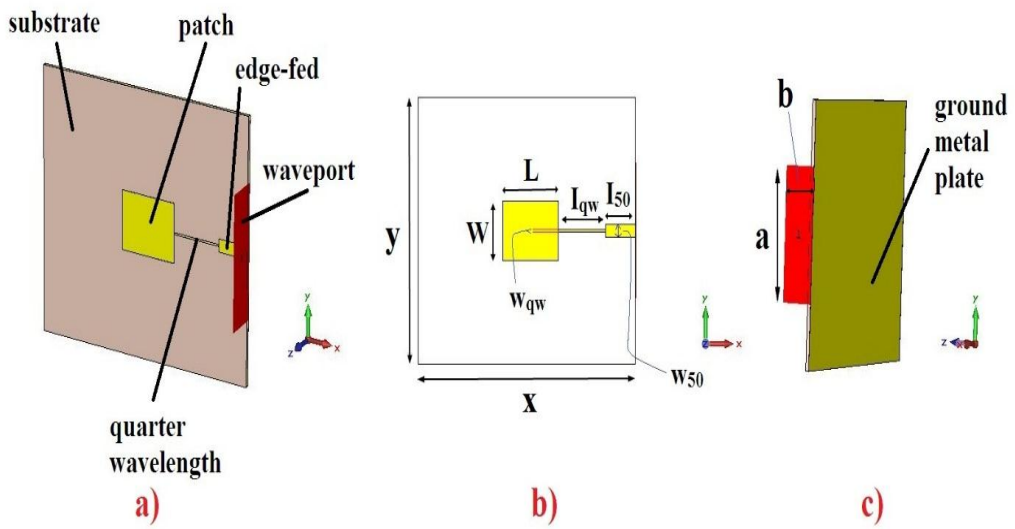

Figure 6-1. (a) Substrate, patch, edge-fed, quarter wavelength and waveport (b) dimensions, (c) ground metal plate and dimensions of waveport for a 2.4 GHz microstrip patch antenna in microwave (GHz) range.

6.2.2. Result and Discussion

Numerical reflectance result can be seen in Figure 6-2. In Figure 6-2, minimum reflectance results are obtained around 0.029, 0.739 and 0.280 at 2.380 GHz, 3.320 GHz and 4.788 GHz, respectively. First resonance at 2.380 GHz is more important because 2.380 GHz is around 2.4 GHz and we would like to design an antenna for 2.4 GHz operation.

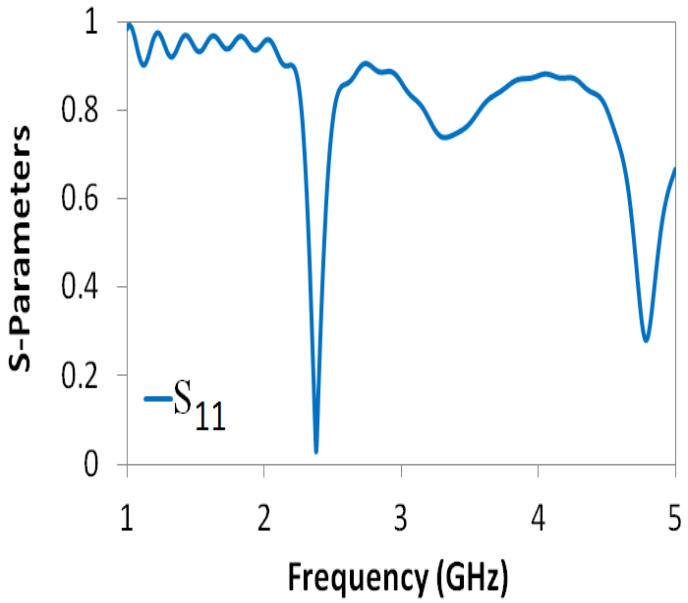

Figure 6-2. Reflectance result for a 2.4 GHz microstrip patch antenna design in Figure 6-1 in microwave (GHz) range from 1 GHz to 5 GHz (The resonance frequencies at 2.380 GHz, 3.320 GHz and 4.788 GHz).

In Figure 6-3a, a metamaterial absorber based energy harvester with four legs is horizontally adding at the top of the patch on the designed a 2.4 GHz microstrip patch antenna in Figure 6-1. Dimensions, FR4 substrate, Copper resonator and four resistors of this adding metamaterial absorber based energy harvester can be seen in Figure 6-3b1. Four FR4 (substrate) legs and Copper metal plate of this adding metamaterial absorber based energy harvester can be seen in Figure 6-3b2. Dimensions of FR4 (substrate) legs, which are located between Copper patch layer of the antenna and Copper metal plate of the metamaterial absorber based energy harvester as shown in Figure 6-3a, can be seen in Figure 6-3b3. Dimension values in Figure 6-3b1and in Figure 6-3b3 W, L, h, k and g are given 22, 28, 15, 2.5 and 5 mm, respectively. Thicknesses are same and equal to 0.035 mm for both bottom (metal plate) and top

(resonator) metallic layers. Also, electrical conductivity of the copper is 5.8001×10^{7} S/m as it is used in antenna design above in this chapter. FR4 is used as a substrate for both metamaterial absorber based energy harvester and four legs. The thickness, loss tangent, relative permittivity and relative permeability of the FR4 substrate material are 1.6 mm, 0.025, 4.3 and 1, respectively.

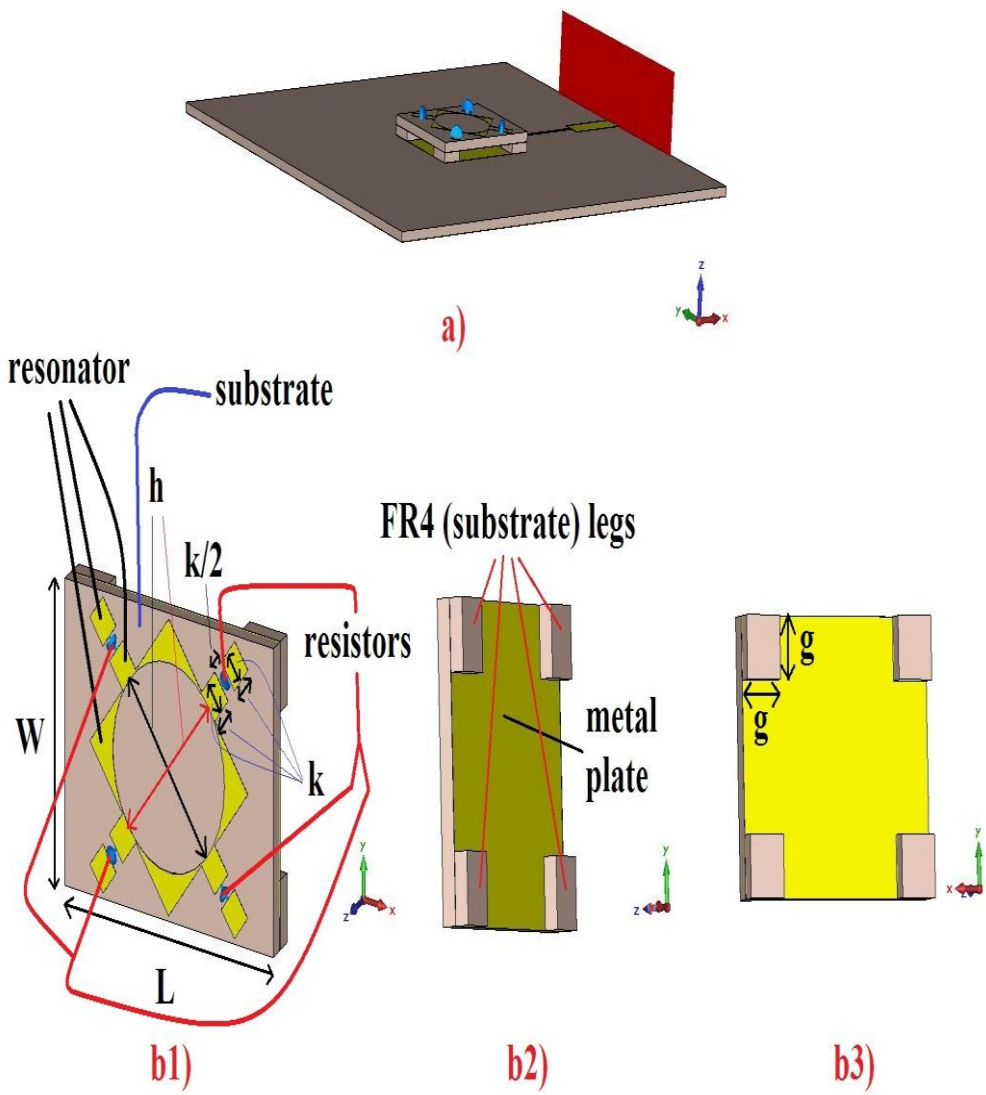

Figure 6-3. (a) Adding four FR4 substrate legs and metamaterial absorber based energy harvester on a 2.4 GHz microstrip patch antenna in microwave (GHz) range (b1) Dimensions, FR4 substrate, Copper resonator and four resistors for a metamaterial absorber based energy harvester (b2) FR4 (substrate) legs and Copper metal plate, (b3) dimensions of FR4 (substrate) legs .

Numerical reflectance and absorption result can be seen in Figure 6-4. In Figure 6-4, maximum absorptions are obtained around 95.06%, 43.83% and 94.90% at 2.348 GHz, 3.156 GHz and 4.804 GHz, respectively. This values are obtained when four 10 ohm resistors are placed across the gaps for the structure in Figure 6-3a.

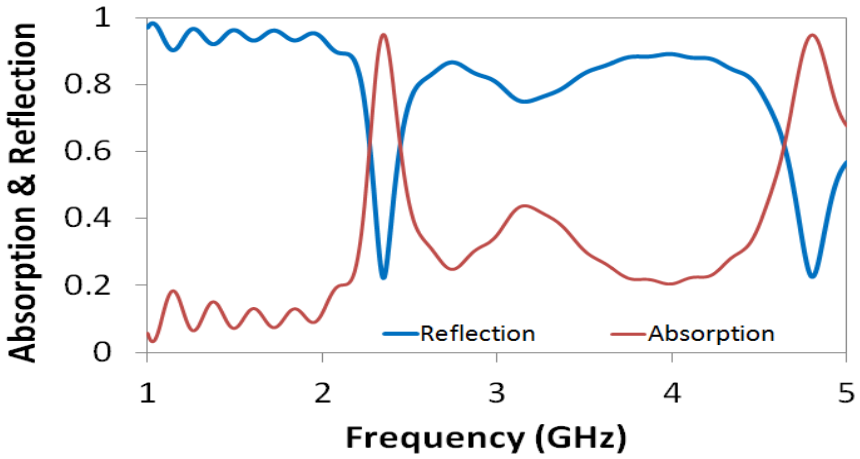

Figure 6-4. Reflectance and absorption results for the design in Figure 6-3a in microwave (GHz) range from 1 GHz to 5 GHz (The resonance frequencies at 2.348 GHz, 3.156 GHz and 4.804 GHz).

Four lumped network elements (resistors) are located as shown in Figure 6-3a. When input powers were chosen 0.500 W, maximum efficiencies are obtained around 4.00% (output power is 0.020 W) at 2.424 GHz, 0.20% (output power is 0.001 W) at 2.764 GHz and less than 0.10% (output power is less than 0.001 W) at 4.908 GHz at 10 ohm as shown in Figure 6-5.

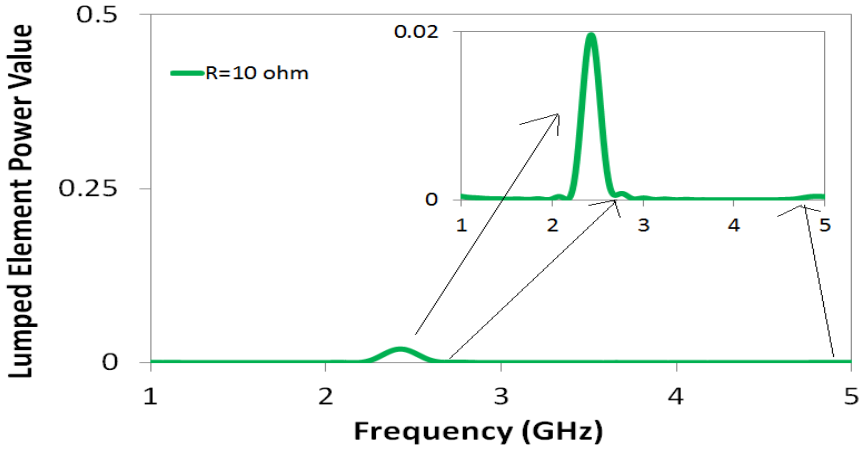

Figure 6-5. Gathered power frequency diagram for four 10 ohm resistors for the design in Figure 6-3a in microwave (GHz) range from 1 GHz to 5 GHz (The resonance frequencies at 2.424 GHz, 2.764 GHz and 4.908 GHz).

In Figure 6-6, increasing quantities of metamaterial absorber based energy harvester with their legs can be seen on the designed 2.4 GHz microstrip patch antenna in microwave (GHz) range. Four 10 ohm resistors are located across the gaps on each resonator for each adding metamaterial absorber based energy harvester. Metamaterial absorber based energy harvester with their legs are horizontally adding 9 – times on top of the each previous adding, so ten layers of metamaterial absorber based energy harvester with their legs are become on designed antenna as shown in Figure 6-6.

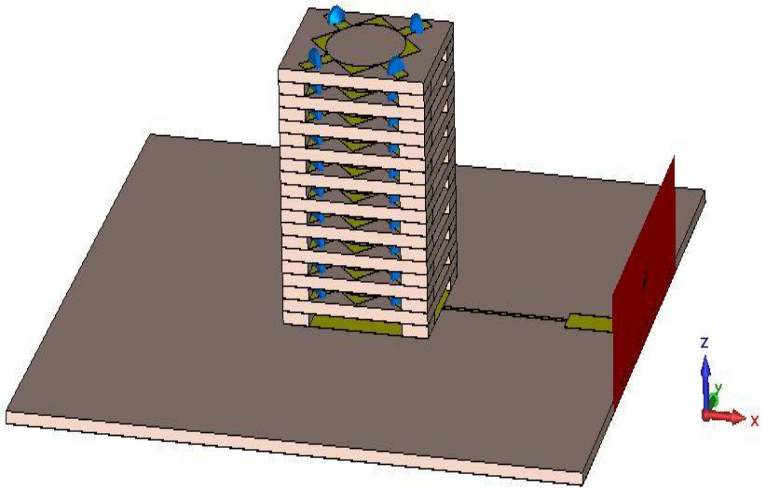

Figure 6-6. Adding ten layers metamaterial absorber based energy harvester with their legs on a 2.4 GHz microstrip patch antenna in microwave (GHz) range (Each layer have four 10 ohm resistors).

Numerical absorption results can be seen in Figure 6-7 for three different (three different quantities of adding metamaterial absorber based energy harvesters with their legs) layers. For adding 2 – layers, maximum absorptions are obtained around 95.51% at 2.348 GHz, 45.19% at 3.160 GHz and 93.01% at 4.804 GHz in Figure 6-7. For adding 5 – layers, maximum absorptions are obtained around 96.83% at 2.340 GHz, 43.95% at 3.136 GHz and 93.05% at 4.820 GHz in Figure 6-7. For adding 10 – layers, maximum absorptions are obtained around 97.78% at 2.344 GHz, 44.21% at 3.148 GHz and 93.69% at 4.820 GHz in Figure 6-7. These values are obtained when four 10 ohm resistors are placed across the gaps on each resonator for each adding metamaterial absorber based energy harvester at the structure in Figure 6-6.

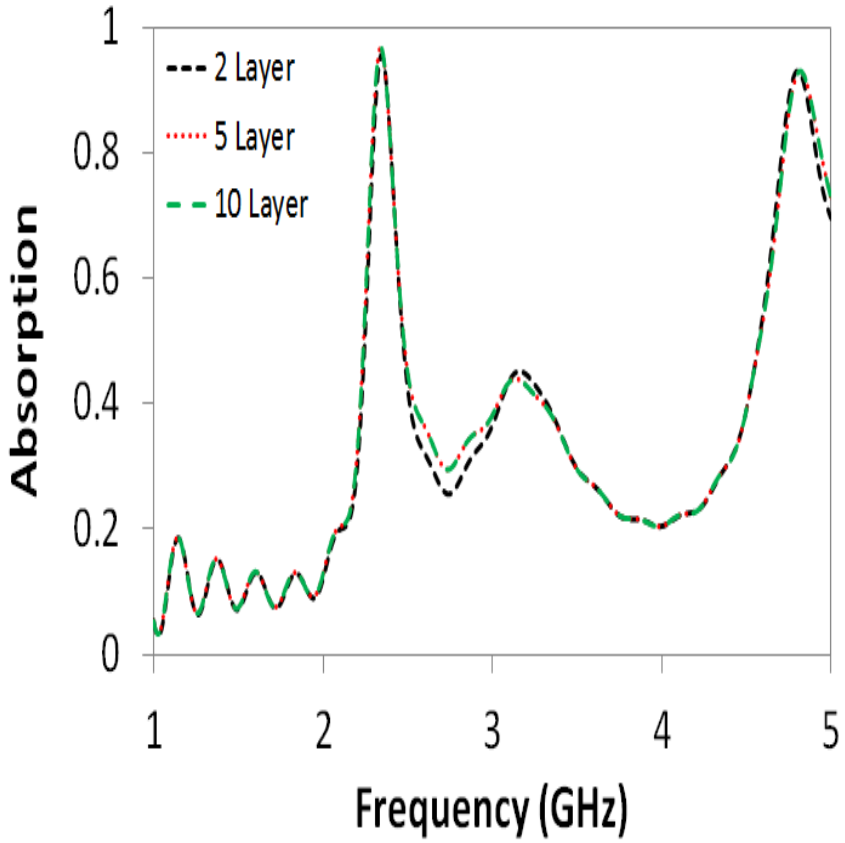

Figure 6-7. Gathered absorption frequency diagram for selected different quantities of adding layers between 2 – 10 layers for the structure in Figure 6-6.

For adding 2 – layer, maximum efficiencies are obtained around 3.40% (output power is 0.017 W) at 2.392 GHz, 0.40% (output power is 0.002 W) at 3.356 GHz and 0.60% (output power is 0.003 W) at 4.884 GHz at 10 ohm as shown in Figure 6-8. For adding 5 – layer, maximum efficiencies are obtained around 4.40% (output power is 0.022 W) at 2.392 GHz, 0.60% (output power is 0.003 W) at 2.956 GHz and 1.40% (output power is 0.007 W) at 4.900 GHz at 10 ohm as shown in Figure 6-8. For adding 10 – layer, maximum efficiencies are obtained around 10.00% (output power is 0.050 W) at 2.408 GHz, 1.00% (output power is 0.005 W) at 3.176 GHz and 2.00% (output power is 0.010 W) at 4.904 GHz at 10 ohm as shown in Figure 6-8. These values are obtained when four 10 ohm resistors are placed across the gaps on each resonator for each adding metamaterial absorber based energy harvester at the structure in Figure 6-6.

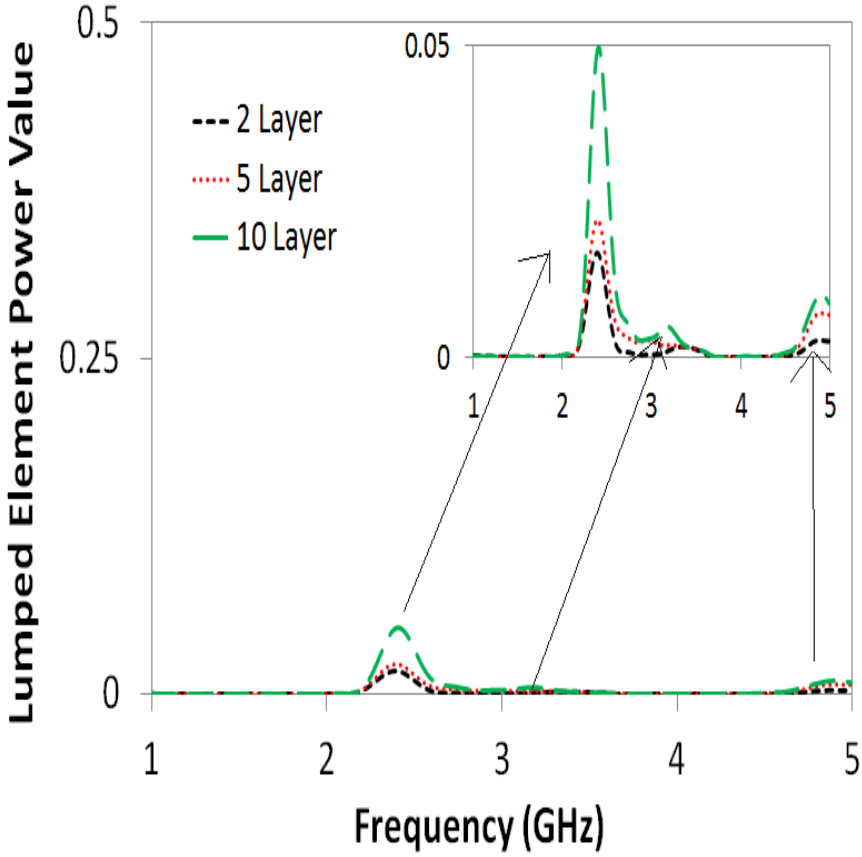

Figure 6-8. Gathered power frequency diagram for selected different quantities of adding layers between 2 – 10 layers for the structure in Figure 6-6.

The electric field, magnetic field, and surface current distributions are given in Figure 6-9 at the first resonance frequency in order to understand better the physical mechanism of the structure in Figure 6-6. Concentrations of these distributions are from on and near of edge-fed, quarter wavelength, patch to on gaps and some parts of resonators of adding layers. The basis of this is the design can be used as a voltage source due to the confinement of the EM waves at the resonance frequency. In Figure 6-9a, electric field at the top of the substrate layer of the microstrip patch antenna behaves as a dipole. Furthermore, typical radiation pattern and three – dimensional far – field pattern are given in Figure 6-10 at the first resonance frequency. The same far – field is shown from two different directions in Figure 6-10b1 and in Figure 6-10b2. In Figure 6-10(b1 or b2), electromagnetic waves propagate +z direction.

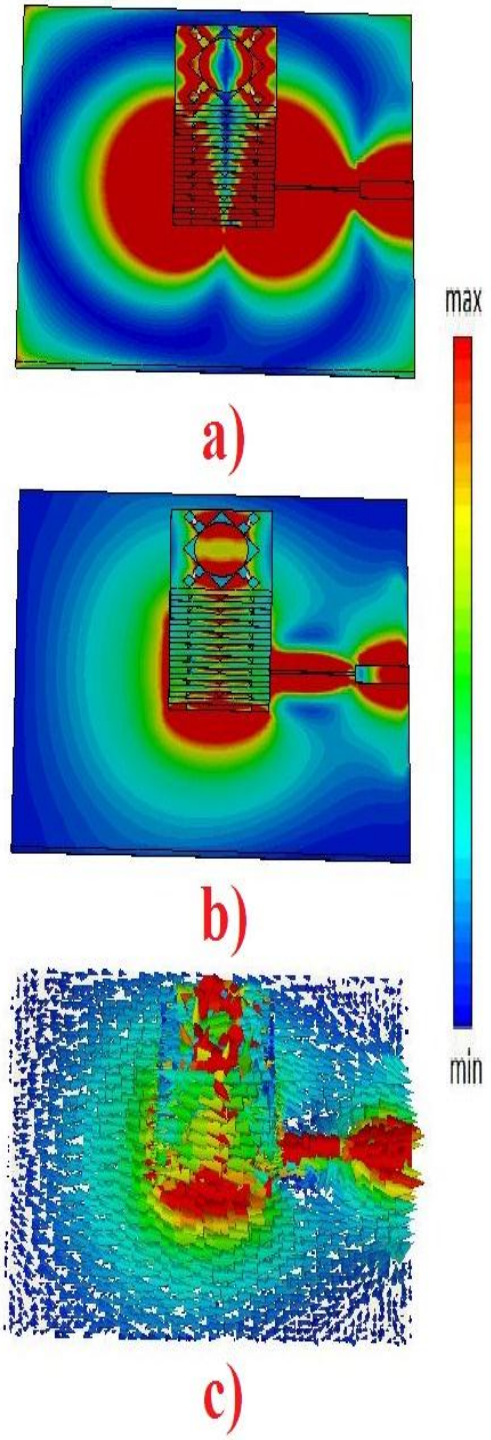

Figure 6-9. For the structure (adding 10 – layers metamaterial absorber based energy harvester with their legs on the designed 2.4 GHz microstrip patch antenna in microwave (GHz) range) in Figure 6-6 (a) Electric field distribution (b) Magnetic field distribution (c) Surface current distribution at the resonance frequency of 2.344 GHz at 10 ohm.

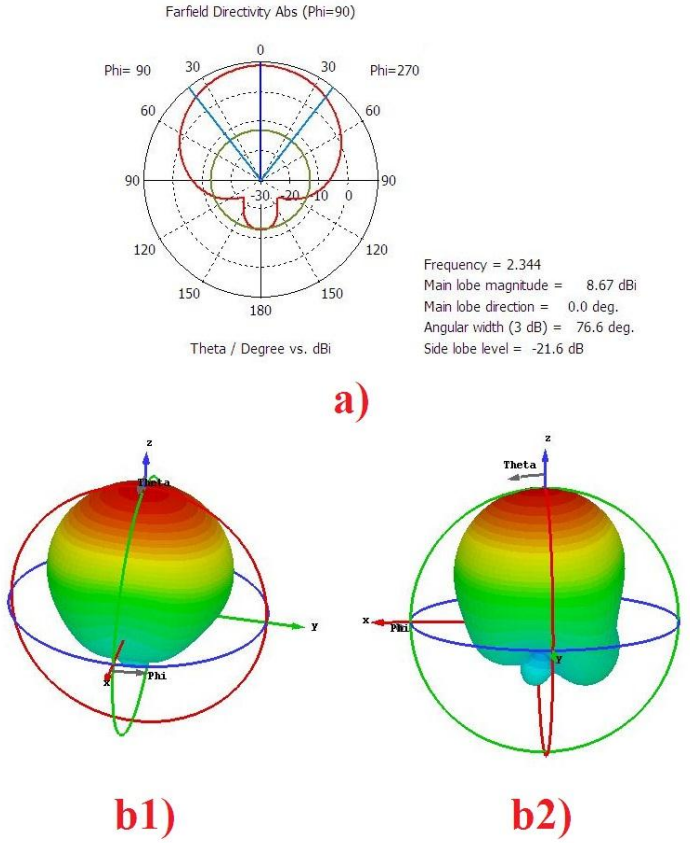

Figure 6-10. For the structure (adding 10 – layers metamaterial absorber based energy harvester with their legs on the designed 2.4 GHz microstrip patch antenna in microwave (GHz) range) in Figure 6-6 (a) typical radiation pattern (b1) and (b2) view of three – dimensional far – field pattern from two different sides at the resonance frequency of 2.344 GHz at 10 ohm.

In Figure 6-11a, a metamaterial absorber based energy harvester (without any legs due to placing vertical) is vertically adding at the top of the patch on the designed a 2.4 GHz microstrip patch antenna in Figure 6-1. Dimensions, FR4 substrate, Copper resonator and four resistors of this adding metamaterial absorber based energy harvester can be seen in Figure 6-11b1. Copper metal plate of this adding metamaterial absorber based energy harvester can be seen in Figure 6-11b2. In Figure 6-11b1, dimension values W, L, h and k are given 22, 28, 15 and 2.5 mm, respectively. Thicknesses are same and equal to 0.035 mm for both bottom (metal plate) and top (resonator) metallic layers. Also, electrical conductivity of the copper is 5.8001×10^{7} S/m as it is used in antenna design above in this chapter. FR4 is used as a substrate for metamaterial absorber based energy harvester. The thickness, loss tangent, relative

permittivity and relative permeability of the FR4 substrate material are 1.6 mm, 0.025, 4.3 and 1, respectively.

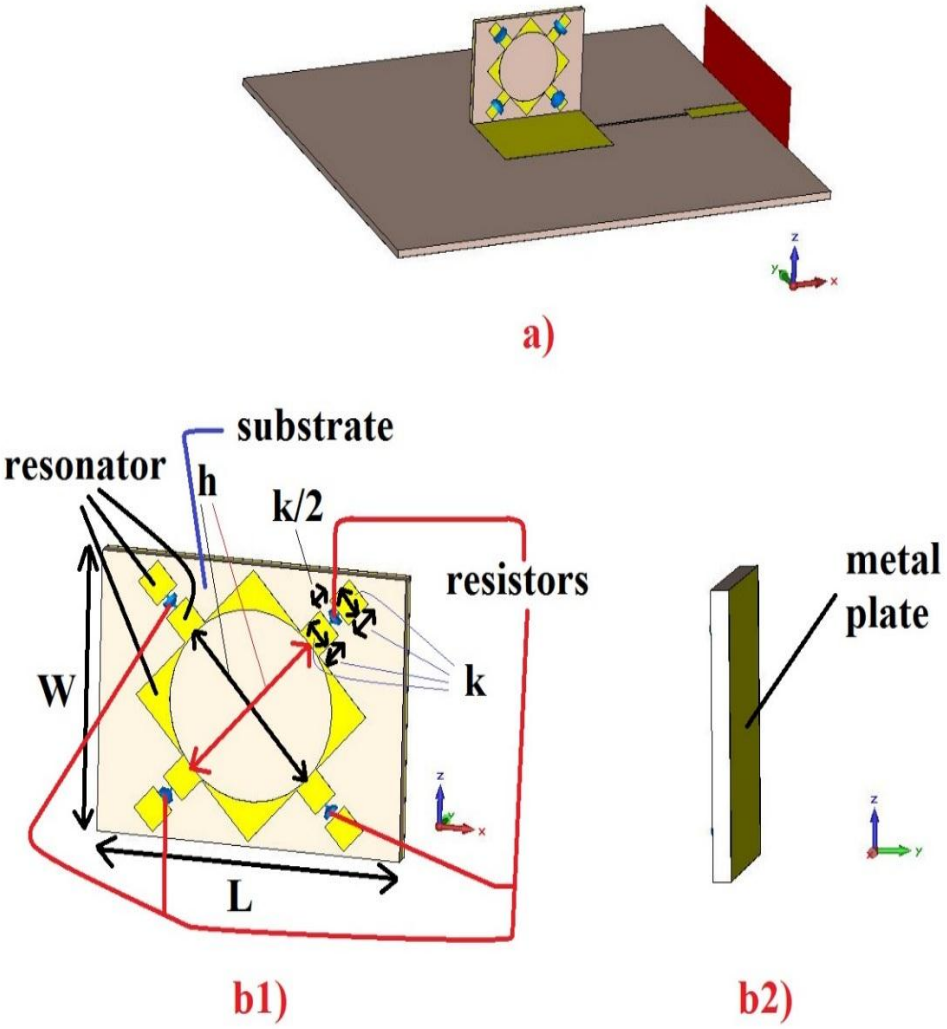

Figure 6-11. (a) Adding metamaterial absorber based energy harvester on a 2.4 GHz microstrip patch antenna in microwave (GHz) range (b1) Dimensions, FR4 substrate, Copper resonator and four resistors for a metamaterial absorber based energy harvester (b2) Copper metal plate for a metamaterial absorber based energy harvester.

Numerical reflection and absorption result can be seen in Figure 6-12. In Figure 6-12, maximum absorptions are obtained around 99.01%, 50.26% and 91.99% at 2.376 GHz, 3.336 GHz and 4.860 GHz, respectively. This values are obtained when four 10 ohm resistors are placed across the gaps for the structure in Figure 6-11a.

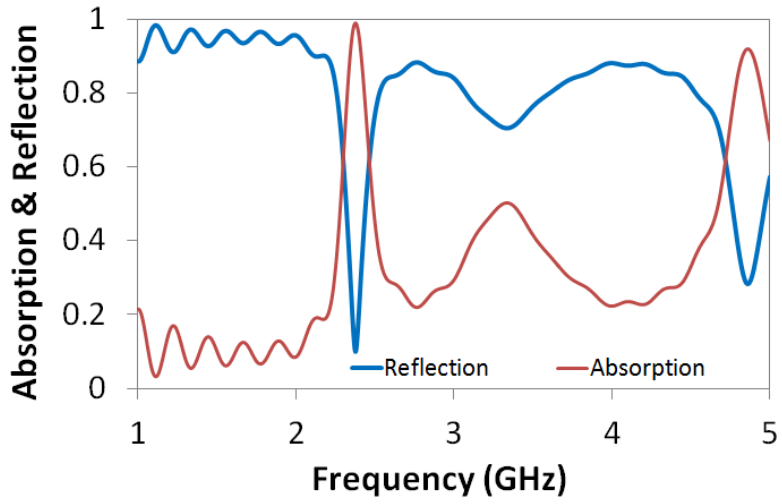

Figure 6-12. Reflectance and absorption results for the design in Figure 6-11a in microwave (GHz) range from 1 GHz to 5 GHz (The resonance frequencies at 2.376 GHz, 3.336 GHz and 4.860 GHz).

Four lumped network elements (resistors) are located as shown in Figure 6-11a. When input powers were chosen 0.500 W, maximum efficiencies are obtained around 0.20% (output power is less than (but approximately near to) 0.001 W) at 2.372 GHz, around 0.20% (output power is less than (but approximately near to) 0.001 W) at 3.740 GHz and less than 0.10% (output power is less than 0.001 W) at 4.908 GHz at 10 ohm as shown in Figure 6-13.

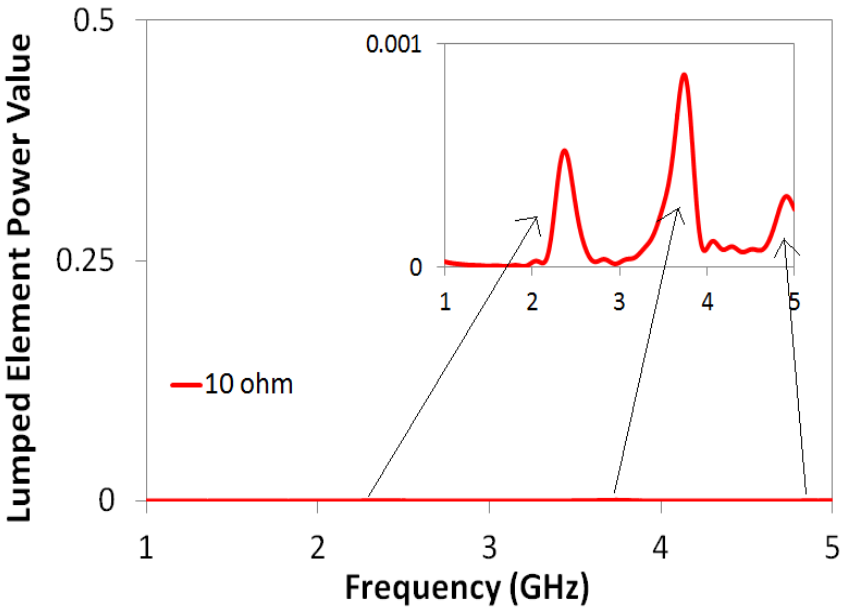

Figure 6-13. Gathered power frequency diagram for four 10 ohm resistors for the design in Figure 6-11a in microwave (GHz) range from 1 GHz to 5 GHz (The resonance frequencies at 2.372 GHz, 3.740 GHz and 4.908 GHz).

In Figure 6-14, increasing quantities of metamaterial absorber based energy harvester without their Copper metal plates can be seen on the designed 2.4 GHz microstrip patch antenna in microwave (GHz) range. Four 10 ohm resistors are located across the gaps on each resonator for each adding metamaterial absorber based energy harvester. Metamaterial absorber based energy harvester without their Copper metal plates are vertically adding 12 – times next to the each previous adding, so thirteen layers are become on designed antenna as shown in Figure 6-14. Copper metal plate is only used for the back of the first adding metamaterial absorber based energy harvester. It is not adding for backs of others. There are not any overflows from the top of the patch on the microstrip antenna after thirteen layers have adding.

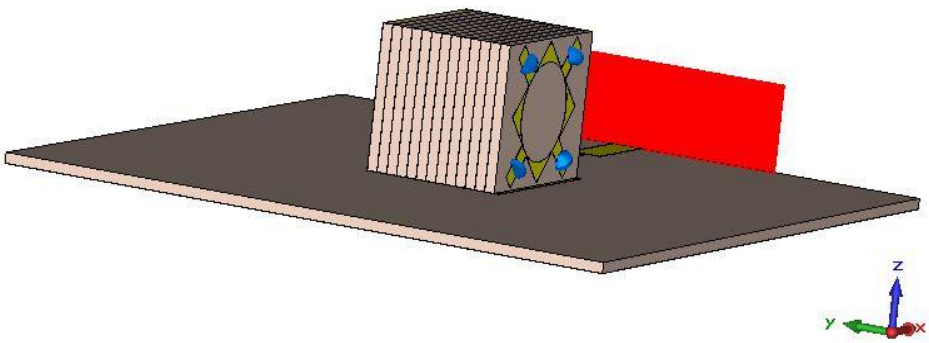

Figure 6-14. Adding thirteen layers metamaterial absorber based energy harvesters without their Copper metal plates (excluded for the first layer) on a 2.4 GHz microstrip patch antenna in microwave (GHz) range (Each layer have four 10 ohm resistors).

Numerical absorption results can be seen in Figure 6-15 for three different (three different quantities of adding metamaterial absorber based energy harvesters without their Copper metal plates (excluded for the first layer)) layers. For adding 2 – layers, maximum absorptions are obtained around 98.76% at 2.376 GHz, 51.09% at 3.336 GHz and 91.88% at 4.860 GHz in Figure 6-15. For adding 7 – layers, maximum absorptions are obtained around 99.19% at 2.368 GHz, 52.97% at 3.332 GHz and 91.56% at 4.864 GHz in Figure 6-15. For adding 13 – layers, maximum absorptions are obtained around 96.43% at 2.348 GHz, 52.74% at 3.320 GHz and 86.46% at 4.876 GHz in Figure 6-15. These values are obtained when four 10 ohm resistors are placed

across the gaps on each resonator for each adding metamaterial absorber based energy harvester at the structure in Figure 6-14.

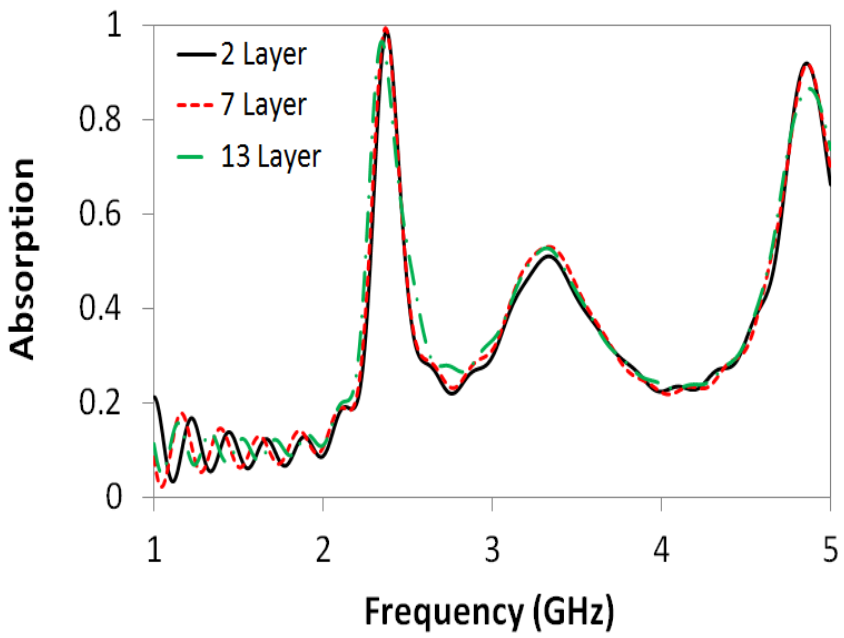

Figure 6-15. Gathered absorption frequency diagram for selected different quantities of adding layers between 2 – 13 layers for the structure in Figure 6-14.

For adding 2 – layer, maximum efficiencies are obtained around 0.20% (output power is 0.001 W) at 2.468 GHz, 0.60% (output power is 0.003 W) at 3.728 GHz and 0.20% (output power is approximately 0.001 W) at 4.916 GHz at 10 ohm as shown in Figure 6-16. For adding 7 – layer, maximum efficiencies are obtained around 1.00% (output power is 0.005 W) at 2.484 GHz, 1.40% (output power is 0.007 W) at 3.636 GHz and 2.20% (output power is 0.011 W) at 4.832 GHz at 10 ohm as shown in Figure 6-16. For adding 13 – layer, maximum efficiencies are obtained around 13.80% (output power is 0.069 W) at 2.392 GHz, 0.80% (output power is 0.004 W) at 3.556 GHz and 6.00% (output power is 0.030 W) at 4.908 GHz at 10 ohm as shown in Figure 6-16. These values are obtained when four 10 ohm resistors are placed across the gaps on each resonator for each adding metamaterial absorber based energy harvester at the structure in Figure 6-14.

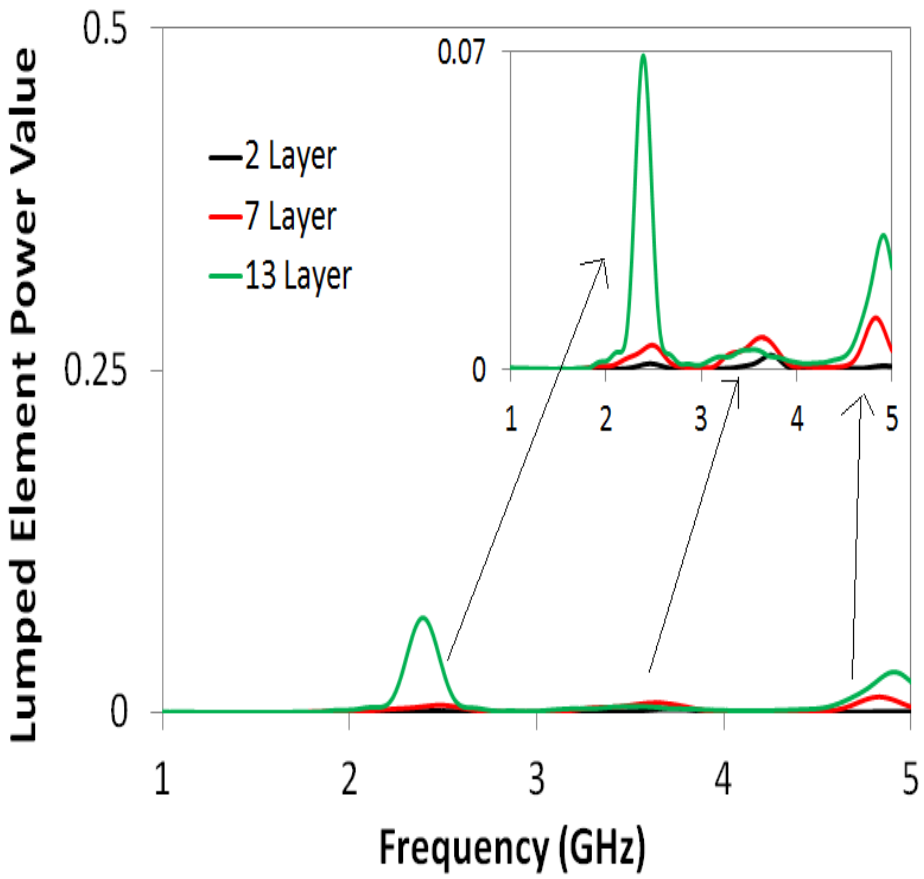

Figure 6-16. Gathered power frequency diagram for selected different quantities of adding layers between 2 – 13 layers for the structure in Figure 6-14.

The electric field, magnetic field, and surface current distributions are given in Figure 6-17 at the first resonance frequency in order to understand better the physical mechanism of the structure in Figure 6-14. Concentrations of these distributions are from on and near of edge-fed, quarter wavelength, patch to on gaps and some parts of resonators of adding layers. The basis of this is the design can be used as a voltage source due to the confinement of the EM waves at the resonance frequency. In Figure 6-17a, electric field at the top of the substrate layer of the microstrip patch antenna behaves as a dipole. Furthermore, typical radiation pattern and three – dimensional far – field pattern are given in Figure 6-18 at the first resonance frequency. The same far – field is shown from two different directions in Figure 6-18b1 and in Figure 6-18b2. In Figure 6-18(b1 or b2), electromagnetic waves propagate +z direction.

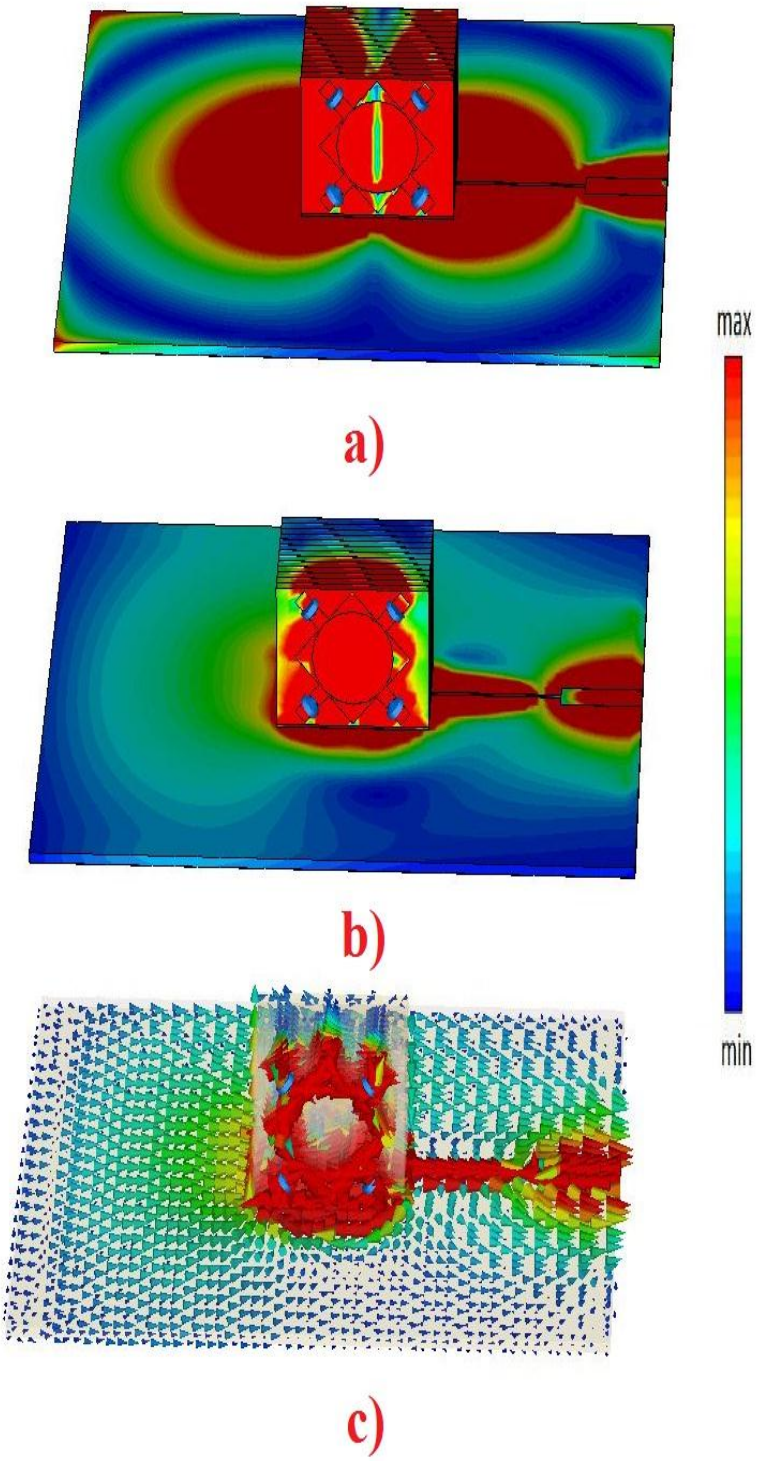

Figure 6-17. For the structure (adding 13 – layers metamaterial absorber based energy harvester without their Copper metal plate (excluded for the first layer) on the designed 2.4 GHz microstrip patch antenna in microwave (GHz) range) in Figure 6-14 (a) Electric field distribution (b) Magnetic field distribution (c) Surface current distribution at the resonance frequency of 2.348 GHz at 10 ohm.

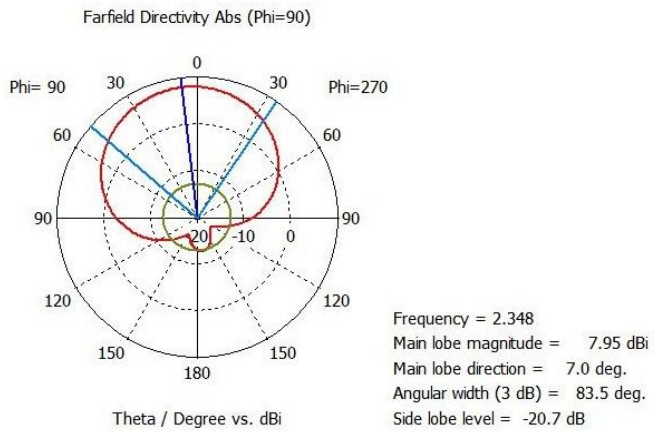

a)

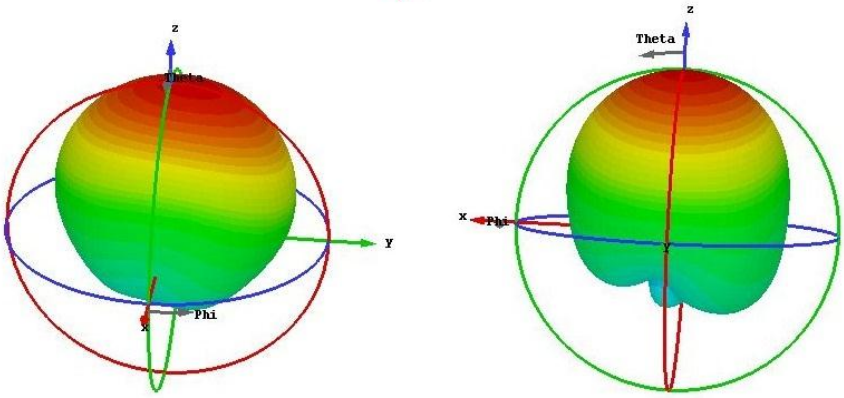

b1) b2)

Figure 6-18. For the structure (adding 13 – layers metamaterial absorber based energy harvester without their Copper metal plate (excluded for the first layer) on the designed 2.4 GHz microstrip patch antenna in microwave (GHz) range) in Figure 6-14 (a) typical radiation pattern (b1) and (b2) view of three – dimensional far – field pattern from two different sides at the resonance frequency of 2.348 GHz at 10 ohm.

6.3. A microstrip patch antenna in 2.4 GHz operation and a metamaterial absorber based energy harvester with Rogers RT5880 substrate with/without Rogers RT5880 substrate legs on its patch

6.3.1. Design and Simulation

In Figure 6-19b, the parametric dimensions of a 2.4 GHz (in the microwave (GHz) frequency regime) microstrip patch antenna structure can be seen. A ground metal plate at the bottom of the structure, a substrate in the middle of the structure, patch,

edge-fed and quarter wavelength at the top of the structure are exist. Study has been done with finite integration technique (FIT)-based numerical simulator. Copper metal element is used at the bottom layer (as a ground metal plate) and top (as patch, edge-fed and quarter wavelength) of this structure as metallic layers as shown in Figure 6-19a and Figure 6-19c. Thicknesses are same and equal to 0.035 mm for both bottom and top metallic layers. Also, electrical conductivity of the copper is 5.8001×10^{7} S/m. Rogers RT5880 is used as a substrate with copper metal for microstrip patch antenna as shown in Figure 6-19. The thickness, loss tangent, relative permittivity and relative permeability of the Rogers RT5880 substrate material are 1.6 mm, 0.0009, 2.2 and 1, respectively. Dimension values of the (Copper, Rogers RT5880 and Copper) microstrip patch antenna structure x, y, W, L, w_{qw}, I_{qw}, w_{50} and I_{50} are given as 110, 98.5, 49.38, 41.32, 0.72, 24.05, 4.84 and 15 mm, correspondingly [Figure 6-19b]. Dimension values of the rectangular waveport a (width) and b (height) are given as 50 and 15 mm, respectively [Figure 6-19c]. S-parameter settings are normalized to fixed impedance (50 ohms). For the x-, y-, and z- directions, open (add space) boundary conditions are selected.

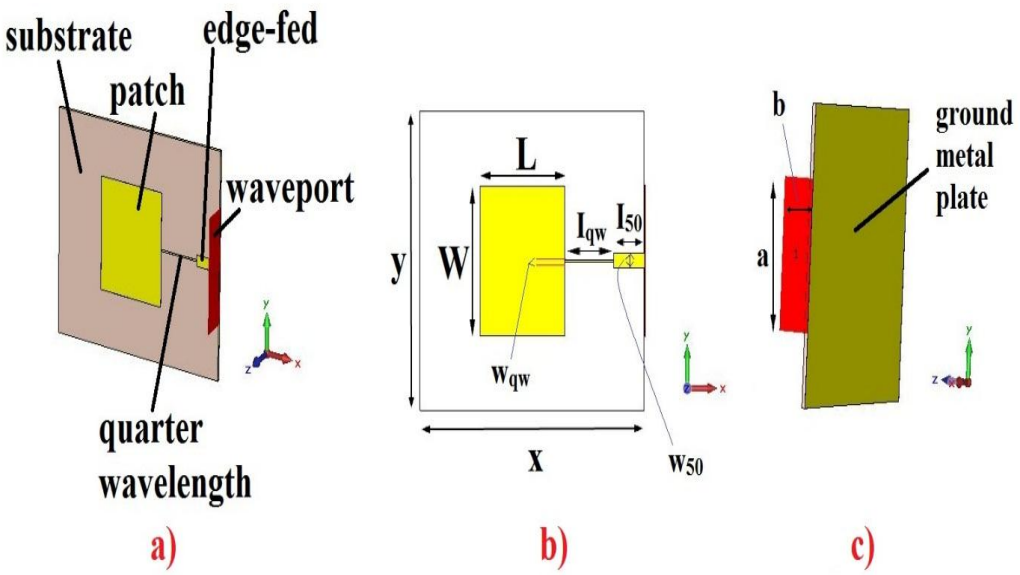

Figure 6-19. (a) Substrate, patch, edge-fed, quarter wavelength and waveport (b) dimensions, (c) ground metal plate and dimensions of waveport for a 2.4 GHz microstrip patch antenna in microwave (GHz) range.

6.3.2. Result and Discussion

Numerical reflectance result can be seen in Figure 6-20. In Figure 6-2, minimum reflectance results are obtained around 0.034, 0.059 and 0.671 at 2.324 GHz, 3.852 GHz and 4.796 GHz, respectively. First resonance at 2.324 GHz is more important because 2.324 GHz is around 2.4 GHz and we would like to design an antenna for 2.4 GHz operation.

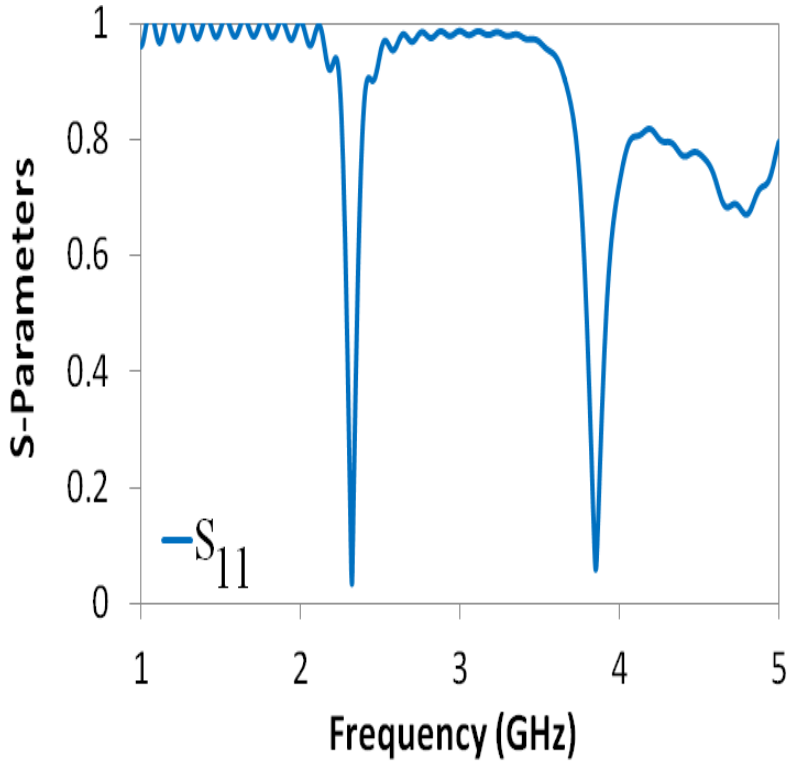

Figure 6-20. Reflectance result for a 2.4 GHz microstrip patch antenna design in Figure 6-19 in microwave (GHz) range from 1 GHz to 5 GHz (The resonance frequencies at 2.324 GHz, 3.852 GHz and 4.796 GHz).

In Figure 6-21a, a metamaterial absorber based energy harvester with four legs is horizontally adding at the top of the patch on the designed a 2.4 GHz microstrip patch antenna in Figure 6-19. Dimensions, Rogers RT5880 substrate, Copper resonator and four resistors of this adding metamaterial absorber based energy harvester can be seen in Figure 6-21b1. Four Rogers RT5880 (substrate) legs and Copper metal plate of this adding metamaterial absorber based energy harvester can be seen in Figure 6-21b2. Dimensions of Rogers RT5880 (substrate) legs, which are located between Copper patch layer of the antenna and Copper metal plate of the metamaterial absorber based

energy harvester as shown in Figure 6-21a, can be seen in Figure 6-21b3. Dimension values in Figure 6-21b1and in Figure 6-21b3 W, L, h, k and g are given 49.38, 41.32, 25, 5 and 5 mm, respectively. Thicknesses are same and equal to 0.035 mm for both bottom (metal plate) and top (resonator) metallic layers. Also, electrical conductivity of the copper is 5.8001×10^{7} S/m as it is used in antenna design above in this chapter. Rogers RT5880 is used as a substrate for both metamaterial absorber based energy harvester and four legs. The thickness, loss tangent, relative permittivity and relative permeability of the Rogers RT5880 substrate material are 1.6 mm, 0.0009, 2.2 and 1, respectively.

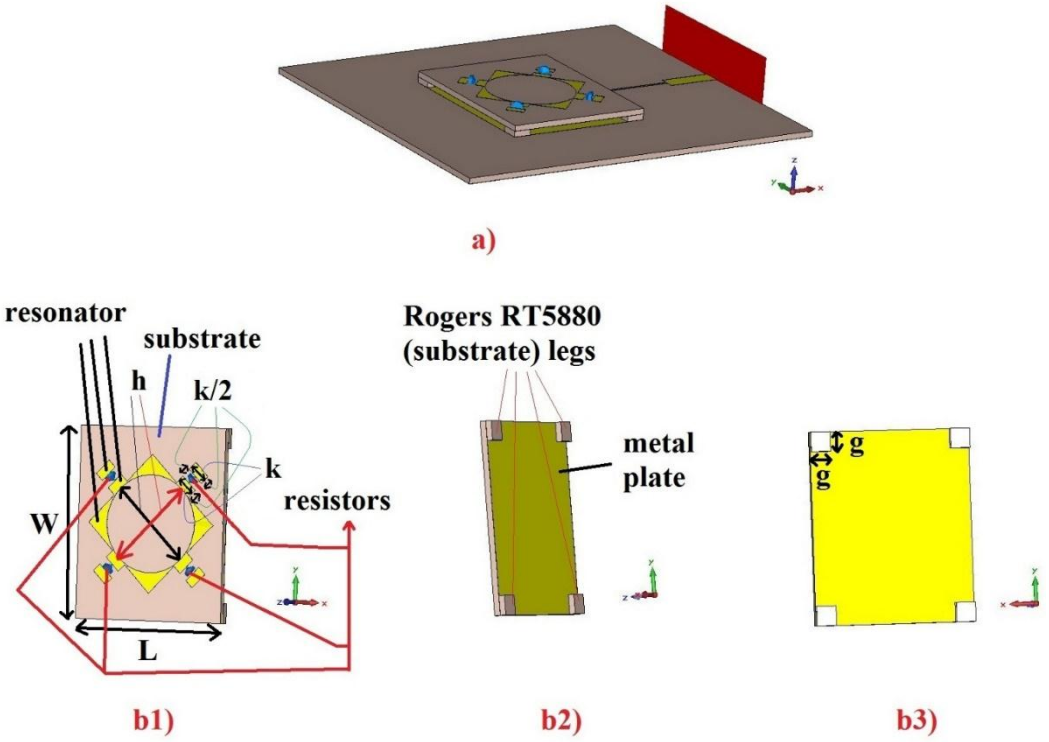

Figure 6-21. (a) Adding four Rogers RT5880 substrate legs and metamaterial absorber based energy harvester on a 2.4 GHz microstrip patch antenna in microwave (GHz) range (b1) Dimensions, Rogers RT5880 substrate, Copper resonator and four resistors for a metamaterial absorber based energy harvester (b2) Rogers RT5880 (substrate) legs and Copper metal plate, (b3) dimensions of Rogers RT5880 (substrate) legs.

Numerical reflection and absorption result can be seen in Figure 6-22. In Figure 6-22, maximum absorptions are obtained around 96.15%, 99.59% and 73.55% at 2.312 GHz,

3.860 GHz and 4.760 GHz, respectively. This values are obtained when four 4700 ohm resistors are placed across the gaps for the structure in Figure 6-21a.

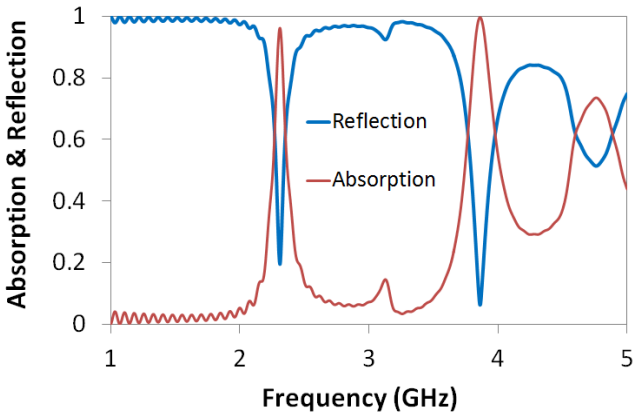

Figure 6-22. Reflectance and absorption results for the design in Figure 6-21a in microwave (GHz) range from 1 GHz to 5 GHz (The resonance frequencies at 2.312 GHz, 3.860 GHz and 4.760 GHz).

Four lumped network elements (resistors) are located as shown in Figure 6-21a. When input powers were chosen 0.500 W, maximum efficiency is obtained around 6.00% (output power is 0.030 W) at 2.304 GHz at 4700 ohm as shown in Figure 6-23.

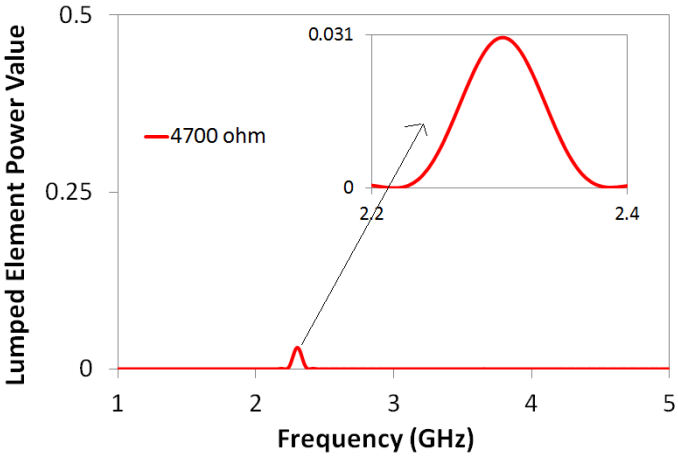

Figure 6-23. Gathered power frequency diagram for four 4700 ohm resistors for the design in Figure 6-21a in microwave (GHz) range from 1 GHz to 5 GHz (The resonance frequency at 2.304 GHz).

In Figure 6-24, increasing quantities of metamaterial absorber based energy harvester with their legs can be seen on the designed 2.4 GHz microstrip patch antenna in

microwave (GHz) range. Four 4700 ohm resistors are located across the gaps on each resonator for each adding metamaterial absorber based energy harvester. Metamaterial absorber based energy harvester with their legs are horizontally adding 5 – times on top of the each previous adding, so six layers of metamaterial absorber based energy harvester with their legs are become on designed antenna as shown in Figure 6-24.

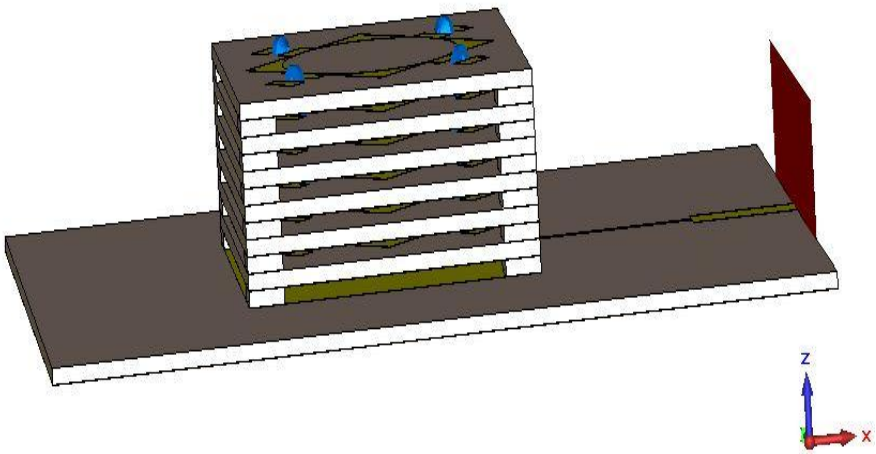

Figure 6-24. Adding six layers metamaterial absorber based energy harvester with their legs on a 2.4 GHz microstrip patch antenna in microwave (GHz) range (Each layer have four 4700 ohm resistors).

Numerical absorption results can be seen in Figure 6-25 for three different (three different quantities of adding metamaterial absorber based energy harvesters with their legs) layers. For adding 2 – layers, maximum absorptions are obtained around 97.22% at 2.304 GHz, 95.34% at 3.848 GHz and 85.17% at 4.756 GHz in Figure 6-25. For adding 4 – layers, maximum absorptions are obtained around 96.25% at 2.304 GHz, 88.53% at 3.888 GHz and 94.09% at 4.768 GHz in Figure 6-25. For adding 6 – layers, maximum absorptions are obtained around 97.08% at 2.304 GHz, 95.85% at 3.912 GHz and 87.62% at 4.780 GHz in Figure 6-25. These values are obtained when four 4700 ohm resistors are placed across the gaps on each resonator for each adding metamaterial absorber based energy harvester at the structure in Figure 6-24.

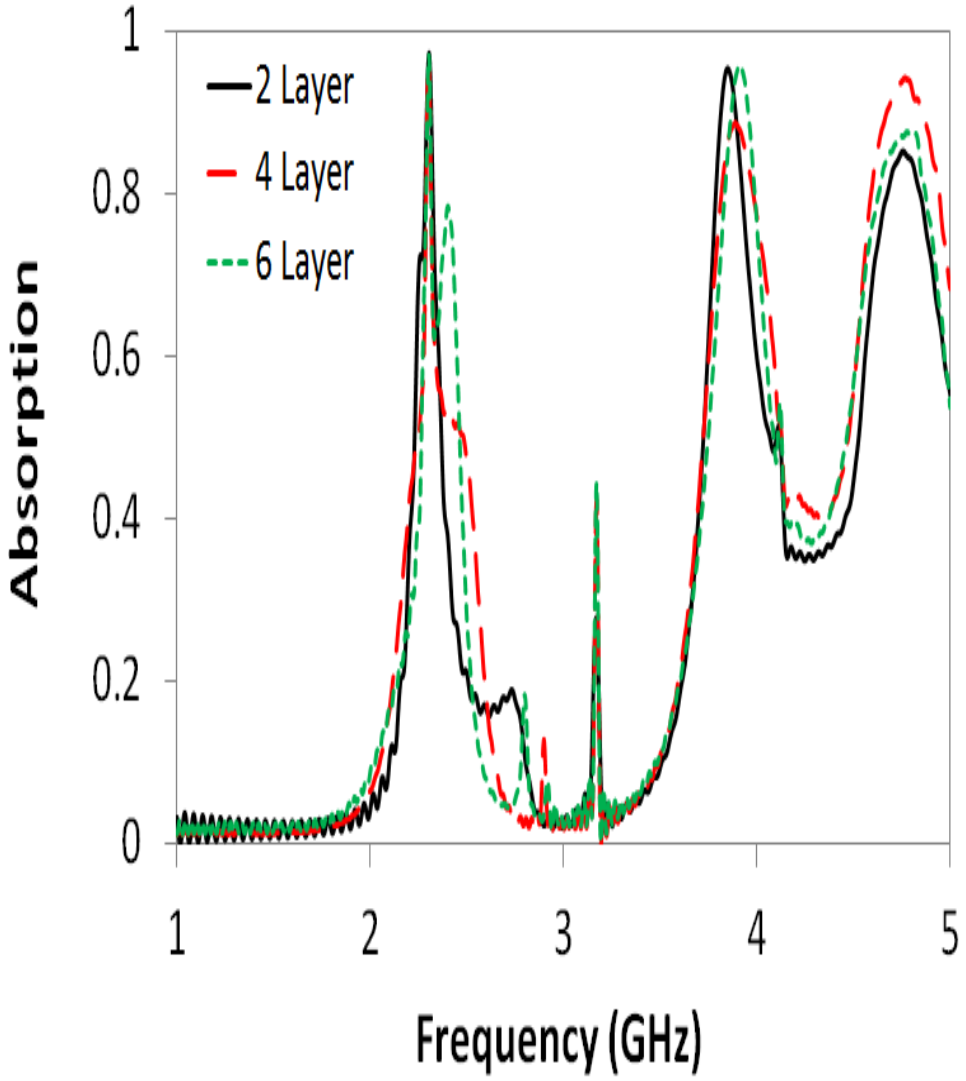

Figure 6-25. Gathered absorption frequency diagram for selected different quantities of adding layers between 2 – 6 layers for the structure in Figure 6-24.

For adding 2 – layer, maximum efficiency is obtained around 30.00% (output power is 0.150 W) at 2.296 GHz at 4700 ohm as shown in Figure 6-26. For adding 4 – layer, maximum efficiency is obtained around 51.00% (output power is 0.255 W) at 2.300 GHz at 4700 ohm as shown in Figure 6-26. For adding 6 – layer, maximum efficiency is obtained around 61.20% (output power is 0.306 W) at 2.300 GHz at 4700 ohm as shown in Figure 6-26. These values are obtained when four 4700 ohm resistors are placed across the gaps on each resonator for each adding metamaterial absorber based energy harvester at the structure in Figure 6-24.

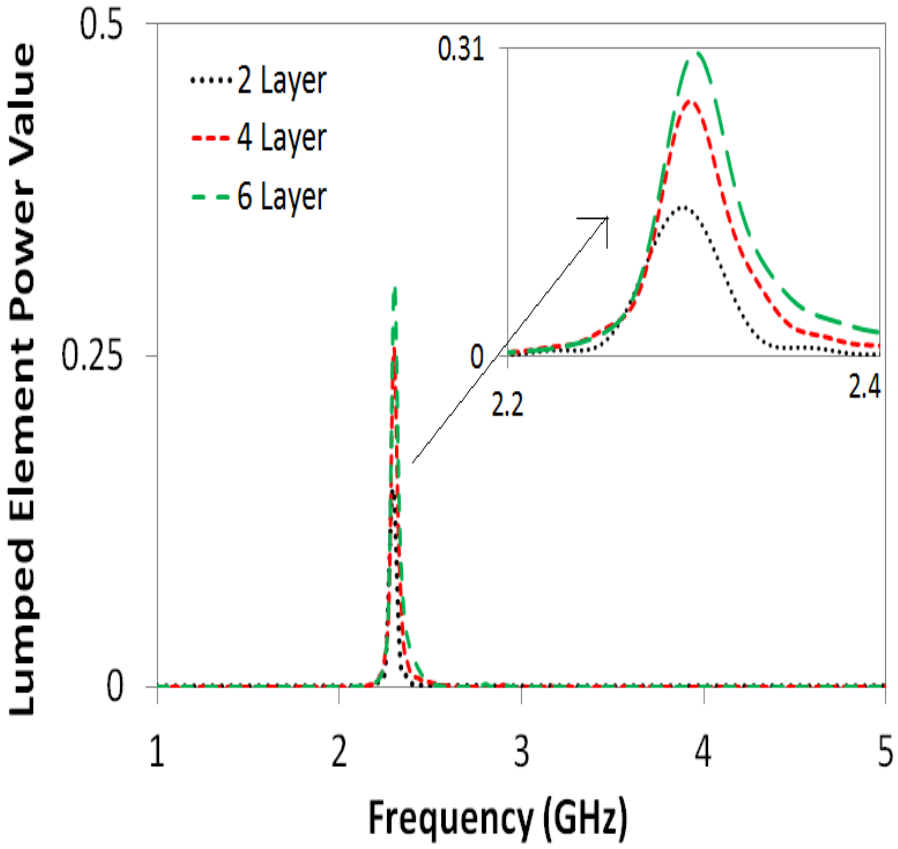

Figure 6-26. Gathered power frequency diagram for selected different quantities of adding layers between 2 – 6 layers for the structure in Figure 6-24.

The electric field, magnetic field, and surface current distributions are given in Figure 6-27 at the first resonance frequency in order to understand better the physical mechanism of the structure in Figure 6-24. Concentrations of these distributions are from on and near of edge-fed, quarter wavelength, patch to on gaps and some parts of resonators of adding layers. The basis of this is the design can be used as a voltage source due to the confinement of the EM waves at the resonance frequency. In Figure 6-27a, electric field at the top of the substrate layer of the microstrip patch antenna behaves as a dipole. Furthermore, typical radiation pattern and three – dimensional far – field pattern are given in Figure 6-28 at the first resonance frequency. The same far – field is shown from two different directions in Figure 6-28b1 and in Figure 6-28b2. In Figure 6-28(b1 or b2), electromagnetic waves propagate +z direction.

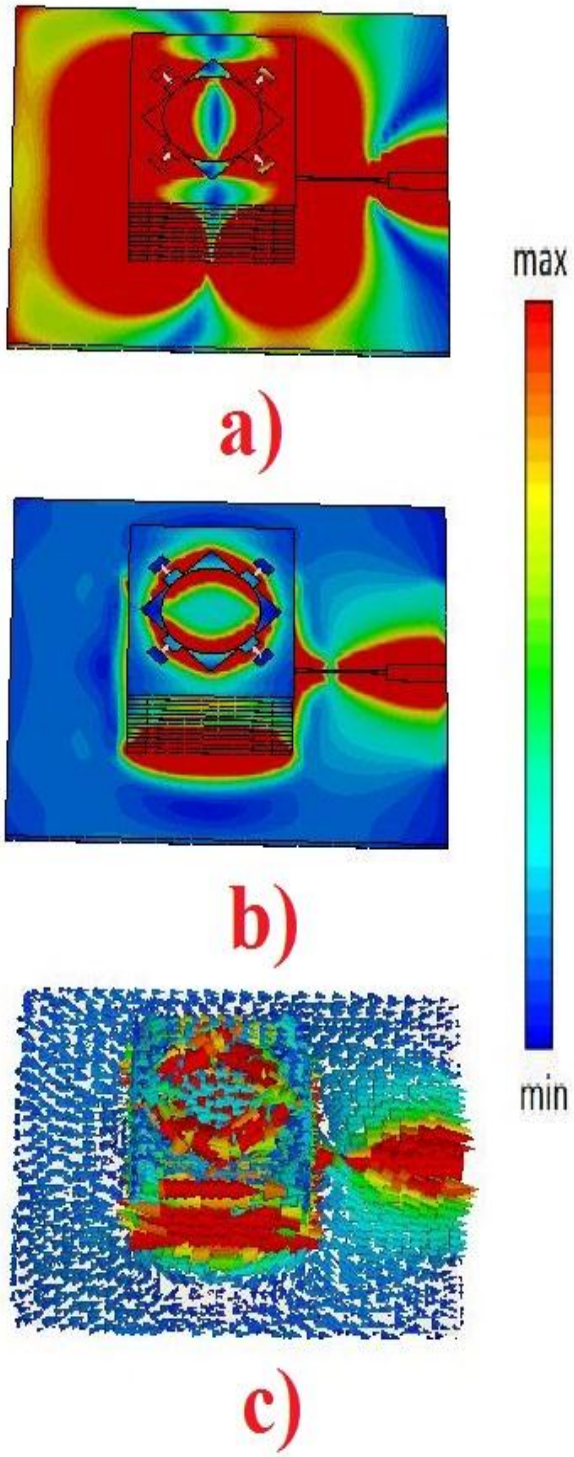

Figure 6-27. For the structure (adding 6 – layers metamaterial absorber based energy harvester with their legs on the designed 2.4 GHz microstrip patch antenna in microwave (GHz) range) in Figure 6-24 (a) Electric field distribution (b) Magnetic field distribution (c) Surface current distribution at the resonance frequency of 2.304 GHz at 4700 ohm.

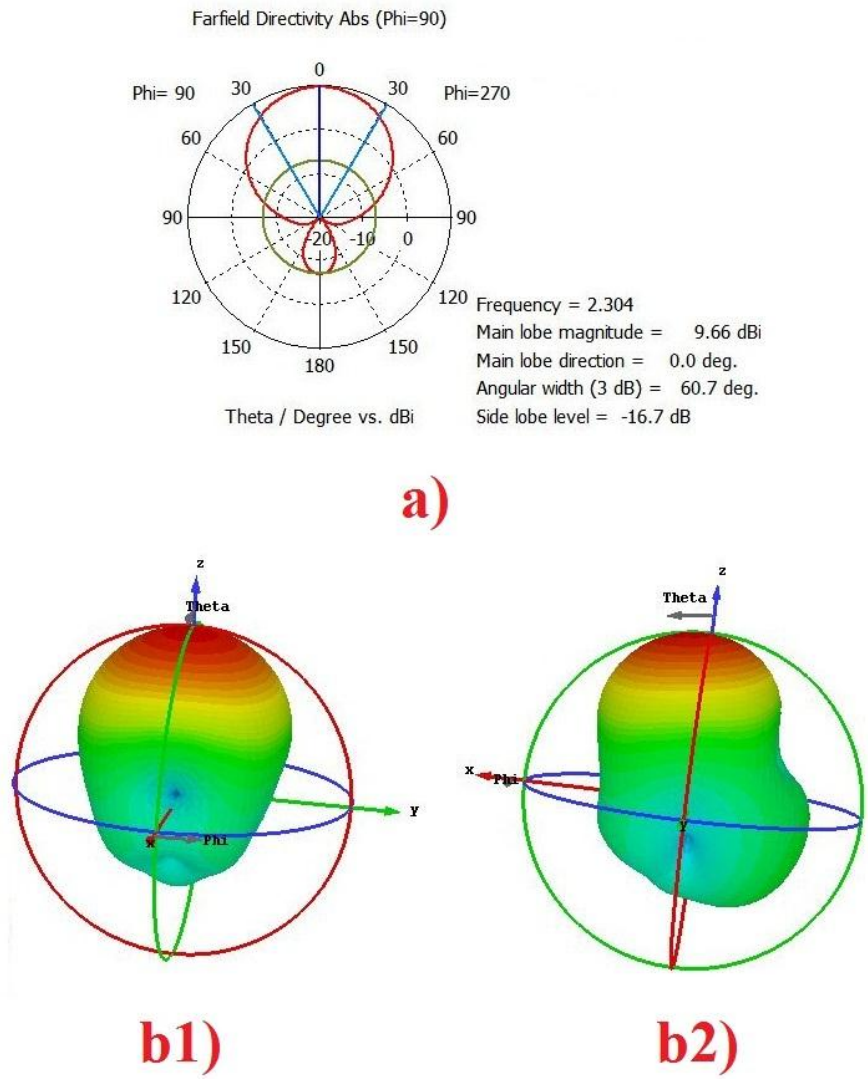

Figure 6-28. For the structure (adding 6 – layers metamaterial absorber based energy harvester with their legs on the designed 2.4 GHz microstrip patch antenna in microwave (GHz) range) in Figure 6-24 (a) typical radiation pattern (b1) and (b2) view of three – dimensional far – field pattern from two different sides at the resonance frequency of 2.304 GHz at 4700 ohm.

In Figure 6-29a, a metamaterial absorber based energy harvester (without any legs due to placing vertical) is vertically adding at the top of the patch on the designed a 2.4 GHz microstrip patch antenna in Figure 6-19. Dimensions, Rogers RT5880 substrate, Copper resonator and four resistors of this adding metamaterial absorber based energy harvester can be seen in Figure 6-29b1. Copper metal plate of this adding metamaterial absorber based energy harvester can be seen in Figure 6-29b2. In Figure 6-29b1, dimension values W, L, h and k are given 49.38, 41.32, 25 and 5 mm, respectively.

Thicknesses are same and equal to 0.035 mm for both bottom (metal plate) and top (resonator) metallic layers. Also, electrical conductivity of the copper is 5.8001×10^{7} S/m as it is used in antenna design above in this chapter. Rogers RT5880 is used as a substrate for metamaterial absorber based energy harvester. The thickness, loss tangent, relative permittivity and relative permeability of the Rogers RT5880 substrate material are 1.6 mm, 0.0009, 2.2 and 1, respectively.

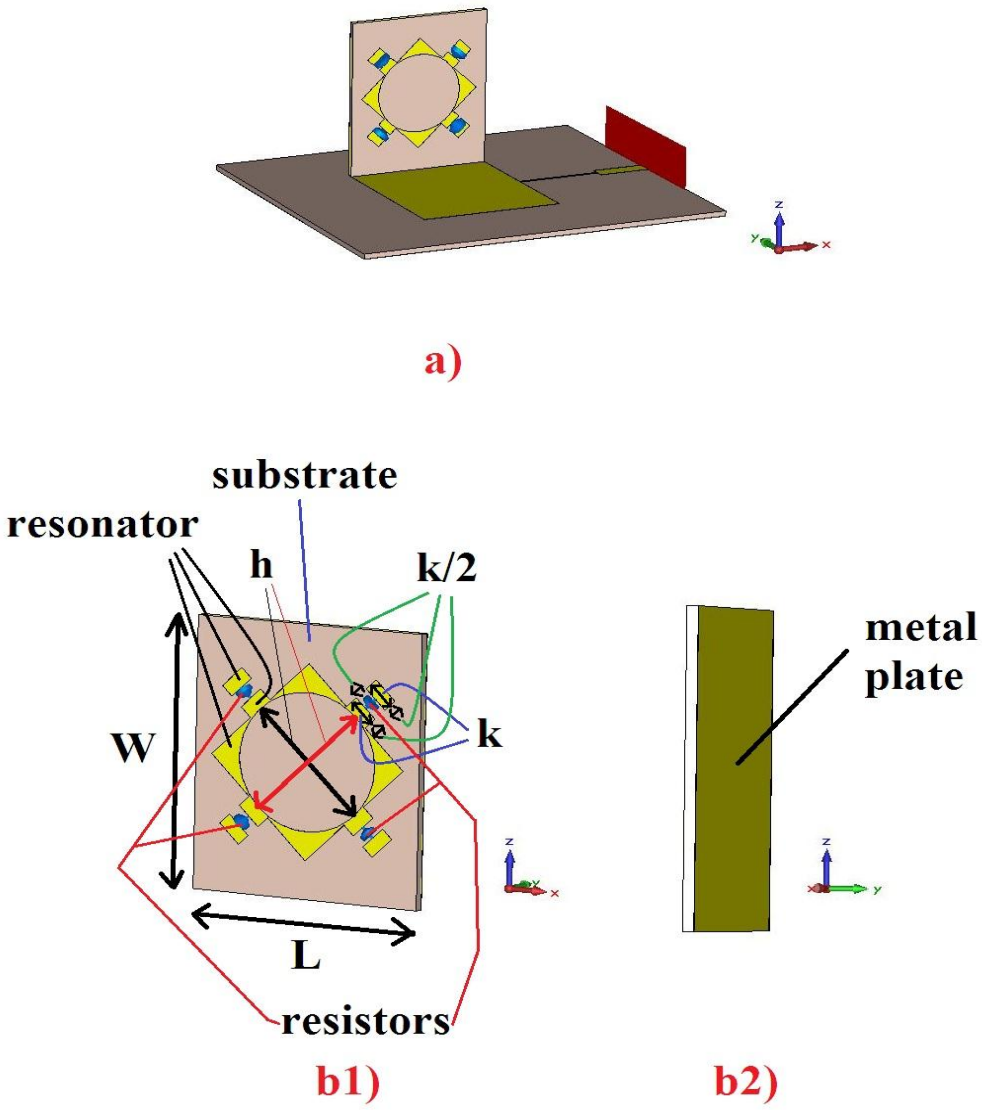

Figure 6-29. (a) Adding metamaterial absorber based energy harvester on a 2.4 GHz microstrip patch antenna in microwave (GHz) range (b1) Dimensions, Rogers RT5880 substrate, Copper resonator and four resistors for a metamaterial absorber based energy harvester (b2) Copper metal plate for a metamaterial absorber based energy harvester.

Numerical reflectance and absorption result can be seen in Figure 6-30. In Figure 6-30, maximum absorptions are obtained around 77.16%, 83.40% and 81.38% at 2.336 GHz, 3.820 GHz and 4.584 GHz, respectively. This values are obtained when four 4700 ohm resistors are placed across the gaps for the structure in Figure 6-29a.

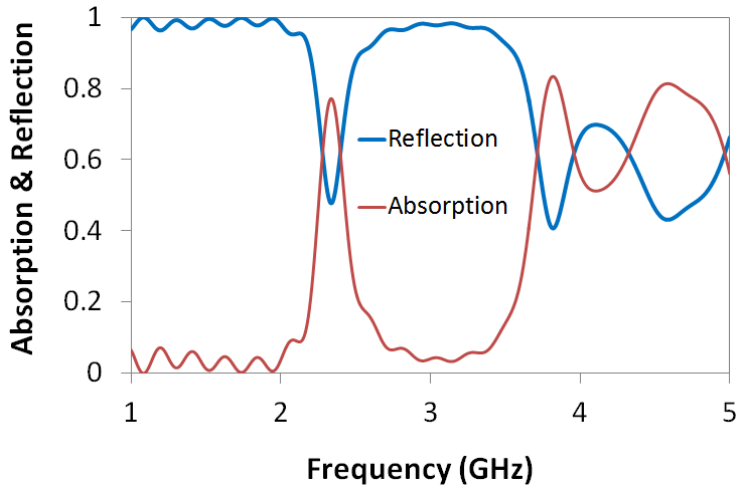

Figure 6-30. Reflectance and absorption results for the design in Figure 6-29a in microwave (GHz) range from 1 GHz to 5 GHz (The resonance frequencies at 2.336 GHz, 3.820 GHz and 4.584 GHz).

Four lumped network elements (resistors) are located as shown in Figure 6-29a. When input powers were chosen 0.500 W, maximum efficiency is obtained less than 0.10% (output power is less than 0.001 W) at 2.240 GHz at 4700 ohm as shown in Figure 6-31.

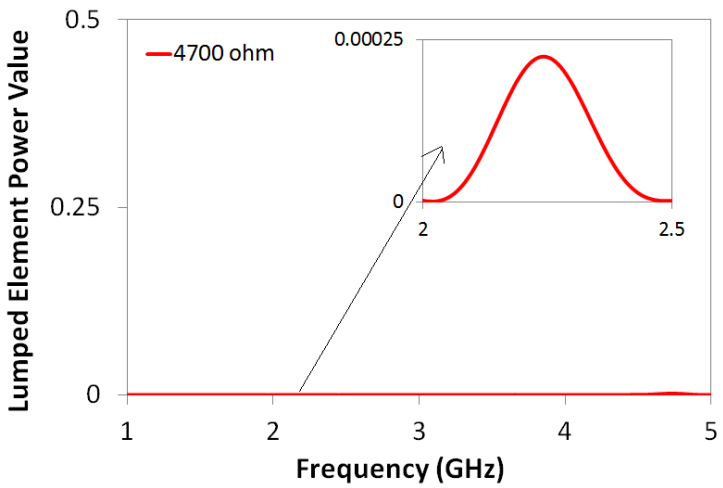

Figure 6-31. Gathered power frequency diagram for four 4700 ohm resistors for the design in Figure 6-29a in microwave (GHz) range from 1 GHz to 5 GHz (The resonance frequency at 2.240 GHz).

In Figure 6-32, increasing quantities of metamaterial absorber based energy harvester without their Copper metal plates can be seen on the designed 2.4 GHz microstrip patch antenna in microwave (GHz) range. Four 4700 ohm resistors are located across the gaps on each resonator for each adding metamaterial absorber based energy harvester. Metamaterial absorber based energy harvester without their Copper metal plates are vertically adding 29 – times next to the each previous adding, so thirty layers are become on designed antenna as shown in Figure 6-32. Copper metal plate is only used for the back of the first adding metamaterial absorber based energy harvester. It is not adding for backs of others. There are not any overflows from the top of the patch on the microstrip antenna after thirty layers have adding.

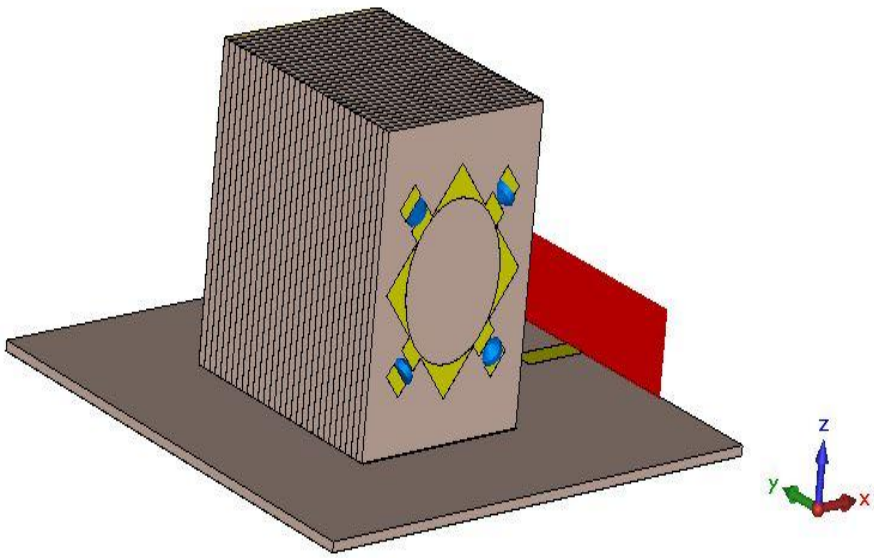

Figure 6-32. Adding thirty layers metamaterial absorber based energy harvesters without their Copper metal plates (excluded for the first layer) on a 2.4 GHz microstrip patch antenna in microwave (GHz) range (Each layer have four 4700 ohm resistors).

Numerical absorption results can be seen in Figure 6-33 for three different (three different quantities of adding metamaterial absorber based energy harvesters without their Copper metal plates (excluded for the first layer)) layers. For adding 2 – layers, maximum absorptions are obtained around 88.79% at 2.276 GHz, 90.90% at 3.772 GHz and 79.53% at 4.704 GHz in Figure 6-33. For adding 16 – layers, maximum absorptions are obtained around 99.92% at 2.300 GHz, 92.20% at 3.792 GHz and 71.98% at 4.520 GHz in Figure 6-33. For adding 30 – layers, maximum absorptions

are obtained around 99.98% at 2.284 GHz, 85.92% at 3.716 GHz and 65.80% at 4.408 GHz in Figure 6-33. These values are obtained when four 4700 ohm resistors are placed across the gaps on each resonator for each adding metamaterial absorber based energy harvester at the structure in Figure 6-32.

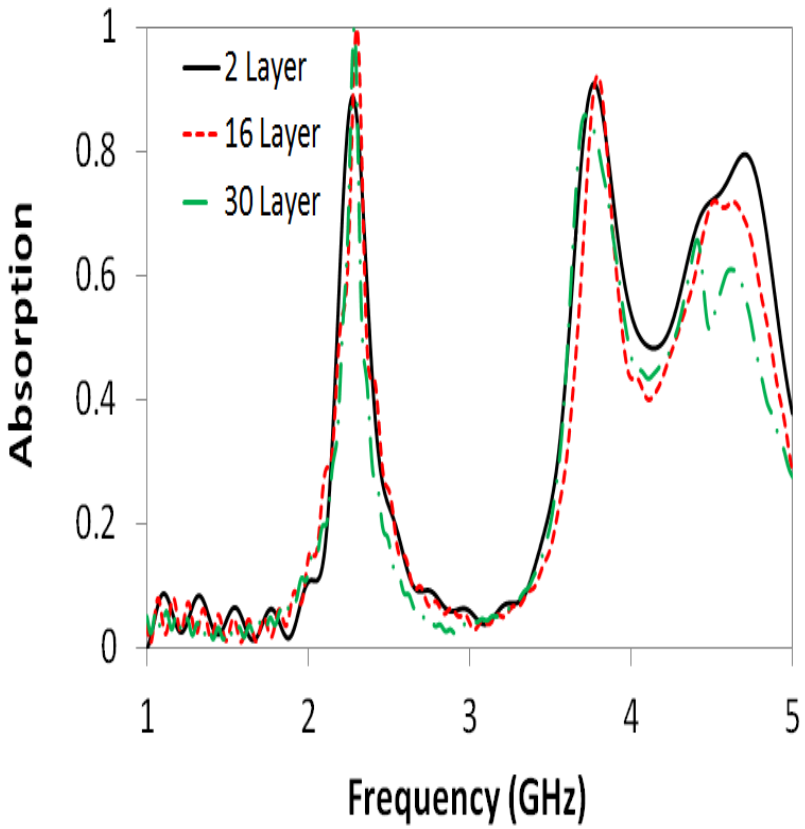

Figure 6-33. Gathered absorption frequency diagram for selected different quantities of adding layers between 2 – 30 layers for the structure in Figure 6-32.

For adding 2 – layer, maximum efficiency is obtained around 0.10% (output power is less than (but approximately near to) 0.001 W) at 2.332 GHz at 4700 ohm as shown in Figure 6-34. For adding 16 – layer, maximum efficiency is obtained around 17.60% (output power is 0.088 W) at 2.300 GHz at 4700 ohm as shown in Figure 6-34. For adding 30 – layer, maximum efficiency is obtained around 24.80% (output power is 0.124 W) at 2.284 GHz at 4700 ohm as shown in Figure 6-34. These values are obtained when four 4700 ohm resistors are placed across the gaps on each resonator for each adding metamaterial absorber based energy harvester at the structure in Figure 6-32.

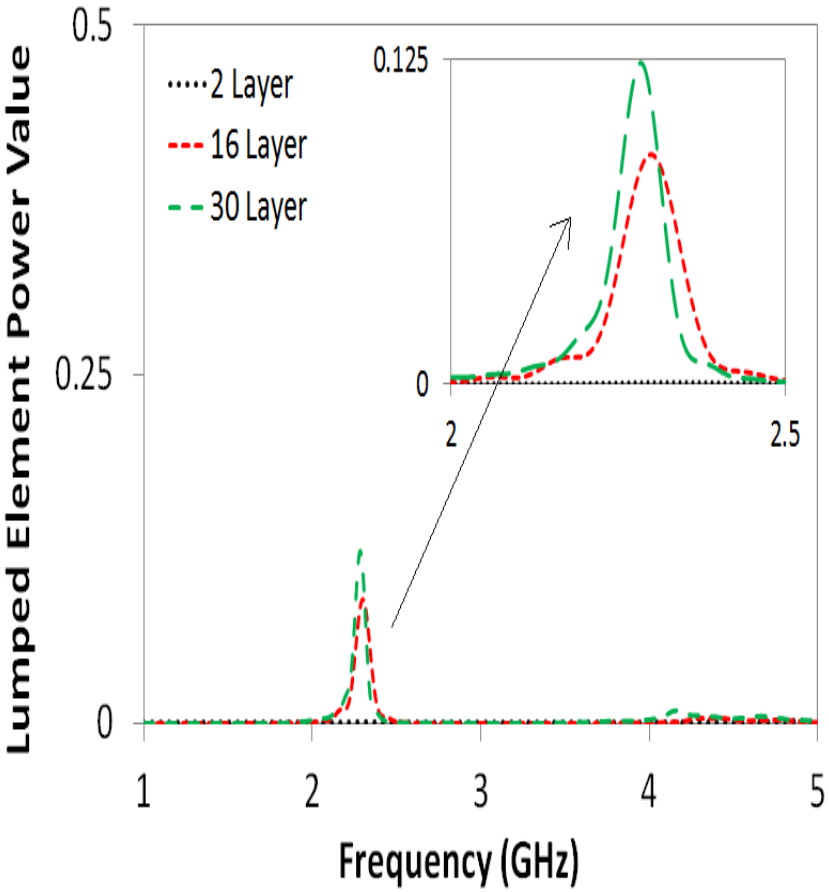

Figure 6-34. Gathered power frequency diagram for selected different quantities of adding layers between 2 – 30 layers for the structure in Figure 6-32.

The electric field, magnetic field, and surface current distributions are given in Figure 6-35 at the first resonance frequency in order to understand better the physical mechanism of the structure in Figure 6-32. Concentrations of these distributions are from on and near of edge-fed, quarter wavelength, patch to on gaps and some parts of resonators of adding layers. The basis of this is the design can be used as a voltage source due to the confinement of the EM waves at the resonance frequency. In Figure 6-35a, electric field at the top of the substrate layer of the microstrip patch antenna behaves as a dipole. Furthermore, typical radiation pattern and three – dimensional far – field pattern are given in Figure 6-36 at the first resonance frequency. The same far – field is shown from two different directions in Figure 6-36b1 and in Figure 6-36b2. In Figure 6-36(b1 or b2), electromagnetic waves propagate +z direction.

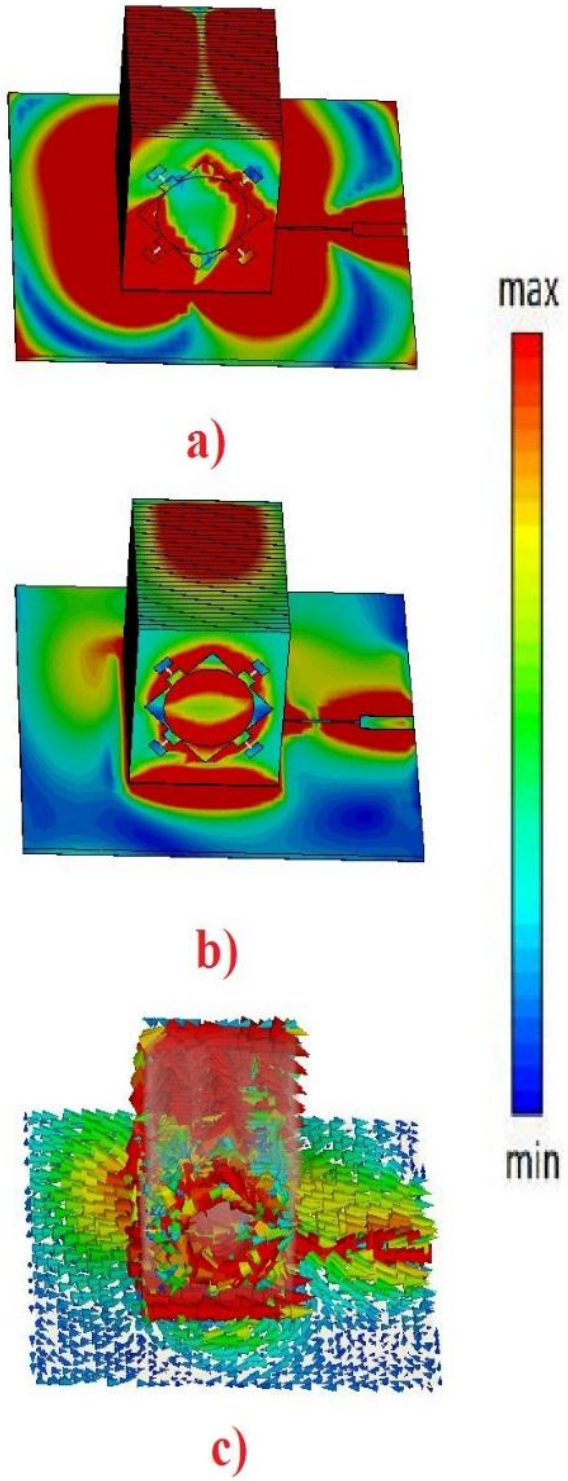

Figure 6-35. For the structure (adding 30 – layers metamaterial absorber based energy harvester without their Copper metal plate (excluded for the first layer) on the designed 2.4 GHz microstrip patch antenna in microwave (GHz) range) in Figure 6-32 (a) Electric field distribution (b) Magnetic field distribution (c) Surface current distribution at the resonance frequency of 2.284 GHz at 4700 ohm.

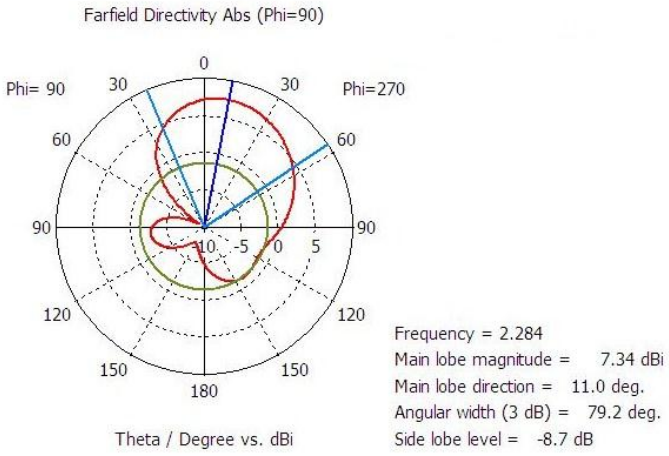

a)

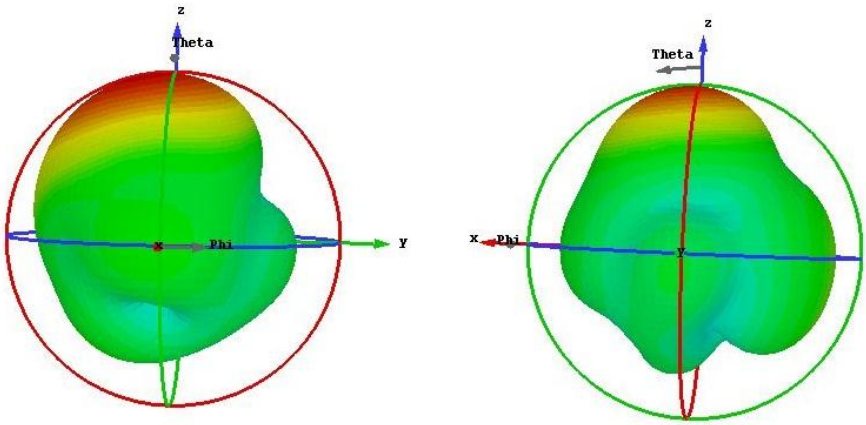

b1) b2)

Figure 6-36. For the structure (adding 30 – layers metamaterial absorber based energy harvester without their Copper metal plate (excluded for the first layer) on the designed 2.4 GHz microstrip patch antenna in microwave (GHz) range) in Figure 6-32 (a) typical radiation pattern (b1) and (b2) view of three – dimensional far – field pattern from two different sides at the resonance frequency of 2.284 GHz at 4700 ohm.

6.4. Conclusion

In this chapter, reflection results, absorption results, total lumped elements power values, field and surface current distributions and typical and 3-D far – field radiation patterns are numerically analysed for FR4 and Rogers RT5880 substrate materials.

Maximum total lumped elements power efficiency is numerically obtained around 61.20% (output power is 0.306 W when input power is 0.500 W) at 2.300 GHz resonance frequency at 4700 ohm (value of lumped elements (resistors)) when six metamaterial absorber based energy harvesters with their Rogers RT5880 legs are horizontally adding at the top of the Copper metal patch in designed microstrip patch antenna for 2.4 GHz operation. This efficiency value (a predictable low result) (61.20%) can not be near to 100% because of the direction of incident EM waves. Proposed structures can be used for many application such as antennas, EM filters, sensors.

CHAPTER 7

CONCLUSION AND FUTURE WORK

Many metamaterial absorber studies are available in literature for different working frequency regions, but metamaterial absorber based energy harvesters are available in literature for low frequency regions. Also, usage of graphene material on metamaterial absorber based energy harvester was a weakness.

First of all, a basic metamaterial absorber was designed and analyzed. Later, in Chapter 2, same metamaterial absorber was converted into two different metamaterial absorber based energy harvester. The difference between MA and MA based EH is collected electromagnetic energy at a point is harvested by resistor.

Similar viewed MA based EH structures in three different frequency region were designed and analysed in Chapter 3 in order to pass from lower frequency to higher frequency. With the same idea, another new similar viewed MA based EH structures were designed and analysed in Chapter 4. Therefore, the positive effects of parametric dimensions and resonators on results were seen.

Graphene material is generally utilized at the top of structure in MA study because of its enhancement effect on results. However, it has negative effect on MA based EH if it is used at the top of structure. Therefore, graphene material is utilized at the bottom of structure in Chapter 5 in order to get rid of from the weakness, strength and limitation. This situation can be called as a novelty.

In chapter 6, horizontal and vertical multilayer metamaterials on two different microstrip patch antennas have extremely enhancement effect on results. 6.00% power efficiency is specifically increased to 61.20% power efficiency when multilayer metamaterials are horizontally adding at the top of antenna in 2.4 GHz operation. This means power efficiency is improved 10.2 times.

Utilization of designs can be in several applications such as antennas, EM filters, sensors, THz imaging systems, infrared spectroscopy, infrared cameras, solar cells, and so on.

Materials, which are utilized in designs of structures, are chose according to their working frequency ranges in electromagnetic spectrum region. Although high costs (expensive material price) or low efficiency effect (due to properties of material) of any materials, many materials are used in designs in this thesis study in order to see effects of each material and obtain highest efficiency. It should be note that this study is not a feasibility study. All these efficient studies can be extremely valuable with lower cost of material in the future because high costs of materials will not continue forever. Therefore, productions can be realized cheaper and then feasibility studies can be done as future work. Parameters of structures can be suitable for experimental studies and fabrication in future by advancing technology.

Some of the results reported in this thesis have been presented in SOLARTR 2014 Solar Conference & Exhibition, and in International Conference on Renewable Energy Technologies and Applications (RETA'16), and in URSI – Turkey'2016 8th Scientific Congress. One journal paper from this thesis was published in Journal of Alloys and Compounds (JALCOM) journal.

BIBLIOGRAPHY

[1] B. Li, L. Wang, B. Kang, P. Wang, and Y. Qiu, Review of recent progress in solid-state dye- sensitized solar cells, Solar Energy Materials & Solar Cells, 90 (2006) 549-573.

[2] C. Li, M. Liu, N. G. Pschirer, M. Baumgarten, and K. Müllen, Polyphenylene-based materials for organic photovoltaics, Chemical Reviews, 110 (2010) 6817-6855.

[3] F. Dincer, O. Akgol, M. Karaaslan, E. Unal, and C. Sabah, Polarization angle independent perfect metamaterial absorbers for solar cell applications in the microwave, infrared, and visible regime, Progress in Electromagnetics Research, 144 (2014) 93-101.

[4] G. Hashmi, M. H. Imtiaz, and S. Rafique, Towards high efficiency solar cells: Composite metamaterials, Global Journal of Researches in Engineering Electrical and Electronics Engineering, 13 (2013) 11-16.

[5] A. Vora, J. Gwamuri, N. Pala, A. Kulkarni, J. M. Pearce, and D. Ö. Güney, Exchanging ohmic losses in metamaterial absorbers with useful optical absorption for photovoltaics, Scientific Reports, 4 : 4901 (2014) 1-13, DOI: 10.1038/srep04901.

[6] V. G. Vesalago, The electrodynamics of substances with simultaneously negative values of ε and μ, Soviet Physics Uspekhi, P. N. Lebedev Physics Institute, 10 (1968) 509-514.

[7] W. Cai, and V. Shalaev, Optical Metamaterials Fundamentals and Applications, Springer New York Dordrecht Heidelberg London (2010) ISBN 978-1-4419-1150-6, e-ISBN 978-1-4419-1151-3, DOI: 10.1007/978-1-4419-1151-3.

[8] S. Takeda, and T. Yoshinaga, Left-handed metamaterial technologies significant for information and communication devices, Quarterly Review No. 34 (2009) 36-49.

[9] J. Valentine, S. Zhang, T. Zentgraf, E. Ulin-Avila, D. A. Genov, G. Bartal, and X. Zhang, Three-dimensional optical metamaterial with a negative refractive index, Nature, 455 (2008) 376-379, DOI: 10.1038/nature07247.

[10] W. J. Padilla, D. N. Basov, and D. R. Smith, Negative refractive index metamaterials, Materials Today, 9 (2006) 28-35.

[11] V. M. Shalaev, Optical negative-index metamaterials, Nature Photonics, 1 (2007) 41-48, DOI: 10.1038/nphoton.2006.49.

[12] C. M. Watts, X. Liu, and W. J. Padilla, Metamaterial electromagnetic wave absorbers, Advanced Optical Materials, 24 (2012) OP98–OP120.

[13] J. B. Pendry, Negative refraction makes a perfect lens, Physical Review Letters, 85 (2000) 3966-3969.

[14] D. R. Smith, W. J. Padilla, D. C. Vier, S. C. Nemat-Nasser, and S. Schultz, Composite medium with simultaneously negative permeability and permittivity, Physical Review Letters, 84, (2000) 4184-4187.

[15] J. B. Pendry, Perfect cylindrical lenses, Optics Express, 11 (7) (2003) 755-760.

[16] N. Fang, H. Lee, C. Sun, and X. Zhang, Sub-diffraction-limited optical imaging with a silver superlens, Science, 308 (2005) 534-537.

[17] Y. Zhang, and M. A. Fiddy, Covered image of superlens, Progress in Electromagnetics Research, 136 (2013) 225-238.

[18] F. Dincer, M. Karaaslan, E. Unal, K. Delihacioglu, and C. Sabah, Design of polarization and incident angle insensitive dual-band metamaterial absorber based on isotropic resonator, Progress in Electromagnetics Research, 144 (2014) 123-132.

[19] D. Li, Z. Szabó, X. Qing, Er-Ping Li, and Z. N. Chen, A high gain antenna with an optimized metamaterial inspired superstrate, IEEE Transactions on Antennas and Propagation, 60, (2012) 6018-6023.

[20] M. Cai, and E. P. Li, A novel terahertz sensing device comprising of a parabolic reflective surface and a bi-conical structure, Progress in Electromagnetics Research, 97 (2009) 61-73.

[21] S. A. Maier, Plasmonics: Fundamentals and Applications, Springer (2007) ISBN 0-387-33150-6.

[22] S. Tretyakov, P. Barois, T. Scharf, V. Kruglyak, and I. Bergmair, Nanostructured metamaterials: Exchange between experts in electromagnetics and material science, Publications Office of the European Union (2010) ISBN 978-92-79-07563-6, DOI: 10.2777/54953.

[23] K. Yamamoto, and S. Nomura, Energy compensated mode in a waveguide composed of lossy left-handed metamaterial, Optics Communications, 276 (2007) 191-195.

[24] M. Karaaslan, and M. Bakir, Chiral metamaterial based multifunctional sensor applications, Progress in Electromagnetics Research, 149 (2014) 55-67.
[25] C. Sabah, F. Dincer, M. Karaaslan, E. Unal, O. Akgol, E. Demirel, Perfect metamaterial absorber with polarization and incident angle independencies based on ring and cross-wire resonators for shielding and a sensor application, Optics Communications, 322 (2014) 137-142.
[26] R. A. Shelby, D. R. Smith, and S. Schultz, Experimental verification of a negative index of refraction, Science, 292 (2001) 77-79.
[27] D. Schurig, J. J. Mock, B. J. Justice, S. A. Cummer, J. B. Pendry, A. F. Starr, and D. R. Smith, Metamaterial electromagnetic cloak at microwave frequencies, Science, 314 (2006) 977-980.
[28] C. Sabah, H. T. Tastan, F. Dincer, K. Delihacioglu, M. Karaaslan, and E. Unal, Transmission tunneling through the multi-layer double-negative and double-positive slabs, Progress in Electromagnetics Research, 138 (2013) 293-306.
[29] J. B. Pendry, D. Schurig, and D. R. Smith, Controlling electromagnetic fields, Science, 312 (2006) 1780-1782.
[30] X. Chen, Implicit boundary conditions in transformation-optics cloaking for electromagnetic waves, Progress in Electromagnetics Research, 121 (2011) 521-534.
[31] J. A. Silva-Macêdo, M. A. Romero, and B.-H. V. Borges, An extended FDTD method for the analysis of electromagnetic field rotations and cloaking devices, Progress in Electromagnetics Research, 87 (2008) 183-196.
[32] C. Sabah, and S. Uckun, Multilayer system of Lorentz/Drude type metamaterials with dielectric slabs and its application to electromagnetic filters, Progress in Electromagnetics Research, 91 (2009) 349-364.
[33] H - T. Chen, Interference theory of metamaterial perfect absorbers, Optics Express, 20 (2012) 7165-7172.
[34] J. Lee, and S. Lim, Bandwidth-enhanced and polarisation-insensitive metamaterial absorber using double resonance, Electronics Letters, 47 (2011) 8-9.
[35] F. Dincer, M. Karaaslan, E. Unal, O. Akgol, E. Demirel, and C. Sabah, Polarization and angle independent perfect metamaterial absorber based on discontinuous cross-wire-strips, Journal of Electromagnetic Waves and Applications, 28 (2014) 741-751.

[36] M. Esen, I. Ilhan, M. Karaaslan, E. Unal, F. Dincer, and C. Sabah, Electromagnetic absorbance properties of a textile material coated using filtered arc-physical vapour deposition method, Journal of Industrial Textiles, 45(2) (2015) 298-309, DOI: 10.1177/1528083714534710.

[37] C. Sabah, F. Dincer, M. Karaaslan, E. Unal, and O. Akgol, Polarization-insensitive FSS-based perfect metamaterial absorbers for GHz and THz frequencies, Radio Science, 49 (2014) 306-314.

[38] F. Bilotti, L. Nucci, and L. Vegni, An SRR based microwave absorber, Microwave and Optical Technology Letters, 48 (2006) 2171-2175.

[39] N. I. Landy, S. Sajuyigbe, J. J. Mock, D. R. Smith, and W. J. Padilla, Perfect metamaterial absorber, Physical Review Letters, 100 (2008) 207402-1 – 207402-4.

[40] B. Wang, T. Koschny, and C. M. Soukoulis, Wide-angle and polarization-independent chiral metamaterial absorber, Physical Review B, 80 (2009) 033108-1 – 033108-4.

[41] B. Zhu, Y. Feng, J. Zhao, C. Huang, Z. Wang, and T. Jiang, Polarization modulation by tunable electromagnetic metamaterial reflector/absorber, Optics Express, 18 (2010) 23196-23203.

[42] L. Li, Y. Yang, and C. Liang, A wide-angle polarization-insensitive ultra-thin metamaterial absorber with three resonant modes, Journal of Applied Physics, 110 (2011) 063702-1 – 063702-5.

[43] F. Dincer, M. Karaaslan, E. Unal, O. Akgol, and C. Sabah, Design of polarization- and incident angle-independent perfect metamaterial absorber with interference theory, Journal of Electronic Materials, 43 (2014) 3949-3953.

[44] Y. Avitzour, Y. A. Urzhumov, and G. Shvets, Wide-angle infrared absorber based on a negative-index plasmonic metamaterial, Physical Review B, 79 (2009) 045131-1 – 045131-5.

[45] Z. Rahimi, The Finite Integration Technique (FIT) and the application in lithography simulations, Als Dissertation genehmigt von der Technischen Fakultät der Universität Erlangen-Nürnberg, (2011).

[46] H. Tao, C. M. Bingham, A. C. Strikwerda, D. Pilon, D. Shrekenhamer, N. I. Landy, K. Fan, X. Zhang, W. J. Padilla, and R. D. Averitt, Highly flexible wide angle

of incidence terahertz metamaterial absorber: Design, fabrication, and characterization, Physical Review B, 78 (2008) 241103-1 – 241103-4.

[47] H. Tao, C. M. Bingham, D. Pilon, K. Fan, A. C. Strikwerda, D. Shrekenhamer, W. J. Padilla, X. Zhang, and R. D. Averitt, A dual band terahertz metamaterial absorber, Journal of Physics D: Applied Physics, 43 (2010) 225102 (5pp).

[48] J. Yoon, M. Zhou, Md. A. Badsha, T. Y. Kim, Y. C. Jun, and C. K. Hwangbo, Broadband epsilon-near zero perfect absorption in the near-infrared, Scientific Reports, 5:12788 (2015) 1-8.

[49] H. Li, L. H. Yuan, B. Zhou, X. P. Shen, Q. Cheng, and T. J. Cui, Ultrathin multiband gigahertz metamaterial absorbers, Journal of Applied Physics, 110 (2011) 014909-1 – 014909-8.

[50] B. Zhu, Z. Wang, C. Huang, Y. Feng, J. Zhao, and T. Jiang, Polarization insensitive metamaterial absorber with wide incident angle, Progress in Electromagnetics Research, 101 (2010) 231–239.

[51] S. Walia, C. M. Shah, P. Gutruf, H. Nili, D. R. Chowdhury, W. Withayachumnankul, M. Bhaskaran, and S. Sriram, Flexible metasurfaces and metamaterials: A review of materials and fabrication processes at micro- and nano-scales, Applied Physics Reviews, 2 (2015) 011303-1 – 011303-14.

[52] M. Bakir, M. Karaaslan, F. Dincer, K. Delihacioglu, and C. Sabah, Perfect metamaterial absorber-based energy harvesting and sensor applications in the industrial, scientific, and medical band, Optical Engineering, 54(9) (2015) 097102-1 – 097102-5.

[53] M. Lallart, D. Guyomar, C. Richard, L. Petit, and AJZ, Nonlinear optimization of acoustic energy harvesting using piezoelectric devices, The Journal of Acoustical Society of America, 128 (2010) 2739-2748.

[54] N. Zhu, R. W. Ziolkowski, and H. Xin, A metamaterial-inspired, electrically small rectenna for high-efficiency, low power harvesting and scavenging at the global positioning system L1 frequency, Applied Physics Letters, 99 (2011) 114101-1 – 114101-3.

[55] O. M. Ramahi, T. S. Almoneef, M. AlShareef, and M. S. Boybay, Metamaterial particles for electromagnetic energy harvesting, Applied Physics Letters, 101 (2012) 173903-1 – 173903-5.

[56] A. M. Hawkes, A. R. Katko, and S. A. Cummer, A microwave metamaterial with integrated power harvesting functionality, Applied Physics Letters, 103 (2013) 163901-1 – 163901-3.

[57] T. S. Almoneef, and O. M. Ramahi, A 3-dimensional stacked metamaterial arrays for electromagnetic energy harvesting, Progress in Electromagnetics Research, 146 (2014) 109-115.

[58] O. T. Gunduz, and C. Sabah, Polarization angle independent perfect multiband metamaterial absorber and energy harvesting application, Journal of Computational Electronics, Springer, 15 (2016) 228-238.

[59] E. D. Palik, Handbook of Optical Constants of Solids, Academic Press, (1985), ISBN 0-12-544420-6.

[60] C. Gu, S. Qu, Z. Pei, H. Zhou, and J. Wang, A wide-band, polarization-insensitive and wide-angle terahertz metamaterial absorber, Progress in Electromagnetics Research Letters, 17 (2010) 171-179.

[61] W. Zhu, and X. Zhao, Metamaterial absorber with random dendritic cells, The European Physical Journal Applied Physics (EPJ AP), 50 (2010) 21101-p1 – 21101-p4.

[62] M. P. Hokmabadi, D. S. Wilbert, P. Kung, S. M. Kim, Theoretical and experimental investigation of hybrid broadband terahertz metamaterial absorber, Proceedings of SPIE, 8632 (2013) 86321X-1 – 86321X-6.

[63] M. S. Dresselhaus, Solid State Physics; Part II; Optical Properties of Solids, MIT Solid State Physics Course, 2001.

[64] J. Wang, C. Fan, P. Ding, J. He, Y. Cheng, W. Hu, G. Cai, E. Liang, and Q. Xue, Tunable broad-band perfect absorber by exciting of multiple plasmon resonances at optical frequency, Optics Express, 20 (2012) 14871-14878.

[65] S. V. Boriskina, H. Ghasemi, and G. Chen, Plasmonic materials for energy: From physics to applications, Materials Today, 16 (2013) 375-386.

[66] K. Yao, and Y. Liu, Plasmonic metamaterials, Nanotechnology Reviews, 3(2) (2014) 177-210.

[67] P. Rufangura, and C. Sabah, Polarisation insensitive tunable metamaterial perfect absorber for solar cells applications, The Institution of Engineering and Technology

(IET) Optoelectronics, 10 (2016) 211-216, http://dx.doi.org/10.1049/iet-opt.2016.0003.

[68] C. J. Docherty, and M. B. Johnston, Terahertz properties of graphene, Journal of Infrared, Millimeter and Terahertz Waves, 33 (2012) 797-815.

[69] J. Ding, B. Arigong, H. Ren, M. Zhou, J. Shao, M. Lu, Y. Chai, Yuankun Lin, and Hualiang Zhang, Scientific Reports, 4:6128 (2014) 1-7.

[70] W. Zouaghi, D. Voß, M. Gorath, N. Nicoloso, and H. G. Roskos, How good would the conductivity of graphene have to be to make single-layer-graphene metamaterials for terahertz frequencies feasible? Carbon, 94 (2015) 301-308.

[71] N. Papasimakis, Z. Luo, Z. X. Shen, F. D. Angelis, E. D. Fabrizio, A. E. Nikolaenko, and N. I. Zheludev, Optics Express, 18 (2010) 8353-8359.

[72] J. Li, Y. Zhou, B. Quan, X. Pan, X. Xu, Z. Ren, F. Hu, H. Fan, M. Qi, J. Bai, L. Wang, J. Li, and C. Gu, Graphene-metamaterial hybridization for enhanced terahertz response, Carbon, 78 (2014) 102-112.

[73] Y. Zou, P. Tassin, T. Koschny, C. M. Soukoulis, Interaction between graphene and metamaterials: split rings vs. wire pairs, Optics Express, 20 (2012) 12198-12204.

[74] F. Valmorra, G. Scalari, C. Maissen, W. Fu, C. Schönenberger, J. W. Choi, H. G. Park, M. Beck, and J. Faist, Low-bias active control of terahertz waves by coupling large-area CVD graphene to a terahertz metamaterial, Nano Letters, 13 (2013) 3193-3198.

[75] O. V. Kotov, M. A. Kol'chenko, and Y. E. Lozovik, Ultrahigh refractive index sensitivity of TE-polarized electromagnetic waves in graphene at the interface between two dielectric media, Optics Express, 21 (2013) 13533-13546.

[76] V. P. Gusynin, S. G. Sharapov, and J. P. Carbotte, Magneto-optical conductivity in graphene, Journal of Physics: Condensed Matter, 19 (2007) 026222 (25pp).

[77] X. He, Tunable terahertz graphene metamaterials, Carbon, 82 (2015) 229-237.

[78] X. He, Z.-Y. Zhao, and W. Shi, Graphene-supported tunable near-IR metamaterials, Optical Society of America, Optics Letters, 40 (2015) 178-181.

[79] K. S. Novoselov, A. K. Geim, S. V. Morozov, D. Jiang, Y. Zhang, S. V. Dubonos, I. V. Grigorieva, and A. A. Firsov, Electric field effect in atomically thin carbon films, Science, 306 (2004) 666-669.

[80] A. Yilmaz, and C. Sabah, Diamond-shaped hole array in double-layer metal sheets for negative index of refraction, Journal of Electromagnetic Waves and Applications, 27 (2013) 413-420.

[81] K. B. Alici, and E. Ozbay, Theoretical study and experimental realization of a low-loss metamaterial operating at the millimeter-wave regime: Demonstrations of flat- and prism-shaped samples, IEEE Journal of Selected Topics in Quantum Electronics, 16 (2010) 386-393.

[82] R. W. Ziolkowski, Metamaterial-based source and scattering enhancements: from microwave to optical frequencies, Opto-Electronics Review, 14(3) (2006) 167-177.

[83] Y. Cui, Y. He, Y. Jin, F. Ding, L. Yang, Y. Ye, S. Zhong, Y. Lin, and S. He, Plasmonic and metamaterial structures as electromagnetic absorbers, Laser and Photonics Reviews, 8 (2014) 495-520.

[84] G. Ghosh, Handbook of optical constant of solids, Volume 5: Handbook of thermo – optic coefficients of optical materials with applications, Academic Press, Burlington: Elsevier, 1998.

[85] P. B. Johnson, and R. W. Christy, Optical constants of the noble metals, Physical Review B, 6 (1972) 4370-4379.

[86] M. M. Gajibo, M. K. A. Rahim, N. A. Murad, O. Ayop, B. D. Bala, and H. A. Majid, X-band operations metamaterial absorber with extended circular ring topology for size reduction, Indonesian Journal of Electrical Engineering and Computer Science, 6 (2017) 180-184, DOI: 10.11591/ijeecs.v6.i1.pp180-184.

[87] S. Franzen, Surface plasmon polaritons and screened plasma absorption in indium tin oxide compared to silver and gold, The Journal of Physical Chemistry C, 112 (2008) 6027-6032.

[88] H. Kim, and C. M. Gilmore, A. Pique´, J. S. Horwitz, H. Mattoussi, H. Murata, Z. H. Kafafi, and D. B. Chrisey, Electrical, optical, and structural properties of indium–tin–oxide thin films for organic light-emitting devices, Journal of Applied Physics, 86 (1999) 6451-6461.

[89] T. Minami, Present status of transparent conducting oxide thin-film development for Indium-Tin-Oxide (ITO) substitutes, Thin Solid Films, 516 (2008) 5822-5828.

[90] G. V. Naik, and A. Boltasseva, A comparative study of semiconductor-based plasmonic metamaterials, Metamaterials, 5 (2011) 1-7.

[91] R. Waterhouse, Microstrip patch antennas – a designer`s guide, Kluwer Academic Publishers, Boston, MA, 2003.

[92] G. Breed, The fundamentals of patch antenna design and performance, High Frequency Electronics (2009) 48.

[93] D. Orban, and G. J. K. Moernaut, The basics of patch antennas, updated, Orban microwave products (www.orbanmicrowave.com), (As seen in the September 29, 2009 edition of the RF Globalnet (www.rfglobalnet.com) newsletter.).

[94] E. Dogan, E. Unal, D. Kapusuz, M. Karaaslan, and C. Sabah, Microstrip patch antenna covered with left handed metamaterial, ACES Journal, 28 (2013) 999-1004.

[95] Y. D. Sirmaci, C. K. Akin, and C. Sabah, Fishnet based metamaterial loaded THz patch antenna, Optical and Quantum Electronics, 48:168 (2016), 1-10, DOI 10.1007/s11082-016-0449-6.

[96] R. Salhi, M. Labidi, M. A. Boujemaa, and F. Choubani, Dual – band microstrip patch antenna based on metamaterial refractive surface, Applied Physics A, 123:420 (2017) 1-10, DOI: 10.1007/s00339-017-1030-2.

[97] K. A. Devi, C. H. Ng, C. F. Kwong, C. K. Chakrabarty, and Norashidah Md. Din, Investigations on characteristics of metamaterial based patch antenna for RF energy harvesting at GSM 900, Electrical and Electronic Engineering, 5(1A) (2015) 7-13, DOI: 10.5923/c.eee.201501.02.